CHARACTERIZATION OF FUNCTIONAL HUMAN ANTIBODIES TARGETING HENIPAVIRUS AND FLAVIVIRUS GLYCOPROTEINS

By

Michael Patrick Doyle

Dissertation

Submitted to the Faculty of the

Graduate School of Vanderbilt University

in partial fulfillment of the requirements

for the degree of

DOCTOR OF PHILOSOPHY

in

Microbe-Host Interactions

June 30th, 2021

Nashville, Tennessee

Approved by:

Ivelin S. Georgiev, Ph.D.

Christopher Aiken, Ph.D.

Suman Das, Ph.D.

Tina Iverson, Ph.D.

Eric S. Skaar, Ph.D., M.P.H.

James E. Crowe, Jr., M.D.

ACKNOWLEDGMENTS

I would first like to thank my thesis mentor Dr. James Crowe. Dr. Crowe provided me all the resources to succeed in my PhD studies, and allowed me to explore many projects no matter the risk nor reward. His infectious passion for improving human health has been incredibly inspiring, and has given me a drive that I will surely carry throughout my career. Thank you to Rob Carnahan, who ultimately became like a second mentor to me. I always appreciated feeling as if you had our backs, and enjoyed all of our brainstorming sessions for sometimes tumultuous collaborative projects. I never became totally LEAN proficient, but I learned so much about leadership, organization, and scientific management from you. To my committee members Ivelin Georgiev, Chris Aiken, Tina Iverson, Suman Das, and Eric Skaar, thank you for your continual guidance and encouragement over the last 4 years.

I would like to specifically thank all of the technical staff, past and present, that have made my work possible. First, thank you to Nurgun Kose. It can be a difficult task being a new graduate student in the Crowe lab, but you helped guide me through the hybridoma process, and laid the foundation for what would be all of my studies spanning multiple viral families. I really cannot give enough credit to you for everything that has resulted from my graduate studies. Pavlo Gilchuk, thank you for always challenging me to think about my work from a skeptical but optimistic perspective. I learned so much about how to be a rigorous scientist from you, both technically and intellectually. I only wish we had worked on more projects together. Iuliia Gilchuk, thank you for your patience, especially early on during my graduate studies. Sharing a bay with a young, clueless graduate student (especially as a highly organized, exceptional

scientist) mustn't have been easy, but you made me feel like I was a part of the team from day one. Thank you Robin Bombardi for all of your help with everything sequencing and designing constructs for Ryan Irving, thank you for always being someone I could share a joke with on those tough days (and for never getting too mad when I would always seem to put my shipments in at the last minute), and for teaching me the ropes. To all other past and present research associates, staff scientists, and lab managers, thank you for everything you've done to get me to this point. It is not an overstatement to say that, without iCore, Robocore, and Techcore, this work would never have been possible.

Next, I'd like to thank my fellow trainees with whom I've gone on this journey of graduate school. First, my closest friends in the lab, Nate Chapman, Taylor Engdahl, and Ben Fowler. At times when it felt like I was failing, both personally or professionally, you lifted me up and gave me encouragement. I will cherish our friendships forever, and hope I have brought the same positivity to your training experiences. Lauren Williamson, my mentor during my Crowe lab rotation, is someone whose tireless work ethic and rigor I sought to emulate, as impossible a task as that may have been. Thank you to Seth Zost for never once saying no to helping me, and, of course, for sharing Philadelphia-themed memes on occasion. Other trainees, both past and present, with whom I never became as close with but respect immensely for their intellectual curiosity and ability to function in such an environment, I've enjoyed my time with you tremendously and look forward to keeping up with all of your career successes.

Thank you to our collaborators who made major contributions to much of the work highlighted in this dissertation. First, a major thanks to Christopher Broder and Moushimi Amaya of

Uniformed Services University for allowing me to perform synergy neutralization assays in your laboratory. Bob Cross, Tom Geisbert, Chad Mire, and Vika Borisevich of The University of Texas Medical Branch, thank you for providing reagents and for your tireless work in high containment to validate our antibodies using authentic viruses both *in vitro* and *in vivo*. A huge thanks to the scientists at Mapp Biopharmaceutical, especially Zach Bornholdt, Brandyn West, and Larry Zeitlin. This collaboration is what will make translation of the antibodies highlighted in this work possible. The work in chapter V was made possible by collaborators Justin Julander at Utah State University, as well as Michael Diamond and Adam Bailey at Washington University. Finally, thank you to the funding sources behind this work: The Chemical Biology of Infectious Diseases T32 (5T32AI112541), NIH NRSA F31 fellowship (F31AI152332), and the Center of Excellence in Translational Research U19 (U19AI142764).

On a personal note, thank you to Kevin Kramer, Ariana von Lersner, Nate Klopfenstein, John Kramer, Ashley Harris, Noah Bradley, Joe Balsamo, Mac Castro, Sam and Jackie Dooyema, Ben and Mackenzie Coleman, and all of my other friends with whom I've shared so many memories in Nashville. Whether it be going to college football games, camping, or even just having a beer in Hillsboro, you all made my life outside of lab fulfilling, and I hope our friendships last a lifetime. Thank you to my parents Mike and Sandy, step-parents Paul and Catherine, and brothers Joe and Nick, for always supporting my goal of seemingly being a lifetime student. You never once questioned my passion for science and for pursuing a higher degree. Thank you to my dog Josi, whose namesake reflects my love of the Nashville Predators, and who became one of my best friends despite almost driving me to bankruptcy with vet bills. Finally, thank you to my partner Clare Laut. We came into graduate school not knowing each other, and will leave as each

other's best friends. Without your support, I can say without a doubt I would not be writing this document. I love you and look forward to spending my life with you.

TABLE OF CONTENTS

LIST OF TABLES

LIST OF FIGURES

ABBREVIATIONS

6HB	6-helix bundle
ACE2	Angiotensin converting enzyme 2
AGM	African Green monkey
BCR	B cell receptor
CD	Cluster of differentiation
CDR	Complementarity determining region
CedV	Cedar virus
CH	Constant heavy
CL	Constant light
CNS	Central nervous system
DENV	Dengue virus
DPP4	Dipeptidyl peptidase 4
E	Envelope glycoprotein
EBV	Epstein-Barr virus
EC_{50}	50% effective concentration
F	Fusion glycoprotein
Fab	Fragment antigen binding
FACS	Fluorescence-activated cell sorting
Fc	Fragment crystallizable
FFU	Focus forming unit
FRNT	Focus reduction neutralization test
GhV	Ghana virus
GP	Glycoprotein
HA	Hemagglutinin
HeV	Hendra virus
HIV	Human immunodeficiency virus
humAb	Human monoclonal antibody
IC_{50}	50% inhibitory concentration
IC_{80}	80% inhibitory concentration
JEV	Japanese encephalitis virus
K_D	Dissociation constant
LLPC	Long-lived plasma cell
mAb	Monoclonal antibody
MERS	Middle East respiratory syndrome
MojV	Mojiang virus
NA	Neuraminidase
NiV_B	Nipah Bangladesh virus
NiV_M	Nipah Malaysia virus
NPC1	Neimann-Pick C1
NS1	Non-structural protein 1
PFU	Plaque forming unit
prM	Pre-membrane protein

PRNT	Plaque reduction neutralization test
RBD	Receptor binding domain
RBP	Receptor binding protein
RdRp	RNA-dependent RNA polymerase
RF	Replication factory
RSV	Respiratory syncytial virus
S	Spike glycoprotein
SARS-CoV-2	Severe acute respiratory syndrome coronavirus (2)
scFv	Single chain fragment variable
SDS-PAGE	Sodium dodecyl sulfate - polyacrylamide gel electrophoresis
SSPE	Subacute sclerosing panencephalitis
ssRNA	Single-stranded RNA
TI	Trimer interface
TRIM-21	Tripartite motif-containing protein 21
UTR	Untranslated region
VH	Variable heavy
VL	Variable light
WNV	West Nile virus
ZIKV	Zika virus

CHAPTER I

INTRODUCTION

Thesis overview

This dissertation documents my body of work seeking to characterize the human antibody response to viral infections caused by henipaviruses or flaviviruses. The goal of this work was to provide basic knowledge regarding adaptive immune responses to highly pathogenic viruses, develop therapeutic monoclonal antibody candidates to target said viruses, inform design of rational next-generation vaccines, and establish principles for development of antibody cocktails with synergistic potency. I have divided this dissertation into six (VI) chapters. I have attempted to order chapters based on my intellectual contributions, starting with largely collaborative efforts, and ending with projects completely conceived by me under the mentorship of Dr. Crowe.

In Chapter I, I provide a broad overview of human antibodies, and how these molecules have been used as therapeutics to combat viral infections in the past. This is followed by a more detailed description of the two viral families I will be discussing in subsequent chapters, *Paramyxoviridae* and *Flaviviridae.* Each of these sections will be concluded by a discussion of what is known regarding vaccines and therapeutics against these viruses, and will highlight gaps of knowledge in the field that are addressed in the following three chapters. Chapters II-V encompass my primary research efforts in the areas introduced in Chapter I. Chapter II is an overview of the preliminary isolation and characterization efforts undertaken to discover human

monoclonal antibodies against the henipavirus receptor binding protein. I built numerous technical tools to assess antibodies that had been structurally characterized by Jinhui Dong. I used ELISA, flow cytometry, and BLI to further characterize these antibodies to assess the mechanisms used by HENV-26 and HENV-32, helping to establish structure-function relationships to the crystallographic reconstructions of these antibodies in complex with antigen. The data in this chapter set the stage for the bulk of my thesis work, informing the sites of neutralization vulnerability targeted by human mAbs to this henipavirus glycoprotein.

In chapter III, I expand upon the knowledge gained through the highly collaborative work discussed in chapter II to develop next-generation, rationally selected antibody cocktails. Here, I characterize a large panel of mAbs targeting the henipavirus receptor binding protein for binding and neutralization. I first comprehensively categorize and map the six distinct antigenic sites bound by this large panel of antibodies. I then show that two distinct classes of antibodies, termed "receptor-blocking" and "receptor-enhanced," function via distinct molecular mechanism and protect hamsters from Nipah Bangladesh challenge. I further highlight the ability of these mAbs to function synergistically, and provide data to support this concept both *in vitro* and *in vivo*. This chapter concludes with a vignette describing bispecific antibodies bearing the antigen binding properties of both "receptor-blocking" and "receptor-enhanced" mAbs, with data suggesting these may also be viable therapeutic candidates. Chapter IV is the third and final chapter on my human henipavirus immunity work. Here, I introduce the targeted discovery approach used to isolate a human monoclonal antibody targeting a previously undescribed antigenic site on the henipavirus receptor binding protein. I define this antibody's ability to bind only to a full-length construct of receptor binding protein (RBP), differentiating it from

antibodies described in Chapter III. I then highlight *in vitro* and *in vivo* activity studies that show this antibody, HENV-270, is able to neutralize virus and protect hamsters from Nipah Bangladesh challenge. I end Chapter IV with structure-function studies of HENV-270, which suggest this mAb recognizes the C-terminus of the RBP stalk domain and may function by preventing RBP from interacting with the fusion (F) glycoprotein.

Chapter V describes my body of work on characterization of human antibodies targeting the yellow fever virus (YFV) envelope (E) protein. I describe the discovery campaign I undertook to isolate rare human antibodies from subjects inoculated with the live-attenuated YFV vaccine. I then focus on one antibody, YFV-136, which I find to be highly potent against YFV-17D vaccine strain. I use a mechanistic neutralization assay to show that YFV-136 neutralizes primarily at a pre-attachment step in the viral replication cycle. I show, using escape mutation analysis, competition binding studies, and HDX-MS that this mAb binds a complex antigenic site encompassing domains I and II. Antibodies targeting this site have been previously described, suggesting an immunodominant site of recognition by neutralizing and protective mAbs. I finish this chapter with in vivo studies performed by collaborators in hamsters and humanized mice, which show YFV-136 may be a viable therapeutic candidate.

Finally, Chapter IV is a discussion of the broader implications of this work, and where I hope my colleagues take this project in future studies. First, I lay out broad conclusions of my studies, and attempt to draw on broader themes learned through my studies. Next, I attempt to make clear the caveats of my studies, and then delve into where I believe this project could be taken in future studies. I will conclude with a discussion on the implications of this work, and how the data I

have accrued can further vaccine and therapeutic development, not just in the henipavirus/flavivirus fields, but across viruses generally. Overall, I believe my work has thoroughly characterized the humoral response to the henipavirus RBP, provided candidate therapeutics against henipaviruses and YFV poised for evaluation in the clinic, and elucidated novel sites of vulnerability on RBP and E that can be reverse engineered to produce rational, targeted vaccines should a henipavirus or flavivirus emerge in an epidemic or pandemic setting.

Part I: Antibodies

Overview of antibody origin, structure, and function

The human immune response is divided into two broad systems: innate and adaptive immunity (Flajnik and Kasahara 2010). The innate immune system is responsible for immediately responding to microbial insults in a manner that is not entirely specific to the microbe itself. Innate defenses are diverse in repertoire, including physical barrier functions, antimicrobial peptides, complement systems, and responses by phagocytic cells that can clear infections and begin healing affected areas after the insult is cleared (Janeway and Medzhitov 2002). In contrast, the adaptive arm of the human immune system is considered to be pathogen specific, inducing "immune memory" to pathogens in order to respond to infection by the same pathogen in the future. Adaptive immunity is further divided into cellular and humoral arms. T and B cells, respectively, are responsible for each of these responses, though they are intimately linked throughout the response to an infection. B cells are lymphocytes that mature in the bone marrow to display a membrane bound immunoglobulin known as a B cell receptor (BCR). B cells, and the molecules they display and secrete, will be the focus of this section of the introduction.

The antibody is the functional effector of the humoral immune system. Antibodies can either be secreted or bound to the B cell membrane, in which they are referred to as BCRs. Structurally, the antibody is a dimer of heterodimers assembled into a Y-shaped molecule **(Figure 1-1)**. This can further be divided into disulfide linked heavy and light chains, with each chain being divided into variable and constant regions. The heavy and light chain variable regions, or VH and VL, are responsible for binding to antigen. Heavy and light together form the two functional regions of an antibody, Fab (fragment antigen binding) and Fc (fragment crystallizable). The Fab contains both VH and VL (as well as the constant light (CL) constant heavy 1 (CH1) domains), making it the region that is most involved in antigen binding. Both VH and VL can be broken into 4 highly conserved framework regions (FR) and 3 highly variable complementarity determining regions (CDR). CDR loops, especially the heavy chain CDR3 (HCDR3), make up the majority of antigen contact residues.

While binding alone can provide an antibody its function (such as preventing a virus from attaching to a cell, or occluding the enzymatic function of a toxin), Fc is responsible for endowing the antibody molecule with effector functions. These include, but are not limited to, complement deposition, antibody dependent cell-mediated cytotoxicity, and antibody dependent cell-mediated phagocytosis (Lazar, Dang et al. 2006). The Fc domain function is primarily dependent upon the antibody isotype and subtype. Antibodies are divided into 5 isotypes: IgA, IgD, IgE, IgG, and IgM (Schroeder and Cavacini 2010). IgD is thought to be largely membrane bound, is found only on naïve B cells, and has unknown function. IgM forms a pentameric or hexameric structure when secreted, as the Fc region binds to another protein known as J chain.

IgM antibodies are generally elicited early in infection, have sequences that largely mirror germline, and have exquisite ability to carry out complement deposition. IgE is induced by a Type II allergic immune response, and binds to either parasitic or non-pathogenic insults (allergens). Binding by IgE to antigen ultimately results in activation of mast cells, basophils, and eosinophils via Fcε receptors. This binding event induces degranulation of leukocytes, resulting in a release of pro-inflammatory molecules responsible for symptoms of allergic reaction. IgA can be secreted as both monomer and J-chain linked dimer, and is a major effector of the mucosal immune system (Boyaka 2017). Mucosa secrete massive amounts of IgA, with as much as 60 mg per kg body weight produced per day (de Sousa-Pereira and Woof 2019). Finally, IgG is the primary isotype of antibodies in circulation, and is the primary contributor to the humoral response to viral and bacterial infections. Work in this thesis focuses on antibodies of IgG isotype.

Antibody diversity is the result of three principles: combinatorial diversity, junctional diversity, and somatic hypermutation. These principles work to drive antibody specificity to distinct antigens over time to maximize effectiveness. While T cell receptors also derive heterogeneity via combinatorial and junctional diversity, somatic hypermutation is a unique feature of BCR/antibody diversity. Combinatorial diversity results from the combination of genes that make up the heavy and light chain of the antibody. The heavy and light chain loci are formed by combinations of V, D and J genes (or V and J only for kappa and lambda loci for light chains). (Brack, Hirama et al. 1978, Schatz, Oettinger et al. 1989). This combination involves the random combination of one of each V, (D), and J genes that make up the variable regions of the antibody, respectively (Matsuda, Ishii et al. 1998). As this occurs on both heavy and light chains, pairings of different heavy and

light chains result in another source of antibody diversity. During recombination, random insertions and deletions of nucleotides at the junctions between the V, D, and J genes results in a second source of diversity, being junctional diversity (Jeske, Jarvis et al. 1984). Combinatorial and junctional diversity allow for mature, naïve B cells, which will display IgM and IgD on the cell surface, to recognize almost unlimited antigens. Upon binding of cognate antigen, typically within secondary lymphoid tissues where cells have the opportunity to sample antigen displayed by subcapsular macrophages and follicular dendritic cells, B cells can enter germinal centers in the lymph node to undergo affinity maturation via somatic hypermutation (Junt, Moseman et al. 2007). During affinity maturation, random mutations are introduced into the heavy and light chain loci, many of which are focused on the CDRs (Schramm and Douek 2018). Concurrently, B cells will undergo isotype switching (also known as class switch recombination), where the constant domain of IgM is changed out for IgG or IgA (or in the case of allergy, IgE) (Stavnezer, Guikema et al. 2008). The isotype fate of a B cell is in part dependent upon the tissue localization of the germinal center reaction. Mucosa associated lymphoid tissue (MALT), for example, has a higher propensity for producing IgA-secreting B cells due to the importance of IgA in mucosal immunity (Boyaka 2017).

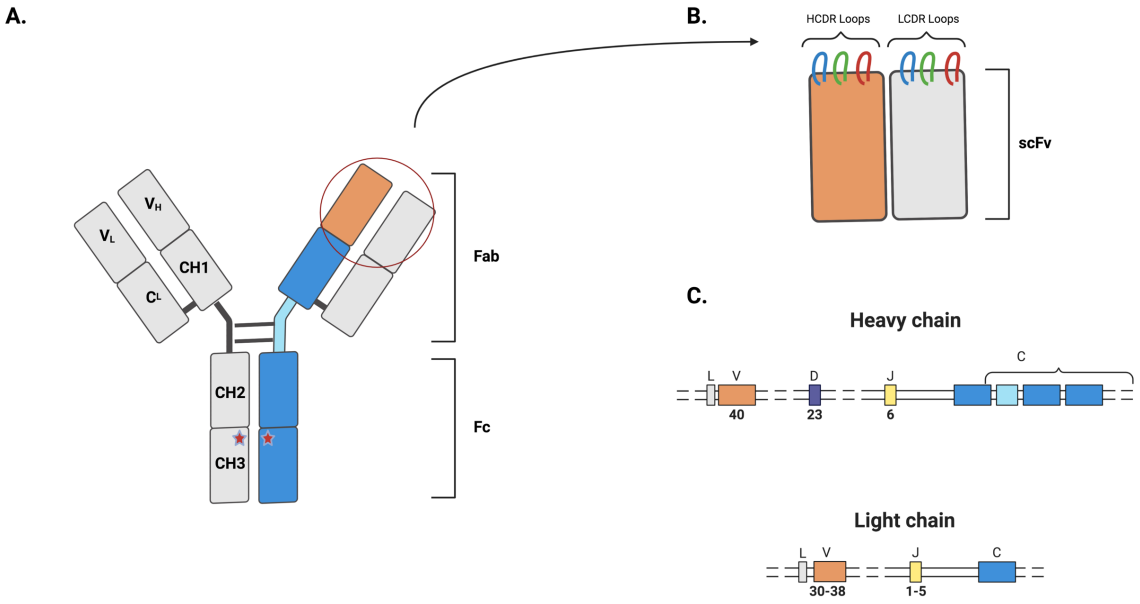

Figure 1-1: Structural and genetic features of antibodies. A) Structure of the full IgG polyprotein. **B)** Zoomed in image of the scFv region, with heavy and light chain CDR loops highlighted. **C)** Heavy and light chain gene loci, with VDJ and C regions for heavy chain, VJ and C regions for light chain. This figure was generated using Biorender.

During the course of an immune response, affinity matured, class-switched B cells will have a variety of potential fates (Hammarlund, Thomas et al. 2017). First, B cells can take on a plasmablast phenotype, a CD19+CD20- (CD = cluster of differentiation) cell type that lacks surface immunoglobulin and is optimized for massive secretion of antibody to respond to a primary infection. As the infection is resolved, a subset of B cells will become $CD19^{+}$ memory B cells. These are characterized by primarily membrane-bound IgG that can be easily stimulated upon re-exposure to infection. More recently, a third B cell compartment known has long lived plasma cells (LLPCs) has been studied and appreciated. These are cells characterized by $CD19^{-}CD27^{+}CD38^{+}$ that secrete exceptionally high affinity antibodies that traffic to the bone marrow following infection (Mei, Wirries et al. 2015). LLPCs are the primary source of antibodies in the serum, as peripheral memory B cells have a low capacity for Ig secretion. Upon

re-exposure to antigen, memory B cells can re-enter germinal centers, undergo affinity maturation, and take on any of the three fates described here. Together, these B cell subsets make up the B2 compartment. A distinct compartment of B cells, known as B1 cells, are derived from the fetal liver to produce an innate-like immune response, but will not be discussed further (Hardy and Hayakawa 2015). It is also worth noting the plasticity in B cell phenotypes. Surface markers for each type described here are done so as generalities, as unique subsets with distinct markers have been described.

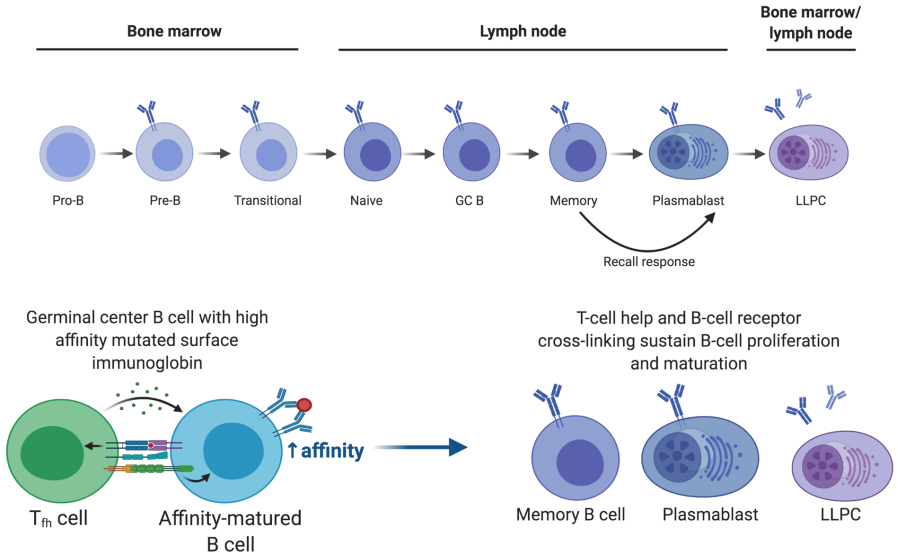

Figure 1-2: B cell development pathway. Top: B cell development, beginning from pre B cell in bone marrow to peripheral memory and long lived plasma cells. Bottom: Germinal center reaction and resulting mature B cell populations. Adapted from "B cell maturation antigen during plasma cell" by Biorender.com (2021). Retrieved from https://app.biorender.com/biorender-templates

History of isolation and use of antibodies as antiviral therapy

Prior to the development of technologies for isolating polyclonal and monoclonal antibodies, there existed a long history of using both human and animal sera or plasma as therapy for infectious diseases. This began roughly 120 years ago, when horses were vaccinated with bacterial antigens in order to harvest serum as a treatment option during severe infections (Casadevall and Scharff 1994). Treatment regimens often required the intravenous dosing of

large volumes of serum from organisms that resolved infection with ill-defined composition. While these therapies were actually considered largely successful, there were problems with maintenance of animal sources of serum, lot to lot variability, and moderate to severe side effects due to byproduct ingredients. As a result, new methods of harnessing the treatment efficacy of serum therapy in a scalable, safe manner were explored. This first required a technique that would allow for continuous culture of B cells, a feat that had eluded researchers to date. Crucial studies by Kohler and Milstein in the 1970s resulted in the development of what is now known as "hybridoma technology," and it is these studies that formed the basis for the technology used in this dissertation (Kohler and Milstein 1975). This involves the immortalization of murine (and now human) B cells by fusion with a multiple myeloma cell line after initial immortalization of B cells using Epstein-Barr virus (EBV). This allows for continuous culture, screening, and production of antibodies from the initial B cell population. This technology has previously been used to develop antibodies used in the clinic for both infectious and non-infectious indications, such as the murine anti-CD3 antibody used to prevent transplant rejections, and Palivizumab for prophylaxis of neonates against respiratory syncytial virus (RSV) (Casadevall, Dadachova et al. 2004). Multiple iterations of hybridoma technology can be found throughout the literature, with numerous antibodies of murine and human origin isolated against infectious disease targets.

Antibody isolation technology from hybridoma cell lines has rapidly developed over the previous decade. Specifically, newer methods have advantages in both speed and throughput. For example, bulk isolation of B cells from human or animal origin, followed by fluorescence activated cell sorting of antigen-specific cells, has allowed for isolation of thousands of antibodies against a particular target in a short period of time. Speed has been further increased

by coupling of single-cell isolation pipelines to next-generation sequencing technologies, in which paired heavy and light chain sequences from sorted antibodies can be analyzed and expressed in micro-scale for pre-clinical studies. Recent Defense Advanced Research Projects Agency (DARPA)-funded studies have highlighted the utility of this platform (Gilchuk, Bombardi et al. 2020). Similarly, libraries of phage, yeast, or mammalian cells displaying human antibody libraries can be screened to identify antibodies against specific antigen targets using similar technologies, and have been implemented by both academic and industry groups with great success (McCafferty, Griffiths et al. 1990, Boder and Wittrup 1997, Bowers, Horlick et al. 2011). Finally, newer frontiers of single cell technology and microfluidics have provided new ways for screening and isolating candidate antibodies for the purposes of therapeutic development (Leung, Klaus et al. 2016).

As far as antibodies approved for use in humans to combat viral diseases, the list is fairly limited in comparison to other diseases, with the majority of the field growth occurring recently due to a viral pandemic. The most widely used of the list is Palivizumab (Johnson, Oliver et al. 1997). This mAb, developed by MedImmune (now AstraZeneca), is used prophylactically in cases of premature birth to prevent infection by respiratory syncytial virus (RSV) (Wu, Pfarr et al. 2008). As RSV is the leading cause of hospitalizations in children, this antibody addressed a severely unmet medical need (Goldstein, Fergie et al. 2021). Despite this, Palivizumab is only moderately potent in its neutralization of RSV, requiring massive doses for protection, which in turn is prohibitively expensive in many cases. This limitation is driving the clinical development of next generation antibodies targeting RSV (Wu, Pfarr et al. 2007). More recently, Ansuvimab produced by Ridgeback Biotherapeutics and a Regeneron antibody cocktail were approved for

the treatment of disease caused by Ebola Zaire (Pascal, Dudgeon et al. 2018, Mulangu, Dodd et al. 2019). Finally, numerous mAbs, both as monotherapy and cocktail, have entered the clinic for the treatment of COVID-19. Examples include Eli Lilly's Bamlanivimab and Regeneron's casirivimab/imdevimab cocktail, though both are currently only being used under Emergency Use Authorization (EUA) and are not yet formally approved for use by the Federal Drug Administration (FDA) (Hansen, Baum et al. 2020, Chen, Nirula et al. 2021).

Functional mechanisms used by antiviral antibodies

Viral pathogens are infectious virion particles made up of genetic information surrounded by a protein coat and host-derived plasma membrane (if enveloped) that can contain surface glycoproteins. Productive infection of host cells by a virus hinges upon viral attachment to a cognate receptor and/or set of attachment factors. Intuitively, antibodies can function by inhibiting this attachment step. Antibodies that function in this manner have the added benefit of targeting a region of a viral glycoprotein that likely necessitates some level of functional conservation derived from the amino acid level. Antibody binding to conserved residues will inhibit receptor interactions preventing viral infection and is therefore a valuable quality for therapeutic molecules. Examples of successful antibody-mediated receptor blocking include CD4 binding blockade of HIV, NPC1 blockade of Ebolavirus, ACE2 blockade of SARS/SARS-CoV-2, DPP4 blockade of MERS, among others (Lynch, Tran et al. 2012, Yu, Zhang et al. 2015, Gilchuk, Kuzmina et al. 2018, Rappazzo, Tse et al. 2021). For viruses where a *bona fide* receptor has not been defined, such as flaviviruses, pre- versus post-attachment neutralization assays can define antibodies for their ability to prevent attachment of virus to host cells (Vogt, Dowd et al. 2011, Qiu, Lei et al. 2018).

Upon attachment to a host cell, a virion must fuse viral and host membranes to allow for ejection of the viral genome into the host cell. This either occurs at the cell membrane independently of pH, or within the low pH endosome in a pH-dependent fashion. In either case, this process involves a conformational rearrangement of one or more viral glycoproteins to facilitate the energetic merging of viral and host membranes. Once fused, the viral genome is able to access the host cytosol. Direct conformational "locking" of a fusion glycoprotein is one way this is achieved (Kaufmann, Vogt et al. 2010, Fibriansah, Ibarra et al. 2015, Hellert, Buchrieser et al. 2020). Antibodies targeting paramyxovirus and pneumovirus F proteins have been shown to function by this method (McLellan, Chen et al. 2013). This is also a postulated mechanism for anti-flavivirus mAbs isolated against viruses including Zika (Zhang, Kostyuchenko et al. 2016).

Beyond interruption of receptor binding and membrane fusion, it has recently been appreciated that antibodies can potentiate structural rearrangements to a viral glycoprotein that have functional consequences. First, this "triggering" event can lead to a premature rearrangement of a viral glycoprotein, rendering virus unable to productively enter host cells. An example of this type of activity can be found in the coronavirus field, where antibodies targeting sarbecovirus spike (S) glycoproteins can induce shedding of a protein subdomain, and can subsequently trigger S to rearrange into a post-fusion conformation in the absence of receptor (Walls, Xiong et al. 2020, Wec, Wrapp et al. 2020). This concept is also applicable to human parainfluenza viruses (PIV), where premature triggering of F renders virus unable to infect cells (Bottom-Tanzer, Rybkina et al. 2019). The induction of allosteric changes to a viral glycoprotein can also have consequences in the context of antibody cocktails. For instance, antibodies targeting the

filovirus GP have been shown to induce allosteric changes and lead to more robust binding by a second antibody to an occult epitope (Howell, Brannan et al. 2017, Gilchuk, Murin et al. 2020). This leads in to the concept of synergy: two antibodies in a cocktail having activity that exceeds that of the individual antibody at the same concentration. Synergistic pairs of antibodies have been described for a number of viral targets such as HIV, coronaviruses, filoviruses, and others, though in many cases the basis for this synergy is unknown (Zhong, Haynes et al. 2009, Miglietta, Pastori et al. 2014, Gilchuk, Murin et al. 2020). It is likely that allosteric potentiation serves as a basis of synergy observed in many of these cocktails. Even in the absence of synergistic activity, antibodies have been shown to function by causing structural changes to viral glycoproteins that disrupt the protein's function. A recent example of this function can be found in the influenza field, with multiple groups discovering antibodies to an antigenic site at the trimer interface (Lee, Boutz et al. 2016, Bajic, Maron et al. 2019, Bangaru, Lang et al. 2019). These mAbs bind to a hidden site that is hidden within the trimeric structure of influenza HA. Electron microscopy studies show that these antibodies disassociate HA trimers, suggesting antibodies to this site function by disrupting virion-bound HA, likely preventing it from functioning in attachment and/or fusion.

Many enveloped viruses are assembled at and bud from the host cell plasma membrane. During this process, viral glycoproteins are inserted into the host membrane, and are displayed to the extracellular milieu during the budding process. Antibodies that target these proteins have the ability to arrest the process of budding, preventing virions from being fully released from the host cell. This concept is well-described in the influenza field, where inhibition of neuraminidase can prevent cleavage of sialic acid, leaving budding virions "stuck" within the host cell (Gilchuk,

Bangaru et al. 2019, Stadlbauer, Zhu et al. 2019). This has been described for other viral pathogens as well, though is likely not thoroughly characterized due to the inability of traditional neutralization assays to capture the activity of these mAbs (Kajihara, Marzi et al. 2012, Jin, Galaz-Montoya et al. 2018).

While this dissertation focuses on antibodies with *in vivo* virus neutralization functions, the Fc domain has the ability to confer activity to both neutralizing and non-neutralizing antibodies. As described for antibodies that inhibit egress, antibody binding to cell surface displayed viral antigens can recruit cellular effectors to infected cells. Effector cells can then recognize the Fc region of the antibody via Fc receptors, resulting in killing of the infected cells (Chung, Nybakken et al. 2006). Although the functions described above account for most antiviral antibodies isolated to date, viral infections have the ability to induce antibodies with atypical functions. In the case of non-enveloped viruses, antibodies may target incoming virions for proteasomal degradation in a TRIM-21 dependent manner, a function that has been seen in anti-bacterial antibodies as well (Foss, Bottermann et al. 2019, Velayutham, Kumar et al. 2019). It is important to note that antibodies may function by two or more of the above mechanisms simultaneous. It is likely that, in the context of a polyclonal response to a viral infection, antibodies with diverse functions work in concert to mediate clearance of virus and ultimately protection from disease.

Mechanisms of evasion from antibody-mediated immunity

RNA viruses have the intrinsic ability to introduce amino acid substitutions into viral glycoproteins by way of error prone RNA-dependent RNA polymerase (RdRp) complexes

(Smith 2017). The error-prone nature of RdRp typically results in the propagation of diverse viral populations in the context of an infections, sometimes referred to as viral quasispecies or viral swarms (Andino and Domingo 2015). Occasionally, amino acid substitutions in viral glycoproteins can decrease the binding of antibodies without incurring a fitness cost on the virus. As this allows the virus to propagate unimpeded by an antibody response, viruses that bear these substitutions will gain a survival advantage and become dominant. The consequences of viral escape can apply to both the natural immune response to the virus or therapeutics used to combat infection. Escape from antibody-mediated neutralization can be readily shown *in vitro* for numerous potent antibody therapeutic candidates targeting diverse RNA viruses (Greaney, Starr et al. 2021). Recent studies in immunocompromised patients chronically infected with SARS-CoV-2 have definitively shown selection of viral populations that escape from antibodies *in vivo* (Starr, Greaney et al. 2021). In these studies, though, the use of antibody cocktails curtailed the possibility of complete failure of the therapy.

Viruses have also evolved other mechanisms to evade humoral immune responses. Numerous viruses, perhaps most notably HIV, use glycans to "shield" vulnerable sites on the viral glycoprotein provide a barrier to antibody-mediated neutralization by specific subsets of antibodies (Fenouillet, Gluckman et al. 1994). It is likely that glycans play a role in shielding henipaviruses from humoral immunity, as studies showing removal of glycans on RBP render henipaviruses more susceptible to neutralization by polyclonal preparations. Decoy proteins are employed by numerous viruses to misdirect immune responses to non-productive antigens. Examples of this include secreted versions of the RSV attachment glycoprotein (sG) and secreted filovirus glycoprotein (sGP) (Bukreyev, Yang et al. 2008, de La Vega, Wong et al. 2015).

Finally, and perhaps the most sophisticated example, is the ability of poxviruses, whose massive genomes encode for hundreds of proteins, to produce cytokine receptor decoys in order to completely misdirect the antiviral immune response (Pontejo, Alejo et al. 2015, Hernaez and Alcami 2018).

Part II: Henipaviruses

Introduction to the *Henipavirus* genus

Viruses classified by the International Committee on Taxonomy of Viruses (ICTV) in the genus *Henipavirus (*subfamily *orthoparamyxovirinae,* family *Paramyxoviridae,* order *Mononegavirales*) are a recently discovered class of viruses, which include the two human pathogens, Hendra (Guirakhoo, Pugachev et al. 2002) and Nipah (NiV) (Rima, Balkema-Buschmann et al. 2019). Henipaviruses are pleomorphic, enveloped viruses with a single stranded RNA genome of negative polarity (Chua, Wong et al. 2007). In comparison to other genera within the *Paramyxoviridae* family, henipaviruses have an exceptionally large genome, with an average size of ~18 kilobases. As with all paramyxoviruses, the henipavirus genus follows the rule of six, in which the number of nucleotides in the viral genome is always a multiple of six, to allow for nucleoprotein binding (Egelman, Wu et al. 1989). The exceptional size of the henipavirus genus is primarily the result of the presence of large 5' and 3' untranslated regions (UTRs) flanking each of protein-coding regions of the genome (Wang, Yu et al. 2000). The RNA genome contains six genes encoding up to nine proteins, depending on RNA editing sites and alternate open reading frames within the phosphoprotein (P) gene **(Figure 1-2)**. Like other paramyxoviruses, the viral envelope contains two distinct glycoproteins: the receptor binding protein (RBP) and fusion protein (F). Following translation and genome

replication, the RBP and F are trafficked to the host cell surface. F is recycled through endosomes, allowing for cleavage by cathepsin L into the mature fusion protein, which is again trafficked to the cell surface (Pager and Dutch 2005, Pager, Craft et al. 2006). These solvent-exposed proteins are also the primary targets of the humoral immune system, and are the focus of vaccine and antibody therapeutic development (reviewed extensively in (Amaya and Broder 2020)).

The henipavirus RBP is a type II integral membrane protein, meaning it contains a single-pass transmembrane domain with a solvent-exposed C-terminus. In its entirety, it contains a cytoplasmic tail, short transmembrane helix, alpha-helical stalk, and six-bladed beta-propeller head domain (Yuan, Swanson et al. 2011). The head domain contains the receptor-binding domain. HeV and NiV RBPs both use the host cells receptors ephrin-B2 and ephrin-B3 (Bonaparte, Dimitrov et al. 2005, Negrete, Levroney et al. 2005, Negrete, Wolf et al. 2006, Xu, Broder et al. 2012). This family of membrane-bound receptor tyrosine kinases are expressed throughout the vascular endothelium and the central nervous system (CNS), with ephrin-B3 especially concentrated in the CNS (Benson, Romero et al. 2005). While both viral attachment proteins are able to use both receptors, there is a great deal of controversy regarding differential affinities between HeV and NiV RBP. The current paradigm is that HeV and NiV can both use ephrin-B2, but NiV has a higher affinity for ephrin-B3 than HeV (Negrete, Chu et al. 2007). Unsurprisingly, as is discussed later in this introduction, this receptor tropism drives the severe disease caused in humans by HeV and NiV.

Upon binding by HeV or NiV to its cognate receptor, a conformational cascade occurs in the quaternary structure of RBP, which in turn triggers cell fusion by F. This triggering event allows F to undergo a conformational rearrangement from pre-fusion to post-fusion. The post-fusion conformation involves a six-helix bundle (6HB) and an exposed fusion peptide (Xu, Chan et al. 2015). This fusion peptide inserts into the host membrane, ultimately allowing for fusion of viral and host membranes, and ejection of the henipavirus RNA genome into the host cytosol in a pH-independent manner. The "triggering" of F by RBP has been explained by two prevailing models: the clamp model, and the provocateur model. In the clamp model, which has been extensively studies in the case of Measles virus, RBP and F are pre-associated, and receptor binding breaks up this complex, therefore "unclamping" F to allow it to undergo structural rearrangements (Plemper, Hammond et al. 2002). Recent work, though, suggests the provocateur model more likely explains henipavirus fusion. In the provocateur, RBP and F are adjacent to each other in the viral membrane. Upon receptor binding, RBP associates with F, "provoking" it to change to its post-fusion conformation (Chan, Lu et al. 2012, Liu, Stone et al. 2013). This triggering likely occurs when the RBP head domains move from a "heads down" to "heads up" conformation, which exposes a region of the stalk domain critical for interacting with F. The RBP and F proteins of HeV and NiV share roughly 83% and 89% amino acid sequence similarity, respectively (Steffen, Xu et al. 2012).

While RPB and F proteins are primarily responsible for productive infection of host cells and are the targets of the human humoral immune response, other non-structural proteins contribute to infection in other important ways. C, V, and W proteins, which are products of the P protein gene (C from an alternate reading frame, V and W from RNA editing) function as innate immune

antagonists (Rodriguez, Wang et al. 2003, Uchida, Horie et al. 2018, Tsimbalyuk, Cross et al. 2020). Specifically, these proteins can bind to members of the STAT family of ISG transcription factors, sequestering them into high molecular weight complexes in the cytoplasm, and preventing translocation to the nucleus. The V protein appears to be especially important for the pathology induced by henipaviruses, as NiV unable to produce V is non-lethal in a hamster model of infection (Yoneda, Guillaume et al. 2010).

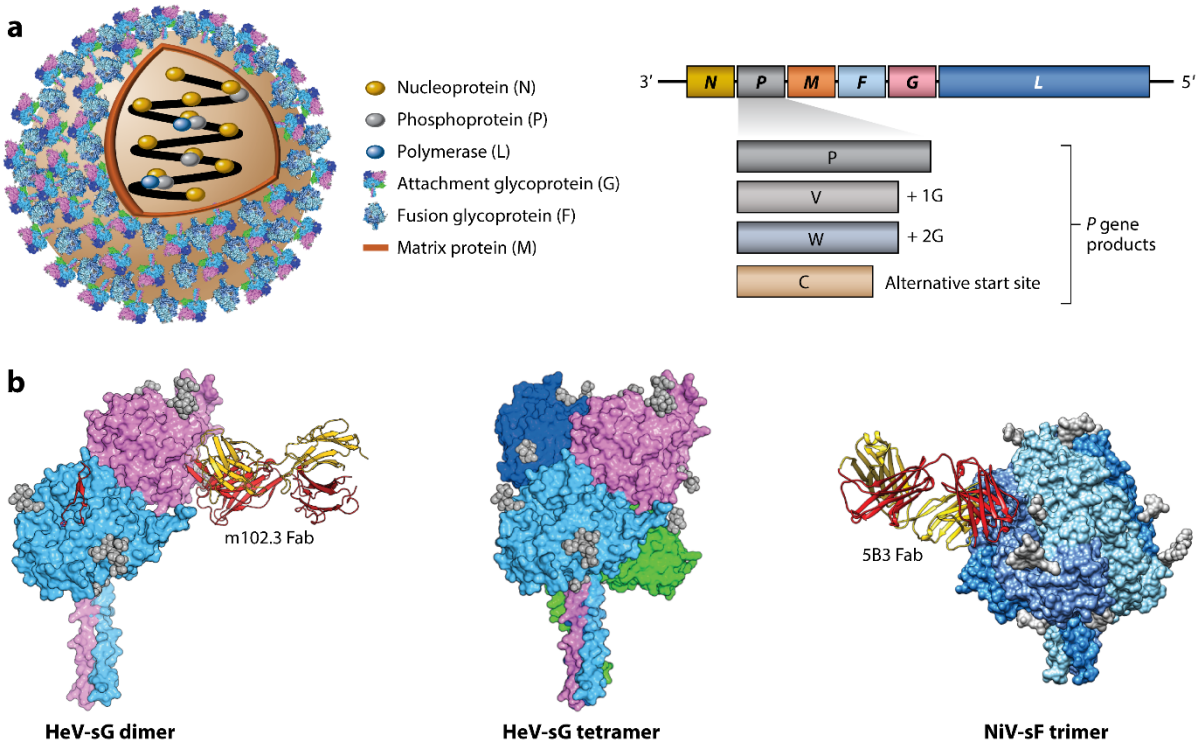

Figure 1-3: Henipavirus genome organization and glycoprotein structure. a) Spherical representation of a henipavirus virion (left). A linear representation of the henipavirus negative sense RNA genome, with structural and non-structural protein genes annotated (Colling, Lunt et al.). **b)** Dimeric HeV-sG (RBP) bound to Fab from neutralizing antibody m102.3 (left). Homotetrameric modeled representation of HeV-RBP (middle). Tetrameric HeV-F bound to fab from protective antibody 5B3 (Colling, Lunt et al.). Figure reproduced with permission (Rightslink license ID 1110536-1) as in (Amaya and Broder 2020).

Henipavirus history and epidemiology

In 1994, HeV, initially named "equine morbillivirus," and subsequently named after the place of its discovery in Hendra, Australia, was the first discovered henipavirus (Murray, Rogers et al. 1995). The first outbreak of HeV began as an unidentified respiratory and encephalitic syndrome in horses, which was subsequently transmitted to two humans who came into contact with the infected horses. Cultured virus from infected horses and human kidney post-mortem confirmed an etiologic agent that appeared related to known morbilliviruses (Selvey, Wells et al. 1995). In 1995, a third human case arose in a sugar cane farmer in Mackay, which was unfortunately fatal. In this case, however, this appeared to be a recurrence incident, where encephalitis and death occurred long after exposure (Murray 1996, O'Sullivan, Allworth et al. 1997). This clinical manifestation suggested a process similar to subacute sclerosing panencephalitis (SSPE), a phenomenon recognized in survivors of measles virus infection (Tan, Goh et al. 2002). Serological surveillance confirmed that *Pteropus* species of bats, colloquially known as flying foxes, were the reservoir species for HeV (Young, Halpin et al. 1996). Since its discovery, HeV has only caused seven human cases, although four of these have been fatal, and almost annual equine cases occur in eastern regions of Australia. Despite annual occurrences of HeV disease, infection is typically isolated to one or a few horses, suggesting HeV transmission between horses is also inefficient (Middleton 2014).

In late 1998, the second name giving virus of the henipavirus genus, Nipah, was described after an outbreak of encephalitis among pig farmers in Malaysia, as well as abbatoir (slaughterhouse) workers in Singapore (Chua, Goh et al. 1999, Paton, Leo et al. 1999). Initially thought to be Japanese encephalitis, this larger outbreak infected more than 250 people, and resulted in over

100 deaths. Virus isolated from the cerebrospinal fluid of infected humans confirmed a Hendra-like virus was the causative agent (Chua, Goh et al. 1999). Subsequently, this virus was named Nipah after the Malaysian village where it was first described. As with HeV, NiV is reservoired in flying foxes, and in the Malaysia outbreak, was transmitted to humans through infected pigs. Unlike humans, pigs presented with a mild respiratory disease, though massive numbers of pigs were culled to contain the virus. Since 1999, outbreaks of a genetically distinct strain of NiV have been described in Bangladesh, and more recently, in Kerala, India (Arunkumar, Chandni et al. 2019). This strain, termed NiV Bangladesh, differs by <10% at the nucleotide level, but is characterized by much higher mortality (>90% case fatality ratio, respiratory and neurological manifestations, and human to human transmission (Lo, Lowe et al. 2012, Mire, Satterfield et al. 2016). Spillover by NiV Bangladesh differs from NiV Malaysia, primarily infecting humans after consumption of date palm sap contaminated with bat excreta (Luby, Rahman et al. 2006).

While HeV and NiV are the only two henipaviruses confirmed to cause disease in humans, three other henipaviruses have been described to varying degrees: Cedar virus (CedV), Ghana virus (GhV), and Mojiang virus (MojV). The most thoroughly described of the three (and the only henipavirus of these three that was actually isolated), CedV, was isolated from Pteropus bats in Australia (Marsh, de Jong et al. 2012). Despite using ephrin-B2 as a host cell receptor (along with A type receptors, and not ephrin-B3), CedV is non-pathogenic in mammals, and is currently being studied as a potential henipavirus vaccine vector (Laing, Navaratnarajah et al. 2019). Ghana virus, which also utilizes ephrin-B2, was sequenced from bats in Ghana, and its pathogenic potential is currently unknown (Voigt, Hoffmann et al. 2019). Finally, Mojiang virus was identified from sequencing of rat feces (Wu, Yang et al. 2014). While it has been implicated

in the death of two miners in Southern China due to atypical pneumonia, MojV was neither isolated nor sequenced from these human subjects. The lack of viral isolates or sequences from these miners calls into question whether or not MojV is pathogenic to humans. MojV has been characterized to use a divergent receptor from other identified henipaviruses, though the exact identity of the receptor is unknown (Rissanen, Ahmed et al. 2017).

Despite the henipavirus genus only having five official members, it is likely there are many henipavirus-like pathogens that have yet to be described. Human serological studies in Cameroon and Trinidad have identified humans and bats with neutralizing antibody titers against Nipah virus (Pernet, Schneider et al. 2014, Schulz, Seifert et al. 2020). In the case of humans surveyed in Cameroon, contact with butchered bats appears to correlate with seropositivity, suggesting that these undescribed viruses are harbored in bat populations. Recently, sero-surveillance of bats in Bangladesh has shown that henipaviruses are far more widespread than previously thought, with Malaysia-like strains isolated from Bangladesh (Epstein, Anthony et al. 2020). These studies have raised concerns that henipaviruses may pose a significant global public health threat, either via pandemic spread or bioterror events (Luby 2013).

Henipavirus disease in humans

While studies on henipavirus transmission are still lacking, infections are thought to occur via the oronasal route (Goh, Tan et al. 2000). This concept has been exemplified by the ability of NiV Bangladesh to more efficiently transmit between humans. The higher rate of human-to-human transmission is likely a result of NiV Bangladesh causing more respiratory illness (Hossain, Gurley et al. 2008). For both HeV and NiV, symptom onset typically begins at one to

two weeks post-infection. Disease progression occurs rapidly, with fever, chills, headache, myalgia, and confusion typically leading to hospitalization on average three days after disease onset. Disease then typically progresses to severe respiratory and/or encephalitic syndromes, followed by death around day nine. Pathologies are the result of systemic vasculitis, with an emphasis on pulmonary and CNS vasculature, leading to ischemia and thrombosis in affected areas (Goh, Tan et al. 2000). For those who survive the disease, which can be as low as 10% of those infected in some outbreaks, late-onset encephalitis can occur several years after infection, though the mechanism of this delayed disease is currently unknown (Tan, Goh et al. 2002). Recent studies, though, have shown that non-human primate survivors of NiV infection have detectable viral antigen in the brain long after infection, suggesting a lasting CNS reservoir may exist for henipaviruses (Johnston, Briese et al. 2015, Liu, Coffin et al. 2019).

Human adaptive immune responses to henipavirus infection

The adaptive immune response to henipaviruses has been largely unstudied. Because of the high mortality rate of HeV and NiV, the immune response is thought to be insufficient in most cases. Two surviving patients from the 2018 NiV outbreak in Kerala were enrolled in a longitudinal study to assess cellular and humoral immunity. In both patients, large expansions of CD8+ T cells were observed, and these cells expressed markers indicative of acute effector functions. Importantly, both patients developed detectable NiV-specific IgM and IgG 8 days post-infection, suggesting humans elicit humoral responses to henipaviruses (Arunkumar, Devadiga et al. 2019). The HeV and NiV glycoproteins, RBP and F, are the major proteins targeted by neutralizing antibodies. In animal models of infection, serum neutralizing antibodies have been shown to be a correlate of protection, as passive therapy using immune serum can fully protect against infection

(Guillaume, Contamin et al. 2004). Concurrently, multiple vaccine trials in animal models have been done with the goal of eliciting neutralizing antibodies, many of which have been successful (recent examples include (Loomis, Stewart-Jones et al. 2020, Geisbert, Bobb et al. 2021).

Animal models of henipavirus disease

For study of antivirals and vaccines *in vivo*, there are currently three popular models; Syrian golden hamsters, ferrets, and the gold standard is the African Green Monkey. Each of these models allows for productive infection of animals without genetic manipulation, while also largely recapitulating henipavirus disease seen in humans. Mice, however, have traditionally not been used as a model of henipavirus infection, as many studies have shown them to be completely refractory to disease. This is likely due to the inability of HeV and NiV to antagonize the murine innate immune system. One study, however, did show the ability of HeV to productively infect aged mice, though this model has not been widely adopted (Dups, Middleton et al. 2012). While there is ongoing work developing models of henipavirus infection using transgenic mouse models, as well as studies in livestock (horses, pigs, etc.), this discussion will focus primarily on the established models listed above in the context of NiV (though all are also models of HeV).

The hamster model of NiV is the primary small animal model used to assess therapeutic and vaccines. This model, developed in 2003 at the Pasteur Institute, mirrors human disease, with viral antigen being detected in multiple organ systems upon intranasal or intraperitoneal inoculation (Wong, Grosjean et al. 2003). This model has been used to test numerous vaccine candidates, as well as passive serum transfer studies (Guillaume, Contamin et al. 2004, Guillaume, Contamin et al. 2006). Follow-up studies on this model have determined that the

route of inoculation, as well as dose of infection, determine disease outcome. Higher dose inoculation leads to a primarily respiratory presentation of disease, whereas low dose induces central nervous system pathologies later in the course of infection (Rockx, Brining et al. 2011). Despite the caveat of this dose-dependence on disease outcome, hamsters are still considered a premier small animal model of infection.

Ferrets have been used as a model of numerous viral infections, as clinical presentation in ferrets mimics disease in humans for many pathogens. The University of Texas Medical Branch (UTMB) developed a ferret model of NiV that more fully recapitulates the pathological changes seen in humans than hamsters. In this model, both respiratory and neurological disease develop concurrently within six to ten days post-inoculation (Bossart, Zhu et al. 2009). This is similar to the incubation period observed in humans. This model has been used to test vaccine and therapeutic candidates, including human antibodies (Bossart, Zhu et al. 2009, Dong, Cross et al. 2020, Mire, Chan et al. 2020). We use this model of Nipah Bangladesh to assess the therapeutic potential of antibodies discussed in chapter II.

The gold standard model for NiV disease (and Hendra) is the African Green monkey (AGM) (Geisbert, Daddario-DiCaprio et al. 2010). This model was initially developed using NiV Malaysia and has been shown to largely recapitulate human disease. AGMs have been particularly useful for dissecting the pathogenic differences between NiV Malaysia and NiV Bangladesh. In follow-up studies by the group who developed the model, NIV Bangladesh was shown to be more highly pathogenic in AGMs, with more severe viremia and time to death observed. Consequently, the therapeutic window for previously described antibody therapeutics

was found to be shorter in AGMs inoculated with NiV Bangladesh (Mire, Satterfield et al. 2016). This was a crucial finding, as most studies done previously used NiV Malaysia, further displaying the utility of the AGM model of NiV.

Therapeutic monoclonal antibodies targeting henipaviruses

As highlighted above, the paradigm of passive immunization using monoclonal antibodies (mAbs) for combating infectious disease has shown to be efficacious for a variety of microorganisms, including a number of RNA viruses. To date, very few studies have sought to define the human humoral immune response to HeV or NiV infection. Multiple studies have used mouse hybridoma technology to isolate monoclonal antibodies. These mAbs target the fusion glycoproteins of HeV and/or NiV, and display *in vitro* neutralization capacity (Avanzato, Oguntuyo et al. 2019, Dang, Chan et al. 2019). Most excitingly, phage display technology has yielded a monoclonal antibody, designated m102.4, targeting RBP of both HeV and NiV viruses, that is able to fully protect multiple animal models, including the model of henipavirus infection that most closely mirrors human infection, the AGM (Zhu, Dimitrov et al. 2006, Zhu, Bossart et al. 2008, Bossart, Geisbert et al. 2011). While these studies have yielded exciting results, these antibodies do not represent the true human immune response to infection, and the technologies used to isolate these mAbs have many drawbacks. Murine antibodies lack the antibody diversity observed in humans, while phage display technology uses random heavy and light chain pairings, leading to pairings that may otherwise have been eliminated during a natural human immune response. Also, naïve human Ig libraries tend to be limited in diversity. Studies presented in this dissertation address these drawbacks by performing discovery of fully human monoclonal antibodies in the context of a naturally immune individual.

Part III: Yellow fever virus

Introduction to the *Flavivirus* genus

The *Flavivirus* genus, classified within the *Flaviviridae* family along with *Hepacivirus* and *Pestisvirus* genera (as well as a number of currently unassigned viruses), is a diverse genus of enveloped, positive-sense single stranded RNA (+ssRNA) viruses (Simmonds, Becher et al. 2017). Flaviviruses encompass many of the most common human arboviral pathogens, including West Nile virus (WNV), Dengue virus (DENV), Japanese encephalitis virus (JEV), among many others transmitted by either mosquitoes or ticks. The name-giving virus of the *Flaviviridae* family (*flavus* being Latin for "yellow") is yellow fever virus (YFV). Yellow fever virus represents a complicated juxtaposition of vaccine success long before the age of rational vaccine design, while also still being responsible for enormous human disease burdens in South America and Sub-Saharan Africa. Recent estimates suggest as many as 60,000 people a year succumb to YFV infection (2010).

The RNA genome of flaviviruses encodes for three structural and seven non-structural proteins (Pierson and Diamond 2020). Envelope (E) and pre-Membrane/Membrane (prM) are solvent exposed, membrane anchored proteins that mediate attachment, fusion, entry, and maturation of viral particles throughout the virus replication cycle (Rey, Heinz et al. 1995, Smit, Moesker et al. 2011, Rey, Stiasny et al. 2017). These proteins, as well as the non-structural protein 1 (NS1) are the primary targets of function humoral immune responses (Muller and Young 2013, Slon Campos, Mongkolsapaya et al. 2018, Reyes-Sandoval and Ludert 2019). The E protein is a class II fusion protein containing three distinct domains. Domain III (DIII) is the putative receptor

binding domain responsible for attachment to host cells, and is linked to Domain II (DII) via Domain I (DI) (Crill and Roehrig 2001). DII contains the hydrophobic fusion loop (FL), which inserts into host endosomal membranes during viral fusion (Allison, Schalich et al. 2001). While the flavivirus receptors/attachment factors are poorly defined, heparin sodium sulfate, lectins, and other membrane bound sugars are thought to participate in attachment (Chen, Maguire et al. 1997, Tassaneetrithep, Burgess et al. 2003).

Upon attachment by E to its undefined attachment factor, viral particles are brought into host cells via clatherin-mediated endocytosis or micropinocytosis (Hackett and Cherry 2018). In the low pH environment of late endosomes, protonation of histidine residues on E induces a massive conformational rearrangement of E proteins, which under neutral pH, lie flat 90 anti-parallel dimers on the viral surface with (pseudo) 3-fold icosahedral symmetry (Kuhn, Zhang et al. 2002). During rearrangement, these dimers reassemble into trimeric spikes, where FL is solvent exposed, allowing for insertion into the endosomal membrane (Chao, Klein et al. 2014). This is proceeded by fusion of viral and host membranes, ejection of the RNA genome into the host cytoplasm, and direct translation and replication of the positive sense RNA genome. Replication occurs in “replication factories” formed from endoplasmic reticulum membranes. In these RFs, immature virions are assembled, where heterotrimers of prM and E form “spiky” particles (Prasad, Miller et al. 2017). As virions traverse the golgi apparatus, prM is cleaved by the host protease furin, but the pr peptide remains bound to the FL to prevent premature fusion (Elshuber, Allison et al. 2003). At this stage, E proteins arrange into the herringbone pattern of 90 anti-parallel dimers. Upon virus release into the extracellular milieu, pr is liberated, resulting in mature particles that can productively infect host cells. The process of prM cleavage is

inefficient, though, particularly for certain viruses in the DENV serogroup. This results in mosaic viruses bearing both mature and immature regions (Junjhon, Edwards et al. 2010). This has serious implications in the host humoral response to some flaviviruses, though YFV is thought to mature more efficiently (Junjhon, Lausumpao et al. 2008). With this general background of flaviviruses, the remainder of this introduction will focus specifically on YFV.

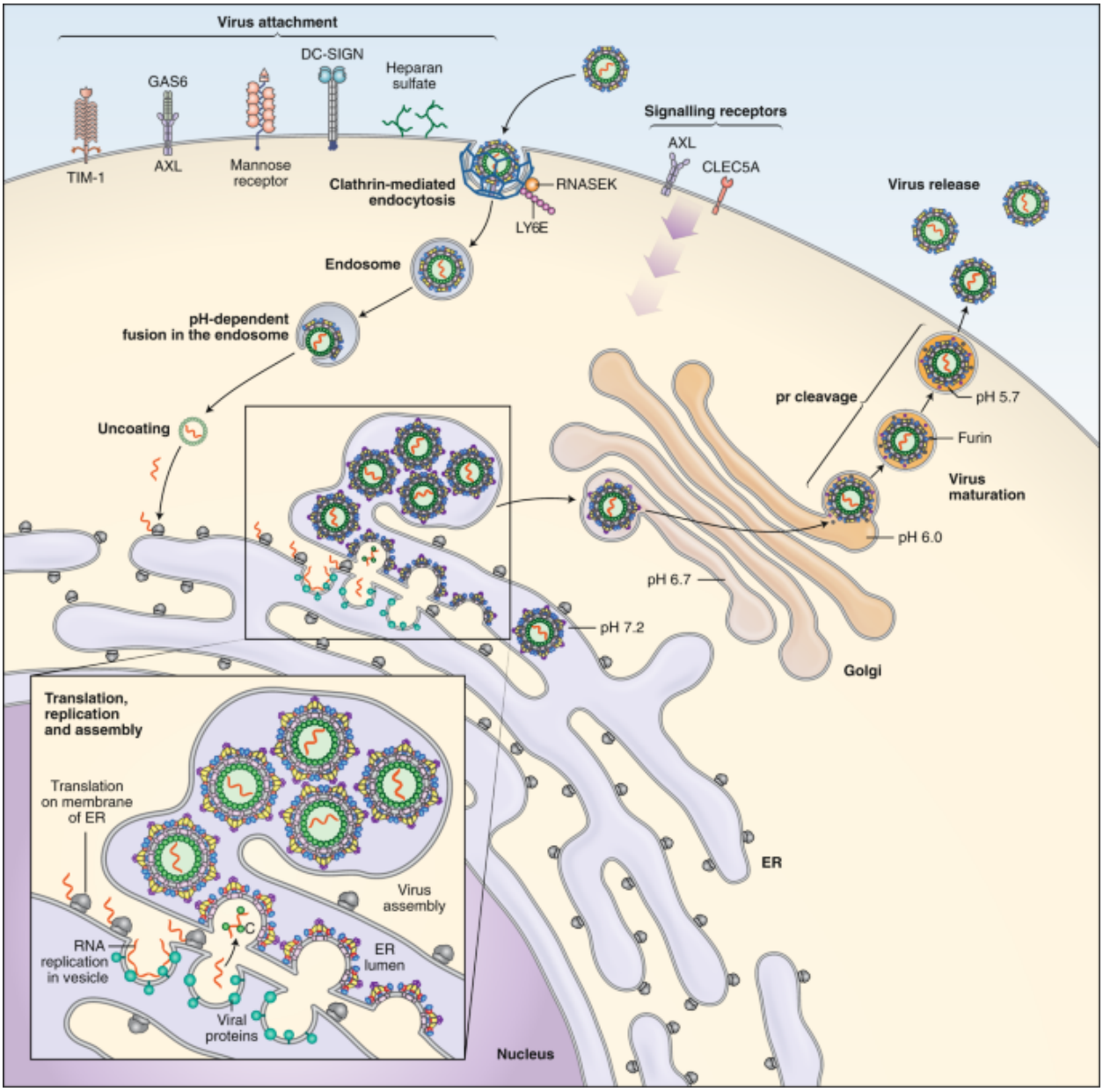

Figure 1-4: Flavivirus replication cycle. Figure replicated with permission (Rightslink license ID 1110536-2) from(Pierson and Diamond 2020). Upon attachment to a diverse set of attachment factors, virus enters cells via clatherin-mediated endocytosis. The low pH environment of the endosome allows for fusion to occur. Positive sense RNA genomes are used directly for translation of structural and non-structural proteins and serve as a template for genome replication in assembly factories that bud off the endoplasmic reticulum lumen. Immature virions traverse through the golgi apparatus, where furin cleaves the pr peptide from prM. Upon release, pr is fully liberated from viral particles to render virions infectious.

Yellow fever virus history

Recorded human infections by YFV are thought to be traced as far back as 1495 (Chippaux and Chippaux 2018). The first officially documented cases, though, occurred approximately 200 years later in the Caribbean islands Barbados and St. Kitts. From here, outbreaks were seeded in North America. In 1793, a massive outbreak of YFV occurred in Philadelphia, Pennsylvania, resulting in nearly 10% of the city's population being killed by the virus (Currie 1803).Other outbreaks plagues the American south later in the 17th century, resulting in hundreds of thousands of cases and tens of thousands of deaths (Jennings 1878). This massive public health concern led to the formation of a commission to understand the origins of the virus, which found that mosquitoes appeared to be the source (Reed, Carroll et al. 1900). Later studies confirmed that YFV, which was initially thought to be caused by a bacterial agent (later characterized as a "filterable agent"), uses *Aedes* spp. mosquitoes as vectors for transmission (Bauer and Hudson 1928).

Initial attempts at a YFV vaccine were made under the assumption that disease was of bacterial etiology. It wasn't until the 1920's when Max Theiler serially passaged virus isolated from an infected patient (now known as the Asibi strain) in murine tissues that a potential vaccine came to the foreground (Theiler and Smith 1937). In these studies, Theiler noted that, while virus had the increased ability to infect murine CNS tissues (neurotropism), the viscerotropism of YFV substantially decreased. This attenuated YFV strain, while representing a major step towards a

vaccine, still held concerns for severe adverse events, specifically neurological disease. To this end, Theiler and colleagues devised a scheme for further attenuation. To achieve this, the Asibi strain was passaged 176 times in chick embryos, with 100 of these passages being done specifically in isolated nervous tissues (Theiler and Smith 1937). Incredibly, other groups were unable to replicate this, meaning this new, avirulent strain of YFV arose by chance mutations. This strain was given the name 17D. YFV-17D vaccine strain is still used today, and is considered one of the great accomplishments in vaccinology though the molecular determinants of YFV-17D's attenuated virulence is still unknown (Norrby 2007). A number of amino acid substitutions in the E protein, as well as mutations to the gene encoding the RNA-dependent RNA polymerase, are thought to play a role, though no mechanistic studies have been published to date (Davis, Beck et al. 2019). This is potentially due to the inability of YFV-17D to generate genetic diversity, though further studies are warranted.

Despite massive vaccination campaigns and vector control having eradicated YFV from the United States, YFV is still a massive global public health threat. For example, ongoing epidemics continually occur in regions of Brazil and Sub-Saharan Africa (Kraemer, Faria et al. 2017, Cunha, Tubaki et al. 2020). In Brazil, urban cycles, where *Aedes aegyptii* mosquitoes transmit virus between people (as opposed to the sylvatic cycle, where virus is maintained in non-human primate populations by transmission via *Aedes albopictus* mosquitoes), have encroached into massive populations centers such as Sao Paolo (Cunha, Tubaki et al. 2020). While vaccination campaigns are being waged in these regions, global shortages of YFV-17D have become a concern due to the inefficient methods of propagating virus in chicken embryos (Gershman, Angelo et al. 2017). Fractional doses, which appear promising, have been used in

these scenarios though there is not a full understanding of the implications of not using a full dosing regimen (Wu, Peak et al. 2016, Juan-Giner, Kimathi et al. 2021).

Humoral response and therapeutic antibodies against YFV

To date, a comprehensive understanding of the antigenic landscape of YFV in the context of natural infection is poorly understood. Studies have focused primarily on two viral glycoproteins: E and NS1. As with all flaviviruses, YFV E is the primary target of the humoral response, and antibodies to this protein are primarily responsible for virus neutralization (Daffis, Kontermann et al. 2005). Almost all studies looking at the human humoral response have been done using YFV-17D-vaccinated subjects, with only limited published data discussing these responses in the setting of natural infection. That being said, studies of vaccinated individuals have shed light on some principles of antibody recognition of YFV antigens.

There are limited studies of monoclonal antibodies as therapeutics against YFV in the literature. 2C9-cIgG was originally isolated from mice and chimerized into a human IgG backbone. This mAb, which binds DII on YFV E, has shown efficacy in hamster and mouse models of infection, though studies to further characterize the mechanism of action of 2C9 are not described in the literature. Further studies of 2C9 sought to develop a second antibody in order to create a cocktail containing 2C9 that is refractory to mutational escape. This resulted in 864-cIgG, which binds DIII on YFV E, a known site of neutralization vulnerability. Despite this, 864-cIgG did not abrogate disease in a mouse model of disease caused by YFV-17D (Thibodeaux, Garbino et al. 2012, Julander, Thibodeaux et al. 2014, Calvert, Dixon et al. 2016). A second antibody, termed 2A10G6, has been described for its ability to neutralize diverse flaviviruses, including YFV

(Deng, Dai et al. 2011). This mAb recognizes a fusion loop-proximal epitope and protects animals from Dengue and West Nile virus infection, though studies have not been done using YFV *in vivo*. The most recent, and perhaps most well characterized mAb, is 5A. This mAb was isolated by panning a phage display library constructed from the repertoires of two individuals who recovered from natural YFV infection (Daffis, Kontermann et al. 2005). This antibody was later characterized for its ability to potently neutralize virus in vitro and protect mice from both vaccine and virulent strains of YFV. In this same study, 5A was determined to bind DII on YFV E and function at both a pre- and post-attachment step. A full structural characterization was performed on 5A in complex with YFV E in both pre and post fusion states (Lu, Xiao et al. 2019).

Perhaps the most comprehensive analysis of the humoral response to YFV was a longitudinal analysis of circulating memory B cells and plasmablasts in two human recipients of YFV-17D (Wec, Haslwanter et al. 2020). These donors were sampled at numerous time points over the course of a year post-inoculation. While this study gives a thorough description of the immunological characteristics of YFV-specific B cells following vaccination, it also further characterizes epitopes recognized by antibodies produced by these cell populations. For one, antibodies targeting DIII on YFV E appear to be rare. This is a critical finding due to the fact that antibodies against this domain are traditionally thought to be the most potently neutralizing against diverse flaviviruses. As expected, a majority of the isolated mAbs recognize the fusion loop epitope. In both donors, though, 5A-like antibodies made up the majority of neutralizers, with 90% of mAbs from this group showing neutralizing activity against YFV-17D. Many of these antibodies, from both donors, use a common heavy and light chain pairing, VH4-4/VL1-

51. Wec and colleagues outline the potential for a “public clonotype” response against the 5A epitope elicited by highly abundant germline VH and VL genes. While this publication does not detail the therapeutic activity of any antibodies in this large panel (>700), the extreme potency outlined by some mAbs here suggests they may be suitable for clinical development.

While E is the primary determinant of the humoral response to infection, NS1 appears to be an important target of antibodies in the context of flavivirus infection. NS1 is a multifunctional protein, serving as a component of the flavivirus replication complex, while also appearing to be involved in the pathogenesis. In one study, NS1 proteins from various flaviviruses were shown to disrupt cell layers that correspond to the tropism of said viruses (i.e. WNV, an encephalitic flavivirus, disrupted blood-brain barrier, Zika virus (ZIKV) disrupted the fetal/placental interface, DENV disrupted vascular endothelium, etc.) (Puerta-Guardo, Glasner et al. 2019). Antibodies of murine and human origin have been shown to provide protection against infection from ZIKV, WNV, DENV, and YFV in animal models of infection (Chung, Nybakken et al. 2006, Wessel, Kose et al. 2020, Modhiran, Song et al. 2021). Interestingly, NS1 appears to be displayed on the surface of infected cells as a dimer (whereas secreted NS1 is thought to be hexameric) (Akey, Brown et al. 2014, Edeling, Diamond et al. 2014). Most protective antibodies are thought to function in an Fc-dependent function by clearing infected cells, though Fc-independent anti-NS1 antibodies have been discovered (Yu, Liu et al. 2021). These Fc-independent mAbs likely function by blocking the activities of secreted NS1 or by preventing the ability of NS1 to bind back to the surface of infected cells. Despite the knowledge gained from these studies of the mAb response to YFV, work still needs to be done to fully define the most effective approach for treatment of this infection. While human antibodies targeting YFV NS1

are of interest to the field, and may offer a therapeutic avenue to combat YFV, the work in chapter V will focus of antibodies against YFV E.

CHAPTER II

STRUCTURAL AND MECHANISTIC INSIGHTS INTO TWO SITES ON THE HENIPAVIRUS RECEPTOR BINDING PROTEIN TARGETED BY PROTECTIVE HUMAN MONOCLONAL ANTIBODIES

This chapter is an adaptation of the following published manuscript:

Dong J*, Cross RW*, **Doyle MP***, et al. Potent henipavirus neutralization by antibodies recognizing diverse sites on Hendra and Nipah virus receptor binding protein. *Cell* 2020; 183, 1536-1550. (*contributed equally).

Contributions: Nurgun Kose and Jarrod Mousa isolated antibodies. Jinhui Dong performed x-ray crystallography. Robert Cross performed BSL-4 *in vitro* and *in vivo* studies. I performed binding assays, receptor-blocking assays, kinetics, and oligomer disruption assays. Jinhui, James Crowe, and I wrote the manuscript.

INTRODUCTION

Hendra virus (Guirakhoo, Pugachev et al.) and Nipah virus (NiV), belonging to the *Henipavirus* genus in the *Paramyxoviridae* family, are zoonotic pathogens that cause severe viral disease in humans characterized by serious respiratory illness and encephalitis with high mortality (Weatherman, Feldmann et al. 2018). Fruit bats of the *Pteropus* genus are natural reservoirs of both HeV and NiV, and the viruses are understood to have co-evolved with these bats (Halpin, Hyatt et al. 2011, Vidgen, de Jong et al. 2015). Transmission of HeV to humans can occur indirectly from fruit bats following direct human contact with infected horses (Murray, Selleck et al. 1995, Selvey, Wells et al. 1995, Field 2016). Transmission of NiV to humans may occur directly from fruit bats, infected pigs, or from infected humans (Clayton, Middleton et al. 2012, Weatherman, Feldmann et al. 2018). There are two distinct major strains of NiV, designated NiV

Malaysia (NiV_M) and NiV Bangladesh (NiV_B) (Lo, Lowe et al. 2012). NiV_B may be more pathogenic than NiV_M, as suggested by differences in mortality rates and transmission patterns (Gurley, Montgomery et al. 2007, Homaira, Rahman et al. 2010, Mire, Satterfield et al. 2016). Recently, 20 new species of viruses in the *Henipavirus* genus, including Ghana virus (GH-M74a henipavirus) and Cedar virus, were identified in bats in Africa (Drexler, Corman et al. 2012) or Australia (Marsh, de Jong et al. 2012). In 2014, a novel henipavirus-like virus, designated Mòjiāng virus, whose genes have high nucleotide sequence identities to those of the known henipaviruses, was found in yellow-breasted rats (*Rattus flavipectus*) in China after miners in the region succumbed to irregular pneumonia with unknown etiology (Wu, Yang et al. 2014). These viruses have high potential to cause significant human epidemics following their spillover from wildlife reservoirs to humans and domestic animals due to their wide host tropism and high pathogenicity (Smith and Wang 2013). Henipavirus spillovers are appreciated to be increasing in frequency and distribution due to changes in wild reservoir species distribution and food sources (such as due to changing climate and human related habitat losses) resulting in increased contact with human populations and agriculture (Plowright, Eby et al. 2015, Walsh, Wiethoelter et al. 2017, Kessler, Becker et al. 2018, Martin, Yanez-Arenas et al. 2018). Furthermore, human-to-human transmission of NiV in India and Bangladesh shows that a large human outbreak is possible (Chadha, Comer et al. 2006, Gurley, Montgomery et al. 2007). There is also concern about the potential to weaponize henipaviruses (Luby 2013). There are no licensed human vaccines or antiviral treatments for HeV or NiV infections (Broder, Xu et al. 2013).

The two henipavirus surface proteins, RBP and F, mediate viral entry by viral attachment to cells and fusion between the viral envelope and host cell membrane (Aguilar and Iorio 2012). HeV or NiV first attach to host cells by binding to the receptors ephrin-B2 or ephrin-B3 using the viral

receptor binding proteins HeV-RBP or NiV-RBP (Bonaparte, Dimitrov et al. 2005, Negrete, Levroney et al. 2005, Negrete, Wolf et al. 2006). Like other members in the *Orthoparamyxovirinae* subfamily, henipavirus attachment proteins are required to enable fusion proteins to function in fusion, and conformational changes of the attachment proteins caused by receptor binding activate F proteins to undergo the transition from the pre-fusion to the post-fusion form in order to complete the fusion process (Bossart, Fusco et al. 2013, Jardetzky and Lamb 2014, Wong, Young et al. 2017).

HeV-RBP and NiV-RBP proteins consist of an N-terminal cytoplasmic tail, a single transmembrane helix, a stalk region, and a globular C-terminal receptor binding domain (RBD) with a 6-bladed propeller fold. The two RBPs have about 80% amino acid sequence identity to each other, but < 30% amino acid sequence identity to the other henipaviruses. In paramyxoviruses, the ectodomains of the RBPs typically assemble into homotetramers (Bose, Jardetzky et al. 2015). The RBP stalk regions form a parallel four helix bundle, while the head domains are organized into a tetramer of two separate dimers (Yuan, Thompson et al. 2005, Yuan, Leser et al. 2008, Bose, Welch et al. 2011, Yuan, Swanson et al. 2011, Welch, Yuan et al. 2013). In contrast, although isolated head domains of paramyxovirus RBPs can be expressed as monomers in solution, these proteins can dimerize in crystalline phase with the same or similar dimeric interfaces as seen in the naturally occurring ectodomains (Crennell, Takimoto et al. 2000, Lawrence, Borg et al. 2004, Santiago, Celma et al. 2010). Similarly, the RBP ectodomain or the full-length HeV-RBP and NiV-RBP form tetramers in solution by forming disulfide bonds in the stem region, and head domains are monomers in solution (Bowden, Crispin et al. 2010, Maar, Harmon et al. 2012). A negative-stain EM study of NiV-RBP ectodomain showed that the protein assembles into an asymmetric tetramer, with a dimer of head domains at its apex and two

monomeric head domains on sides of a central stalk (Wong, Young et al. 2017). In the crystalline state, isolated HeV-RBP head domains can form dimers with a conserved dimeric interface, as occurs with other paramyxovirus RBPs (Bowden, Crispin et al. 2010). In summary, henipaviruses possess quaternary structures of RBPs in which the stem regions form a major homo-tetrameric interface, while the head domains can associate as dimers or tetramers with a very dynamic quaternary arrangement.

To date, naturally occurring human monoclonal antibodies (mAbs) for HeV or NiV isolated from immune individuals have not been described. MAbs binding to HeV/NiV have been isolated by phage display from a henipavirus-naïve human Fab library (Zhu, Dimitrov et al. 2006). An affinity-matured variant of one of those clones, designated m102.4, was converted to a recombinant IgG1 form in which it exhibited neutralization of HeV and NiV (Zhu, Bossart et al. 2008) and protected animals after lethal NiV Malaysia challenge (Bossart, Zhu et al. 2009, Rockx, Bossart et al. 2010, Bossart, Geisbert et al. 2011). Crystal structures of the HeV-RBP head domain in complex with a derivative of the Fab m102.4 (designated m102.3) revealed that binding of the mAb heavy chain complementarity determining region 3 (CDRH3) loop binds to the receptor binding site on RBP for ephrin-B2/ephrin-B3 (Xu, Rockx et al. 2013). m102.4 was well tolerated and exhibited linear pharmacokinetics in a recent Phase 1 human trail and has been used on compassionate grounds in the post-exposure therapy of 14 humans following high-risk HeV exposures since 2010, highlighting the benefit and practicality of mA postexposure therapy (Playford, Munro et al. 2020).

The demonstrated activity of the m102.4 antibody represents an important conceptual advance. However, the treatment failure of m102.4 in a day 5 and 7 treatment regimen of NiV_B in African

green monkeys (Mire, Satterfield et al. 2016) suggests a more potent antibody regimen may of benefit. Second, cocktails of human mAbs that recognize diverse sites on viral glycoproteins and neutralize by differing mechanisms may be desirable for therapeutic development for RNA viruses that easily escape virus neutralization. Third, it is preferable in human therapeutic antibody development to use naturally occurring human mAbs from immune donors that possess naturally paired heavy and light chains and naturally occurring somatic mutations.

Here, we report the identification and characterization of naturally occurring human mAbs against HeV and NiV isolated directly from an immune human individual. We determined the crystal structures of the HeV-RBP head domain in complex with the two most potent neutralizing cross-reactive human mAbs, HENV-26 and HENV-32. The structures suggest that the two mAbs neutralize these viruses by very different molecular mechanisms. These antibodies could be developed as promising mAb prophylactic or therapeutic molecules, and the protective epitopes defined by recognition of these human antibodies informs rational vaccine development and testing for these lethal viruses.

RESULTS

Isolation of human mAbs

To generate human cell lines secreting human mAbs to HeV, we obtained peripheral blood mononuclear cells from an individual in Australia with occupation-related exposure to the equine HeV-RBP subunit vaccine (Equivac®). At the time of study, the individual had a serum 50% virus neutralization titer of 1:40, 1:16 or ≤1:4 for HeV, NiV_M or NiV_B, respectively. We transformed B cells in the blood sample with Epstein-Barr virus, as described in the Experimental Procedures section. We screened supernatants from EBV-transformed B cell lines for binding to HeV-RBP and NiV-RBP head domain proteins and fused the resulting B cell lines to make hybridomas secreting 10 different fully human naturally occurring mAbs.

Binding activity of human mAbs to HeV-RBP head domain in ELISA

In order to determine the breadth of mAb binding, we screened the mAbs in ELISA for binding to recombinant RBP head domain proteins from multiple henipaviruses: HeV, NiV_M [strain Malaysia], or NiV_B [strain Bangladesh] (Bowden, Aricescu et al. 2008). Determination of half maximal effective concentration (EC_{50}) for binding of each mAb against the autologous HeV-RBP or heterologous NiV-RBP head domain proteins revealed that most of the clones bound at very low concentrations (**Table 2-1, Figure 2-1A**). Four of the HeV-reactive clones also cross-reacted with NiV_B-RBP head domain.

Neutralizing activity of human mAbs

To evaluate the inhibitory activity of the isolated mAbs, we tested the mAbs in an *in vitro* neutralization assay using HeV. All 10 of the HeV-RBP-reactive mAbs neutralized HeV, with

half-maximal inhibitory concentration (IC_{50}) values < 0.92 μg/mL (**Table 2-1, Figure 2-1B)**. Several mAbs displayed high neutralizing potency (IC_{50} values < 0.1 μg/mL; **Table 2-1**). The ELISA binding results discussed above suggested that cross-reactive mAbs in our panel might possess neutralizing activity to multiple henipaviruses. To test this hypothesis, we screened the mAbs in NiV_B and NiV_M neutralization assays and found that 4 of the 10 mAbs also neutralized both of the heterologous NiV_M and NiV_B strains (**Table 1)**. Five of the 6 remaining mAbs neutralized HeV well but neutralized NiV only incompletely, and one mAb (HENV-43) did not neutralize NiV (**Table 2-1)**. In parallel, we tested the m102.4 antibody for comparative purposes and found the IC_{50} values to be 257 ng/mL (Guirakhoo, Pugachev et al.), 20 ng/mL (NiV_M) or 49 ng/mL (NiV_B).

Competition-Binding Group[a]	Clone	Binding to RBP Head Domain from Indicated Virus in ELISA EC_{50} Values[b] in μg/mL *(Area under the Curve)*			Neutralization of Indicated Virus IC_{50} Values[c] in μg/mL *(Area under the Curve)*			Neutralization of Indicated Virus IC_{80} Values[c] in μg/mL *(Max % Inhibition)*		
		HeV	NiV_B	NiV_M	HeV	NiV_B	NiV_M	HeV	NiV_B	NiV_M
A	HENV-1	0.19 *(3.27)*	>[d] *(0.61)*	> *(0.67)*	0.63 *(187)*	> *(7.98)*	> *(22.6)*	1.70 *(100)*	> *(32.7)*	> *(34.9)*
B	HENV-32	0.36 *(3.71)*	0.96 *(6.6)*	0.42 *(8.0)*	0.27 *(198)*	0.38 *(194)*	0.31 *(201)*	1.26 *(100)*	1.14 *(100)*	2.15 *(100)*
	HENV-21	0.42 *(3.30)*	2.44 *(5.5)*	0.87 *(7.2)*	1.94 *(133)*	1.91 *(140)*	2.01 *(129)*	5.54 *(100)*	4.09 *(100)*	8.44 *(92.4)*
	HENV-10	0.21 *(5.49)*	> *(0.63)*	> *(0.76)*	0.62 *(181)*	1.07 *(140)*	0.22 *(152)*	1.71 *(100)*	9.42 *(96.3)*	1.44 *(84.2)*
B/C	HENV-2	0.13 *(5.81)*	0.51 *(6.4)*	0.28 *(9.0)*	0.78 *(166)*	1.39 *(143)*	0.75 *(186)*	2.57 *(100)*	4.88 *(95.8)*	2.67 *(100)*
C	HENV-9	0.60 *(3.19)*	> *(0.57)*	0.75 *(4.2)*	0.37 *(195)*	> *(11.9)*	8.93 *(69.2)*	1.88 *(100)*	> *(35.2)*	> *(61.5)*
	HENV-43	0.86 *(6.87)*	> *(0.59)*	1.49 *(1.4)*	0.61 *(178)*	> *(9.2)*	> *(45.2)*	2.39 *(100)*	> *(40.0)*	> *(51.9)*
D	HENV-18 [e]	0.21 *(5.80)*	> *(0.56)*	> *(0.60)*	0.38 *(211)*	> *(5.7)*	> *(51.1)*	1.16 *(100)*	> *(31.4)*	> *(50.8)*
	HENV-19 [e]	0.25 *(3.69)*	> *(0.52)*	> *(0.61)*	0.35 *(209)*	> *(7.2)*	8.08 *(43.1)*	0.89 *(100)*	> *(33.9)*	> *(49.2)*
E	HENV-26	0.14 *(5.39)*	0.09 *(10.5)*	0.07 *(11.0)*	0.07 *(281)*	0.03 *(289)*	0.040 *(293)*	0.19 *(100)*	0.12 *(100)*	0.11 *(100)*

Table 2-1: Binding and neutralization characteristics of 10 human mAbs. Experiments were conducted with two or three biological replicates, each with two technical replicates, with consistent results. Binding data from one representative experiment are shown, with neutralization data combined from three independent experiments. [a]Competition-binding group, as determined by data in Figure 1.[b]50% maximal effective concentration. [c]50% maximal inhibitory concentration. [d]The ''>'' symbol indicates half-maximal binding or neutralization is not achieved below the highest concentration tested: 20 mg/mL for HeV RBP binding, 50mg/mL for NiV_M or NiV_B binding, or 50 mg/mL for neutralization of each of the three viruses. [e]After all functional studies were completed, antibody variable gene sequencing later revealed the independently derived clones HENV-18 and -19 shared identical antibody variable gene sequences.

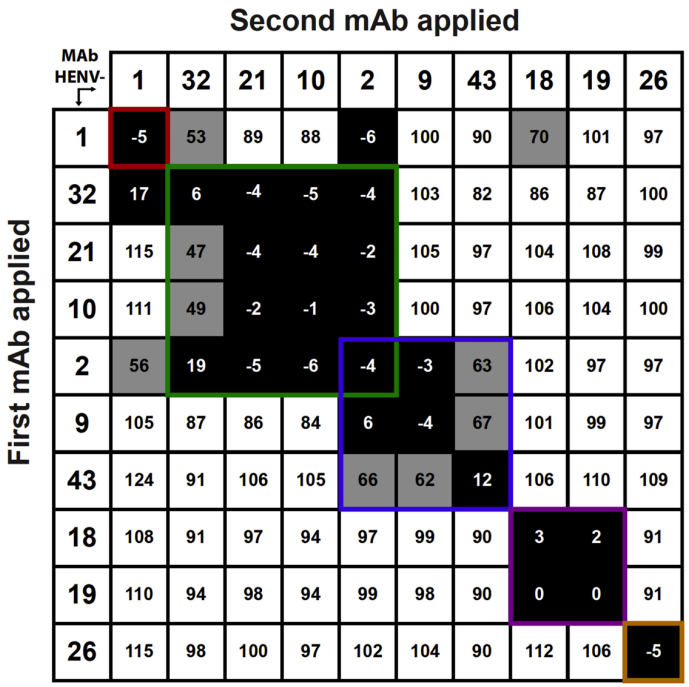

Figure 2-1: Competition binding of 10 human mAbs. Numbers in boxes are the percentage binding signal of the second mAb applied after binding of the first mAb, compared with binding signal of the second mAb alone. The antibodies were defined as competing antibodies if the first antibody reduced binding of the second antibody by more than 70 percent. The antibodies were defined as non-competing antibodies if the first antibody reduced binding of the second antibody by less than 40 percent. Binding signals 40 to 70% were considered intermediate competition (grey boxes with black numbers). Inferred competition-binding groups A to E (designated in order left to right and top to bottom) are indicated with colored boxes, A) red, B) green, C) blue, D) purple, E) yellow.

Binding activity of human mAbs to HeV, NiV_M, or NiV_B RBPs on the surface of mammalian cells

The antibody discovery experiments and the ELISAs above were conducted with recombinant soluble forms of henipavirus RBP head domains. We next sought to determine the binding capacity of the most potent mAbs, HENV-26 and HENV-32, to full-length RBPs expressed on the surface of mammalian cells. We transfected 3 x 10^7 cells with cDNAs encoding the full-length HeV, NiV_M, or NiV_B RBP, allowed the cells to express the proteins, and then incubated the transfected cells with mAbs and tested for cell surface binding by flow cytometric detection. The results showed that these antibodies bound to the authentic full-length RBPs at low concentrations (**Figure 2-2A**). The EC_{50} values for binding of HENV-26 or HENV-32 ranged from 325 to 343 ng/mL or 680 to 836 ng/mL respectively for binding to HeV, NiV_M, or NiV_B. We tested kinetics of binding of these antibodies to RBPs on a biosensor to determine affinity (**Figure 2-2B**). The K_D for HENV-26 was 2.9, 2.2 or 1.0 nM and for HENV-32 was 2.1, 2.2, or 2.8 nM for HeV, NiV_M, or NiV_B, respectively.

A Binding assays of HENV-26 or HENV-32 to full-length HeV-RBP or NiV-RBPs detected by flow cytometric analysis.

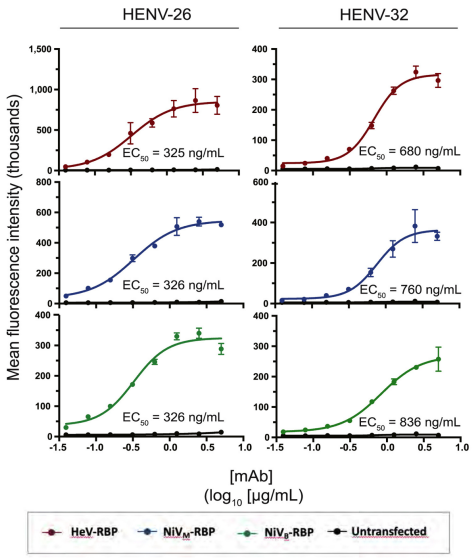

B Kinetics of binding of HENV-26 or HENV-32 to full-length HeV-RBP or NiV-RBPs in biolayer interferometry to determine affinity of binding.

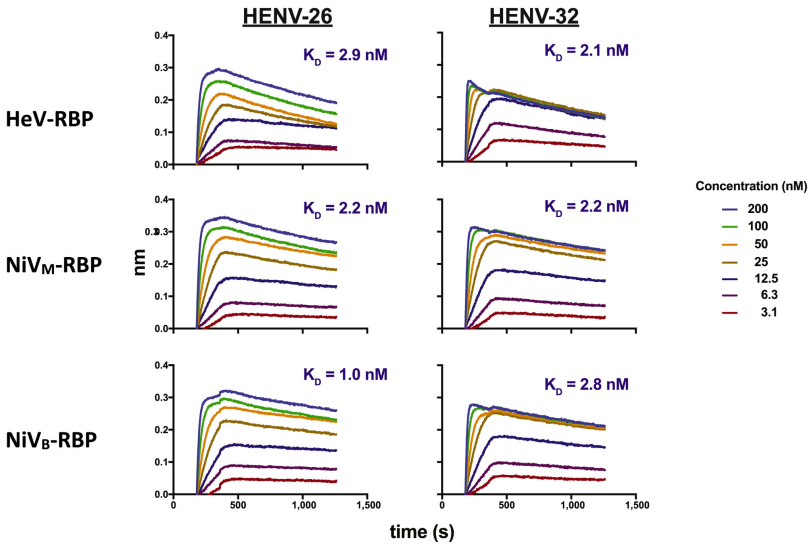

Figure 2-2: Binding to cell surface displayed antigen and kinetics. A) Binding to cells transfected with HeV-RBP (red), NiV_M-RBP (blue), NiV_B-RBP (green), or un-transfected (black) cells was analyzed using an Intellicyt iQue instrument. Values are expressed as mean fluorescence intensity (MFI) of PE-conjugated secondary antibody signal and were plotted in GraphPad to interpolate EC_{50} values by non-linear regression analysis. Serial dilutions of HENV-26 or HENV-32 were performed in triplicate, with data representative of three independent assays shown. Error bars indicate SEM. **B.** Binding kinetics of Fab fragments corresponding to HENV-26 and HENV-32 were performed on an Octet RED instrument (FortéBio). Recombinant histidine-tagged RBP head domain was immobilized to HIS1K biosensor tips (FortéBio) at 10 µg/mL in kinetics buffer. After a brief baseline step, serial dilutions of HENV-26 or HENV-32 Fab starting at 200 nM then were associated to coated biosensor tips, followed by a dissociation step in 1x kinetics buffer. Curve-fitting was performed to extrapolate equilibrium dissociation constant values.

Major antigenic sites recognized by human mAbs

To determine whether Abs from distinct binding groups targeted different antigenic regions on the HeV-RBP surface, we performed a quantitative competition-binding assay using a real-time biosensor. We tested all mAbs in a tandem blocking assay in which HeV-RBP was attached to the biosensor. The data suggest that mAbs in this panel form at least 5 major competition-binding groups, consistent with recognition of 5 different antigenic regions on the HeV-RBP head domain (**Figure 2-1**). The potently neutralizing mAbs HENV-26 and HENV-32 segregated into different competition-binding groups. Interestingly, mAb HENV-2 competed with 5 other mAbs, suggesting that it may bind to overlapping regions from 2 or 3 antigenic sites, though this is likely an experimental artifact often seen in biolayer interferometry competition studies.

Competition-binding studies with the ephrin-B2 receptor

Henipaviruses use the human ephrin-B2 protein as a receptor for attachment and entry (Bonaparte, Dimitrov et al. 2005, Negrete, Levroney et al. 2005). We sought to determine if any of the anti-HeV-RBP mAbs neutralized virus by blocking virus attachment to ephrin-B2. We competed recombinant ephrin-B2 protein with mAbs or buffer for binding to biosensor tips coated with HeV-RBP head domain. MAb HENV-26 reciprocally competed with ephrin-B2 for binding to HeV-RBP, while mAbs HENV-19 and HENV-32 did not (**Figure 2-3A**), suggesting that HENV-26 neutralizes by binding to the receptor binding site on HeV-RBP. MAb HENV-26 also competed with ephrin-B2 for binding to full-length HeV-RBP expressed on the surface of 293F cells (**Figure 2-3B)**.

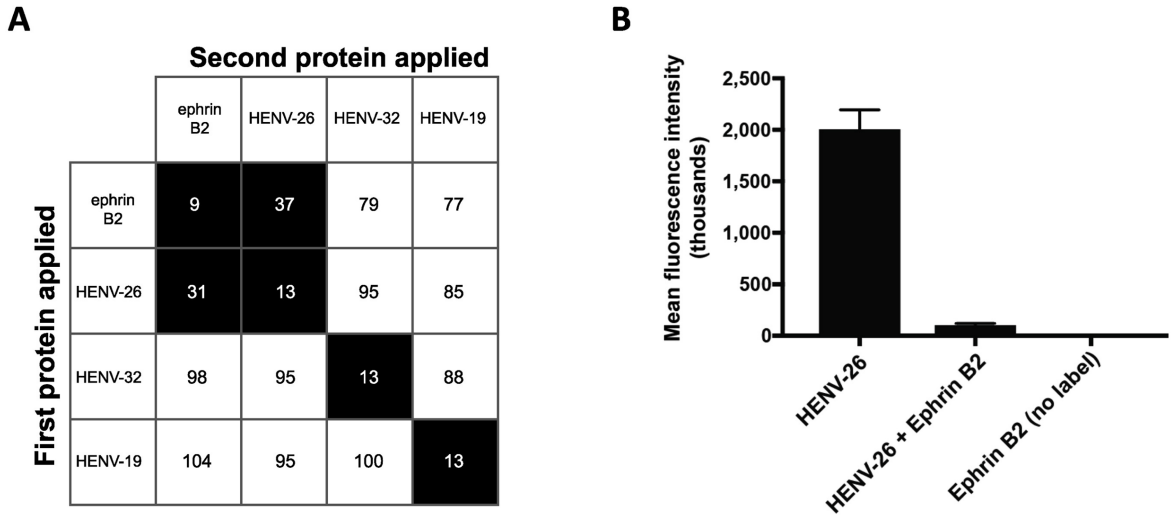

Figure 2-3: Antibody competition with host receptor ephrin-B2. A) Numbers in boxes are the percentage binding signal of the second protein applied after binding of the first protein, compared with binding signal of the second protein alone. The proteins were defined as competing if the first protein reduced binding of the second protein by more than 70 percent. The proteins were defined as non-competing if the first protein reduced binding of the second protein by less than 40 percent. **B)** 293F cells were transfected to display the full-length HeV-RBP protein on the cell surface. Cells were incubated with soluble ephrinB2 protein or FACS buffer, then HENV-26 labeled with AlexaFluor-647 was added to cells and incubated. Cells then were washed and analyzed using an Intellicyt iQue flow cytometry instrument. Binding of HENV-26 in the presence or absence of ephrinB2 was expressed as mean fluorescence intensity (MFI).

Crystal structures of HENV-26 and HENV-32 in complex with HeV-RBP or NiV-RBP proteins

Next, we determined the structure of antigen-antibody complexes for two mAbs using crystallography. We selected the two most potent and cross-reactive mAbs from the panel, HENV-26 and HENV-32, for crystallographic studies and first determined their heavy and light chain variable gene sequences. HENV-26 Fab complexed with HeV-RBP head domain was crystallized in spacegroup $P3_22$, and the crystal structures were solved at 2.60 Å **(Figure 2-4A)**. Overlays of the epitope on the surface of HeV-RBP recognized by HENV-26 with that of the ephrin-B2 receptor binding site shows that the antibody epitopes overlap greatly with the receptor binding site, consistent with the competition-binding experiments. Therefore, HENV-26

neutralizes HeV (as well as NiV) via competitive inhibition of viral attachment to the viral receptor.

It was apparent from the competition-binding studies with HENV-26 or with ephrin-B2 shown above that the potent neutralizing mAb HENV-32 bound to an antigenic site distinct from the receptor binding domain epitope recognized by HENV-26. Therefore, we next determined the structure of Ab-Ag complexes for HENV-32 with HeV-RBP using crystallography. The structure revealed the molecular details of HENV-32 binding to an epitope distinct from that of HENV-26. HENV-32 in complex with HeV-RBP head domain crystallized in spacegroup C2 with a resolution of 2.0 Å **(Figure 2-4A)**. Based on previous studies, these structural data suggest HENV-32 recognizes an antigenic site that lies at the putative dimeric interface of HeV-RBP **(Figure 2-4B)**. This led to the hypothesis that HENV-32 may function by disrupting the dimeric and/or tetrameric structure of HeV-RBP, rendering virus afusogenic. I purified the full ectodomain of HeV-RBP by affinity chromatography, followed by size exclusion in an attempt to fully isolate monomeric, dimeric, and tetrameric species of RBP. Each of the fractions corresponding to different oligomeric states was incubated with HENV-26 or HENV-32 Fab and analyzed by non-reducing SDS-PAGE. I observed no change in the presence of dimeric or tetrameric species after incubation with HENV-26 or HENV-32, suggesting disruption of oligomers is not the mechanism by which HENV-32 neutralizes HeV and NiV **(Figure 2-4C)**.

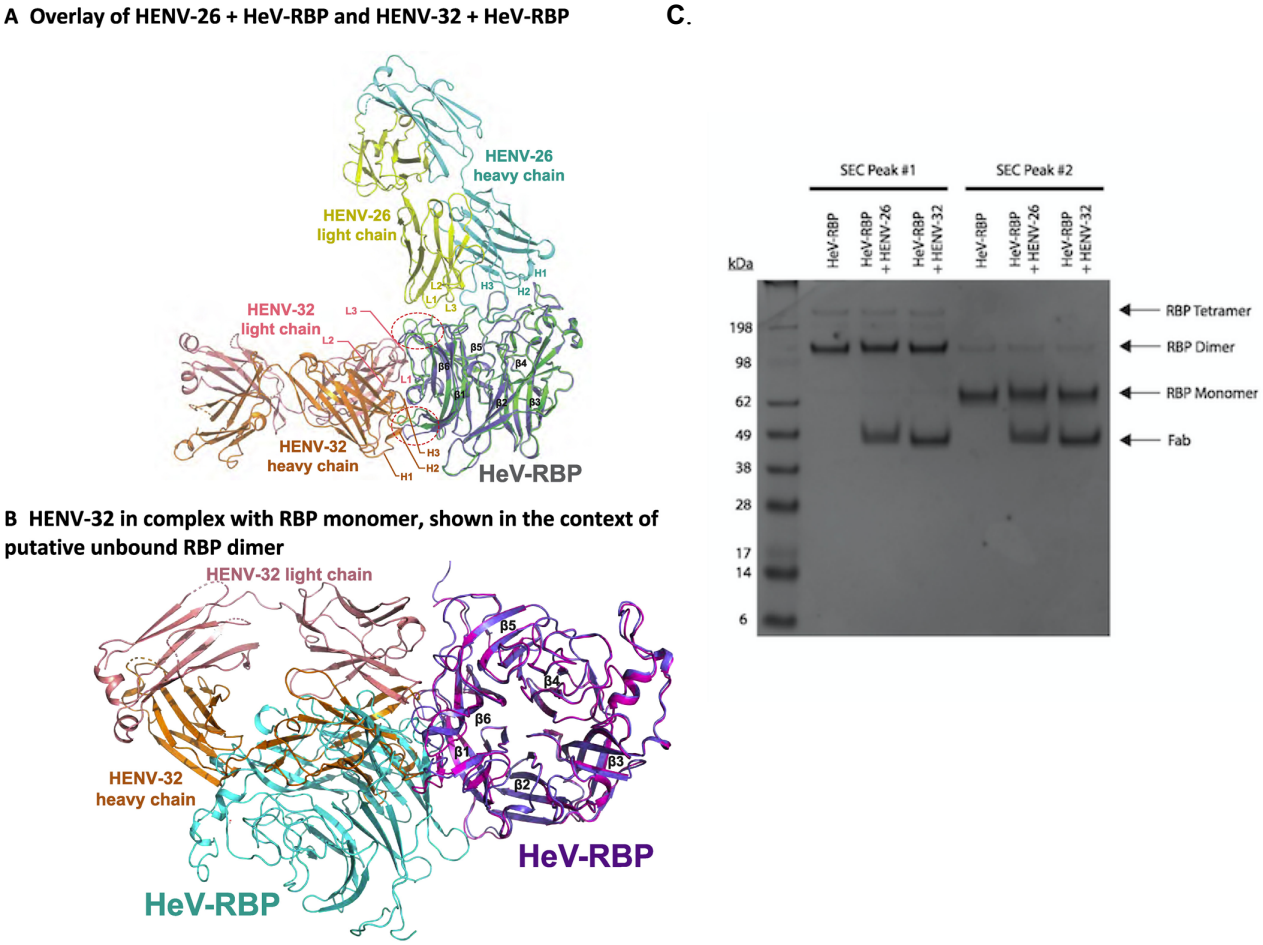

Figure 2-4: Structural insights into HENV-26 and HENV-32 function. A) Superimposition of the crystal structures of HeV-RBP head domain in complex with HENV-26 or HENV-32. HeV-RBP head domain in the HeV-RBP/HENV-26 complex is colored in green, and that in the HeV-RBP/HENV-32 in light blue. The HENV-26 heavy chain is colored in cyan, HENV-26 light chain in yellow, HENV-32 heavy chain in orange, and HENV-32 light chain in salmon. The CDRs of both mAbs and the individual blades of the HeV-RBP head domain are labeled. Regions in the HeV-RBP head domain with large structural differences between structures are indicated within broken red lines. **B)** Superimposition of HeV-RBP structures in the HENV-32/HeV-RBP complex and ephrinB2/HeV-RBP complex. The HeV-RBP structure in the HENV-32/HeV-RBP complex is shown in light blue, and HeV-RBP in the ephrinB2/HeV-RBP complex in yellow. EphrinB2 in the complex is shown in gray. The overlay suggests that the conformation of HeV-RBP β6/S2-S3 and β5/S4- β6/S1 loops in the HENV-32/HeV-RBP complex causes potential steric clashes between the loops and the ephrinB2 G-H loop. The potential steric clashes between the HENV-32 bound HeV-RBP structure and ephrinB2 G-H loop are represented with broken red lines, and the residues with potential steric clashes are shown in stick, and corresponding residues of the ephrinB2 bound HeV-RBP structure are shown as line representation. **C)** Lack of dimer disruption mediated by HENV-26 or HENV-32. HeV-RBP full ectodomain was expressed in Expi293F cells and purified sequentially by HisTrap affinity chromatography followed by size exclusion chromatography (SEC). Size exclusion peaks corresponding to dimeric (SEC peak #2) or tetrameric (SEC peak #1) species were each incubated with HENV-26 or HENV-32 Fab for 1 h at room temperature. Each preparation was then analyzed by 4%–12% Bis-Tris SDS-PAGE using SimplyBlue SafeStain Coomassie G-250 stain.

Lack of cross-reactivity with RBPs from Cedar virus or Ghanaian bat henipavirus

We also examined whether or not HENV-26 of HENV-32 could recognize more distantly related henipaviruses including Cedar virus (CedV) and Ghanaian bat henipavirus (GhV). The RBP of the more distantly related henipavirus Mòjiāng virus was not tested as it is more divergent in sequence, is antigenically distinct, and lacks an ephrin-B2/B3 binding domain (Rissanen, Ahmed et al. 2017). The HENV mAbs did not bind to recombinant forms of RBPs from CedV or GhV in ELISA, whereas CedV- or GhV-specific control antibodies did bind (**Figure 2-5A**). There are numerous differences in the epitopes when RBP sequence alignments between HeV/NiV and CedV or GhV are compared that suggest why the antibodies do not recognize CedV or GhV (**Figure 2-5B)**.

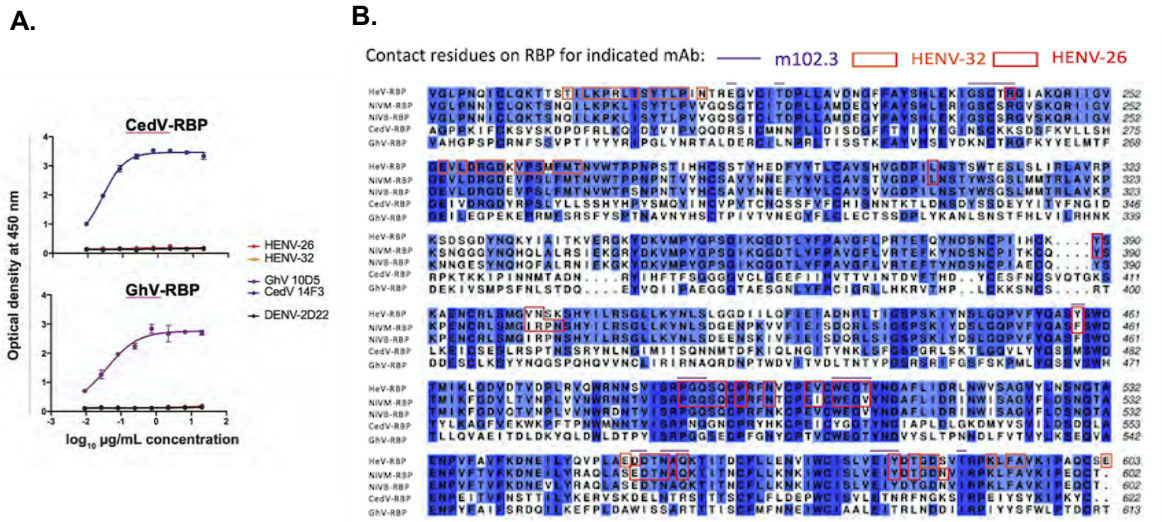

Figure 2-5: Cross-reactivity to divergent henipaviruses. A) CedV-RBP or GhV-RBP ELISA. Binding of HENV-26 or HENV-32 was tested in ELISA using recombinant CedV-RBP head domain or GhV-RBP full ectodomain. MAbs to CedV-RBP (14F3) or GhV-RBP (10D5) were used as controls. **B)** Epitope mapping of RBP head domains of HeV, NiV_M, and NiV_B. The RBP amino acid sequences of the three viruses were aligned with MUSCLE (1), and the figure was made with sequence alignment editor, ALINE (2). For comparison, the sequences of Cedar virus RBP (CedV-RBP) and Ghana virus RBP (GhV-RBP) also are shown.

Post-exposure efficacy of human mAbs in a ferret model of henipavirus infection

To determine the therapeutic activity of these cross-neutralizing Abs, we tested two antibodies in ferrets. We focused on potent cross-reactive antibodies for challenge with NiV_B. We selected the two mAbs HENV-26 and HENV-32, because they bound non-overlapping antigenic regions in the competition-binding experiments and structural studies. Female ferrets (~3-5 months old) received 15 mg/kg of antibody by the intraperitoneal route on days 3 and 5 (for a total of 30 mg/kg cumulative dose) after intranasal inoculation with 5,000 PFU of NiV_B. The serum 50% virus neutralizing titers for NiV_B for ferrets treated with HENV-26 were 1:369 (day 5) and 1:765 (day 7), while the titers for ferrets treated with HENV-32 were 1: 135 (day 5) and 1:132 (day 7). HENV-26 and HENV-32 each reduced disease and protected ferrets from death when delivered 3 and 5 days after virus challenge (**Figure 2-6A,B**). All untreated control animals exhibited a clinical course and pathology consistent with previous reports of henipavirus infection in ferrets including: pulmonary complications, lymphopenia, neutrophilia, thrombocytopenia, and hypoalbuminemia (Mire, Versteeg et al. 2013). Circulating viral genomes were detected beginning on day 5, with a mean value of 5.64 (+/- 0.26 SD) log_{10} genomes/g tissue (**Figure 2-6C**). Viral genomes were detected in all tissues tested (**Figure 2-6D**), and infectious virus was detected at low levels in spleen, kidney, adrenal glands, lung (data not shown). These data suggest HENV-26 and HENV-32 may be therapeutic candidates for treatment of Nipah Bangladesh disease (**Figure 6C**).

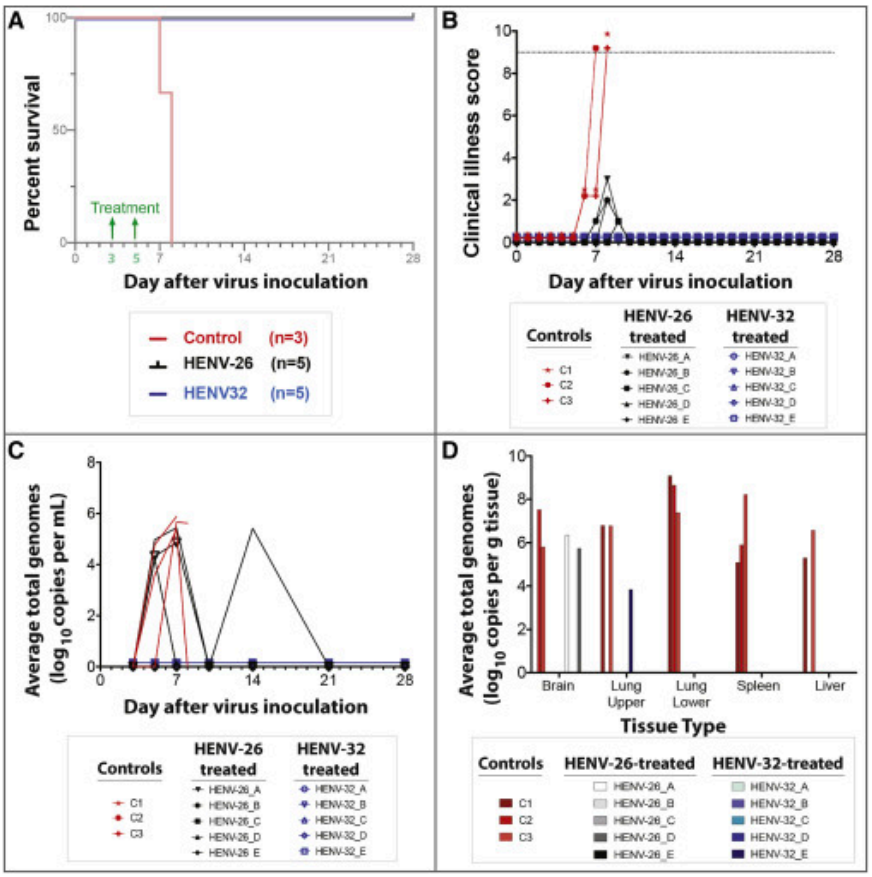

Figure 2-6: Ferret Nipah Bangladesh challenge studies. A) Kaplan-Meier survival curve of ferrets infected with NiV_B. **B)** Clinical scores of ferrets infected with NiV_B. Dotted line represents the threshold for euthanasia criteria. **C)** Circulating viral genomes from ferrets infected with NiV_B. **D)** Viral genomes present in select tissues at study endpoints.

DISCUSSION

We obtained the first panel of naturally occurring human mAbs from a human individual immune to HeV and found mAbs that were potently neutralizing, including 4 that exhibited breadth of recognition for the major strains of NiV. The two most potent, cross-reactive mAbs, HENV-26 and HENV-32, afforded post-exposure protection against the notably more pathogenic Bangladesh strain of NiV in an animal model (Clayton, Middleton et al. 2012, Lo, Lowe et al. 2012, Mire,

Satterfield et al. 2016). There is no FDA-approved HeV or NiV vaccine or effective treatment for these viruses, and NiV can be transmitted person to person. These two mAbs could be considered lead candidates for prophylaxis or therapy of HeV or NiV infections. HENV-26 directly competes with ephrin-B2 for RBP binding, while HENV-32 does not, and crystal structures revealed very distinct antigenic sites. The two mAbs do not compete with each other for HeV/NiV binding, and they neutralize the viruses by very different mechanisms. Therefore, a combination prevention or treatment formulation combining these two mAbs could be considered. MAb combinations may be desirable for treatment of RNA virus infections to prevent virus escape and may produce cooperative effects.

The cross-reactivity of the antibodies we isolated for recognition and neutralization of HeV, NiV_M and NiV_B, and protection against those viruses, is desirable since it is plausible that a single regimen of monotherapy or a cocktail of these antibodies could prevent or treat each of the three viruses. We tested for breadth of binding for other more distantly related henipaviruses but did not detect cross-reactivity to other viruses. This finding was not surprising, since the RBPs of NiV and HeV have been reported to elicit only a limited cross-reactive antibody response, and cross-protection between Mòjiāng virus or Ghana virus, and the highly pathogenic henipaviruses was not detected (Li, Li et al. 2020).

To explore structural mechanisms of binding and neutralization of the two mAbs, we solved the crystal structures of the mAbs in complex with HeV-RBP and/or NiV-RBP head domains. HENV-26 targets the central cavity and top loops of mainly blade 4, 5, and 6 of the propeller-fold of HeV-RBP and NiV-RBP head domains, overlapping the ephrin-B2/B3 binding sites, thus directly

competing with ephrin-B2/B3 for RBP binding. Therefore, HENV-26 neutralizes HeV or NiV by blocking the receptor binding site of the viruses, thus protecting animals against viral infection by inhibition of viral entry. The major interacting residues of RBPs are conserved between HeV-RBP and NiV-RBP (**Figure S4D**), making the mAb cross reactive to both viruses. All of the HENV-26 CDRs participate in the formation of the Ab-Ag interface, in contrast to the interaction mode of the previously described phage display library derived antibody m102.3 (Xu, Rockx et al. 2013).

In contrast, HENV-32 binding causes conformational changes at the β5S4/β6S1 loop and β6S4/β1S1 loops. If HENV-32 bound HeV-RBP is superimposed onto ephrin-B2-bound HeV-RBP, the conformational changes at these two loops result in steric clashes between the ephrin-B2 G-H loop and residues in these loops of HeV-RBP (**Figure S5C).** We considered whether HENV-32 could compete with the binding of ephrin-B2 via an allosteric effect. However, we did not observe competition between HENV-32 and ephrin-B2 for HeV-RBP binding in a BLI assay (**Figure S3A**). Therefore, the binding of HENV-32 to the putative dimeric interface of RBP head domains likely neutralizes HeV or NiV by altering dynamic features of the surface protein on virions. There is extensive literature defining the dimeric architecture of the RBP (Bowden, Crispin et al. 2010), which forms a functional tetrameric unit when two disulfide-linked dimers associate (Bossart, Crameri et al. 2005, Negrete, Chu et al. 2007, Bowden, Aricescu et al. 2008), and a disulfide bond in the stalk stabilizes the tetramer (Maar, Harmon et al. 2012). The henipavirus RBP interacts with host cellular B class ephrins, triggering conformational alterations in RBP that lead to the activation of the F glycoprotein, which facilitates the membrane fusion process (Steffen, Xu et al. 2012, Bradel-Tretheway, Zamora et al. 2019, Navaratnarajah, Generous et al. 2020).

Possibly, HENV-32 binding causes rearrangement of the quaternary structure of the RBPs in the head domains in such a way that the orientation of the receptor-binding sites of the RBPs are no longer suitable for receptor binding, preventing viral attachment to cells. However, we found that a soluble recombinant form of ephrin-B2 can bind in the presence of HENV-32. Another possibility is that HENV-32 interferes with the activation of HeV/NiV fusion proteins by RBPs, in a mechanism suggest by previous studies of a rabbit antibody with inhibitory activity that likely binds near the epitope recognized by the human mAb HENV-32 (Aguilar, Ataman et al. 2009). The rearrangement of quaternary structure caused by HENV-32 binding also might make the activation residues in the stem regions of the RBPs inaccessible to the fusion proteins, thus inhibiting viral entry to cells. Further studies are needed to clarify these possibilities.

The solved crystal structures of these Ab-Ag complexes also inform opportunities for future rational antibody engineering efforts to improve binding affinities of the mAbs. HENV-26 CDRH1 residue R31 makes only loose van der Waals interactions with HeV-RBP V502 or NiV-RBP residues I502 and P403. Insertions and mutations at R31 position might enhance binding. As mentioned above, there are significant rearrangements of polar interactions between the HENV-26/HeV-RBP and HENV-26/NiV-RBP complexes at the interface between CDRL1 and RBP region D555 – Q559. This finding suggests that CDRL1 may be a malleable region for improvement of binding. HENV-32 CDRL3 residue N93 interacts with a hydrophobic patch on HeV-RBP (comprising residues P200, L202, and F593) and with the mainchain carbonyl oxygen atom of residue P200 via an H-bond. It could be interesting to examine the effects of mutations of CDRL3 residue N93 to aliphatic residues (valine, leucine, or isoleucine) on binding affinity, because the mutation might improve the hydrophobic effect between N93 and the hydrophobic

patch but lose a H-bond between Ab and Ag.

Vaccine development for NiV is a high priority for many recommending bodies. The epitopes recognized by these broad and potent antibodies could be used in structure-based reverse vaccinology design programs to design new vaccine candidates. Thus, the studies provide important new conceptual data on henipavirus immunity, but there are significant limitations of these studies. First, the mAbs in this study were isolated from a single human immune individual, and it is uncertain how generalizable these findings would be in a population. Second, the studies focus on antibodies to RBP, since the individual studied had exposure to a vaccine RBP and we screened for antibodies reacting to the RBP head domain; from these studies we cannot determine the role for antibodies to the RBP stem, potential complex quaternary epitopes at the head/stem interface, or fusion protein in immunity to henipaviruses and more antigenic sites are possible. Third, there may be a role for non-neutralizing antibodies to henipaviruses, but we did not explore that mode of immunity here. These limitations point to the need for additional in-depth studies of this type for immunity to henipaviruses.

METHODS

Expression and purification of HeV and NiV attachment glycoproteins

The DNA segments correspondent to the head domain of HeV-RBP (residues 185 – 604), head domain of NiV_M-RBP (residues 183 – 602) (Bowden et al., 2008), and head domain of NiV_B-RBP (residues 185 – 602) were sequenced optimized for expression, synthesized, and cloned into the pcDNA3.1 (+) (HeV and NiV_M) or pcDNA3.1 (+)-C-6His (NiV_B) expression DNA plasmid downstream of the signal peptide from the pHLsec vector (MGILPSPGMPALLSLVSLLSVLLMGCVA) or osteonectin (MRAWIFFLLCLAGRALA)(GenScript). A TEV protease cleavage site and a His-tag also were incorporated at the C-terminus of HeV and NiV_M constructs to facilitate protein purification. Expi293F cells were transfected transiently with plasmids encoding HeV-RBP, NiV_M-RBP, or NiV_B-RBP head domains, and culture supernatants were harvested after 6 to 7 days. The head domains were purified from the supernatants by nickel affinity chromatography with HisTrap Excel columns (GE Healthcare Life Sciences). For protein production used in crystallization trials, 5 μM kifunensine was included in the culture medium to produce the head domains with high mannose glycans. The high mannose glycoproteins subsequently were treated with endoglycosidase F1 (Millipore) to obtain homogeneously deglycosylated HeV-RBP or NiV_M-RBP head domains (Bowden et al., 2008).

PBMC isolation and hybridoma generation

The study was approved by the Vanderbilt University Medical Center Institutional Review Board. Peripheral blood was collected at Vanderbilt after written informed consent from a healthy donor with prior history of inadvertent inoculation with recombinant HeV-RBP in an equine HeV

vaccine. PBMCs from the donor were isolated by density gradient separation on Ficoll, cryopreserved and stored in the vapor phase of liquid nitrogen until use. Generation of human hybridoma cell lines secreting human mAbs was performed as described previously (Smith, Zhou et al. 2012). Briefly, human B cells in the PBMC suspension were immortalized by transformation with EBV in the presence of CpG10103, cyclosporin A, and a Chk2 inhibitor and plated in 384-well culture plates. On day 7 to 10 after EBV transformation, the supernatants from transformed B cells were used to screen for the presence of antibodies binding to recombinant HeV-RBP head domain in ELISA. Cells from the wells containing B cells secreting HeV-RBP-reactive antibodies were fused with HMMA2.5 myeloma cells using a BTX ECM 2001 electro cell manipulator by an electrofusion method (Yu, McGraw et al. 2008). After fusion, human hybridomas were selected in medium with HAT solution containing ouabain. The hybridomas were cloned by flow cytometric sorting of single cells into 384-well plates and then expanded in culture. Particular clones for downstream studies were selected by choosing the clone for each independently derived hybridoma line that exhibited the highest level of IgG secretion.

Production of IgG for mAbs from hybridoma cells

The selected cloned cell lines secreting mAbs were grown initially in hybridoma growth medium (ClonaCell-HY medium E from STEMCELL Technologies, 03805) and then switched to serum-free medium (GIBCO Hybridoma-SFM, Invitrogen, 12045084) for antibody expression and purification. Cloned hybridoma cells were expanded sequentially to 225 cm^2 flasks for mAb production. The supernatants from hybridoma cultures were filtered with 0.45 μm pore diameter filter flasks, and then the IgG from the hybridoma cell line supernatants was purified by affinity chromatography using protein G columns (GE Life Sciences, Protein G HP Columns). Purified

IgG generated from hybridomas was used for all EC_{50} and IC_{50} studies, competition-binding studies, HDX-MS studies, and animal studies. To generate the corresponding fragment antigen-binding (Fab) fragments for crystallization trials, papain digestion of purified mAb IgG was performed using the Pierce Fab Preparation Kit (ThermoFisher Scientific). The resulting Fabs were purified from the digestions by affinity chromatography by coupling a protein G affinity column and an anti-human CH1 column (GE Healthcare Life Sciences).

Characterization of antibody isotype, subclass, and variable genes

The isotype and subclass of secreted antibodies were determined by ELISA. Antibody heavy and light chain variable region genes were sequenced from antigen-specific hybridoma lines that had been cloned biologically using flow cytometric single cell sorting. Briefly, total RNA was extracted using the RNeasy Mini kit (Qiagen, 74106) and reverse-transcriptase PCR (RT-PCR) amplification of the antibody gene cDNAs was performed using the PrimeScript One Step RT-PCR kit (Clontech, RR055A) according to the manufacturer's protocols with gene-specific primers as previously described. PCR products were purified using Agencourt AMPure XP magnetic beads (Beckman Coulter) and sequenced directly using an ABI3700 automated DNA sequencer without cloning. The identities of gene segments and mutations from germlines were determined by alignment using ImMunoGeneTics database (Brochet, Lefranc et al. 2008, Giudicelli and Lefranc 2011).

Determination of half maximal effective concentration (EC_{50}) for binding

To determine EC_{50} concentrations for binding, we performed ELISA using 384-well plates that were coated overnight at 4°C with 2 μg/mL of a recombinant form of soluble head domain of HeV-

RBP or NiV-RBP protein. The plates were blocked for 1 hour with 2% non-fat dry milk and 2% goat serum in PBS-T. After washing the plates 4 times with PBS-T, primary mAbs or hybridoma cell culture supernatants were applied to wells, and the plates were incubated at room temperature for 1 hour. Alkaline phosphatase-conjugated secondary antibodies (goat anti-human IgG Fc, Meridian Life Science), with a dilution of 1:4,000 in blocking solution, were placed into each well following plate wash with PBS-T. After 1-hour incubation, the plates were washed 4 times with PBS-T, and substrate solution (1 mg/mL pNPP disodium salt hexahydrate, Sigma) was added to each well. The plates were incubated at room temperature for approximately 30 min before reading the optical density at 405 nm with a Biotek plate reader. To obtain half maximal effective concentration (EC_{50}) values of human mAbs binding to HeV-RBP or NiV-RBP, ELISA experiments were performed with purified antibodies in three-fold serial dilutions, starting at 20 μg/mL for HeV, and 50 μg/mL for NiV_M-RBP or NiV_B-RBP, and EC_{50} values were estimated by a sigmoidal dose-response nonlinear curve fitting procedure with Prism software (GraphPad). Each dilution was performed in quadruplicate, and the experiment was conducted twice independently.

K_D determination by bio-layer interferometry (BLI)

Kinetic assays with BLI were performed on an Octet RED biosensor instrument (Pall FortéBio, Menlo Park). Recombinant histidine-tagged RBP (head domain) was immobilized to HIS1K biosensor tips (FortéBio) at 10 μg/mL in proprietary kinetics buffer (FortéBio). After a brief baseline step, serial dilutions of HENV-26 or HENV-32 Fab starting at 200 nM then were associated to coated biosensor tips for 300 seconds, followed by a 900 second dissociation step in 10x kinetics buffer. Data Analysis HT 11.0.2 software was used for curve-fitting to extrapolate

equilibrium dissociation constant values. Association and dissociation steps were aligned to reference wells to account for dissociation of antigen from the biosensor tip. Global fitting using a 1:1 model with Savitzky-Golay filtering was used to fit curves.

Biolayer interferometry (BLI) to determine competition-binding groups

Competition-binding experiments were performed on the Octet RED biosensor, as described previously (Flyak, Ilinykh et al. 2015). In brief, HeV-RBP or NiV-RBP with a C-terminal His-tag at 20 μg/mL was loaded onto Ni-NTA coated biosensor tips for 2 min. After 1 min wash in a kinetic buffer (1% BSA, 0.002% Tween 20 in PBS), the biosensor tips were dipped into the first antibody solution at a concentration of 50 μg/mL for 5 min, and then biosensors were switched into a second antibody solution at a concentration of 50 μg/mL for 5 min. The ratio of the maximal signal from the seconding antibody after the first antibody binding to the maximal signal of the second antibody tested alone was calculated and expressed as a percentage.

Biolayer interferometry to test for mAb blocking of HeV-RBP protein binding to the host receptor ephrin-B2

The human antibodies also were used in competition binding with a recombinant form of the host receptor ephrin-B2 to determine if the mechanism of neutralization was blockade of receptor binding. The studies were performed using BLI on an Octet RED instrument. Streptavidin (SA) sensor tips were coated in 5 μg/mL biotinylated, recombinant HeV-RBP head domain protein diluted in proprietary Kinetics Buffer 10X (Pall FortéBio) for 30 seconds. Following a brief baseline step, 25 μg/mL HENV-26, HENV-32, or soluble ephrin-B2 in buffer was associated to the coated sensor tips for 100 seconds. Tips then were dipped into wells containing a second

antibody or ephrin-B2. The data were analyzed using FortéBio software, with percentage binding determined by comparing the maximal binding signal of the second protein associated to that of the same protein associated alone.

Cell-surface display flow cytometric assay to test for mAb blocking of HeV-RBP protein binding to the host receptor ephrin-B2

A suspension of 293F cells was transfected with cDNA encoding the full length HeV-RBP protein using PEI for 72 hours. Transfected cells were harvested and plated in V-bottom 96-well plates at 50,000 cells/well. After a wash step, cells were incubated with 50 μg/mL soluble ephrin-B2 protein or FACS buffer for 30 minutes. Without washing, 2 μg/mL HENV-26 labeled with AlexaFluor-647 (Invitrogen) was added to cells and incubated for 30 minutes. Cells then were washed and analyzed using an Intellicyt iQue flow cytometry instrument. Binding of HENV-26 in the presence or absence of ephrin-B2 was expressed as mean fluorescence intensity (MFI).

Crystallization and structural determination of antibody-antigen complexes

Purified Fabs were mixed with deglycosylated HeV-RBP or NiV-RBP head domain in a molar ratio of 1:1, and the mixtures were purified further by size-exclusion chromatography with a Superdex-200 HiLoad column (GE Healthcare Life Sciences) to obtain antibody-antigen complexes. The complexes were concentrated to about 10 mg/mL and subjected to crystallization trials. HeV-RBP head domain in complex with the Fab HENV-26 was crystallized in 30% MPD, 0.1 imidazole pH 6.5, 0.2 M ammonium sulfate, and 10% PEG 3350, and NiV-RBP head domain in complex with the Fab HENV-26 was in 1.0 M sodium malonate pH 7.0, 0.1 M Bis-Tris propane pH 7.0. Protein crystals were flash-frozen in liquid nitrogen after a quick soaking in the

corresponding cryo-protection solutions (same as the crystallization solution for HeV-RBP/HENV26 complex, the solution of 25% sodium malonate pH 7.0 and 0.1 M Bis-Tris propane pH 7.0 for NiV-RBP/HENV-26 complex). Diffraction data were collected at the beamline 21-ID-G at the Advanced Photon Source. The diffraction data were processed with XDS (Kabsch 2010) and CCP4 suite (Winn, Ballard et al. 2011). The crystal structures were solved by molecular replacement using the structure of the head domain of HeV-RBP or NiV-RBP in human ephrin-B2-HeV-RBP or ephrin-B2-NiV-RBP complex (PDB ID 2VSK and 2VSM) and Fab structure of MR78 (PDB ID 5JRP) with the program Phaser (McCoy, Grosse-Kunstleve et al. 2007).The structure was refined and rebuilt manually with Phenix (Adams, Afonine et al. 2010) and Coot (Emsley and Cowtan 2004), respectively. The models have been deposited into the Protein Data Bank. PyMOL software (Schrodinger 2015) was used to make all of the structural figures.

CedV-RBP and GhV-RBP ELISA

Constructs for CedV-RBP head domain and GhV-RBP full ectodomain were transfected transiently into Expi293F cells using ExpiFectamine transfection reagents (ThermoFisher). Cell supernatants were harvested 7 days post-transfection. CedV-RBP head domain was purified using HisTrap affinity chromatography as described above for HeV-RBP and NiV-RBP head domains (SigmaAldrich). Full-length ectodomain GhV-RBP containing a GCN tetramerization domain was purified using S-protein agarose (EMD Millipore). To test HENV-26 and HENV-32 for binding to CedV-RBP and GhV-RBP, 384-well plates were coated with 5 µg/mL CedV-RBP head domain or cell supernatant from GhV-RBP transfected cells and incubated overnight at 4°C. The following day, plates were blocked with DPBS-T containing 2% milk and 1% goat serum at room temperature for 1 hour. After a wash step, 3-fold serial dilutions of HENV-26, HENV-32, or

control mAbs for CedV (14F3) or GhV (10D5) kindly provided by Christopher Broder were added to plates and incubated for 1 hour at room temperature. Secondary antibody (goat anti-human IgG-HRP for HENV-26 and HENV-32, goat anti-mouse human adsorbed Ig-HRP for controls) diluted 1:1,000 in DBPS-T containing 1% milk and 1% goat serum were added to plates. TMB substrate was used to develop plates, and the reaction was quenched using 1N HCl 10-15 minutes later. Absorbance at 450 nm was read using a Biotek plate reader, and binding curves were generated using non-linear regression analysis in GraphPad Prism software.

HeV and NiV viruses

Nipah virus number 1999011924 was obtained from a patient from the 1999 outbreak in Malaysia. The passage 3 (P3) virus stock of NiVM we used for used for neutralization assays is known to have an N277K polymorphism in the RBP (Mire, Satterfield et al. 2016). The isolate of NiV_B was 200401066 and was obtained from a fatal human case during the outbreak in Rajbari, Bangladesh in 2004 and passaged on Vero E6 cell monolayer cultures twice, making this a passage 2 virus. Hendra virus was obtained from a patient from the 1994 outbreak in Australia. All viruses were kindly provided by Dr. Thomas Ksiazek, UTMB. Each virus was propagated on Vero E6 cells in Eagle's minimal essential medium supplemented with 10% fetal calf serum. The NiV_M, NiV_B and HeV challenge virus stocks were assessed for the presence of endotoxin using The Endosafe-Portable Test System (PTS) (Charles River Laboratories, Wilmington, MA). Each virus preparation was diluted 1:10 in Limulus Amebocyte Lysate (LAL) Reagent Water per the manufacturer's instructions, and endotoxin levels were tested in LAL Endosafe-PTS cartridges as directed by the manufacturer. Each preparation was found to be below detectable limits, whereas positive controls showed that the tests were valid. All experiments involving infectious

henipaviruses were carried out at the UTMB Galveston National Laboratory under biosafety level 4 conditions.

Neutralization assays

The virus neutralizing activity concentrations were determined for NiV_M, NiV_B, and HeV using a plaque reduction assay. Briefly, antibodies were diluted serially two-fold from 50 μg/mL to extinction and incubated with a target of ~100 plaque-forming units (pfu) of NiV_M , NiV_B, or HeV for 45 min at 37 °C. Virus and antibody mixtures then were added to individual wells of six-well plates of Vero76 cells. Plates were stained with neutral red two days after infection, and plaques were counted 24 h after staining. Neutralization potency was calculated based on pfu for each virus in the well without antibody. The neutralization experiments were performed in triplicate, with independent virus preparations and duplicate readings for each replicate. Mean half-maximal inhibitory concentrations were calculated as previously described (Ferrara and Temperton 2018).

Protection study in ferrets

The animal studies were performed at the Galveston National Laboratory, University of Texas Medical Branch at Galveston (UTMB) and were approved by the UTMB Institutional Animal Care and Use Committee (IACUC). This facility is fully accredited by the Association for Assessment and Accreditation of Laboratory Animal Care International. Thirteen female ferrets weighing 0.75–1 kg were housed socially and placed into cohorts for treatment or no treatment. For virus challenge and procedures, animals were anesthetized by isoflurane inhalation. Animals were inoculated intranasally (i.n.) with ~5×10^3 plaque-forming units (pfu) of NiV_B in 0.5 mL

Dulbecco's minimal essential medium (Sigma-Aldrich, St. Louis, MO) on day 0. After challenge, ferrets in the treated cohorts were given mAb HENV-26 or HENV-32 by intraperitoneal (i.p.) injection on day 3 and 5 after challenge at a 15 mg/kg dose, a dosage lower than that used in prior studies in ferrets and nonhuman primates with an antiviral mAb (Bossart, Zhu et al. 2009, Bossart, Geisbert et al. 2011, Geisbert, Mire et al. 2014, Mire, Satterfield et al. 2016, Mire, Chan et al. 2019). Animals were anesthetized for clinical examination including body weight, temperature, respiration quality, and blood collection on days 0, 3, 5, 7, 10, 14, and 28 after challenge. Before and after challenge, animals were assessed daily for clinical score on a scale of 0 of 12 for clinical observations based on coat appearance, body weight loss, social behavior, and provoked behavior; animals scoring 9 or greater were euthanized per the established UTMB IACUC protocol. The remaining subjects were euthanized at the study endpoint on day 28 after challenge.

Specimen collection and processing in NiV- and HeV-infected ferrets

On sampling days, blood was collected and placed in MiniCollect EDTA tubes (Greiner Bio-One, Monroe, NC) for virus load and hematology analysis or MiniCollect serum tubes (Greiner Bio-One) for clinical chemistry analysis. Necropsy was performed on all ferrets, and tissues sampled included lungs, liver, spleen, kidney, adrenal gland, pancreas, and brain (frontal cortex). Ten percent tissue homogenates of liver, spleen, kidney, adrenal gland, and brain were used for virus load analysis.

Measurement of infectious virus load in ferret tissues

Virus titration was performed by plaque assay with Vero cells from all tissue homogenates (10% w/v). In brief, increasing 10-fold dilutions of the samples were adsorbed to Vero cell monolayers

in duplicate wells (200 μL); the limit of detection was 25 pfu/mL for whole blood and 250 pfu/gram for tissue**.**

RNA isolation from ferret tissues

Immediately following sampling, 100 μL of blood was added to 600 μL of AVL viral lysis buffer (Qiagen) for RNA extraction. For tissues, approximately 100 mg was stored in 1 ml RNAlater (Qiagen) for 7 days to stabilize RNA. RNAlater was completely removed, and tissues were homogenized in 600 μL RLT buffer (Qiagen) in a 2-mL cryovial using a tissue lyser (Qiagen) and ceramic beads. The tissues sampled included cerebral spinal cord, brain stem, brain (frontal cortex), lung (left upper and left lower), spleen, and liver. All blood samples were inactivated in AVL viral lysis buffer, and tissue samples were homogenized and inactivated in RLT buffer prior to removal from the BSL-4 laboratory. Subsequently, RNA was isolated from blood using the QIAamp viral RNA kit (Qiagen), and from tissues using the RNeasy Mini Kit (Qiagen) according to the manufacturer's instructions supplied with each kit.

Detection of viral genomes in ferret samples

RNA was isolated from blood or tissues and analyzed using primers/probe targeting the nucleoprotein (N) gene and intergenic region between N and phosphoprotein (P) of NiV for quantitative real-time PCR (qRT-PCR), with the probe used here being 6-carboxyfluorescein (6FAM)-5′ CGT CAC ACA TCA GCT CTG ACA A 3′-6 carboxytetramethylrhodamine (TAMRA) (Life Technologies, Carlsbad, CA). NiV RNA was detected using the CFX96 detection system (Bio-Rad) in One-step probe qRT-PCR kits (Qiagen) with the following cycle conditions: 50°C for 10 minutes, 95°C for 10 seconds, and 40 cycles of 95°C for 10 seconds and 57°C for 30 seconds. Threshold cycle (*CT*) values representing NiV genomes were analyzed with

CFX Manager Software, and data are shown as genome equivalents (GEq). To create the GEq standard, RNA from NiV challenge stocks was extracted and the number of NiV genomes was calculated using Avogadro's number and the molecular weight of the NiV genome.

CHAPTER III

FUNCTIONAL COOPERATIVITY MEDIATED BY RATIONALLY SELECTED COMBINATIONS OF HUMAN MONOCLONAL ANTIBODIES TARGETING THE HENIPAVIRUS RECEPTOR BINDING PROTEIN

This chapter is an adaptation of the following submitted manuscript:

Doyle MP et al. Functional cooperativity mediated by rationally selected cocktails of human monoclonal antibodies targeting the henipavirus receptor binding protein. In review at *Cell Reports.*

Contributions: Nurgun Kose and I isolated antibodies. I performed binding assays, mechanistic assays, and all neutralization assays using VSV or rCedV viruses. I performed protein purification for structural studies. Elad Binshtein performed EM studies. Robert Cross performed BSL-4 *in vitro* and *in vivo* studies. Brandyn West and Zachary Bornholdt (Mapp Biopharmaceutical) generated bispecific antibodies. James Crowe and I wrote the manuscript.

INTRODUCTION

Hendra virus (Guirakhoo, Pugachev et al.) and Nipah virus (NiV), the prototypic henipaviruses, are emerging zoonotic paramyxoviruses known to cause severe disease in humans and diverse other mammalian orders. Multiple species of *Pteropid* bats (flying foxes) act as reservoir hosts for these negative-sense, single-stranded RNA viruses in the *Paramyxoviridae* family with which they are understood to have co-evolved (Halpin, Young et al. 2000, Chua, Koh et al. 2002, Halpin, Hyatt et al. 2011, Vidgen, de Jong et al. 2015). HeV is transmitted from flying foxes to horses and from horses to in-contact humans causing severe respiratory and/or encephalitic disease mediated by endothelial vasculitis in both (Murray, Rogers et al. 1995, Escaffre, Borisevich et al. 2013, Field 2016). HeV was identified in 1994, having caused the death of 14 of

21 infected horses and one of two infected humans in Queensland, Australia (Murray, Selleck et al. 1995, Selvey, Wells et al. 1995). Spillover has occurred sporadically with some seasonal and climatic trend since, causing disease in 105 horses and seven humans, with high case fatality rates (Queensland Government 2020). NiV, which was discovered four years after HeV when hundreds of pig handlers fell ill with encephalitic disease (Chua, Goh et al. 1999), has continued to cause sporadic outbreaks in Bangladesh and India (Arunkumar, Chandni et al. 2019, Soman Pillai, Krishna et al. 2020). More direct routes of infection, including human-to-human transmission, and mortality rates approaching 100%, have been observed during recent NiV outbreaks (Chadha, Comer et al. 2006, Gurley, Montgomery et al. 2007, Clayton, Middleton et al. 2012). Anthropogenic and climatic influences on flying foxes are affecting their roosting, feeding and migration habits as well as their susceptibility to heat-stress, disease and injury (Plowright, Eby et al. 2015, Kessler, Becker et al. 2018). These factors together with their resultant increase in intermediate host contact (humans and domestic animals) are associated with increasing geographic range and frequency of henipavirus disease spillover (Walsh, Wiethoelter et al. 2017, Martin, Yanez-Arenas et al. 2018). While HeV and NiV outbreaks historically have been confined geographically to Australia and Southeast Asia, respectively, risk of pandemic spread of these highly pathogenic agents related to regional and global population densities and difficulty avoiding international transmission via infected travelers has been highlighted by recent experience with SARS-CoV-2 (Morens and Fauci 2020). Such consideration prompted the World Health Organization (WHO) to designate henipavirus infections as priority diseases requiring extensive and immediate research and development (Sweileh 2017). The risk of global health crisis associated with henipaviruses is exacerbated by the lack of licensed antiviral drugs or vaccines for HNV and a dearth of knowledge of the human

immune response to these viruses (Escaffre, Borisevich et al. 2013, Gomez Roman, Wang et al. 2020).

Passive immune transfer studies in both hamsters and ferrets have provided evidence that neutralizing antibodies are a correlate of immunoprotection from henipaviruses (Guillaume, Contamin et al. 2004, Guillaume, Contamin et al. 2006, Bossart, Zhu et al. 2009). These data have been corroborated in multiple studies by investigators using murine, rabbit, or human antibody discovery technologies to isolate potently neutralizing antibodies to HeV and/or NiV (Zhu, Dimitrov et al. 2006, Aguilar, Ataman et al. 2009, Mire, Chan et al. 2020). One of these studies used phage display technology to isolate a human monoclonal antibody (humAb), designated m102.4 (Zhu, Bossart et al. 2008). This mAb potently neutralizes both HeV and NiV *in vitro* and protects against infection and disease in experimental henipavirus challenge models using ferrets or non-human primates (Bossart, Geisbert et al. 2011, Geisbert, Mire et al. 2014, Mire, Satterfield et al. 2016). More recently, two human mAbs, HENV-26 and HENV-32, were shown to neutralize HeV and NiV by distinct mechanisms and protect from NiV Bangladesh (NiV_B) strain challenge in a ferret model (Dong, Cross et al. 2020). While these studies have laid a foundation for our understanding of how to target henipaviruses therapeutically, many questions remain regarding the antigenicity of the attachment glycoprotein, and whether escape mutations from these mAbs can develop *in vivo*.

Here, we isolated humAbs from circulating B cells of an individual with occupation-related exposure to the equine HeV vaccine (Equivac® HeV) (Middleton, Pallister et al. 2014). Members of this large panel of antibodies target diverse antigenic sites, many of which are sites of

vulnerability for neutralization for at least one virus. In particular, two functional classes of antibodies that we have termed “receptor-blocking” or “receptor-enhanced” neutralized HeV and NiV *in vitro* by distinct molecular mechanisms and provided protection when used as monotherapy against lethal challenge in hamsters with the highly virulent NiV_B strain. Antibodies recognizing these sites cooperate for binding to the henipavirus RBP glycoprotein that mediates attachment (formerly designated the G or glycosylated attachment protein, but recently renamed by the International Committee on Taxonomy of Viruses) (Rima, Balkema-Buschmann et al. 2019). These mAbs also synergize for neutralization Cedar virus chimeras displaying the RBP and F proteins of HeV (as well as NiV, data not shown). Cocktails of antibodies from these groups show superior therapeutic efficacy in hamsters, while bispecific antibodies bearing antigen binding fragments from both mAbs also show therapeutic benefit. In this model, “receptor-blocking” mAbs induce conformational changes to the RBP that better expose the “receptor-enhanced” antigenic site. These results suggest these mAbs could be used in a cocktail therapeutic approach to achieve synergistic neutralizing potency against henipavirus infections.

RESULTS

Cross-reactive, neutralizing antibodies target two distinct antigenic sites on HNV-RBP

Peripheral blood mononuclear cells (PBMCs) from an Australian veterinarian with occupation-related exposure to HeV-RBP (Equivac® HeV) were tested for secretion of antibodies binding to recombinant forms of the NiV attachment (RBP) glycoproteins for NiV_B, the NiV Malaysian strain (NiV_M), or HeV. In total, we isolated 41 distinct new mAbs that bind henipavirus RBPs. In order to group this large panel of mAbs rationally into those that recognized similar antigenic

sites, we used a surface plasmon resonance platform to bin antibodies based on the antigenic sites they recognized on recombinant protein comprising the HeV-RBP head domain. This method immobilizes a first antibody on the surface of a gold-coated sensor-chip that captures soluble antigen, and then assesses the ability of a second antibody to bind to the captured antigen. The resulting data showed that mAbs binding to HeV-RBP recognized at least 6 distinct major antigenic sites, designated A-F (**Figure 2-1**).

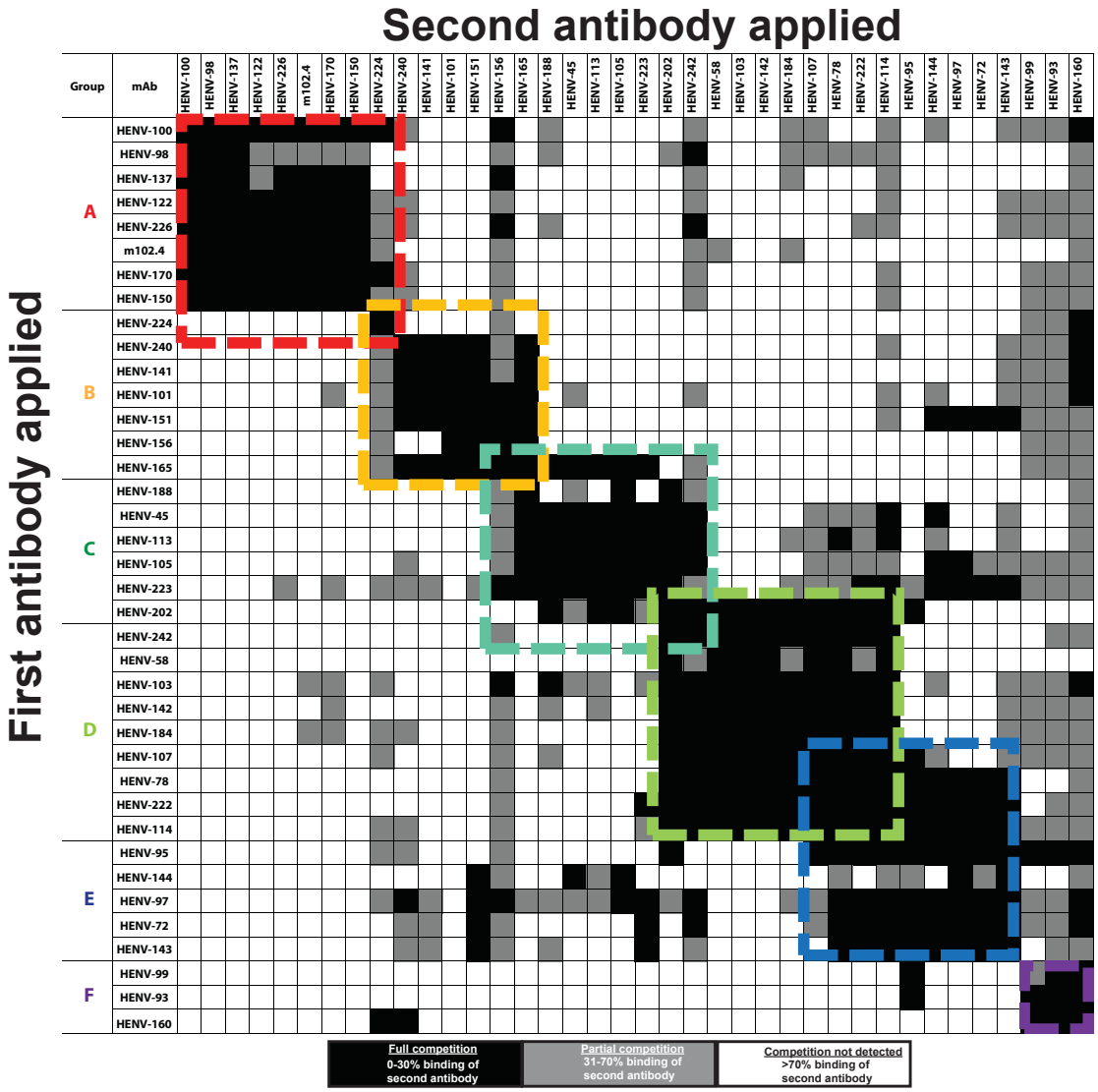

Figure 3-1: Surface plasmon resonance competition-binding of human antibodies against HeV-RBP. A first antibody was applied to a gold-coated sensorchip, and recombinant HeV-RBP head domain was associated to the coupled antibody. A second antibody was applied to the sensorchip to determine binding to RBP. Black boxes indicated a pairwise interaction in which the binding of the second antibody is blocked by the first. White indicates

both antibodies could bind simultaneously. Gray indicates an intermediate competition phenotype. The matrix was assembled using the Carterra Epitope software.

In tandem, we used hydrogen-deuterium exchange mass spectrometry (HDX-MS) to map the antigenic sites of representative antibodies from each group (**Figure 2-2**), along with binding and neutralization assays to determine cross-reactivity and functional activity **(Figure 2-3)**.

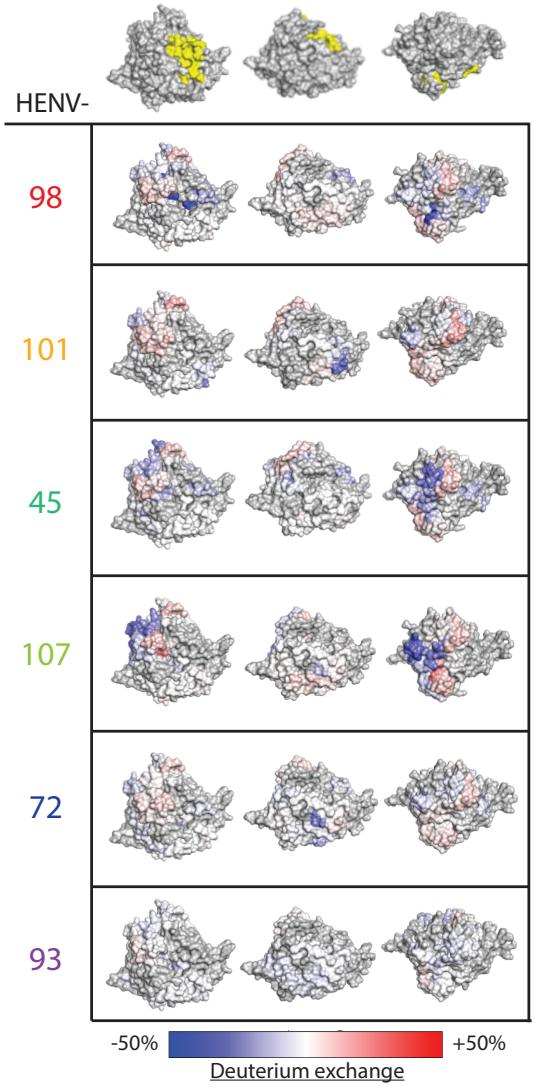

Figure 3-2: Hydrogen-deuterium exchange mass spectrometry profiles for representative mAbs. Decrease (blue) or increase (red) in deuterium exchange on HeV-RBP in the presence of antibody is mapped onto the crystal structure of HeV-RBP (PDB 6CMG). Structures are positioned in 3 orientations, with the top structure noting the ephrin-B2 binding site in yellow.

Antibodies belonging to groups A and C cross-reacted with HeV, NiV_M, and NiV_B-RBP, and neutralized the corresponding viral strains. Group A, specifically, includes the control mAb m102.4, which has been thoroughly characterized for its ability to block viral attachment to the host cell receptors ephrin-B2 and ephrin-B3, and potently neutralize both HeV and NiV(Xu, Rockx et al. 2013, 2020) (Xu, Rockx et al. 2013). As expected, a representative group A mAb HENV-98 caused a decrease in deuterium exchange in a region of the HeV-RBP that corresponds to the receptor-binding site. All group A mAbs also neutralized HeV, NiV_M, and NiV_B strains *in vitro*. Notably, HENV-117 displayed exceptional potency, with half maximal inhibitory concentration (IC_{50}) values of 14, 8, or 15 ng/mL against HeV, NiV_M, or NiV_B, respectively. To date, this is the most broad and potent neutralizing mAb targeting HeV and NiV ever described, suggesting it may possess superior therapeutic activity.

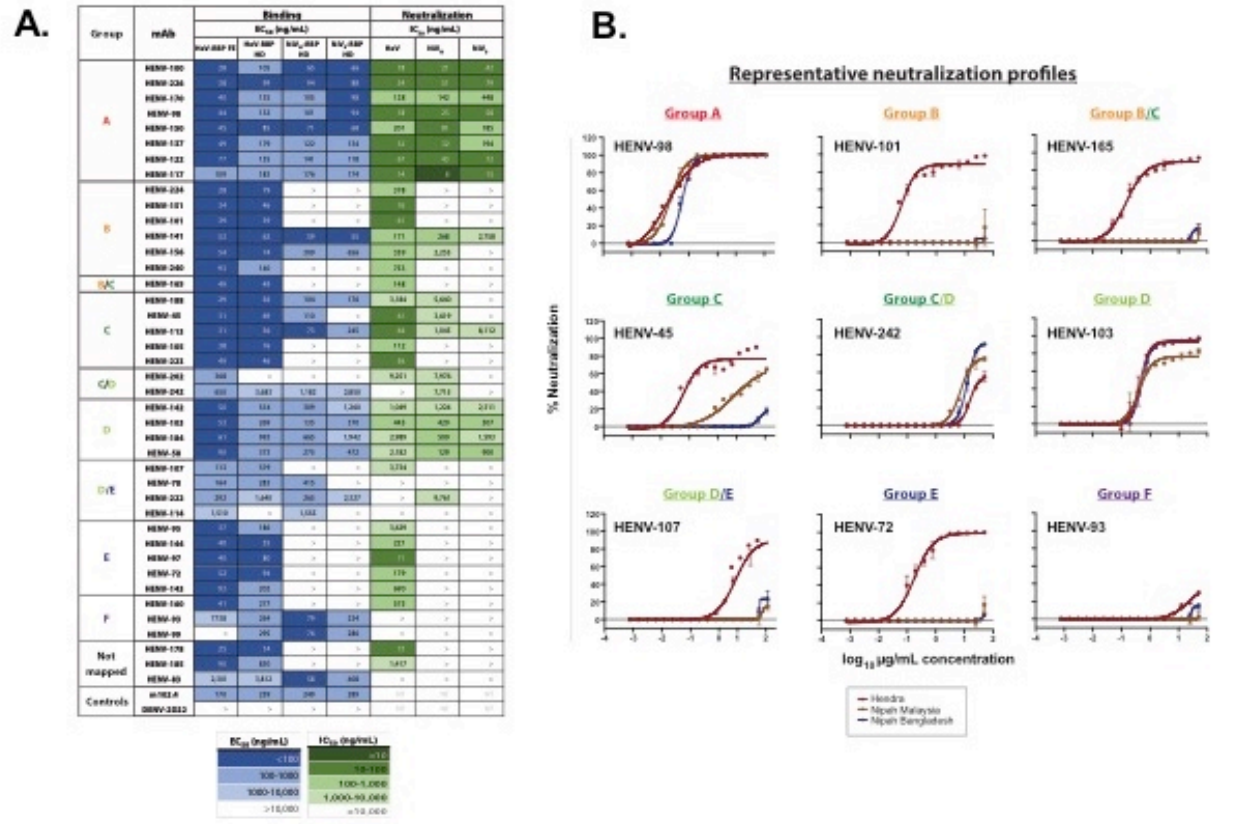

Figure 3-3: Summary of panel binding and neutralization profiles A) Half maximal binding (blue) or neutralization (green) concentrations for antibodies against recombinant proteins or live HeV or NiV, respectively. **B)** Neutralization curve plots for representative antibodies against HeV, NiV Malaysia, or NiV Bangladesh viruses. Representative EC_{50} values for binding from 3 independent experiments are shown. IC_{50} values for neutralization are from a single independent experiment due to limitations of BSL-4 resources.

Group D represents a second class of mAbs that cross-neutralize HeV, NiV_M, and NiV_B, albeit with roughly 10-fold less potency than group A. The group D representative mAb HENV-107 mapped to a distinct site on the HeV-RPB head domain spanning the ß1 and ß6 propeller blades. This region of the head domain likely lies at the interface between protomers within the dimer-of-dimers structure of the HeV-RBP tetramer, suggesting a semi-cryptic site of vulnerability on RBP (Lee and Ataman 2011). This region has been postulated to be important in fusion triggering, as point mutations made to this region render F unable to complete its fusion cascade (Aguilar, Ataman et al. 2009, Liu, Stone et al. 2013).

While mAbs in group C display limited cross-neutralization of HeV and NiV, groups B and E contain mAbs that only neutralize HeV with appreciable potency. Group F mAbs are weakly neutralizing or non-neutralizing and appear to target an antigenic site that lies on the RBP face opposite the receptor-binding domain. This epitope is likely in a site that is poorly accessible in the membrane-anchored form of RBP, lending to the poor neutralizing activity observed for these mAbs. Overall, we discovered and mapped cross-reactive, neutralizing mAbs targeting two distinct major antigenic sites that likely use distinct mechanisms to achieve virus neutralization.

Neutralizing mAbs either compete with, or are enhanced by, ephrin-B2 binding to HeV-RBP. With the knowledge that group A mAbs map to the receptor-binding domain of HeV-RBP, we sought to determine if these antibodies could block binding of soluble ephrin-B2 to cell surface-displayed HeV-RBP. 293F cells were transiently transfected with a cDNA construct encoding full-length HeV-RBP (head, stalk, transmembrane, and cytoplasmic domains) and incubated for 72 hours. These cells then were incubated with saturating concentrations of recombinant, soluble ephrin-B2, followed by addition of anti-RBP mAbs at a concentration of 2 μg/mL to assess the ability of antibodies to bind RPB in its receptor-bound state. Cells were analyzed by flow cytometry, comparing antibody binding in the presence or absence of ephrin-B2 (**Figure 2-4)**. Antibodies in group A displayed a substantial decrease in binding in the presence of ephrin-B2, supporting the hypothesis that mAbs from this group potently neutralize by blocking binding of virus to host cells. This receptor-blocking phenotype is reflected in the activity of the control mAb m102.4, which also displayed decreased signal when associated to receptor-bound RBP.

We also assessed antibodies from all other epitope binning groups for their ability to bind RBP in the presence of ephrin-B2. Antibodies from group F did not bind to surface-displayed HeV-RBP, further suggesting these antibodies cannot access this antigenic site when RBP is in its tetrameric, membrane-anchored form. Group B, C, and E mAbs bound to HeV-RBP with equal signal in the presence or absence of ephrin-B2. Surprisingly, cross-reactive and neutralizing antibodies in group E displayed a "receptor-enhanced" phenotype, in which binding was increased in the presence of ephrin-B2. As HDX experiments suggested this antigenic site lies at the putative interface between protomers within the HeV-RBP dimer, it is likely that receptor binding alters the conformation of HeV-RBP, better exposing this epitope and increasing binding by mAbs to this site. In summary, cross-reactive and neutralizing mAbs displayed either "receptor-blocking" or "receptor-enhanced" phenotypes, suggesting distinct neutralization mechanisms used by antibodies targeting distinct sites.

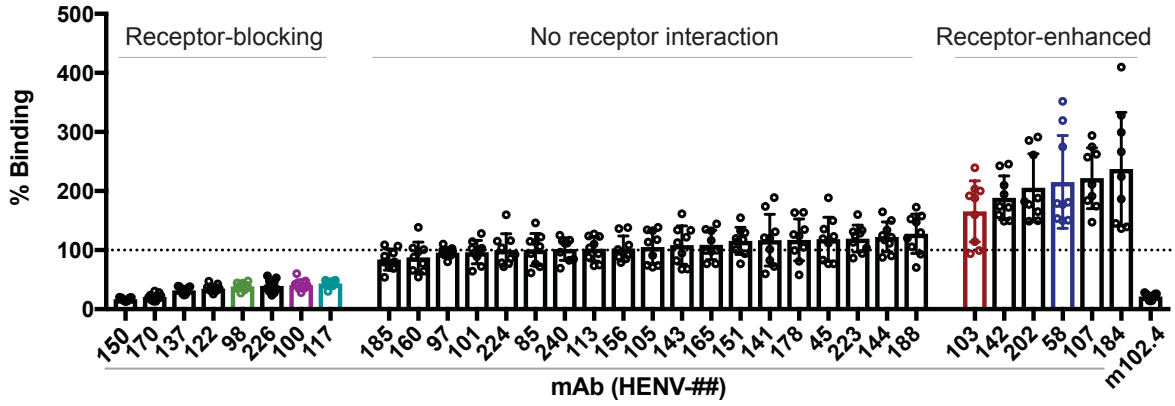

Figure 3-4: Antibody binding to cell-surface-displayed HeV-RBP when ephrin-B2 is bound. Cells transiently transfected with a cDNA encoding the full-length HeV-RBP were incubated with a saturating concentration of recombinantly expressed ephrin-B2. Without washing, cells were incubated with 2 μg/mL antibody, and binding was compared to binding of antibodies in the absence of ephrin-B2. The mAb m102.4 served as a control for receptor competition. Pooled data from 3 independent experiments are shown.

Negative stain electron microscopy (nsEM) elucidates structural determinants of recognition by receptor-blocking and receptor-enhanced mAbs.

To gain insight into the structural determinants of recognition by "receptor-blocking" and "receptor-enhanced" mAbs, we performed nsEM on HeV-RBP complexed with representative Fabs based on the sequence of HENV-117 (blocking) or HENV-103 (enhanced). Initial studies with HeV-RBP ectodomain (head and stalk domains) purified by size exclusion chromatography showed substantial structural heterogeneity of both dimeric and tetrameric complexes (elaborated upon in Chapter IV). In order to generate more structurally homogeneous antigen suitable for 3D reconstruction, we purified HeV-RBP by gradient fixation ultracentrifugation using a 10 to 30% glycerol gradient containing a linear 0 to 0.1% glutaraldehyde gradient. This method achieved highly pure material, appropriate separation of monomeric, dimeric, and tetrameric species, and structural homogeneity induced by mild glutaraldehyde fixation. Dimeric HeV-RPB was complexed with a molar excess of HENV-117 and HENV-103 and assessed using nsEM.

Both HENV-103 and HENV-117 bind simultaneously to the HeV-RBP, further confirming these mAbs recognize distinct antigenic sites (**Figure 2-5A**). By docking the crystal model of the head domain bound the ephrin-B2 receptor to the EM map, we observed that HENV-117 mimics the binding position of the receptor, confirming its ability to block receptor attachment **(Figure 2-5B)**. This mAb represents a next-generation version of HENV-26, which showed a similar receptor blocking phenotype, albeit with decreased potency in comparison. Conversely, HENV-103 approaches the HeV-RBP perpendicular to the receptor binding domain at the putative interface between protomers within the RBP **(Figure 2-5C)**. This antigenic site overlaps with previous published mAbs, including HENV-32, though appears to have a different angle of

approach with more contacts to beta propeller 1. Furthermore, modeling suggests that HENV-117 uses a long CDRH3 loop, binding to RBP in a manner similar to the GH loop of ephrin-B2. In summary, HENV-103 and HENV-117 map to distinct antigenic sites by negative stain EM, with HENV-117 mimicking ephrin-B2 binding, while HENV-103 binds at the putative dimeric interface.

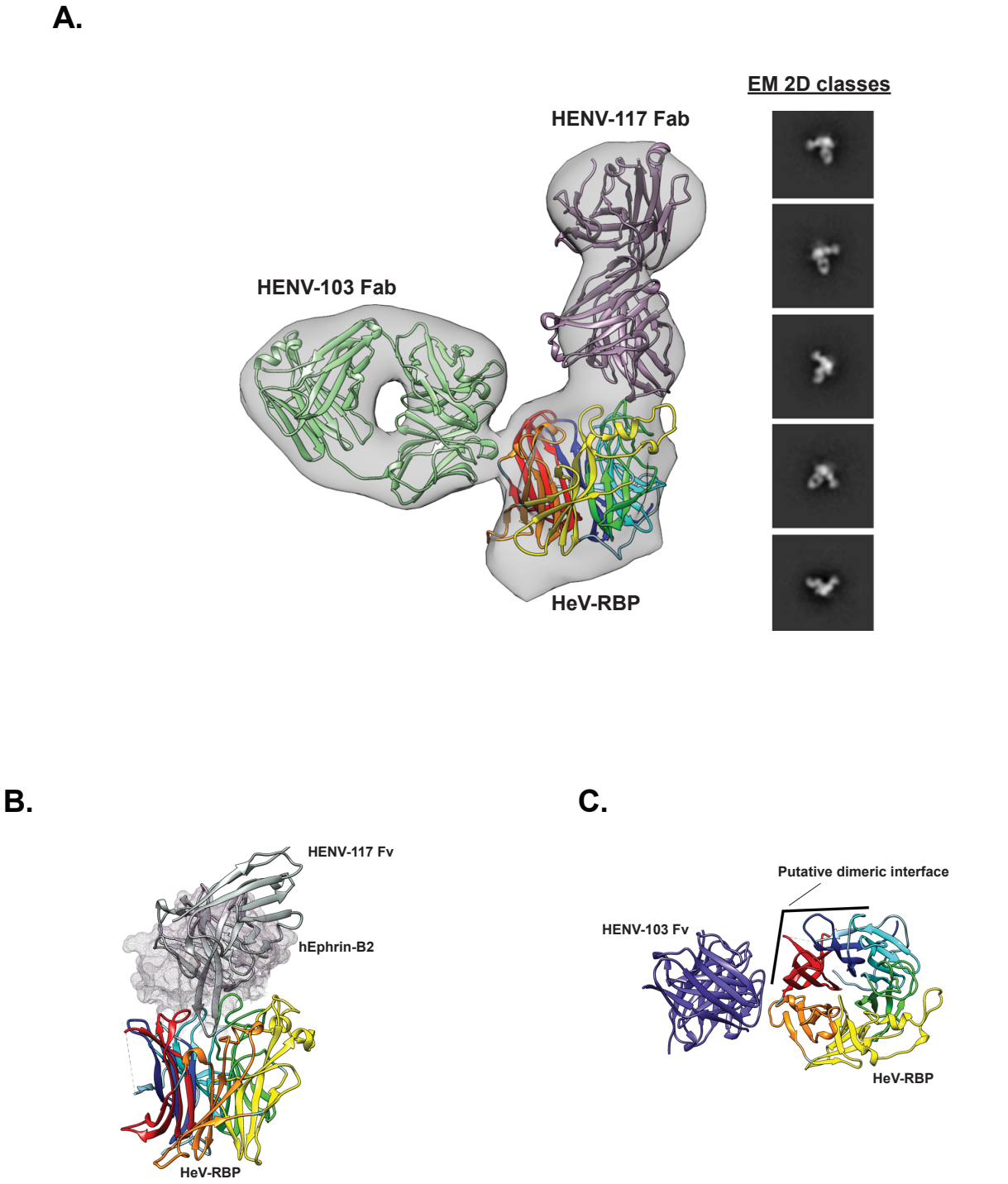

Figure 3-5: Negative stain electron microscopy of Fab-antigen co-complexes A) Three-dimensional reconstruction from negative stain electron microscopy of dimeric HeV-RBP full ectodomain bound to HENV-103 Fab and HENV-117-Fab. The EM map is shown in gray, the Fabs are in purple and green, and the RBP head domain is colored by β-propeller. 2D classes are shown, with box size of 128 at A/pix of 3.5. **B)** The RBP head domain with a model of HENV-117 scFv (Playford, Munro et al.) overlapping with ephrin-B2 receptor electron density (dot surface PRB: 9PDL). **C)** The RBP head domain with a model of HENV-103 Fv (blue) from top (right, looking down on ephrin-B2 binding face) and side (left) view. Black line denoted the putative dimeric interface.

Antibodies provide therapeutic protection in a highly stringent model of Nipah Bangladesh virus challenge in Syrian golden hamsters.

Previous studies of murine and human mAbs targeting HeV and/or NiV suggested passive immunization as a potential strategy for therapeutic intervention. To assess therapeutic activity of antibodies in this large panel, we chose 5 candidate mAbs representing groups A (receptor-blocking HENV-98, HENV-100, HENV-117) and D (receptor-enhanced HENV-58, HENV-103) to test in a highly stringent NiV_B challenge model in hamsters (Wong, Grosjean et al. 2003). Disease in this model follows a two-stage disease pattern with differing sequelae: an acute respiratory distress syndrome (ARDS)-like respiratory tract component starting at day 3 to 4, and an encephalitic component beginning at days 8 to 12. On day 0, Syrian golden hamsters were challenged intranasally with 5×10^6 PFU NiV_B. The following day, hamsters were administered a 10 mg/kg dose of antibody by the IP route and monitored for 28 days after challenge. While the hamster administered a vehicle control solution succumbed at day 3, as much as 60% survival was achieved in animals administered either "receptor-blocking" or "receptor-enhanced" mAbs. **(Figure 2-6)**. The two most protective mAbs from each class were HENV-117 and HENV-103, for which surviving animals in each treatment group were able to maintain body weight throughout the study **(Figure 2-6)**. HENV-117 and HENV-103 were also the two most potent mAbs from groups A and D, suggesting *in vitro* potency by antibodies targeting these sites correlates with *in vivo* efficacy. In summary, receptor-blocking and receptor-enhanced mAbs protect hamsters from NiV_B challenge, with HENV-117 and HENV-103 representing the most promising candidates targeting two distinct antigenic sites.

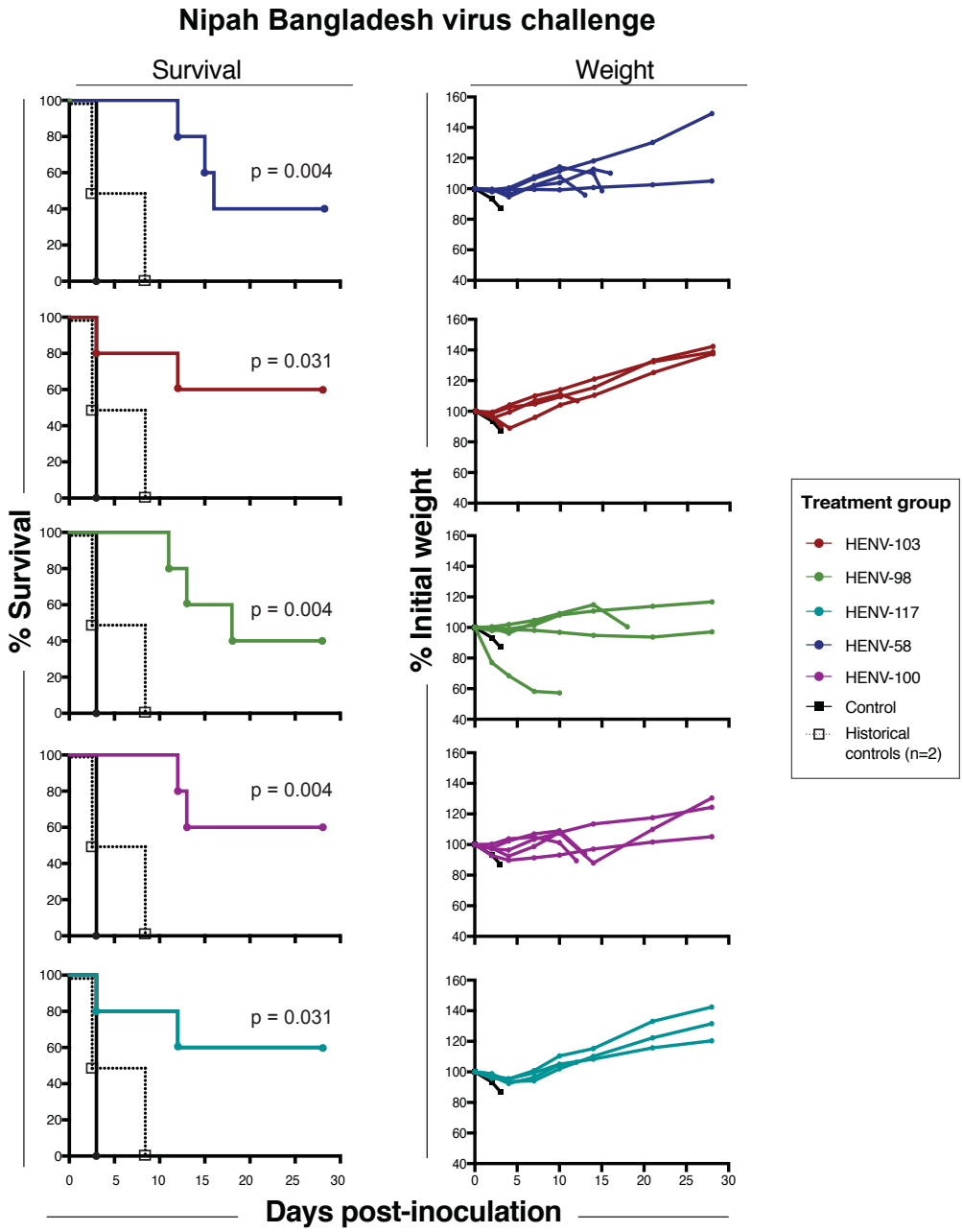

Figure 3-6. Therapeutic protection by antibodies in a hamster model of Nipah Bangladesh. Survival curves (left) and weight maintenance (Colling, Lunt et al.) for hamsters treated with 10 mg/kg antibody (n=5 per group) 24 hours post-inoculation with 5 x 10^6 PFU NiV Bangladesh by the intranasal route. An untreated control animal (n=1) succumbed to infection 3 days post-inoculation. All weight maintenance charts include control animal in black. Two historical controls are plotted on survival curves and pooled with the experimental control to perform statistical analysis by the long rank Mantel-Cox test.

HENV-117 and HENV-103 cooperate for binding to HNV-RBP and reveal synergistic virus neutralization activity.

RNA viruses, including HeV and NiV, use error-prone RNA-dependent RNA polymerase (RdRP) complexes to achieve genome replication (Welch, Tilston et al. 2020). While generation of errors can lead to non-viable genomes in some cases, this process also affords viruses the ability to escape from small and large molecule antivirals by introducing amino acid substitutions in the sites recognized by these molecules (Borisevich, Lee et al. 2016). This escape pattern is of concern and has been observed in both *in vitro* and *in vivo* studies of diverse RNA viruses, showing that antibody monotherapy approaches against viral pathogens may be susceptible to failure. In order to combat escape, cocktails of antibodies targeting the same or differing antigenic sites offer a higher threshold of protection, with escape becoming statistically highly unlikely. Concurrently, studies of antibody cocktails against Ebola virus, HIV, and more recently SARS-CoV-2, show the potential for synergistic activity by neutralizing antibodies, in which one antibody potentiates the activity of another (Miglietta, Pastori et al. 2014, Howell, Brannan et al. 2017, Zost, Gilchuk et al. 2020). With this goal in mind, we sought to determine whether "receptor-blocking" and "receptor-enhanced" mAbs cooperatively bind to and neutralize henipaviruses. We hypothesized that "receptor-blocking" mAbs would mimic the structural rearrangements in HeV-RBP by ephrin-B2, better exposing the "receptor-enhanced" epitope, allowing for synergistic neutralization by combinations of these antibodies. We chose the most potent and protective candidates from each class, HENV-103 and HENV-117, for these studies.

We first tested the ability of HENV-117 to enhance the binding of HENV-103 to cell-surface displayed RBP. Using the surface-display system, we incubated HeV-RBP-transfected cells in

saturating concentrations of mAbs that block ephrin-B2 binding. Without washing, we then added serial dilutions of HENV-103 chemically labeled with an Alexa Fluor-647 tag. Cells then were analyzed by flow cytometry to determine if HENV-103 showed increased binding signal across a dilution series in the presence of "receptor-blocking" mAbs. When cells were incubated with HENV-103 only, half maximal binding was achieved at 5,289 ng/mL. When cells were first incubated with saturating concentrations of HENV-117, the EC_{50} of HENV-103 shifted to 350 ng/mL, representing an increase in binding activity of approximately 15-fold (**Figure 2-7A**). Notably, this cooperativity is unidirectional, as HENV-103 did not increase the binding of HENV-117 **(Figure 2-7A)**. This cooperative phenotype also depends on HENV-117, with increasing HENV-117 concentrations showing increased binding by a constant concentration of HENV-103 **(Figure 2-7B)**. These data suggest that antibodies that bind the ephrin-B2 binding site on HeV-RBP, such as HENV-117, mimic the conformational changes induced by ephrin-B2 binding, making a semi-cryptic epitope recognized by HENV-103 more accessible.

In order to determine whether this cooperative binding phenotype is recapitulated functionally, we performed neutralization tests using solutions containing antibody pairs to measure synergistic neutralization potential. In order to perform these multiple comparison neutralization assays quantitatively in BSL-2 facilities, we used a non-pathogenic henipavirus chimerized with the HeV or NiV_B glycoproteins. In this system, recombinant Cedar virus (rCedV) was engineered genetically to express the RPB and F from HeV or NiV_B, as well as a GFP reporter. The resulting rescued, recombinant, chimeric viruses were termed rCedV-NiV_B or rCedV-HeV. Here, we used a matrix approach to test antibody pairs for neutralization synergy, in which serial dilutions of HENV-117 and HENV-103 were mixed together in a pairwise matrix, followed by incubation

with rCedV-HeV. Virus/mAb mixtures then were added to Vero E6 cell monolayer cultures in 96-well plates. At approximately 22 hours after inoculating cells with virus/antibody mixtures, plates were fixed and GFP+ foci were quantified to enumerate antibody neutralization values. To calculate synergy, neutralization matrix data were uploaded to the open source program "SynergyFinder," and synergy scores were calculated using the zero interactions potency (ZIP) model (Ianevski, He et al. 2020). A score >10 suggests synergistic activity. We observed that HENV-103 and HENV-117 gave an overall ZIP score of 13.1, with select physiologically achievable cocktail concentrations achieving synergy scores >20 **(Figure 2-7C)**. (Mire, Geisbert et al. 2019). These data together with binding studies show that antibodies from these classes cooperate for binding to RBP and synergistically neutralize chimeric and pseudotyped viruses bearing RBP and F proteins from HeV or NiV_B, suggesting they will likely function to synergistically neutralize pathogenic henipaviruses.

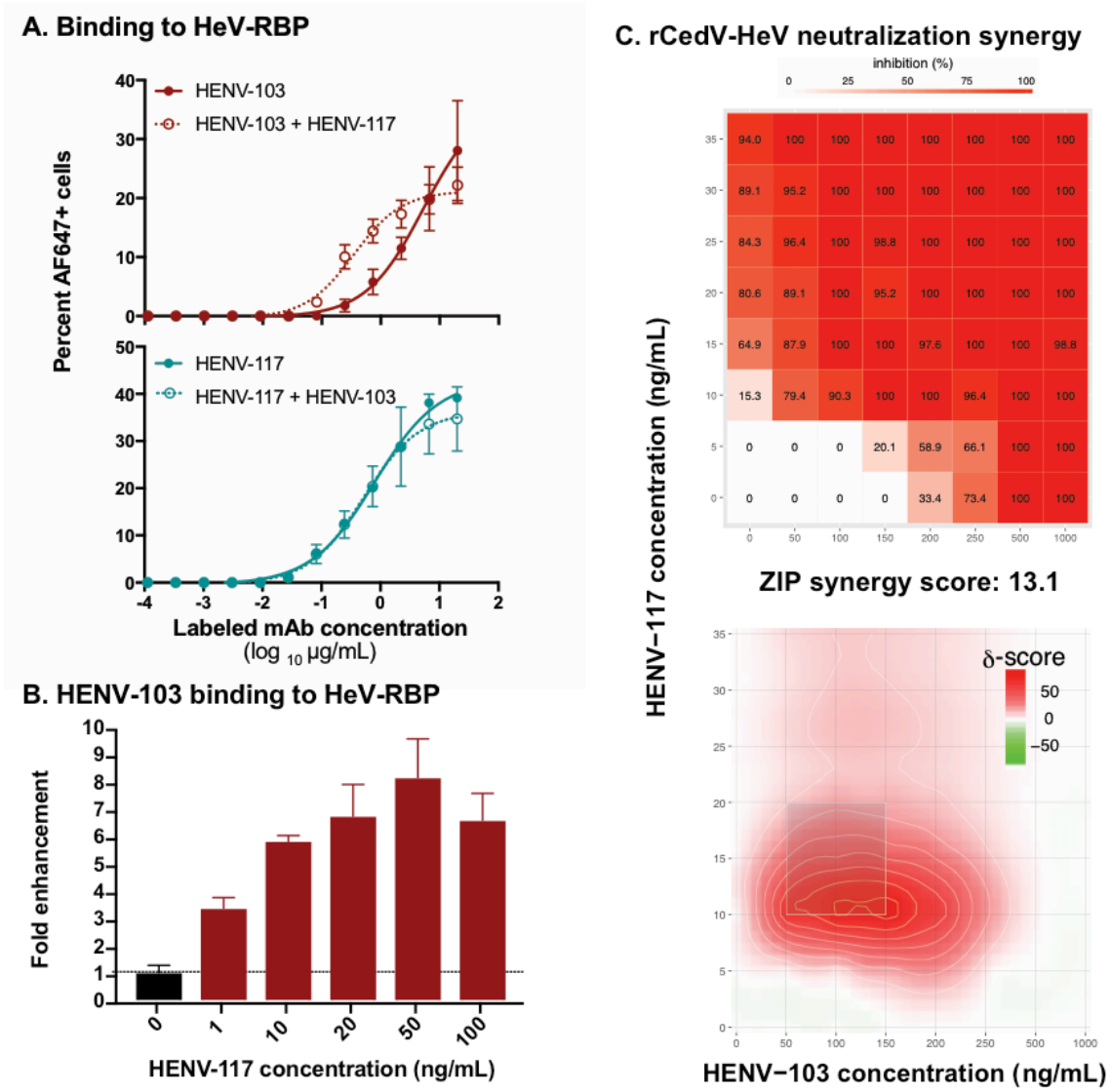

Figure 3-7: Cooperativity in binding and synergy in neutralization by HENV-103 and HENV-117. A) Cooperative binding by HENV-103 and HENV-117 to cell-surface-displayed HeV-RBP. Cells expressing HeV-RBP were incubated with unlabeled HENV-103 or HENV-117, followed by addition of a dilution series of Alexa Fluor 647 (AF647) -labeled HENV-103 or HENV-117. Cells were analyzed by flow cytometry and gated for AF647-positive cells. Data were pooled from 3 independent experiments. **B)** Dependence of HENV-117 effective concentration on HENV-103 binding enhancement. Cells were incubated with varying concentrations of unlabeled HENV-117, followed by incubation with AF647-labeled HENV-103 at 0.5 µg/mL, with enhancement calculated by comparing AF647+ cells to HENV-103 binding to HeV-RBP in the absence of HENV-117. Representative data from 3 independent experiments are shown. **C)** Synergistic neutralization of rCedV-HeV by HENV-103 and HENV-117 combinations. Neutralization values at each matrix concentration (top) and calculated synergy scores (bottom) are shown. Serial dilutions of HENV-103 and HENV-117 were mixed with 4,000 PFU rCedV-HeV-GFP for 2 hours, followed by addition to Vero E6 cell monolayers in 96 well plates. Formalin fixed cells were imaged using a CTL S6 analyzer to count GFP+ cells. Neutralization was calculated by comparing treatment to virus-only control wells. Values were imported into SynergyFinder using a Zero Interactions Potency (ZIP) statistical model. Delta scores >10 indicate likely synergy. Two independent experiments were performed, with data from a single representative experiment shown.

Antibody cocktails and derivative bispecific mAbs provide improved therapeutic activity in hamsters.

Synergy observed *in vitro* by HENV-103 and HENV-117 against VSV-NiV_B and rCedV-NiV_B suggested the potential for *in vivo* synergistic protection from NiV_B infection. To assess this possibility, we took two separate approaches. In the first approach, we tested HENV-103 and HENV-117 as a cocktail therapy in Syrian golden hamsters. Previously, animals were treated with 10 mg/kg for each individual mAb. In this study, animals were treated with 5 mg/kg HENV-103 and 5 mg/kg HENV-117 at 24 hours after intranasal inoculation with NiV_B. Using monotherapy, we found that 3 of 5 animals treated with either HENV-103 or HENV-117 survived throughout the study. However, when given in combination, all animals survived and maintained/gained weight for 28 days after infection (**Figure 5B)**. These data show that HENV-103 and HENV-117 provide synergistic protection in hamsters when administered together 24 hours after infection with NiV_B.

The second approach used two bispecific antibody platforms. The dual variable domain (DVD) construct bears two heavy and light chain variable domains in each "arm," with the domains most Fc-distal corresponding to HENV-117 (Wu, Ying et al. 2007). A similar construct, termed Bis4Ab, differs from DVD in that the Fc-distal HENV-117 component contains a full Fab fragment, whereas the HENV-103 contains only heavy and light chain variable domains in a Fc-proximal scFv format (Thanabalasuriar, Surewaard et al. 2017, Dimasi, Fleming et al. 2019). We first tested these constructs *in vitro* against VSV-NiV_B and found that both DVD and Bis4Ab constructs strongly neutralized VSV-NiV_B with similar potency (**Figure 5A)**. We again tested these in the Syrian golden hamster model of NiV_B infection and found that in the DVD group,

4/5 hamster survived, while protection in the Bis4Ab group mirrored that of monotherapy, with 3/5 hamsters surviving. These data suggest that there may be added complexity to using bispecific antibody platforms (whether or not both antigen binding fragments can engage antigen simultaneously, serum half-life in rodents, etc.) and that combined administration of HENV-103 and HENV-117 provides superior *in vivo* protection in comparison to monotherapy. This feature is complemented by the added benefit of further protection from escape mutation.

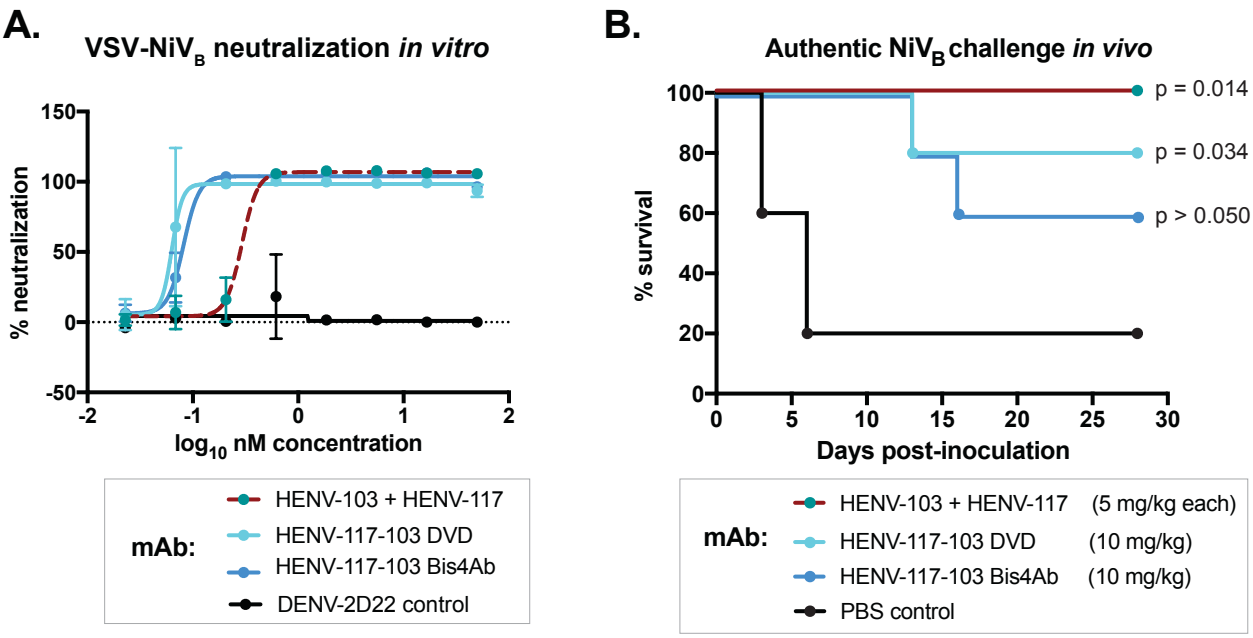

Figure 3-8: Therapeutic protection by antibody cocktails and corresponding bispecific antibodies A) Neutralization of VSV-NiV$_B$ by bispecific antibodies in comparison to equimolar antibody cocktail. Representative data from two independent experiments is shown, each performed in technical triplicate. **B)** Syrian golden hamster challenge studies with HENV-103 and HENV-117 cocktail or corresponding bispecific antibodies. Challenge studies were performed as described above. P values represent statistical significance as determined by Mantel-Cox log rank test. N=5 animals were included in all groups, with control animals treated with PBS at 24 hours post-inoculation.

DISCUSSION

Recent epidemics of Ebola, 2009 H1N1 influenza, and SARS-CoV-2 viruses highlight the need for the development of countermeasures against emerging viruses with pandemic potential before their occurrence. Pathogenic henipaviruses, particularly NiV, are emerging and highly pathogenic agents with confirmed human-to-human transmission for which licensed treatments or vaccines for human use do not yet (Amaya and Broder 2020). In this study, we isolated a panel of mAbs specific for the henipavirus RBP glycoprotein from an individual with prior occupation-related exposure to equine HeV-RBP subunit vaccine. Competition-binding and HDX-MS studies identified at least six distinct antigenic sites recognized by these mAbs. Flow cytometric studies with surface-displayed HeV-RBP showed that potently neutralizing, cross-reactive antibodies either a) blocked HeV-RBP binding to ephrin-B2, or b) showed enhanced binding in the presence of ephrin-B2. Antibodies that block receptor binding also induced the "receptor-enhanced" phenotype, showing that antibodies to these two classes cooperate for binding to HNV-RBP. In addition, these mAbs also showed synergy in neutralization of rCedV-HeV particles. As monotherapy, "receptor-blocking" and "receptor-enhanced" antibodies provided modest protection in a stringent, highly lethal NiV_B challenge model in Syrian golden hamsters. In combination, these antibodies provided complete therapeutic protection in the same model of infection.

A significant concern when using antibodies as therapeutics against emerging infectious diseases due to RNA viruses is the potential for viral 'mutational escape' within an infected host or immune evasion by divergent viral variants. Escape from antibody-mediated neutralization has

been documented even with ultrapotent mAbs targeting conserved epitopes on viral glycoproteins (Greaney, Starr et al. 2020). Using a cocktail of mAbs provides resistance against escape, with the potential added benefit of synergistic antiviral potency, allowing for lower dosing. The potential for spillover of divergent variants of bat-borne paramyxoviruses (henipaviruses and rubulaviruses) is consistent with the inherent propensity of RNA viruses for rapid evolution. Furthermore, flying foxes serve as ideal reservoir hosts because of their dense community roosting patterns and relative resistance to paramyxoviral disease (Baker, Todd et al. 2012, Drexler, Corman et al. 2012, Sasaki, Setiyono et al. 2012, Barr, Smith et al. 2015, Luis, O'Shea et al. 2015, Vidgen, de Jong et al. 2015, Peel, Wells et al. 2019). The discovery of protective antibodies highlighted here, specifically HENV-103 and HENV-117, offer the opportunity to construct a cocktail of antibodies with most-desired protective properties including against mutation escape and spillover variant viruses. Concurrently, a bispecific antibody with activity of both HENV-103 and HENV-117 is an attractive therapeutic option that endows a single therapeutic molecule with the synergistic potency of two individual mAbs. While we showed that two antibodies targeting RBP offer a synergistic benefit, the possibility exists that having antibodies targeting both RBP and F may provide also be of benefit. Recently, highly potent and protective anti-F antibodies have been described and may offer an ideal partner to HENV-103, HENV-117, or both as a triple antibody cocktail (Dang, Chan et al. 2019, Mire, Chan et al. 2020).

As with other paramyxoviruses, humans likely elicit highly functional antibodies against the henipavirus F glycoprotein (Merz, Scheid et al. 1980). This concept is highlighted by palivizumab, an anti-F antibody used as a prophylaxis for premature infants to protect from

infection by respiratory syncytial virus (Meissner, Welliver et al. 1999). Although, as highlighted above, protective anti-F mAbs have been isolated, these have been uniformly of murine origin. The full antigenic landscape of the henipavirus F protein may suggest new sites of vulnerability to neutralization by mAbs and could guide the rational design of henipavirus vaccines. This opportunity is especially important considering the geographical range of henipaviruses, and the fact that a previously undescribed virus from this genus may emerge to cause a pandemic. Having knowledge of the determinants of neutralization for both RBP and F will allow for quick mobilization of platform technologies to develop vaccines, similar to what we have seen in the response to the SARS-CoV-2 pandemic (Zost, Gilchuk et al. 2020).

Wild-type mice are understood to be refractory to infection with henipaviruses. On the contrary, the Syrian golden hamster model of henipavirus infection has been demonstrated to recapitulate the most salient features of human disease, including the biphasic pulmonary disease followed by catastrophic neurological events (Rockx, Brining et al. 2011), making it an ideal model to screen vaccines and therapeutics. However, hamsters require an orders of magnitude higher challenge dose in order to achieve lethal disease compared to ferrets or African Green monkeys (AGM). This requirement likely contributes to a much faster disease progression and a conceivably shorter therapeutic window. Ferrets, and optimally, AGM are likely superior animal models to further preclinical development of these promising antibody candidates. This possibility is especially true of the AGM model of NiV_B infection, in which the therapeutic window for use of antibody therapies (treatment at days 3 to 5) is shorter than that of HeV and NiV_M (treatment at days 5 to 7) (Mire, Satterfield et al. 2016). Studies in these models might further elucidate if

HENV-103 and HENV-117 are improved compared to previously described antibodies (Playford, Munro et al. 2020).

Here, and in previous studies, functional anti-henipavirus RBP-specific mAbs from multiple species have been isolated. These antibodies uniformly recognize the head domain of RBP, suggesting this region is likely the most immunogenic domain of the RBP. Multiple studies interrogating the function of RBP, and its role in triggering the F protein to undergo significant conformational rearrangements, have pointed to the RBP stalk domain as playing a significant role in viral fusogenicity. Specifically, Aguilar *et al.* have shown that the C-terminal portion of the NiV stalk domain can trigger fusion of membranes in the absence of a head domain (Liu, Stone et al. 2013). While it is likely that the stalk domain, which is partially obstructed by the head domain, is immunogenically subdominant, it is possible that rare, circulating memory B cells harboring antibodies targeting this domain exist. Future studies interrogating the antibody response to these viruses also may shed light on the role of mAbs targeting the stalk domain of HNV-RBP, and whether these antibodies have the potential to prevent viral and host membrane fusion.

METHODS

Generation of humAbs

Peripheral blood mononuclear cells (PBMCs) from a human subject were isolated from whole blood and transformed using Epstein-Barr virus (EBV), as previously described (Crowe 2017). Briefly, transformed B cells were expanded and co-cultured with irradiated human PBMCs in 96-well plates. Cell supernatants were screened by ELISA using recombinant HeV-RBP or NiV-RBP head domain proteins. Wells with positive reactivity then were fused to a human-mouse heteromyeloma cell line (HMMA 2.5) and plated by limiting dilution in 384-well plates. The resulting hybridomas were cloned as single cells by fluorescence-activated cell sorting (FACS) to produce clonal hybridoma cell lines. These clonal hybridoma cells were cultured in T-225 flasks containing serum-free medium, and mAb was purified from spent medium by affinity chromatography on an ÄKTA^{TM} pure Fast Protein Liquid Chromatography (FPLC) instrument (GE Healthcare).

Generation of bispecific mAbs

Bispecific mAbs that combined the antigen binding domains of HENV-117 and HENV-103 into a single molecule were designed, expressed, and purified as follows. The heavy chain of the HENV-117-103 DVD combines the heavy chain variable domains of first HENV-117, then HENV-103, each separated by a flexible linker, and then followed by the IgG1 human constant heavy chain domains. Similarly, the light chain of the HENV-117-103 DVD includes the light chain variable domains of both HENV-117 and HENV-103, separated by a flexible linker and then followed by a single human kappa light chain constant domain which naturally pairs with

the corresponding DVD heavy chain. The HENV-117-103 Bis4Ab was constructed by inserting a HENV-103 single-chain variable fragment (scFv) between CH_1 and CH_2 of the HENV-117 heavy chain. The HENV-103 scFv in the bis4Ab format contains a poly glycine-serine linker between its variable domains, and the scFv unit is also flanked by poly glycine-serine linkers. The modified heavy chain is then paired with the standard HENV-117 light chain for expression and purification (Dimasi, Fleming et al. 2019). The heavy and light chains of the HENV-117-103 DVD and the HENV-117-103 Bis4Ab were cloned into pcDNA3 expression vectors. For each of the bispecific mAbs, the corresponding heavy and light chain plasmids were chemically co-transfected into ExpiCHO cells (Gibco) and transiently expressed for 9 days. The supernatant was then clarified by centrifugation and filtration, prior to loading onto a MabSelect SuRe Protein A (GE Healthcare) affinity chromatography column using an ÄKTA™ Fast Protein Liquid Chromatography (FPLC) instrument (GE Healthcare). The column was washed with 1X PBS, and the mAbs were eluted with IgG Elution Buffer (Pierce). Following neutralization with 1 M Tris pH 8.0 to pH ~7, the eluates were concentrated to 5 mg/ml in an Amicon 30K MWCO centrifugal filter (Millipore), and then sterile-filtered using a 0.22 μM syringe filter (Millex-GP).

HeV and NiV viruses

NiV number 1999011924 was obtained from a patient from the 1999 outbreak in Malaysia. The isolate of NiV_B used was 200401066 and was obtained from a fatal human case during the outbreak in Rajbari, Bangladesh in 2004 and passaged on Vero E6 cell monolayer cultures three times. HeV was obtained from a patient from the 1994 outbreak in Australia. All viruses were kindly provided by Dr. Thomas Ksiazek, UTMB. Each virus was propagated on Vero E6 cells in Eagle's minimal essential medium supplemented with 10% fetal calf serum. The NiV_M, NiV_B and HeV challenge

virus stocks were assessed for the presence of endotoxin using The Endosafe-Portable Test System (PTS) (Charles River Laboratories, Wilmington, MA). Each virus preparation was diluted 1:10 in Limulus Amebocyte Lysate (LAL) Reagent Water per the manufacturer's instructions, and endotoxin levels were tested in LAL Endosafe-PTS cartridges as directed by the manufacturer. Each preparation was found to be below detectable limits, whereas positive controls showed that the tests were valid. All experiments involving infectious henipaviruses were carried out at the UTMB Galveston National Laboratory under biosafety level 4 conditions.

Neutralization assays

The virus neutralizing activity concentrations were determined for NiV_M, NiV_B, and HeV using a plaque reduction assay. Briefly, antibodies were diluted two-fold from 100 μg/mL to extinction and incubated with a target of ~100 plaque-forming units (pfu) of NiV_M, NiV_B, or HeV for 45 min at 37 °C. Virus and antibody mixtures then were added to individual wells of six-well plates of Vero 76 cell monolayer cultures. Plates were fixed and stained with neutral red two days after infection, and plaques were counted 24 h after staining. Neutralization potency was calculated based on pfu for each virus in the well without antibody. The neutralization experiments were performed in triplicate, with independent virus preparations and duplicate readings for each replicate. Mean half-maximal inhibitory concentration (IC_{50}) values were calculated as previously described (Ferrara and Temperton 2018).

Surface plasmon resonance (SPR) epitope binning

A continuous flow micro-spotter (CFM) instrument (Carterra) was used to generate antibody-coated SPR sensor chips (Xantec) (Abdiche, Miles et al. 2014). Briefly, mAbs were diluted to 10 μg/mL in sodium acetate pH 4.5 in a 96-well round bottom plate. A mirroring 96-well plate containing activation buffer (EDC and sulfo-NHS in 10 mM MES pH 5.5) was used first to activate the gold-plated surface of the sensor chip, followed by association of antibodies. The coated chip then was moved to an IBIS-MX96 microarray-based surface plasmon resonance imager (Carterra), where it was quenched with 1 M ethanolamine to prevent further coupling of proteins. To bin antibodies, 100 mM HeV-RBP head domain was flowed over the coated sensor chip. One-by-one, antibodies diluted to 10 μg/mL were tested for their ability to associate with antigen captured on the sensor chip. Carterra Epitope software was used to analyze data and construct competition-binding grids.

Hydrogen-deuterium exchange mass spectrometry (HDX-MS) of Fab-HeV-RBP complexes

HDX-MS was performed as previously reported (Bennett, Bombardi et al. 2019). Briefly, antigen (HeV-RBP) and selected mAbs were prepared individually or in complex at a protein-concentration of 10 pmol/μL in 1× PBS pH 7.4 and incubated for 2 h at 0 °C. Deuterium labeling was performed by a 20-fold dilution of 3 μL sample in PBS pH 7.4 in D_2O and incubation at 20 °C for 0 s, 100 s, and 1,000 s. The reaction was quenched by a 2-fold dilution in 1× PBS, 4 M guanidinium/HCl, 100 mM tris(2-carboxyethyl)phosphine to a final pH of 2.3 at 0 °C. Samples were injected immediately into a nano-ACQUITY UPLC system controlled by an HDX manager (Waters Corporation, Milford, MA, USA). Online pepsin digestion was performed at 15 °C, 10,000 psi at a flow of 100 μL/min of 0.1% formic acid in H_2O using an immobilized-pepsin

column. A Waters VanGuard™ BEH C18 1.7 μm guard column was used to trap peptides at 0 °C for 6 min before separation on a Waters ACQUITY UPLC BEH C18 1.7 μm, 1 mm × 100 mm column at a flow of 40 μL/min at 0 °C with a 6 min gradient of 5 to 35% acetonitrile, 0.1% formic acid in H_2O. UPLC effluent was directed into a Waters Xevo G2-XS with electrospray ionization and lock-mass acquisition (human Glu-1-Fibrinopeptide B peptide, m/z=785.8427) for peptide analysis in MS^E-mode. The capillary was set to 2.8 kV, source-temperature to 80 °C, desolvation temperature to 175 °C, desolvation gas to 400 L/h and the instrument was scanned over a m/z-range of 50 to 2000. All experiments were carried out in triplicate. Data analysis was accomplished using Waters ProteinLynx Global Server 3.0.3 software (non-specific protease, min fragment ion matches per peptide of three, FDR 4% and oxidation of methionine as a variable modification) for peptide identification and DynamX 3.0 software (minimum intensity of 500, minimum products 3, minimum products per amino acid 0.3 and a mass error < 15 ppm) for deuterium uptake calculations. Results are reported as an average of triplicate analyses.

Generation of VSV pseudotyped viruses bearing NiV_B glycoproteins

Recombinant VSVs containing genomic inserts for expression of NiV_B G and F proteins were kindly provided by Chad Mire and generated as previously described (Mire, Geisbert et al. 2019). Stocks of each rVSV were propagated and titrated on VSV-G transfected BHK-21 (WI-2), with viral titers determined by counting GFP+ cells using a CTL S6 Analyzer instrument (company/). To generate virus bearing both G and F glycoproteins, cells were inoculated with each VSV at MOI=5 and incubated for 48 hours. Cell supernatants were clarified by centrifugation. Resulting VSV-NiV_B was titrated on Vero cell monolayers using an

xCELLigence instrument to determine the lowest virus concentration that would induce CPE as measured by cell impedance.

Cooperative binding of antibodies to antigen displayed on the surface of cells

A construct containing cDNA encoding full-length HeV-RBP protein was transfected using polyethylenimine into 293F cells, and cells were cultured at 37 °C in 5% CO_2 for 3 days. Cells subsequently were plated at 50,000 cells/well in V-bottom 96-well plates, washed, and incubated with either 20 μg/mL primary mAb in 30 μL or FACS buffer alone for 30 minutes at 4 °C. Without washing, 30 μL serially diluted mAb labeled with Alexa Fluor 647 dye (ThermoFisher) was added to wells and incubated for 30 minutes at 4 °C. Cells were washed and resuspended in FACS buffer and analyzed using an iQue Plus flow cytometer (Intellicyt). Dead cells were excluded from analysis by fluorescent staining with 4′,6-diamidino-2-phenylindole (DAPI).

Negative stain electron microscopy

For electron microscopy imaging of HeV-RBP protein and Fabs complex, we expressed the HeV-RBP full ectodomain (head domain with intact stalk domain) with a C-terminal polyhistidine tag. Expressed protein was isolated by metal affinity chromatography on HisTrap Excel columns (GE Healthcare), followed by GraFix methods using a 10% to 30% glycerol gradient and 0 to 0.1% glutaraldehyde gradient (Stark 2010). Glutaraldehyde was quenched with 1 M Tris-Cl after fractionation. 200 μL fractions were analyzed by SDS-PAGE, with fractions corresponding to monomeric, dimeric, and tetrameric species pooled. Protein was then buffer exchanged into 50 mM Tris-Cl pH 7.5 containing 140 mM NaCl. Fabs corresponding to HENV-103 and HENV-117 were expressed and purified as previously described. Protein complexes

were generated by incubation of HeV-RBP_{ecto} dimer and the two Fab in a 1:5:5 molar ratio overnight at 4 °C. Approximately 3 µL of the sample at ~10 to 15 µg/mL was applied to a glow-discharged grid with continuous carbon film on 400 square mesh copper electron microscopy grids (Electron Microscopy Sciences). Grids were stained with 0.75% uranyl formate (Ohi, Li et al. 2004). Images were recorded on a Gatan US4000 4k × 4k CCD camera using an FEI TF20 (TFS) transmission electron microscope operated at 200 keV and control with SerialEM. All images were taken at 62,000× magnification with a pixel size of 1.757 Å per pixel in low-dose mode at a defocus of 1.5 to 1.8 µm. The total dose for the micrographs was ~35 e− per $Å^2$. Image processing was performed using the cryoSPARC software package. Images were imported, CTF-estimated and particles were picked automatically. The particles were extracted with a box size of 256 pixels and binned to 128 pixels (pixel size of 3.514 A/pix) and 2D class averages were performed to achieve clean datasets. Classes were further classified (2D) to separated different complex variant and classes having the 2 Fab on one RBP domain were selected. *Ab-initio* was used to generate initial 3D volume that was further refined with a mask over one RBP-Fabs complex. The final refine volume has a resolution of ~15Å. Model docking to the EM map was done in Chimera (Pettersen, Goddard et al. 2004). For the RBP head domain PDB: 6PDL was used and for the Fab PDB:12E8 or the prediction model of the Fv that was generated by SAbPred tool was used (Dunbar, Krawczyk et al. 2016). The 3D EM map has been deposited into EMDB (EMDB XXX). Chimera software was used to make all structural figures.

Neutralization synergy of rCedV chimeric viruses

Recombinant Cedar virus (rCedV) chimeras displaying RBP and F proteins of HeV or NiV_B were generated and validated as described elsewhere. Black-walled 96-well plates (Corning Life

Sciences; NY, USA) were coated with 20,000 cells/well Vero E6 cells in DMEM + 10% Cosmic calf serum and incubated overnight. Approximately 24 hours later, HENV-103 and HENV-117 were diluted to indicated concentrations and incubated 1:1 with 4,000 PFU/well rCedV-HeV-GFP or rCedV-NiV_B-GFP and incubated for 2 hours at 37 °C. Following incubation, 90 µL virus/antibody mixtures were added to aspirated cell monolayers and were incubated at 37 °C for 22 hours. Medium containing virus/antibody mixtures was aspirated, and cells were fixed with 100 µL/well 4% formalin for 20 minutes at room temperature. After aspiration, cell monolayers were gently washed 4x with DI water. Formalin-fixed plates were then scanned using the CTL S6 analyzer (Cellular Technology Limited; OH, USA). Fluorescent foci were counted using the CTL Basic Count™ feature and S6 software. Percent neutralization was calculated by normalizing counts to a virus only control. Matrices were then imported into SynergyFinder and analyzed as described before.

Antibody therapy in Syrian golden hamster model of Nipah Bangladesh

3-to-5 week-old Syrian golden hamsters were inoculated with 5 x 10^6 PFU Nipah Bangladesh (passage 3) via the intranasal route. At 24 hours post challenge, 5 animals per group were treated with 10 mg/kg antibody by intraperitoneal administration. Animals were monitored for 28 days for changes in weight, temperature, and clinical appearance. Animals were humanely euthanized at the experimental endpoint. A single untreated animal served as a control in each study highlighted.

CHAPTER IV

A NOVEL SITE OF NEUTRALIZATION VULNERABILITY ON THE STALK DOMAIN OF THE HENIPAVIRUS RECEPTOR BINDING PROTEIN

Contributions: Nurgun Kose and I isolated HENV-270. I performed binding assays, mechanistic assays, alanine scanning mutagenesis, and protein purification for HeV-RBP. Robert Cross performed BSL-4 *in vitro* and *in vivo* studies. VU Mass Spectrometry core peformed HDX-MS studies. Elad Binshtein performed EM studies.

INTRODUCTION

Hendra virus (Guirakhoo, Pugachev et al.) and Nipah virus (NiV) of the genus *Henipavirus* are high consequence pathogens recently appreciated for their ability to cause severe disease in humans. NiV has caused sporadic outbreaks of respiratory and neurological disease resulting in fatality rates as high as 90% (Spiropoulou 2019). Documented human-to-human transmission has occurred in recent outbreaks in geographically new regions of India, and there is a new appreciation for the widespread shedding of virus by *Pteropus* species bats (Arunkumar, Chandni et al. 2019). These concerns have prompted the World Health Organization to prioritize henipaviruses as an epidemic threat in the R&D Blueprint, a tool that distinguishes which diseases pose the greatest public health risk due to their epidemic potential and the insufficient availability of countermeasures (Sweileh 2017). Despite this designation, only a limited number of therapeutic candidate molecules have progressed into clinical trials, and approved vaccines are not available for widespread vaccination campaigns. A more thorough understanding of the human immune responses to these viruses and more advanced development of candidate therapeutics and vaccines is needed.

Henipavirus is a genus of enveloped, negative-sense single-stranded RNA viruses in the family *Paramyxoviridae*, subfamily *Orthomyxovirinae*. The genomes of HeV and NiV encode for six structural proteins: RdRp (L), nucleoprotein (N), phosphoprotein (P), matrix protein (M), receptor binding protein (RBP; formerly designated G, for glycosylated), and the fusion protein (F) (Rima, Balkema-Buschmann et al. 2019). The P gene, via RNA editing and an alternate reading frame, also codes for the IFN-antagonizing V, W, and C proteins (Satterfield, Cross et al. 2015). The two membrane-bound proteins responsible for attachment and entry into host cells are RBP and F. RBP, as suggested by the name, mediates attachment to the host cell receptors ephrin-B2 and ephrin-B3 (Xu, Broder et al. 2012). These receptor tyrosine kinases are widely expressed in the vascular endothelium, and ephrin-B3 is abundant in the central nervous system (Benson, Romero et al. 2005). Upon attachment to one of these ephrin receptors, conformational rearrangements, thought to include the flexing of head domains into a "heads up" position, expose the C-terminal region of the alpha-helical stalk domain (Liu, Stone et al. 2013). This domain acts to trigger the class I fusion protein F, provoking it to undergo massive structural changes from a pre-fusion to post-fusion conformation (Xu, Chan et al. 2015). This conformational cascade exposes the hydrophobic fusion peptide, which inserts into the host cell membrane creating a pore through which the RNA genome enters the host cell.

With the exception of internal targets for small-molecule inhibitors including nucleoside analogs, the primary druggable targets of henipaviruses are RBP and F (Lo, Feldmann et al. 2019). Antibody therapeutic and vaccine discovery efforts have focused on these two membrane-anchored glycoproteins, as these are also the primary targets of the human humoral response to

infection. Two of the most promising vaccine candidates for henipaviruses are composed of soluble, recombinant RBP or F proteins (Loomis, Stewart-Jones et al. 2020, Geisbert, Bobb et al. 2021). The RBP candidate vaccine has begun testing in phase I clinical trials and is used on a regular basis as an equine vaccine in Australia . Antibody discovery campaigns by multiple groups have resulted in candidate therapeutic antibodies targeting either RBP or F. The antibodies 5B3 and mab66, for example, both target the pre-fusion conformation of F and have shown efficacy in animal models of NiV infection (Avanzato, Oguntuyo et al. 2019, Dang, Chan et al. 2019). The mAbs for which protective capacity are best demonstrated, however, are those targeting RBP. A humanized murine monoclonal antibody designated m102.4 blocks receptor binding, has shown efficacy in several animal models of HeV or NiV infection, and has been used on an emergency use basis in multiple human subjects with high risk for developing henipavirus disease (Zhu, Bossart et al. 2008, Bossart, Geisbert et al. 2011, Geisbert, Mire et al. 2014). In previous chapters, I described work characterizing antibodies that primarily target the head domain, with humoral immunity to the stalk domain still to be investigated.

While studies to date have provided numerous vaccine and therapeutic candidates and have identified several sites of vulnerability for neutralization on both F and RBP, much is still unknown about the full antigenic landscape of RBP. All antibodies discovered against RBP to date target structures on the immunodominant head domain formed within a single RBP protomer. The discovery of mAbs recognizing quaternary epitopes spanning multiple head domains or mAbs targeting the stalk domain has not been reported, but such responses likely occur given the discovery of such antibodies in many other virus systems. To address this gap in knowledge, we used a differential antigen screening approach to discover antibodies targeting

the stalk domain using B cells from a human subject with prior occupation-related exposure to the HeV equine vaccine. One mAb we identified, termed HENV-270, binds only to the full-length RBP ectodomain, without detectable reactivity to the head domain. HENV-270 cross-reacts with the RBP of HeV and RBP of both NiV Malaysia (NiV_M) and NiV Bangladesh (NiV_B) lineages and mediated a therapeutic effect in a hamster model of NiV_B infection.

We sought to characterize the full-length ectodomain of HeV-RBP in complex with HENV-270, because this mAb recognized a previously uncharacterized antigenic site that required the presence of the stalk domain for binding. We used a gradient fixation (GraFix) purification scheme to separate HeV-RBP into monomeric, dimeric, or tetrameric species and to limit conformational flexibility of the stalk domain. By negative stain electron microscopy, we solved the structure of HeV-RPB bound to both HENV-270 and ephrin-B2. The structure of the complex revealed a novel site of vulnerability to HENV-270 distal from the receptor binding domain involving stalk domain. Hydrogen deuterium exchange mass spectrometry (HDX-MS) studies indicated an HENV-270 may sterically block regions of the stalk domain distal from the HENV-270 antigenic site. Alanine scanning mutagenesis revealed residues L181 and G183 as critical residues for binding by HENV-270. These residues are located at the C-terminus of the stalk domain, a region that has been implicated in triggering the structural rearrangements of F that are required for fusion of virus and host membranes. These studies provide a full structure of the HeV-RBP ectodomain, reveal a novel site of neutralization vulnerability on the stalk domain, and describe a novel therapeutic antibody candidate against henipavirus disease.

RESULTS

Isolation of HENV-270, a fully human monoclonal antibody that targets an epitope not presented on the HeV-RBP head domain

To date, all reported mAbs isolated against the henipavirus RBP target the globular 6-bladed beta propeller head domain. Recently, synergistic pairs of antibodies targeting the head domain were isolated from a human subject exposed to the HeV equine vaccine Equivac. This subunit vaccine contains the fully oligomeric ectodomain of the RBP including both head and stalk domains. We reasoned that, while previous studies have suggested the stalk is a subdominant domain for human B cell responses, this individual may have generated antibodies targeting this domain in the vaccine antigen. The rationale for seeking such antibodies is that antibodies against this region might reduce viral fusogenicity by preventing RBP from triggering F conformational changes needed for virus-cell membrane fusion. Thus, we sought to isolate mAbs targeting the stalk domain for further studies.

We used a previously described human B cell hybridoma method to isolate mAbs from this human subject with henipavirus immunity (Dong, Cross et al. 2020). To preferentially isolate B cells secreting mAbs targeting novel epitopes not presented on the globular head domain, we used a differential antigen ELISA screening strategy. We screened EBV-transformed B-cell supernatants by ELISA against recombinant, soluble head domain or full ectodomain proteins of HeV-RBP, and pursued isolation of antibody clones that only showed reactivity to the full ectodomain construct. As expected, circulating memory B cells secreting mAbs with these characteristics were rare. We isolated one mAb, HENV-270 that showed robust binding to the

HeV-RBP full ectodomain but did not exhibit detectable binding to head domains from the HeV or NiV-RBPs **(Figure 4-1A).** Using a cell-surface-display receptor competition assay, we found that HENV-270 did not block ephrin-B2, nor was mAb binding enhanced by ephrin-B2, further differentiating this clone phenotypically from previously isolated mAbs **(Figure 4-1B)**.

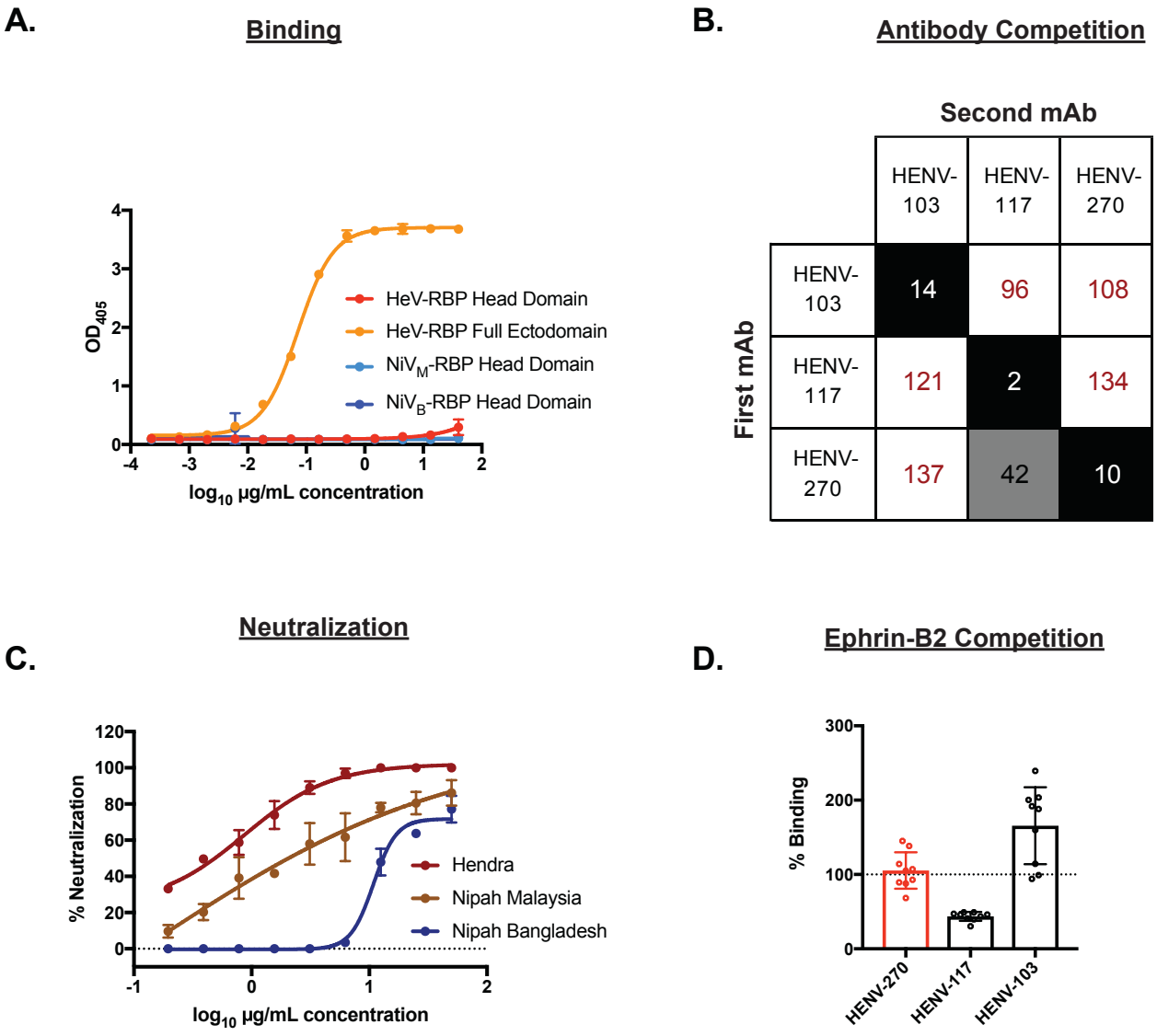

Figure 4-1: Binding and neutralization characteristics of HENV-270 A) Binding of HENV-270 to Hendra RBP full ectodomain (orange), Hendra RBP head domain (red), Nipah Malaysia head domain (light blue), or Nipah Bangladesh head domain (dark blue). **B)** Competition binding to Hendra RBP full ectodomain as assessed by biolayer interferometry. Sensortips were coated in HeV-RBP, with a "first mAb" allowed to bind to antigen. A "second mAb" was then assessed for its ability to bind in the presence of the first antibody. **C)** Neutralization of HeV, NiV_M, or NiV_B by HENV-270 as assessed by plaque reduction neutralization test (PRNT). **D)** Binding of HENV-270 to cell surface displayed HeV-RBP in the presence of host receptor ephrin-B2. Binding is presented as a percentage of residual binding when compared to HENV-270 binding in the absence of ephrin-B2.

We next sought to assess the ability of HENV-270 to neutralize HeV, NiV_M, and NiV_B. In biosafety level 4 conditions, we assessed neutralization potency of HENV-270 against the same three viruses by plaque reduction neutralization tests. While HENV-270 neutralized HeV or NiV_M viruses with half maximal inhibitory concentration (IC_{50}) values of 870 or 153 ng/mL, respectively, this mAb was less potent against NiV_B, with an IC_{50} of 11 μg/mL.

Therapeutic activity of HENV-270 in a stringent hamster model of NiV_B challenge

The Syrian golden hamster model of NiV_B disease represents a highly stringent, small animal model suitable for assessing therapeutic efficacy of small or large molecule drug candidates. Previously, both monotherapy and cocktail/bispecific mAb administration have shown therapeutic benefit at 24 hours after inoculation with a lethal inoculum of NiV_B. We used this model to assess the therapeutic potential of HENV-270. Five hamsters were inoculated intranasally with 5×10^6 plaque forming units of NiV_B. Twenty-four hours after inoculation, animals were administered 10 mg/kg HENV-270 by the i.p. route and monitored for 28 days for changes in weight, temperature, and clinical signs of disease. An untreated hamster served as a contemporary control and 2 historical controls were included in the analysis. As expected, the control animal developed respiratory disease and was euthanized on day +3. All animals in the HENV-270 treatment group survived the first phase of disease and did not develop signs of respiratory disease. Two animals succumbed to disease due to neurological disease during the second phase of disease, while three animals survived the course of the study and maintained/gained weight throughout. Despite the lack of *in vitro* potency against NiV_B, the survival benefit afforded by HENV-270 *in vivo* is comparable to that of the most potent anti-RBP antibodies described to date, including HENV-117, which has an IC_{50} value below 20

ng/mL, nearly 500-fold more potent than HENV-270. These studies highlighted an apparent discrepancy between the *in vitro* neutralizing activity and *in vivo* efficacy for anti-henipavirus antibodies, and identified a new therapeutic candidate antibody against HeV and NiV directed to a new antigenic site.

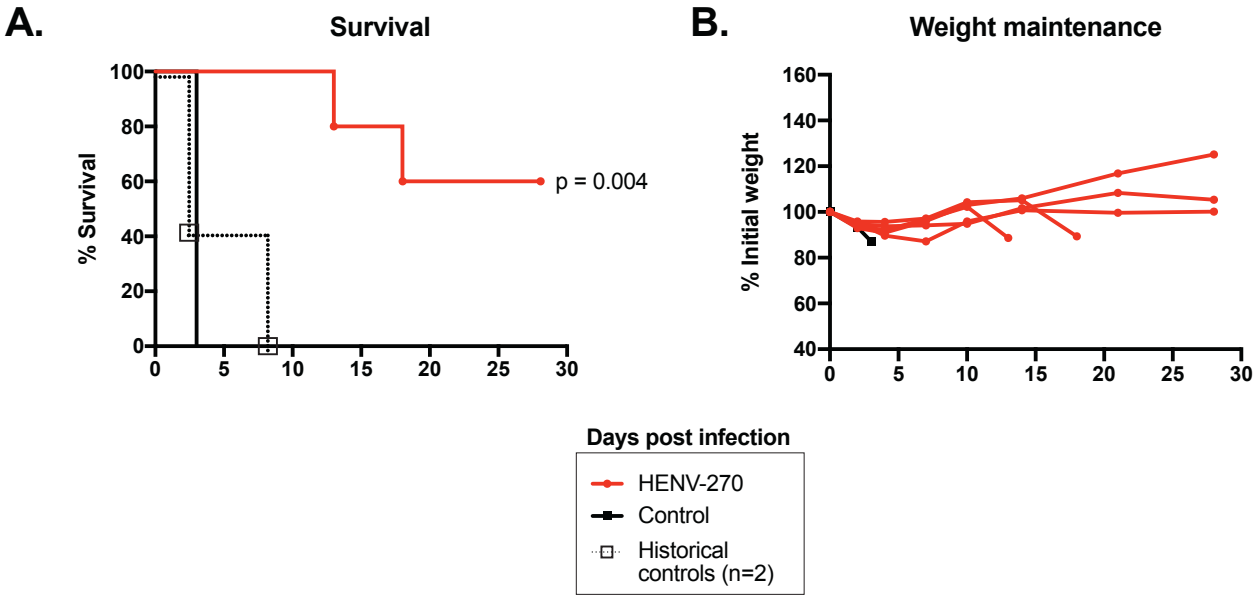

Figure 4-2: Therapeutic protection of NiV-challenged hamsters by HENV-270. Six Syrian golden hamsters were challenged with 5 x 10^6 PFU NiV_B and treated with 10 mg/kg HENV-270 (or n=1 untreated) 24 hours after inoculation. Two historical controls were pooled with the experimental control to perform statistical analysis using Log-Rank Mantel-Cox test.

Structural characterization of HeV-RBP complexed with HENV-270 and ephrin-B2 defines a complex antigenic site encompassing the stalk domain C-terminus

To date, all high-resolution structural characterization of the henipavirus RPB has only elucidated atomic-level structures of the globular head domain. Because HENV-270 requires the intact stalk domain in order to bind at detectable levels, we expressed the full-length ectodomain (head domain +stalk) to use in structural studies. We first employed hydrogen-deuterium exchange mass spectrometry (HDX-MS) studies to identify, at peptide resolution, the region on HeV-RBP bound by HENV-270. We observed nearly identical HDX profiles across two

biological replicates, with a representative map shown **(Figure 4-##)**. The decrease in deuterium exchange observed between residues 30-40 is likely an artifact due to this region of the protein being truncated from the construct used in these studies. As expected based on HENV-270 only showing detectable binding to a construct bearing the stalk domain, we saw a consistent decrease in deuterium exchange in the presence of HENV-270 spanning residues 75-140. This region represents the membrane-proximal portion of the stalk domain, further suggesting HENV-270 binds to the stalk domain of HeV-RBP. Interestingly, we also observed modest decreases in deuterium exchange in multiple regions of the head domain, though these were less pronounced in magnitude. These HDX-MS data suggested HENV-270 binds to the stalk domain. This region has been validated for its functional importance in henipavirus fusion, further suggesting this mAb may function by abrogating the "provocateur" model of henipavirus fusion, wherein fusion inhibition can be accomplished if the C-terminal stalk domain is prevented from interacting with F (Liu, Stone et al. 2013). Interestingly, HENV-270 may also induce some allosteric rearrangements to the RBP head domain, potentially also paying a role in the function of HENV-270.

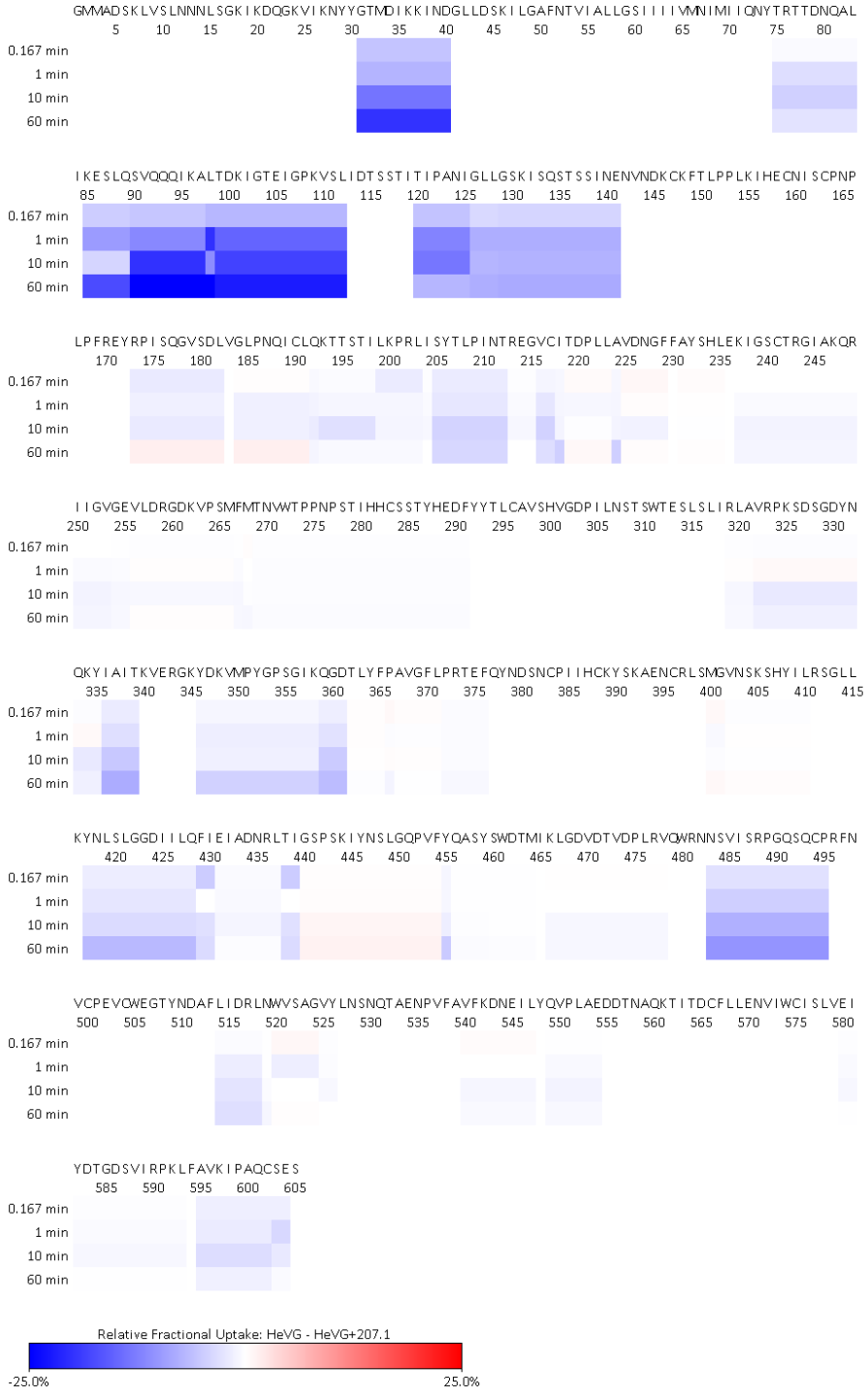

Figure 4-3: Hydrogen-deuterium exchange mass spectrometry (HDX-MS) on HeV-RBP in complex with HENV-270. The full length sequence of HeV-RBP is shown with HDX properties at 1min, 10 min, and 60 min quenches. Blue indicates peptides on RBP that show a decrease in deuterium exchange in the presence of HENV-270. Red indicates an increase in deuterium exchange. Data are representative of two independent experiments.

To better define the antigenic site recognized by HENV-270, we used cryo-electron microscopy (cryoEM) on the full ectodomain construct of HeV-RBP in complex with HENV-270. RBP exhibits structural heterogeneity, and multiple oligomeric species were present after nickel affinity purification of purified recombinant protein that was not resolved by size exclusion chromatography. Therefore, we used gradient fixation to produce RBP suitable for higher resolution structural studies. The full ectodomain of HeV-RBP was overexpressed in Expi293F cells and subsequently purified by Ni-NTA affinity chromatography. At this stage, HeV-RBP was present as species corresponding in apparent molecular weight to soluble monomers, dimers, or tetramers, which re-assembled/disassembled after separation by size-exclusion chromatography. Soluble protein was applied to a 10 to 30% glycerol gradient containing a 0 to 0.1% gradient of the mild fixative glutaraldehyde. A series of 200 µL fractions was taken after ultracentrifugation, quenched with 1M Tris-HCl pH 7.5; after analysis by non-reducing SDS-PAGE, monomeric, dimeric, or tetrameric fractions were pooled **(Figure 4-4A,B)**. Negative-stain EM verified the oligomeric state of each fraction, which was maintained over time without the need for further purification steps (**Figure 4-4C).**

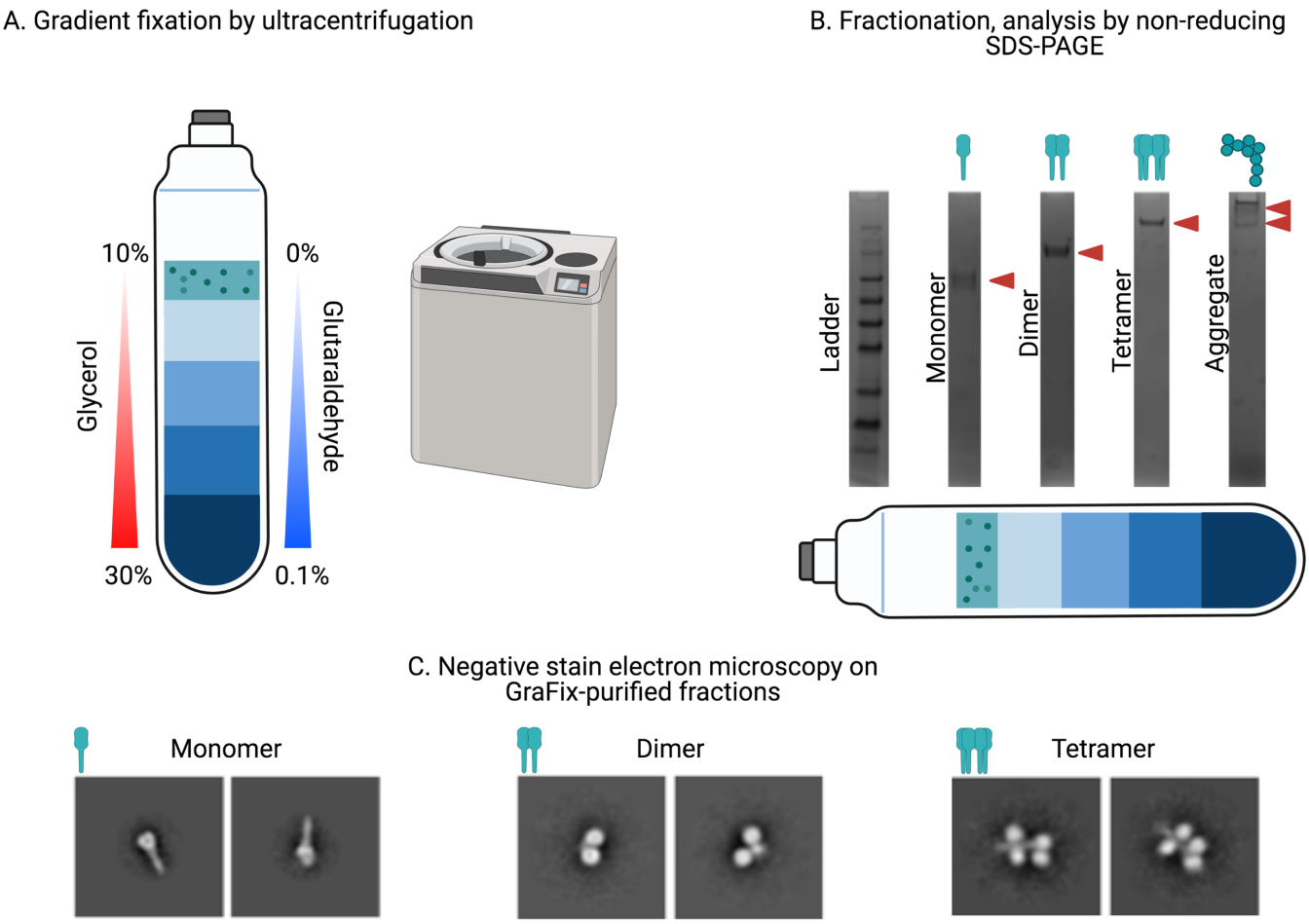

Figure 4-4: Gradient fixation (GraFix) purification of HeV-RBP. A) Schematic for generation of glycerol gradients containing 0-0.1% glutaraldehyde. Protein is overlaid on this gradient and ultracentrifuged to disperse monomeric, dimeric, and tetrameric HeV-RBP species. **B)** Non-reducing SDS-PAGE analysis of 200 µL fractions generated by GraFix. Higher molecular weight complexes migrated to higher glycerol and glutaraldehyde concentrations. **C)** 2D class averages from negative stain electron microscopy performed on fractions corresponding to monomer, dimer, and tetramer HeV-RBP.

To limit complexity, we used monomeric HeV-RBP to create Fab-antigen complexes for cryoEM. We also included soluble, recombinant ephrin-B2 in these complexes to spatially evaluate binding by HENV-270 in relation to receptor binding and increase the complex size and stability. While cryoEM studies are ongoing, we were able to obtain a low-resolution 3D reconstruction using negative stain electron microscopy **(Figure 4-5)**. Because of the conformational flexibility of the stalk domain, coupled to the low resolution provided by this technique, only the head domain of RBP was able to be visualized. Fitting of the crystal structure

of the head domain of HeV-RBP bound to ephrin-B2 showed that HENV-270 Fab binds distal to the receptor binding site, further suggesting HENV-270 does not function by blocking receptor attachment. While only low-resolution reconstruction was obtained, these studies further determined that HENV-270 binds to a novel antigenic site that is distinct from antibodies previously described to be protective *in vivo*.

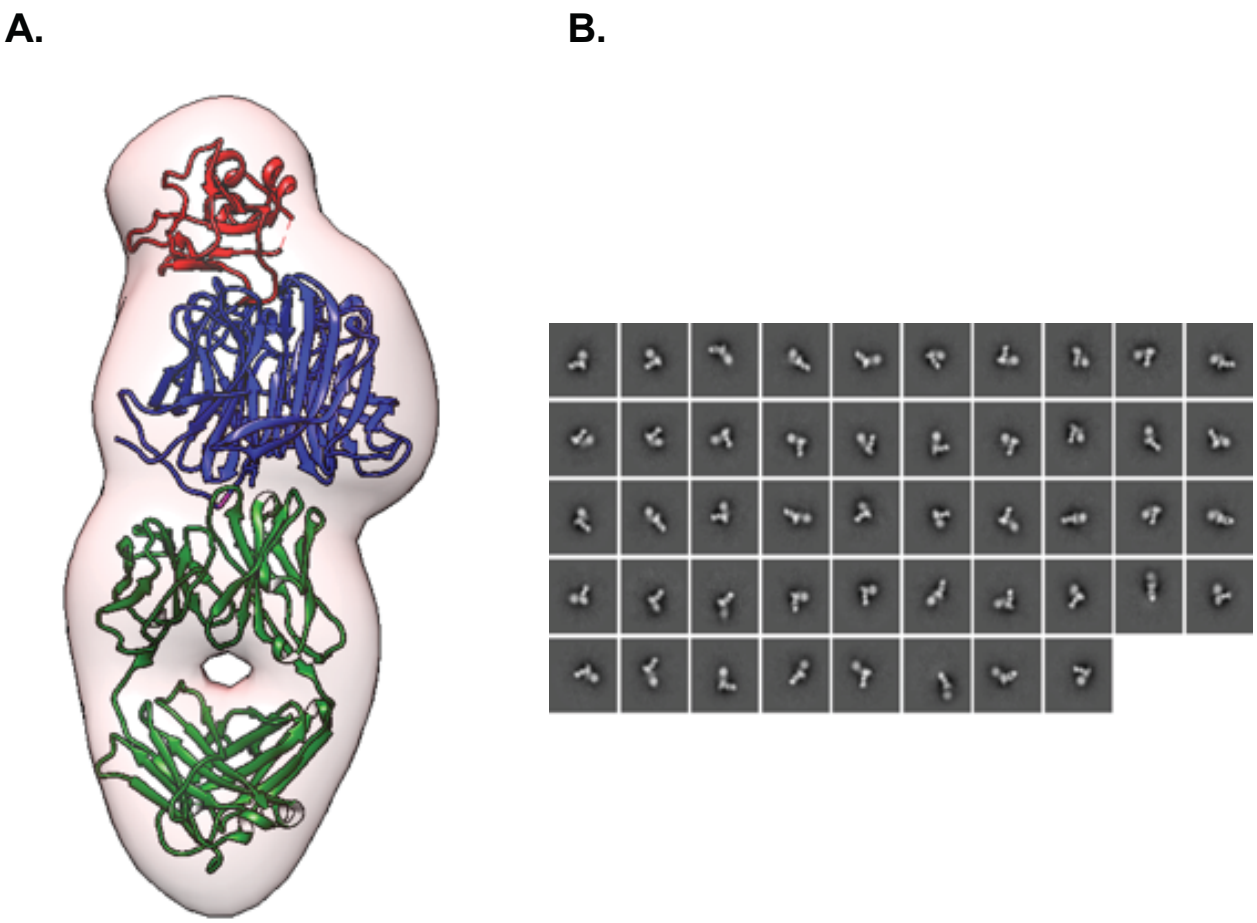

Figure 4-5: Negative stain electron microscopy of HENV-270 bound to receptor-bound HeV-RBP. A) 3D reconstruction of HeV-RBP (blue) bound to HENV-270 Fab (green) and soluble ephrin-B2 (red). **B)** 2D class averages built from 28,276 particles used for 3D reconstruction in A).

Alanine scanning mutagenesis defined stalk residues L181 and G183 on HeV-RBP as critical for binding by HENV-270

To determine which residues in the HeV-RBP:HENV-270 interface are most crucial for binding, we used a cell-surface-display method to screen a scanning alanine mutagenesis library of HeV-RBP constructs. Starting at residue 70 (so as to avoid including the transmembrane or cytoplasmic domains), we changed every residue, one by one, to alanine (or serine if already alanine), and assessed binding of HENV-270 to that variant expressed on the surface of transfected cells. HENV-26 and HENV-32, two mAbs previously characterized for their ability to bind distinct sites on RBP, were used as controls to assure folding and expression of variant RBPs. Across the library, binding by HENV-270 and a cocktail of HENV-26 and -32 correlated strongly. Residues L181 and G183 were bound by the control at levels >70% of binding to WT HeV-RBP, while binding by HENV-270 Fab showed <20% binding to each of the variants. Binding to G183 by HENV-270, specifically, was completely ablated by the alanine substitution. The variant proteins maintained levels of cell-surface expression similar to that of the WT RBP. These substitutions, which can be caused by single nucleotide mutations in henipavirus genome, suggest escape from antibody binding at this position is feasible. Overall, the structure-function analysis determined L181 and G183 in the C-terminus of the HeV-RBP stalk to be critical for binding by HENV-270.

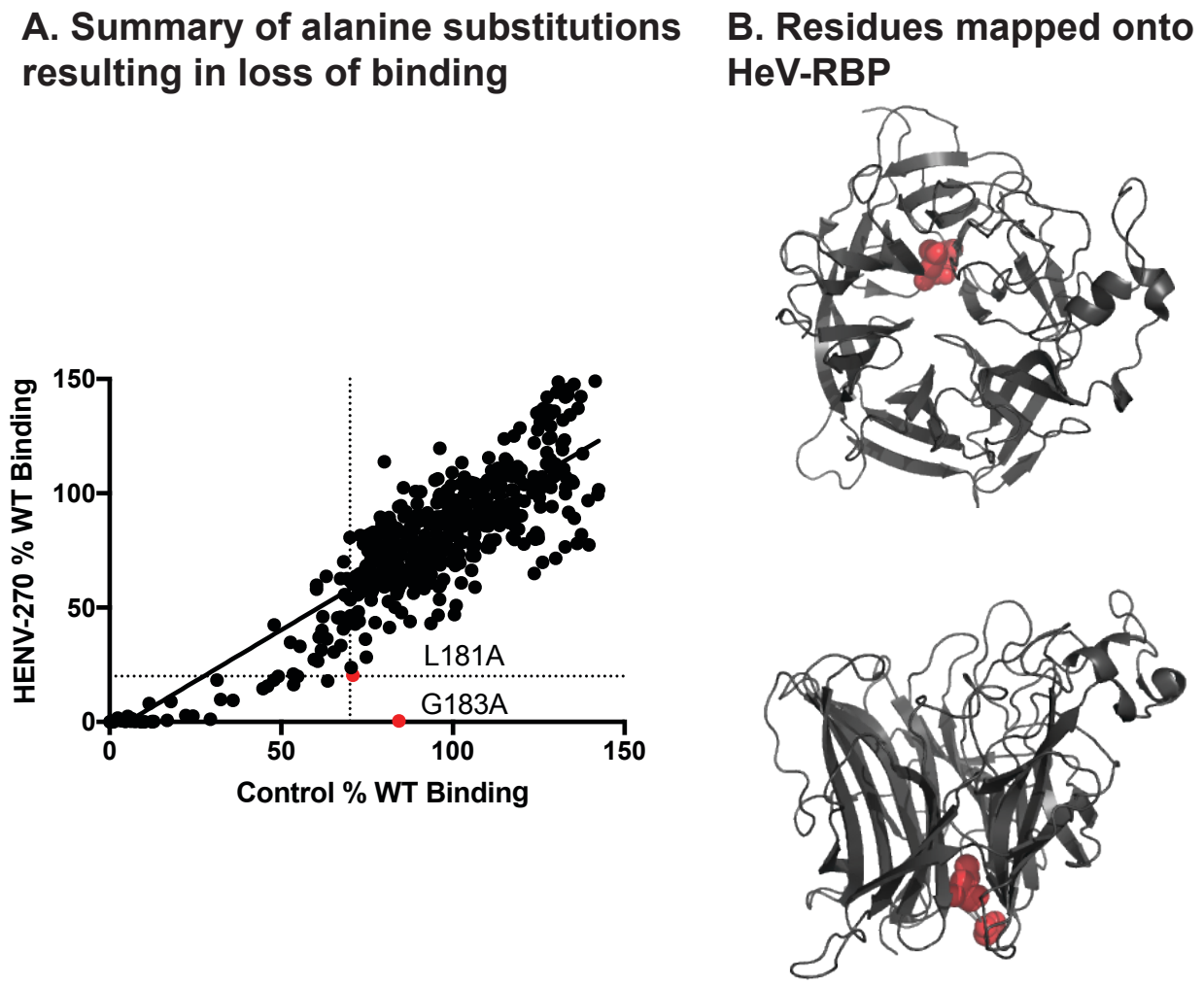

Figure 4-6: Scanning alanine mutagenesis to determine residues critical for binding by HENV-270 Fab. A) Binding by HENV-270 Fab (y-axis) or control cocktail (x-axis) relative to binding of each to WT protein. Residues were considered critical for HENV-270 binding when binding by HENV-270 was <20% binding to WT but >70% binding of control relative to WT. B) Critical residues (red spheres) mapped onto HeV-RBP head domain crystal structure. Top view is looking down on ephrin-B2 binding face, bottom view is looking at side of head domain, with ephrin-B2 binding face on top.

DISCUSSION

HeV and NiV are highly lethal pathogens primed for transmission across human populations. Despite the WHO designating these as priority pathogens, vaccines and therapeutics have not been fully approved for human use to date. Concurrently, structural information regarding the full-length RBP, and the antigenic landscape in the full-length surface protein has been lacking.

We used a differential screen to isolate a human mAb HENV-270 that preferentially binds to the full ectodomain of RBP. This mAb, while showing limited potency *in vitro*, potently protects hamsters from NiV_B challenge. A gradient fixation purification method allowed for determination of the first high-resolution structure of full-length HeV-RBP and did so in a complex with ephrin-B2 and the HENV-270 mAb. These structural studies elucidated a novel antigenic site of neutralization vulnerability on the C-terminus of the RPB stalk domain. This region is implicated in the fusion triggering capability of RBP, suggesting HENV-270 functions by blocking this triggering mechanism directly. Structure-function studies found L181 and G183 to be a critical residue for binding by HENV-270.

HENV-270 is the first monoclonal antibody, of human or animal origin, that targets the stalk domain of a paramyxovirus attachment glycoprotein. Because previous studies have implicated this region as being important for the fusion triggering of F, HENV-270 provides a crucial reagent for further assessment of the fusogenic properties of the RBP stalk domains of HeV and NiV. While studies to date are lacking, it is likely that emerging henipaviruses, such as Cedar and Ghana viruses, utilize a similar strategy for fusion triggering after attachment to cognate host cell receptors. This may provide a general mechanism for therapeutically targeting henipaviruses. The limited size and secondary structure of this region may be amenable to targeting by broadly reactive small molecule or peptide inhibitors. Future studies should assess this possibility, as well as the possibility for HENV-270 to cross-react to these emergent viruses.

METHODS

Generation of humAb HENV-270

HENV-270 was generated using a hybridoma protocol largely described previously (Dong, Cross et al. 2020). Approximately 6 million peripheral blood mononuclear cells (PBMCs) isolated from a human subject by leukapheresis were transformed with Epstein-Barr virus (EBV) and stimulated for lymphoblastoid cell line (LCL) proliferation using CpG DNA oligo, Chk2 inhibitor, and cyclosporine. Cells were plated in 384-well plates and cultured for 7 days prior to expansion onto irradiated feeder layers of human PBMCs (Nashville Red Cross). Cell supernatants were screened 3 to 5 days after expansion for binding to antigen by ELISA. Wells secreting antibody that showed detectable binding to HeV-RBP full ectodomain, but no detectable binding to HeV-RBP head domain, were fused to the multiple myeloma heterohybridoma cell line HMMA 2.5 by a previously described electrofusion technique (Yu, McGraw et al. 2008). Fused cells were plated in selection medium containing hypoxanthine, aminopterin, and thymidine in 384-well plates and incubated for 14 days, with cells being fed with Medium E (STEMCELL) on day 7. Supernatants then were screened again for binding, and positively reactive wells were expanded to 48-well plates. After another round of ELISA screening, positively reactive hybridomas were cloned via fluorescence activated cell sorting into 384-well plates. Cloned hybridomas were expanded for production of IgG and subsequent purification directly from hybridoma cell supernatants or were subjected to 5′ and/or 3′ rapid amplification of cDNA ends (RACE) sequencing to identify paired heavy and light chain sequences. For recombinant, large-scale IgG protein expression, oligos encoding the heavy and light chain genes of HENV-270 were cloned into IgG expression vectors by Twist Biosciences.

ELISA screening of LCL and hybridoma supernatants

Recombinant HeV-RBP head domain or HeV-RBP full ectodomain was associated to 384-well ELISA plates at 1-2 μg/mL overnight at 4°C. Plates were aspirated and blocked with 2% milk + 1% goat serum in DPBS-T for 1 h at room temperature. After washing plates 3x with DPBS-T, 25 μL/well LCL supernatants were added to plates and incubated for 1 h at room temperature. Plates were washed again 3x, and alkaline phosphatase (AP) conjugated goat-anti human IgG secondary antibody diluted 1:4,000 in 1% milk + 1% goat serum in DPBS-T was added to plates and incubated for 1 h at room temperature. After a final wash step, AP substrate buffer was used to develop plates for 30 to 45 minutes at room temperature. Plates were read at 405 nm on a Biotek plate reader to identify wells for positive reactivity to selected antigens.

ELISA binding to determine half-maximal binding concentrations

ELISA binding experiments were performed as previously described (synergy paper citation). Briefly, 384-well plates were coated with 25 μL/well recombinant protein at 2 μg/mL corresponding to HeV-RBP full ectodomain, HeV-RBP head domain, NiV_M-RBP head domain, or NiV_B-RBP head domain. Plates were incubated overnight at 4°C. After aspiration, plates were blocked with 25 μL/well 2% milk, 1% goat serum in DPBS-T for 1 hour at room temperature. After washing 3x with DBPS-T, serial dilutions of mAbs at 25 μL/well were added to plates and incubated for 1 hour at room temperature. After washing, 25 μL/well 1% milk, 1% goat serum in DPBS-T containing a 1:1000 dilution of goat anti-human IgG-AP was added to plates and again incubated for 1 hour at room temperature. Plates were developed using AP substrate tablets dissolved at 1 tablet per 5 mL buffer for 30-45 minutes. Absorbance at 405 nm was determined

using a BioTek plate reader. Standard curves using non-linear regression were generated in GraphPad prism to interpolate EC_{50} values.

Ephrin-B2 blockade assay

Receptor blocking assays were performed exactly as previously described in chapter III. 293F cells were transiently transfected with cDNA encoding the full length HeV-RBP and incubated for 72 hours prior to use. After filtering cell suspensions to prevent clumping, 50,000 cells/well were added to 96-well V-bottom plates and washed with 100 µL/well FACS buffer (DPBS containing 2.5% FBS, 1 mM EDTA). Cells were centrifuged and aspirated prior to addition of 50 µg/mL recombinant, soluble ephrin-B2 at 30 µL/well and incubated for 30 minutes at 4C. Cells were again washed with 100 µL/well FACS buffer. 30 µL/well HENV-270, HENV-103, or HENV-117 was then added to wells at 2 µg/mL and incubated for 30 minutes at 4C. After washing, 30 µL/well FACS buffer containing goat anti-human IgG-PE diluted 1:1000 was added to cells and incubated for 30 minutes at 4C. After a final wash step, FACS containing 1:1000 DAPI was added to cells, which were then analyzed by an Intellicyt iQue benchtop flow cytometer. Cells were first gated for viability. Mean fluorescence intensity (MFI) of antibody binding in the presence of ephrin-B2 was compared to the absence of ephrin-B2 in triplicate and expressed percent binding.

Biolayer interferometry (BLI) competition binding to HeV-RBP

Competition binding to HeV-RBP was performed on an Octet Red 96 instrument. Ni-NTA sensortips were first equilibrated in 1x kinetics buffer (Pall) for 10 minutes. Tips were then immersed in wells containing 25 µg/mL HeV-RBP full ectodomain in 1x kinetics buffer for 60

seconds to allow for association of his-tagged protein. After a brief baseline step, a first antibody was associated to the sensortips at 5 μg/mL for 300 seconds. This step was immediately followed by immersion into a second antibody for 180 seconds. A control tip that only associated a second antibody was used to determine maximal binding of each mAb. These data were analyzed by Octet Data Analysis software to build a competition matrix.

Plaque reduction neutralization tests against HeV, NiV_M, and NiV_B

Virus neutralization assays were performed in biosafety level 4 facilities with all proper precautions taken. Antibodies were serially diluted 2-fold starting at 100 μg/mL and incubated with approximately 100 plaque forming units (PFU) or HeV, NiV_M, or NiV_B and incubated for 45 minutes at 37C prior to being added to Vero E6 cell monolayers. 48 hours after inoculation, cells were fixed and stained with neutral red, with plaques counted 24 hours after fixation/staining. Plaque counts were normalized to a virus only control to enumerate percent neutralization for each treatment. Data were input into GraphPad prism and analyzed by non-linear regression to derive half maximal inhibitory concentration (IC_{50}). Assays were performed in technical duplicate.

Syrian golden hamster Nipah Bangladesh challenge studies

The Syrian golden hamster model of Nipah Bangladesh infection has been described elsewhere and used to assess therapeutic efficacy of human monoclonal antibodies in previous studies. Briefly, 3-5 week old animals were inoculated by the intranasal route with 5 x 10^6 plaque forming units NiV_B (day 0). 24 hours later (day 1), animals were either treated with 10 mg/kg HENV-270 by the intraperitoneal route or left untreated. Animals were monitored for 28 days for

changes in weight, temperature, disease state, and survival. Animals displaying signs of severe disease were humanely euthanized, as were animals that survived through the study endpoint. Survival and weight change data were analyzed in GraphPad Prism, with survival data statistically analyzed using the Log-Rank Mantel-Cox test to compare treatment group with pooled experimental and historical (2 animals) controls.

Hydrogen-deuterium exchange mass spectrometry (HDX-MS) on HeV-RBP when bound to HENV-270

Proteins were prepared at a final concentration of 15 pmol/µl. Labeling occurred in PBS (pH 7.4) in D2O at 20°C for 10, 60, 600 and 3600s . The reaction was quenched with a solution containing PBS, 4 M guanidinium-HCl, and 500 mM tris(2-carboxyethyl)phosphine to pH 2.4 at 0°C. Samples were injected into a nano-Acquity ultraperformance liquid chromatography (UPLC) system with HDX technology. Digestion was performed at 15°C with a flow rate of 150 µl/min of 0.1% formic acid using a pepsin column. Peptides were simultaneously trapped at 0°C on a VanGuard ethylene bridged hybrid (BEH) C18 1.7-µm column. Peptides were separated on an Acquity UPLC BEH C18 1.7-µm, 1-mm by 100-mm column; eluted using 5 to 35% acetonitrile and 0.1% formic acid in H2O; and analyzed using a Xevo G2-XS mass spectrometer in MSE mode. Peptides were identified using Waters ProteinLynx global server 3.0.3, and then analyzed in Waters DynamX 3.0 implementing a score cut-off of 7.5, the peptide must be present in at least 2 files and have at least 0.2 products per amino acid. The relative deuterium uptake for each peptide was calculated by comparing the centroids of the mass envelopes of the deuterated samples versus the un-deuterated controls . Results were averaged across triplicate analyses, at a given time point, and the standard deviation was determined.

Scanning alanine mutagenesis of HeV-RBP

An alanine scanning mutagenesis library based on the full length sequence of HeV-RBP was constructed by Twist biosciences. Excluding the cytoplasmic and transmembrane domains (starting at residue 70), each amino acid was substituted for alanine, or if already alanine, substituted for serine, one-by-one. Each sequence-verified construct was delivered in 96-well plate format. Plasmid was prepared and purified as previously described, with all final concentrations normalized to 100 ng/µL using a Biomek liquid handling instrument. Transfections were performed using the ExpiFectamine reagent. Briefly, 5 µL WT or alanine-substituted HeV-RBP plasmid corresponding to 500 ng cDNA was incubated with 26 µL Opti-MEM containing the ExpiFectamine reagent in sterile, deep-well 96-well plates for 15 minutes at room temperature. After incubation, 450 µL expi293F cells diluted to 2.5 x 10^6 cells/mL were added to wells and incubated for approximately 24 hours at 37C, shaking at 900 RPM in a plate shaker. The next day, 15 µL/well were aspirated (corresponding to ~50,000 cells) from plates and added to V-bottom 96-well plates. Alongside, a 96-well plate with untransfected cells was harvested at 50,000 cells/well. Plates were washed 1x with FACS buffer (DPBS, 1 mM EDTA, 2.5% FBS) and centrifuged at 2000 RPM for 2 minutes. After aspiration, 30 µL/well HENV-270 Fab or a cocktail of HENV-26 and HENV-32 (to control for protein expression and folding) at 2 µg/mL was added to pelleted cells and incubated for 30 minutes at 4C. Cells were washed with FACS buffer, centrifuged, aspirated, and then incubated with 30 µL/well FACS containing 1:1000 dilution of goat anti-human IgG-PE for 30 minutes at 4C. Cells were then washed 2x with FACS buffer prior to addition of 30 µL/well FACS containing DAPI. Stained cells were analyzed on an Intellicyt iQue instrument. Dead cells were excluded by DAPI (VL-1 channel) and gated on PE+ cells (BL-2 channel) to assess binding by HENV-270 Fab or the cocktail

control. Percent binding was calculated for both HENV-270 Fab and control by comparing binding to alanine substituted constructs to pooled binding to WT constructs (6 separate WT constructs were used, each in triplicate). Residues were determined to be critical for HENV-270 Fab binding when binding by HENV-270 Fab was <20% binding to WT, while binding by the control cocktail was >70% binding to WT. Untransfected cells were used as a control for background binding, with % PE+ from each used as a background subtraction.

Negative Stain electron microscopy

For electron microscopy imaging of HeV-RBP$_{ecto}$ protein, Fab and ephrinB2 complex, we expressed the HeV-RBP full ectodomain with His tag. Expressed protein was isolated by metal affinity chromatography on HisTrap Excel columns (GE Healthcare), followed by GraFix using a 10% to 30% glycerol gradient and 0 to 0.1% glutaraldehyde gradient. Fractions (200 μL) were buffer exchange and concentrated. HENV-270 Fab was express recombinantly and purified by HisTrap Excel affinity chromatography columns (GE Healthcare). Complexes were generated by incubation of HeV-RBP$_{ecto}$ monomer, HENV-270 Fab, and ephrin-B2 in a 1:2:2 molar ratio overnight at 4°C. Approximately 3 μL of complex at concentrations of ~10–15 μg/mL was applied to a glow-discharged grid with continuous carbon film on 400 square mesh copper electron microscopy grids (Electron Microscopy Sciences). The grids were stained with 0.75% uranyl formate. Images were recorded on a Gatan US4000 4k×4k CCD camera using an FEI TF20 (TFS) transmission electron microscope operated at 200 keV and control with SerialEM. All images were taken at 50,000× magnification with a pixel size of 2.18 Å per pixel in low-dose mode at a defocus of 1.5–1.8 μm. The total dose for the micrographs was around 20 e−per Å2. Image processing was performed using the cryoSPARC software package. Images were

imported, CTF-estimated and particles were picked automatically. The particles were extracted with a box size of 256 pixels and binned to 128 pixels (pixel size of 4.36 A/pix) and 2D class averages were performed to get clean data set. Acceptable classes with both the Fab and the receptor were further classified (2D) to separate full complex giving 28276 particles. *Ab-initio* was used to generate initial 3D volume that was farther refined. The final refine volume have resolution of ~14A. Model docking to the EM map was done in Chimera. For the ephrin-B2-RBP domain complex PDB: 6PDL was used and for the Fab PDB:12E8 or prediction model of the Fv that generate by SAbPred tool was used. Chimera software was used to make all the structural figures.

CHAPTER V

A HUMAN MONOCLONAL ANTIBODY TARGETING THE YELLOW FEVER VIRUS ENVELOPE PROTEIN DOMAIN II POTENTLY NEUTRALIZES AT A PRE-ATTACHMENT STEP AND PROVIDES THERAPEUTIC PROTECTION IN HAMSTERS

Contributions: Nurgun Kose, Joe Genualdi, and I isolated antibodies. Joe Genualdi and I performed binding assays. I performed neutralization, pre vs. post attachment, competition binding, and escape mutant studies. Justin Julander (Utah State University) performed hamster challenge studies. VU Mass Spectrometry core performed HDX-MS studies.

INTRODUCTION

Yellow fever virus (YFV), the name-giving member of the family *Flaviviridae*, is a historically important human pathogen of global public health concern. Yellow fever disease has been known in the New World since the 1600's, and YFV was first identified in 1927 (Bauer and Hudson 1928). The virus has caused numerous outbreaks of human disease throughout the world. According to the World Health Organization, 47 countries in Africa and Central and South America have regions that are endemic for yellow fever, and the burden of yellow fever disease during 2019 was as high as 109,000 severe cases and 51,000 deaths (Gaythorpe, Hamlet et al. 2021). While only a small proportion of infected individuals will develop severe disease, those who do face hemorrhagic disease and multiorgan failure, with mortality rates approaching 50% (Monath and Vasconcelos 2015). Non-human primates serve as the primary reservoir for YFV, with *Aedes albopictus* mosquitoes propagating viral spread in these populations in what is known as the sylvatic cycle. Occasionally, *Aedes aegyptii* mosquitoes serve as vectors, and can begin to circulate virus in human populations, known as the urban cycle (Douam and Ploss

2018). With infections becoming more frequent in major urban centers like Sao Paolo and Rio de Janeiro, there is concern of more severe YFV epidemics and pandemics (Cunha, Tubaki et al. 2020).

YFV is a small, enveloped virus harboring a positive-sense, single-stranded RNA genome . The YFV genome is translated as a single polyprotein, which is post-translationally cleaved into 3 structural (pr/M, E, C) and 7 non-structural (NS1, NS2a, NS2b, NS3, NS4a, NS4b, NS5) proteins by a combination of host and viral proteins (Chambers, Hahn et al. 1990). The envelope (E) protein is the primary surface-exposed protein on mature particles and is the primary protective target of the humoral immune system (Daffis, Kontermann et al. 2005). E protein comprises three distinct domains, domain I (DI), domain II (DII), and domain III (DIII). DII contains a number of immunodominant epitopes, including the fusion loop (FL), which is responsible for fusion of viral and host membranes in the late endosome. DII and DIII are bridged by DI. Domain III on E contains the putative cellular attachment domain. While a number of attachment factors have been postulated, specific viral receptors have not yet been identified. Virus enters host cells via receptor-mediated endocytosis, where the low pH of late endosomes triggers major conformational changes to the E protein. These changes expose the FL, which inserts into the endosomal membrane, allowing ejection of the RNA genome into the host cytoplasm for direct translation and replication. While E protein is the major target of neutralizing antibodies, the pre-membrane (prM) and nonstructural 1 (NS1) proteins also can elicit protective antibodies. With antibodies to prM, however, the risk of antibody-dependent enhancement of infection by otherwise poorly infectious immature virions is a concern (Smith, Nivarthi et al. 2016).

While the YFV vaccine is considered one of the most successful live-attenuated vaccines to date, the durability of immunity induced by vaccination may be somewhat limited. Also, challenges in the sustainability of manufacturing and distribution have sometimes limited it effectiveness as a public health tool. Shortages of vaccines based on YFV-17D (and related strains) have plagued countries with endemic YFV circulation. Fractional dosing has been explored in outbreak settings when vaccine supply is insufficient, but there are conflicting reports on the effectiveness of this strategy. YFV vaccine shortages stem principally from the limitations inherent in the legacy methods of vaccine strain propagation still being used. When outbreaks do occur in the setting of vaccine insufficiency, specific licensed antiviral treatments targeting YFV are not available. A number of trials using small molecule inhibitors including ribavirin have been unsuccessful.

Recently, highly potent monoclonal antibodies (mAbs) to a number of viral targets have shown efficacy as potential treatments of highly pathogenic agents, including other flaviviruses . A number of antibodies targeting both E and NS1 of YFV have been described. A mAb in designated A5 was identified using phage display technology and showed efficacy in an immunodeficient YFV-17D challenge model. While this antibody is interesting mechanistically, as it neutralized virus *in vitro* at multiple stages in the YFV replication cycle, fully human mAbs with native heavy and light chain pairing are preferred for use in human therapy. Here, we isolated a panel of fully human mAbs targeting E protein in order to identify candidate therapeutic antibodies. Competition-binding studies mapped these antibodies to diverse antigenic sites, one of which elicits antibodies that neutralize YFV. *In vitro* studies of the mechanism of neutralization showed that YFV-136 functions at a pre-attachment step by binding to DII on

YFV-E. Further, escape mutant generation revealed a critical residue on DII that, when substituted from histidine to tyrosine, allows for viral escape from YFV-136 neutralization. Hydrogen-deuterium exchange mass spectrometry (HDX-MS) suggested involvement of DI in antibody binding, potentially via allosteric rearrangements of E within the dimeric, virion-bound architecture. Passive transfer of this mAb protected Syrian golden hamsters in a therapeutic challenge setting, as well as immunocompetent mice from lethal YFV challenge. These studies identified a potently neutralizing monoclonal antibody targeting YFV and pave the way for further development of mAb YFV-136 as a candidate therapeutic antibody.

RESULTS

Isolation of monoclonal antibodies from YFV vaccinees

Peripheral blood mononuclear cells (PBMCs) from subjects who received the YFV vaccine previously were transformed *in vitro* with Epstein-Barr virus (EBV) to screen for YFV-reactive antibodies secreted by transformed memory B cells. We screened cell supernatants for binding to recombinant YFV E protein by ELISA and/or binding to YFV-infected cells by flow cytometry. Cells secreting YFV-reactive antibodies were fused to a myeloma partner to generate hybridoma lines, which were subsequently cloned by fluorescence activated cell sorting (FACS). Antibody was purified from serum-free supernatants by affinity chromatography. Using these methods, we isolated 15 monoclonal antibodies from YFV-immune subjects. These antibodies bound to recombinant E protein by ELISA with varying half maximal effective concentrations (EC_{50}) for binding ranging from 29-15600 ng/mL.

A. YFV-17D E half maximal binding

mAb	YFV E
YFV-59	28.7
YFV-142	33.4
YFV-132	34.6
YFV-59.2	43.6
YFV-40	52.6
YFV-155	56.7
YFV-149	73.7
YFV-147	87.1
YFV-39	100.3
YFV-83	157.9
YFV-136	269.7
YFV-108	292.7
YFV-121	311.1
YFV-146	1769
YFV-99	15600

EC_{50} (ng/mL)
0-50
51-500
501-1000
>1000

B. YFV-17D neutralization

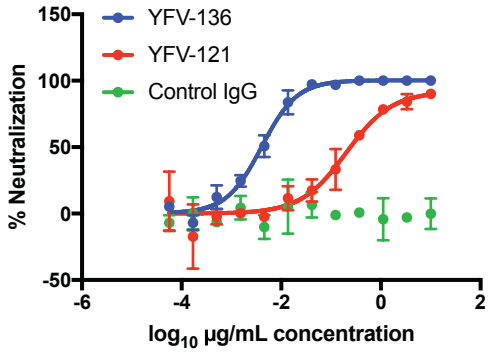

Figure 5-1: Binding and neutralization by humAbs against YFV-E. A) Half maximal effecting binding concentrations for 15 mAbs (YFV-59.2 later found to share identical sequence to YFV-59) Values are representative of three independent experiments. **C)** Neutralization profiles of the two neutralizing mAbs YFV-121 and YFV-136 against YFV-17D.

Neutralization of vaccine and WT YFV strains by mAbs targeting YFV E protein

All antibodies isolated were tested for their ability to neutralize YFV-17D in a focus reduction neutralization test (FRNT). While most antibodies were completely non-functional against YFV-17D, two mAbs from this panel showed varying ability to neutralize virus. YFV-121 was moderately neutralizing, with half maximal inhibitory concentration of 202 ng/mL **(Figure 5-1)**. However, YFV-136 showed exceptional potency, with an IC_{50} below 10 ng/mL. The potency of YFV-136 represents one of the most potent mAbs against YFV ever isolated, prompting us to pursue this mAb for further studies. We next tested YFV-136 for its ability to neutralize diverse YFV strains in BSL-3 conditions.

Competition-binding reveals antibodies target diverse antigenic sites on the E protein

In order to group antibodies based on the major antigenic sites recognized, we used a high-throughput biolayer interferometry instrument (Octet HTX) to perform competition binding **(Figure 5-2)**. In this platform, antigen is loaded onto a biosensor tip, with two antibodies sequentially flowed over the tip. If mAbs do recognize non-overlapping antigenic sites, both antibodies are able to associate to the coated sensors when applied in sequence. If binding of the first antibody applied to the antigen-coated sensor reduces or prevents binding of the second antibody, this finding indicates that the pair of mAbs bind to the same or an overlapping antigenic site. We included the previously described pan-flavivirus reactive mouse mAb 4G2 targeting the fusion loop (FL) for comparative purposes. The human antibodies appeared to recognize five major antigenic sites. One group of mAbs, including YFV-39, -40, and -146, competed for binding with 4G2, indicating that these mAbs target the FL epitope on YFV E. The neutralizing mAbs YFV-121 and -136 grouped together, indicating these mAbs target an overlapping antigenic site of neutralization vulnerability on YFV E. Interestingly, YFV-65 also competed for binding to E with YFV-121 and YFV-136, despite the fact that it did not neutralize YFV-17D when tested at concentrations as high as 10 μg/mL. These data suggest there are multiple antigenic sites on YFV E, with at least one site being a target of potently neutralizing antibodies.

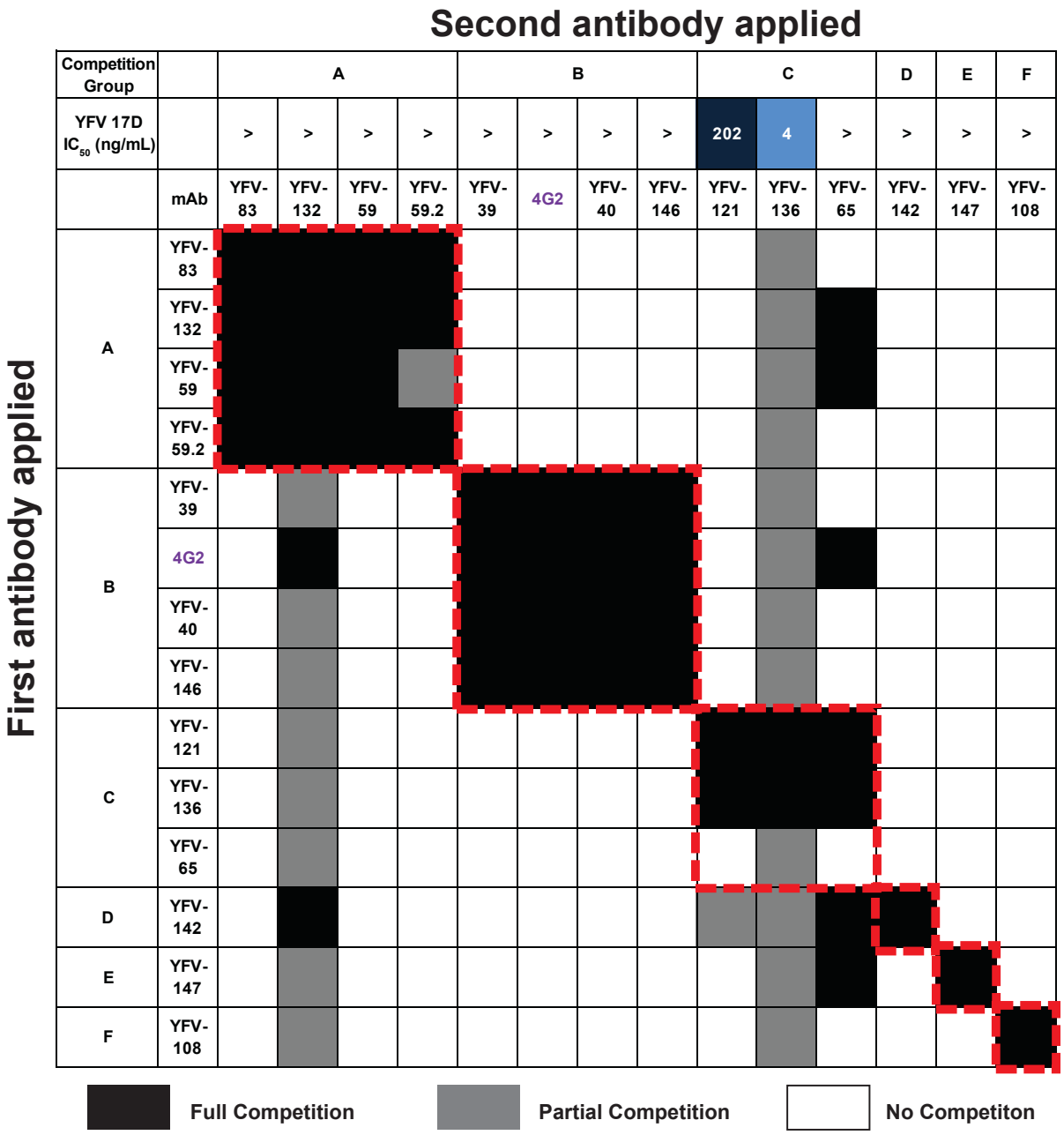

Figure 5-2: Competition binding of mAbs to YFV-E. YFV-E was immobilized to a biolayer interferometry sensortip, with a first antibody associated to antigen. A second antibody was then assessed for its ability to bind in the presence of the first antibody. Each box represents a pairwise event of two mAbs interacting with antigen. Antibodies were clustered based on their competition profiles.

YFV-136 neutralizes YFV-17D virus at a pre-attachment step

Neutralizing antibodies can target major stages in the viral replication cycle, including, but not limited to, attachment, entry, and egress. Antibodies targeting YFV and other flaviviruses

typically function at one or more of these replication steps. To determine the mechanism of action for the most potently neutralizing antibody, YFV-136, we performed pre- and post-attachment neutralization assays **(Figure 5-3)**. In the pre-attachment variation, virus and antibody were pre-mixed prior to addition to Vero cell culture monolayers. In the post-attachment assay, first virus was incubated on cells to allow attachment, the excess, unbound virus was washed away and subsequently antibody was added. YFV-136 and YFV-121 neutralized prior to virus attachment to cells, but both showed substantial loss in potency when added to cells after virus had attached. These data suggest that antibodies YFV-121 and YFV-136 function primarily at a pre-attachment step, likely blocking the ability of virus to bind to host cells.

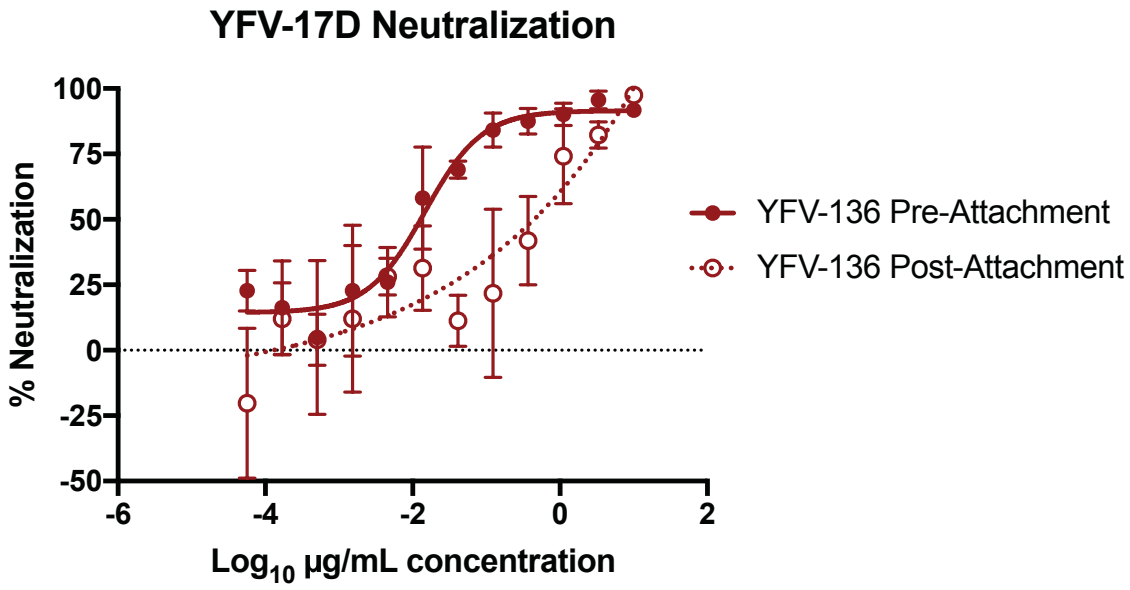

Figure 5-3: Pre vs. post attachment neutralization of YFV-17D by YFV-136. Virus was either pre-incubated with antibody (solid curve) or first added to cells, followed by incubation of pre-inoculated cells with antibody. Cells were kept cold to prevent internalization of virus.

YFV-136 escape mutation studies identify a substitution at H67 that abrogates neutralization capacity

In order to identify mutations in the YFV envelope protein that allow escape from YFV-136 neutralization, we used a real-time cell analysis (RTCA) assay that has previously been utilized to evaluate SARS-CoV-2 antibody escape mutations in high throughput fashion. This system monitors cytopathic effect over time, which in turn allows for identification of escape viruses by observation of late CPE after incubating virus with antibody. For these studies, in 16 wells in a 96 well plate, YFV-17D was incubated with 5 μg/mL YFV-136. In 13/16 wells, complete neutralization and maintenance of cell monolayer integrity was observed throughout the study. However, 3/16 wells showed a late CPE phenotype, suggesting selection of YFV-17D variants that subvert YFV-136 neutralization **(Figure 5-4)**. Supernatants from these wells were harvested and again incubated with 5 μg/mL YFV-136 on the RTCA instrument to confirm escape. In this second round, CPE developed rapidly, similar to a virus-only control, confirming selection of a population of virus that is refractory to YFV-136 neutralization.

Confirmation of viral escape using RTCA was followed by outgrowth of virus in the presence of 10 μg/mL YFV-136 to provide further purifying selection. Viral RNA was then isolated, and prM and E genes amplified and sequenced. In all 3 escape viruses, a single histidine to tyrosine substitution at position 67 on DII of YFV E was selected. This residue in the *b*-strand *is* absolutely conserved across all YFV genotypes, suggesting this escape phenotype would likely be recapitulated in fully virulent YFV strains. Interestingly, DENV serotypes 1-4 contain an N-linked glycan at this site, which may partially explain why this mAb is not cross-reactive across flaviviruses. While this residue lies within the antigenic site recognized by the previously

described mAb 5A, our mechanistic studies that suggest function at a pre-attachment step suggest these mAbs bind to distinct epitopes within DII that are, at least partially, responsible for attachment to host cells. Overall, escape mutation studies identified a key residue in DII responsible for escape from YFV-136, suggesting this mAb functions by binding an epitope including H67 on DII.

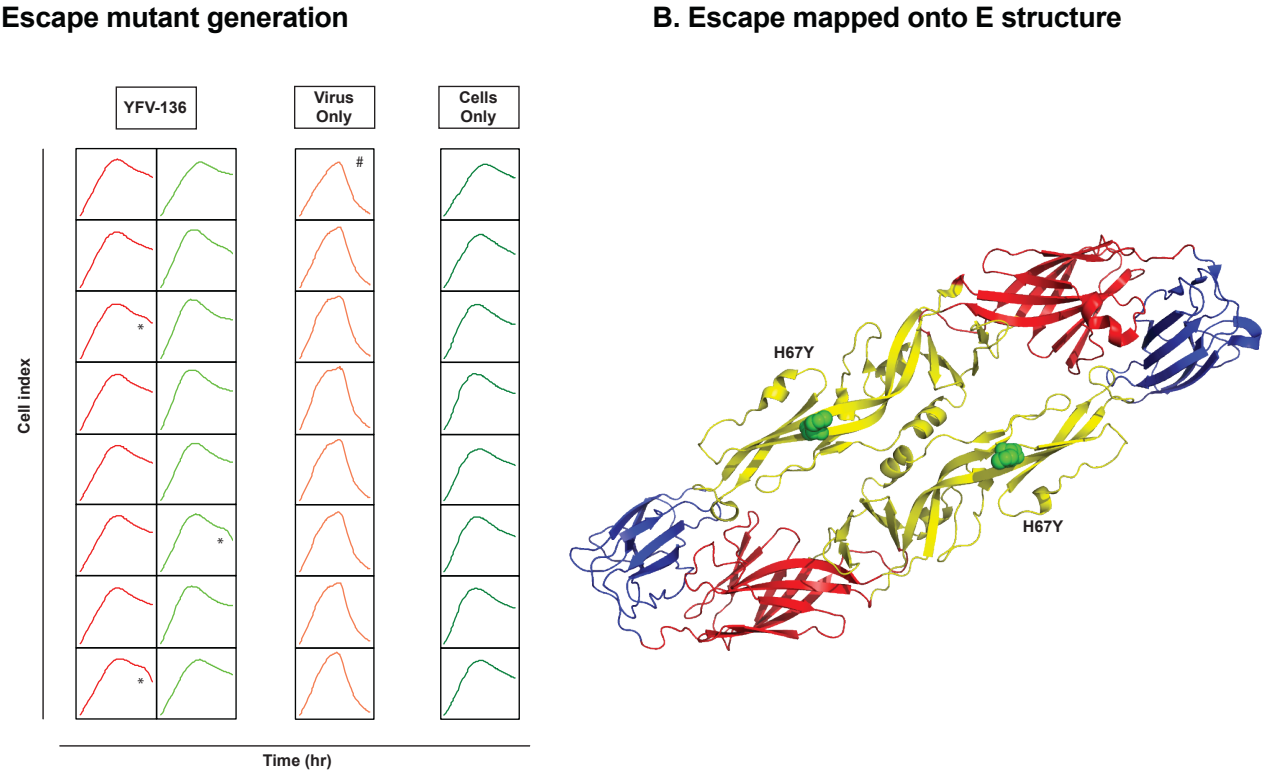

Figure 5-4: Generation of YFV-17D mutants that escape neutralization by YFV-136. A) xCELLigence cell index plots of wells treated with YFV-136, virus only, or an untreated control. * indicates wells with escape virus as determined by a late cytopathic effect (CPE) phenotype. # indicates the well from which a control virus was sequenced to control for mutations that arise during cell culture passage. **B)** Amino acid substitution present in all 3 escape viruses mapped onto envelope protein structure. Blue is DIII, yellow DII, and red DI (PDB ID: 6IW5).

HDX-MS studies suggest YFV-136 engages an antigenic site that includes DII

Escape mutant studies suggested YFV-136 binds to an antigenic site that is proximal to the fusion loop on DII. This site has previously been described as being targeted by monoclonal antibodies with neutralization functions. We next sought to determine the extent to which YFV-136 bears similarity to these previously described mAbs, and if perhaps the exceptional potency of this mAb could be explained by structural determinants of recognition of YFV. We used hydrogen-deuterium exchange mass spectrometry (HDX-MS) to map, at peptide resolution, regions of YFV-E that may be occluded during binding by YFV-136. At all quench times tested, YFV-136 induced a decrease in deuterium exchange in a region on E spanning residues 21-31 **(Figure 5-5).** Interestingly, while this region is proximal to the putative binding site of YFV-136, it is putatively not solvent exposed. This could suggest that YFV-136 is inducing allosteric rearrangements to YFV E that further bury this region within the dimeric architecture of YFV E, and may inform the mechanism by which this antibody functions.

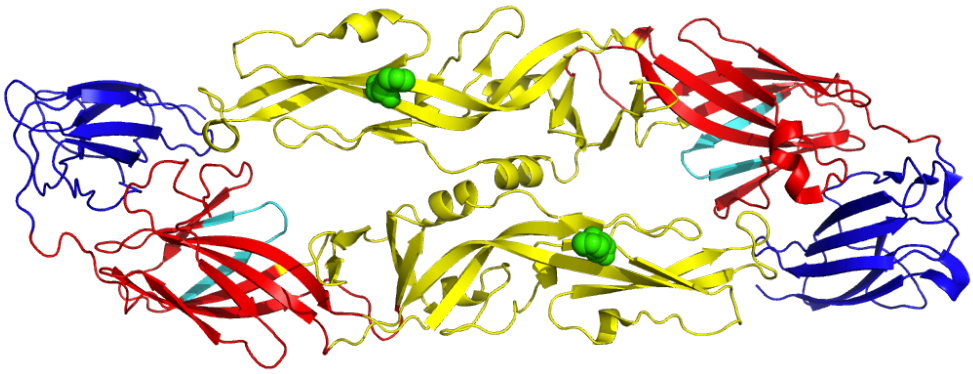

Figure 5-5: Hydrogen-deuterium exchange mass spectrometry mapping of YFV-136 antigenic site. The crystal structure of YFV E (PDB as above) with domain I in red, II in yellow, III in blue. Peptides showing a decrease in deuterium exchange in the presence of YFV-136 are colored in cyan. Green spheres indicate the location of the YFV-136 escape mutant amino acid substitution for reference.

YFV-136 protects hamsters from lethal YFV challenge

Because YFV-136 is the most potently neutralizing antibody in this panel, we chose to study its activity *in vivo*. We first assessed this mAb in a therapeutic model of YFV in Syrian golden hamsters. Animals were administered a 6 x $LD50_{50}$ dose of YFV Jimenez strain by the intraperitoneal route. At 3 days post infection, 10 animals were treated with 50 mg/kg YFV-136, and 15 animals with 20 mg//kg of control antibody DENV-2D22. Whereas 12/15 animals in the control group succumbed to infection, all animals in the YFV-136 group survived thee 21 day study **(Figure 5-6)**. Animals treated with YFV-136 briefly showed weight loss after antibody treatment, but quickly recovered and continued to gain weight throughout the course of the study. Viremia was assessed in all animals at day 6 post inoculation. While 2D22 treated animals showed substantial viremia, animals treated with YFV-136 showed a significant reduction in peripheral virus titers. Finally, we assessed the ability of YFV-136 to prevent YFV-induced liver damage by measuring serum alanine aminotransferase (ALT).

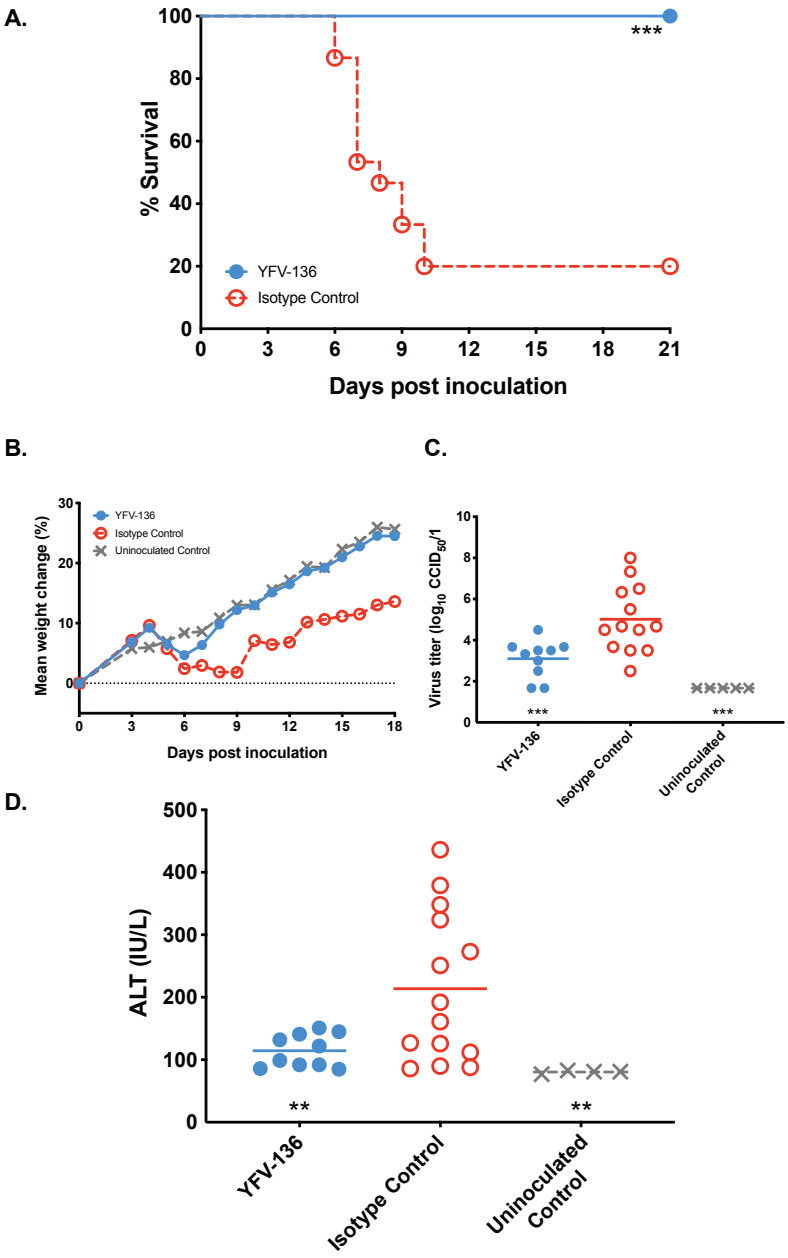

Figure 5-6: Syrian golden hamster challenge studies to assess YFV-136 therapeutic efficacy. A) Kaplan-Meier survival curve of animals treated with 50 mg/kg YFV-136 3 days post inoculation with YFV (strain Jimenez). Statistical analysis was performed using a Log-Rank Mantel-Cox test. **B)** Weight maintenance. **C)** Serum virus titers assessed at 6 days post inoculation. **D)** Serum alanine aminotransferase assesses at 6 days post inoculation as a proxy for liver function. Statistical analyses of **C)** and **D)** were performed using a one-way ANOVA with Dunnett's multiple comparisons test.

DISCUSSION

Yellow fever virus is a re-emerging arbovirus with larger epidemic potential. While a highly efficacious vaccine is available for human use, safety and manufacturing concerns warrant new vaccine and therapeutic development. Here, we use a highly validated hybridoma method to isolate a panel of monoclonal antibodies that target the primary target of anti-YFV functional humoral immunity, the envelope glycoprotein. Two mAbs, YFV-121 and YFV-136, show neutralization activity against YFV-17D, with YFV-136 showing exceptional potency with IC_{50} < 10 ng/mL. This mAb also neutralizes fully virulent strains of YFV. Both neutralizing mAbs bind to overlapping antigenic sites as determined by competition binding, suggesting a single site of neutralization vulnerability represented within this panel of antibodies. Escape mutant studies identified H67 on DII as a critical residue for this antibody's function, which I show to occur at a pre-attachment step using a pre vs. post attachment neutralization assay. Finally, this mAb is highly efficacious in a therapeutic model of YFV in Syrian golden hamsters, suggesting YFV-136 warrants further development as a therapeutic monoclonal antibody for use in humans.

The antigenic site recognized by YFV-136, which lies proximal to the fusion loop (FL) on domain II, has been previously implicated in its importance for humoral immunity generated by YFV-17D vaccination (Wec, Haslwanter et al. 2020). Concurrently, mAbs in this study show a propensity for VH4-4/VL1-51 pairings of heavy and light chain genes, suggesting a public clonotype is elicited by YFV-17D vaccination. We complement these findings, as YFV-136 also uses this pairing. Because these were the only neutralizing mAbs we were able to isolate from these donors, it is possible that the efficacy of YFV-17D largely hinges on its ability to elicit antibodies to this site.

To date, very few studies probing the humoral immune response to yellow fever virus have utilized survivors of natural infection. Most studies, while extremely important, have only focused on vaccinees. The frequency, potency, and sites recognized by the humoral response elicited by vaccination vs. natural infection is an outstanding question in the field. Future studies seeking to isolate therapeutic antibody candidates from survivors have the potential to discover antibodies to sites that are not immunodominant in the context of vaccination. Concurrently, more potent mAbs to similar sites might be found. As with all flaviviruses, it is likely that antibodies targeting domain III have exceptional potency both *in vitro* and *in vivo*. A considerable problem with these mAbs is that they are elicited at low levels despite their obvious potential as therapeutics. With our panel of vaccinee PBMCs, this may be overcome using single cell approached, specifically employing recombinant YFV EDIII as bait to discover these antibodies.

Escape mutation and structural studies here suggest that, while YFV-136 has the ability to bind to recombinant, monomeric protein, it may have the ability to interact with both E protomers within the dimeric, membrane bound structure of YFV-E. This is suggested by the fact that the single escape mutant isolated showed an amino acid substitution in DII, while HDX consistently displayed a decrease in deuterium exchange in DI. It is most likely that critical contacts are focused on the H67 region of DII, but that interactions with DI in the adjacent E protein are possible in the context of binding to whole YFV virions. It is possible that these interactions across adjacent E proteins is what differentiates YFV-136 from YFV-121, a less potent antibody that we show to bind to a similar/overlapping antigenic site. Higher resolution structural studies are warranted in order to parse out these interactions, as well as identify other critical residues that are critical for binding by YFV-136.

METHODS

Generation of human monoclonal antibodies

Peripheral blood mononuclear cells (PBMCs) from human subjects previously vaccinated with YFV-17D (or variant strains) were isolated from whole blood and transformed using Epstein-Barr virus (EBV), as previously described . Briefly, transformed B cells were expanded and co-cultured with irradiated human PBMCs in 96-well plates. Cell supernatants were screened by ELISA using recombinant YFV E protein (Meridian Life Sciences). Wells with positive reactivity then were fused to a human-mouse myeloma cell line (HMMA 2.5) and plated by limiting dilution in 384-well plates. The resulting hybridomas were cloned by fluorescence-activated cell sorting (FACS) to produce clonal hybridoma cell lines. These clonal hybridoma cells were cultured in T-225 flasks containing serum-free medium, and mAb was purified from spent medium by affinity chromatography on an ÄKTA™ pure Fast Protein Liquid Chromatography (FPLC) instrument (GE Healthcare).

ELISA binding of mAbs to YFV E

384 well plates were coated with 2 µg/mL YFV E protein (Meridian) at 25 µL/well and incubated overnight at 4°C. Plates then were washed and blocked using Dulbecco's phosphate-buffered saline with Tween 20 (DPBS-T) containing 2% milk and 1% goat serum for 1 hour at room temperature. Following a wash step, serial dilutions of antibody in DPBS were added to plates and incubated for 1 hour at room temperature. To detect antibody, alkaline phosphatase conjugated goat-anti human IgG diluted 1:4,000 in DPBS-T containing 1% milk and 1% goat serum was added to plates for 1 hour at room temperature and developed using AP substrate

tablets diluted in 1 M Tris, 0.3 mM magnesium chloride. Plates were developed in the dark for 1 hour and read on a BioTek plate reader at 405 nm. Binding curves were interpolated in Prism software (GraphPad) using a non-linear regression analysis.

YFV-17D focus reduction neutralization test (FRNT)

A focus reduction neutralization test was performed as previously described with minor amendments. Briefly, 96-well plates were seeded with Vero cells at 2.5 x 10^4 cells/well and incubated overnight. The following day, serial dilutions of antibody were mixed with 10^2 FFU YFV-17D and incubated at 37°C for 1 hour. 30 µL/well of virus/antibody mixture then was added to Vero cell culture monolayers and incubated at 37°C for 1 hour. Without washing, 110 µL per well of overlay containing a 1:1 mixture of 2.4% methylcellulose and 2x Dulbecco's Modified Eagle Medium (DMEM) with 4% FBS was added to plates, which then were incubated for 72 hours at 37°C in 5% CO_2. To stain foci of virus infection, cells were fixed with 1% paraformaldehyde for 1 hour at room temperature, washed, and permeabilized using permeabilization buffer (0.1% saponin, 0.1% BSA in DPBS) for 10 minutes. Cells then were stained with 1 µg/mL pan-flavivirus murine mAb 4G2 in permeabilization buffer for 1 hour at room temperature. After two washes, goat anti-mouse IgG- horseradish peroxidase (Southern Biotech) diluted 1:1,000 in permeabilization buffer was added to cells and incubated for 1 hour at room temperature. Foci were developed using TrueBlue peroxidase and counted using a spot counter instrument (ImmunoSpot; CTL). Foci counts were normalized to that of a virus-only control, and neutralization curves were interpolated in Prism software using a non-linear regression analysis.

Pre- and post-attachment neutralization of YFV-17D

Pre- and post-attachment neutralization assays were performed as previously described (Williamson, Gilliland et al. 2020). For pre-attachment studies, 600 FFU YFV-17D was mixed with serial dilutions of antibody for 1 hour at 37°C. Cells and virus/mAb mixtures were then pre-chilled for 15 minutes prior to addition of mixtures to cell monolayers for 1 hour at 4°C. Cells then were washed and incubated with pre-warmed DMEM for 15 minutes prior to addition of methylcellulose overlay containing DMEM, as described previously. For post-attachment studies, cell monolayers first were incubated with virus for 1 hour at 4°C. Cells then were washed and incubated with serial dilutions of antibody for 1 hour at 4°C. Excess antibody then was washed off, and cells were incubated for 15 minutes at 37°C with DMEM prior to addition of overlay. Foci were enumerated as described for the focus reduction neutralization test described above.

Biolayer interferometry competition-binding assay

Competition-binding studies were performed using a biolayer interferometry instrument (ForteBio HTX BLI). HIS1K sensortips were pre-incubated in kinetics buffer (Pall) for 10 minutes. After a 60 sec baseline step, his-tagged YFV E protein (Meridian) was associated to the tips at 5 µg/mL for 60 seconds. Readings again were set to baseline for 60 seconds, followed by association of the first antibody at 25 µg/mL for 600 seconds to achieve complete saturation. Tip readings again were baselined and then tips dipped into wells containing a second antibody at 25 µg/mL for 180 seconds. Data then was analyzed using ForteBio data analysis software. All steps were normalized to a buffer-only control, and antibodies were grouped using a Pearson correlation statistical analysis.

Generation and analysis of YFV-17D escape mutations

In a U-bottom 96 well plate, 25 µL YFV-136 at 5 µg/mL was pre-mixed with 25 µL YFV-17D (Breit, Wolvers-Tettero et al.) diluted 1:10 (~5000 FFU) in DMEM without FBS and incubated for 1 hour at 37C. This was done in 16 separate wells within the 96 well plate. Virus was also mixed with DMEM alone and passaged throughout the study to control for substitutions that arise from cell culture adaptation. 50 µL virus/antibody mixture and controls were added to Huh 7.5 cell monolayers in 96-well ePlates (Agilent) and incubated for 1 hour at 37C. 100 µL DMEM containing 5% FBS was then added to each well, plates placed back on the xCELLigence instrument, and cell monolayers were monitored for delayed CPE. Cell supernatants in wells with a delayed CPE phenotype, as well as a virus only control, were subjected to a repeat of this assay to confirm viral escape.

Once escape was confirmed, 6-well plates containing confluent Huh7.5 cell monolayers were inoculated with 100 µL/well escape virus or a virus control in the presence of 10 µg/mL YFV-136 for outgrowth of escape virus. Virus was harvested from 6-well plates, and RNA isolated using Qiagen virus RNA isolation kit. E and prM genes from isolated RNA were reverse transcribed to cDNA and PCR amplified using primers flanking the prM and E genes (One-step RT-PCR kit). Genes were then sequenced by Genewiz using overlapping primers that give coverage across prM and E. The control virus sequence was aligned to the 17D reference sequence to confirm no mutations resulted from adaptation to cell culture.

Hydrogen-deuterium exchange mass spectrometry on YFV-E bound by YFV-136

Proteins were prepared at a final concentration of 15 pmol/µl. Labeling occurred in PBS (pH 7.4) in D2O at 20°C for 10, 100, 1000 and 5000s. The reaction was quenched with a solution

containing PBS, 4 M guanidinium-HCl, and 500 mM tris(2-carboxyethyl)phosphine to pH 2.4 at 0°C. Samples were injected into a nano-Acquity ultraperformance liquid chromatography (UPLC) system with HDX technology. Digestion was performed at 15°C with a flow rate of 150 µl/min of 0.1% formic acid using a pepsin column. Peptides were simultaneously trapped at 0°C on a VanGuard ethylene bridged hybrid (BEH) C18 1.7-µm column. Peptides were separated on an Acquity UPLC BEH C18 1.7-µm, 1-mm by 100-mm column; eluted using 5 to 35% acetonitrile and 0.1% formic acid in H2O; and analyzed using a Xevo G2-XS mass spectrometer in MSE mode. Peptides were identified using Waters ProteinLynx global server 3.0.3, and then analyzed in Waters DynamX 3.0 implementing a score cut-off of 7.5, the peptide must be present in at least 2 files and have at least 0.2 products per amino acid. The relative deuterium uptake for each peptide was calculated by comparing the centroids of the mass envelopes of the deuterated samples versus the un-deuterated controls. Results were averaged across triplicate analyses, at a given time point, and the standard deviation was determined.

Syrian golden hamster YFV Jimenez challenge studies

The Syrian golden hamster model used for these studies has been previously described. 30 female Syrian golden hamsters (LVG/Lak strain) supplied by Charles River were used. Hamsters were block-randomized by weight to experimental groups and individually marked with ear tags. For challenge studies, hamsters were challenged at day 0 with 200 $CCID_{50}$ hamster-adapted YFV Jimenez strain by bilateral i.p. injections in a total of 0.2 mL. At 3 days post-virus inoculation, hamsters were dosed at 50 mg/kg rYFV-136 (1 mL total volume) or 10 mg/kg rDENV-2D22 control and monitored for weight loss and clinical manifestations for 21 days. Blood samples

were taken at days 4 and 6 to assess viremia and ALT. Any surviving animals were humanely euthanized at the experimental endpoint.

Measurement of serum aminotransferase

ALT (SGPT) reagent (Teco Diagnostics, Anaheim, CA) was used, and the protocol was altered for use in 96-well plates. Briefly, 50 µl aminotransferase substrate was placed in each well of a 96-well plate, and 15 µl of sample was added at timed intervals. The samples were incubated at 37˚C, after which 50 µl color reagent was added to each sample and incubated for 10 min as above. A volume of 200 µl of color developer was next added to each well and incubated for 5 min. The plate was then read on a spectrophotometer, and aminotransferase concentrations were determined per manufacturer's instructions.

$CCID_{50}$ assays to assess viral burdens

Virus titer was quantified using an infectious cell culture assay where a specific volume of either tissue homogenate or serum was added to the first tube of a series of dilution tubes. Serial dilutions were made and added to Vero cells. Ten days later cytopathic effect (CPE) was used to identify the endpoint of infection. Four replicates were used to calculate the 50% cell culture infectious doses (CCID50) per mL of plasma or gram of tissues.

CHAPTER VI

SUMMARY AND FUTURE DIRECTIONS

Thesis Summary

Henipaviruses and flaviviruses represent some of the most important global public health threats. Hendra and Nipah viruses pose a pandemic threat, with high mortality, human to human transmission, and bioterror potential prompting the World Health Organization to designate them as priority pathogens. Flaviviruses threaten a large percentage of the global population with infection via mosquito vectors. YFV, specifically, is largely considered one of the most impressive vaccine successes of modern medicine, but has re-emerged in South America and Sub-Saharan Africa This poses a massive threat to some of the most densely populated cities on the planet. Neutralizing antibodies are considered a correlate of protection against both flaviviruses and henipaviruses. Specifically, the RBP of henipaviruses and E protein of YFV are targeted by antibodies shown to offer protection in numerous animal models. To this end, I sought to characterize the human antibody response to these understudied pathogens.

First, I undertook a large antibody discovery campaign using a human subject with occupation-related exposure to the HeV equine vaccine. Serology suggested this donor mounted a robust humoral response to the HeV receptor binding protein. I used hybridoma technology to isolate 43 monoclonal antibodies against RBP and I characterized these antibodies for their ability to bind recombinant HeV and NiV virus antigens. Two groups of antibodies, as determined by SPR competition binding studies and HDX, bound to two distinct antigenic sites on RBP and

neutralized HeV and NiV isolates. The most potent antibodies functioned by blocking attachment of RBP to ephrin-B2, one of the host cell receptors used by henipaviruses. The second group of cross-neutralizing antibodies, which were on average less potent, displayed a "receptor-enhanced" phenotype, in which binding by ephrin-B2 resulted in better binding by these antibodies. Representative mAbs from each group afforded protection as monotherapy in a highly stringent model of NiV_B in hamsters. I down-selected the most promising mAbs from each group: HENV-117 from the receptor blocking group, HENV-103 from the receptor enhanced group. Just as ephrin-B2 enhanced binding by HENV-103, HENV-117 enhanced HENV-103 binding. Functionally, these mAbs synergized for neutralization of VSV-NiV_B and chimeric Cedar viruses. As combination therapy, HENV-103 and HENV-117 afforded superior protection over monotherapy in hamsters. Bispecific antibodies with HENV-103 and HENV-117 antigen binding fragments also afforded protection in this model. This work described a basis for synergy in neutralization and protection by human antibodies targeting distinct antigenic sites on the henipavirus receptor binding protein.

Fusion mechanics of paramyxoviruses is a subject of much controversy. Henipaviruses are thought to abide by a "provocateur" model, in which binding to ephrin-B2 or ephrin-B3 by RPB "provokes" the class I fusion protein F to under structural rearrangements that allow for fusion of viral and host membranes. The stalk region of RBP, specifically, is thought to play a direct role in this fusion mechanism. This suggests that a potential mechanism for antibody-mediated neutralization could be direct blockade of this region on RBP. To isolate mAbs that may target this region, I used a differential screening campaign to select for B cells secreting mAbs that only bind to the full length ectodomain of RBP. While antibodies with this binding pattern were

rare, I isolated an antibody termed HENV-270 that displayed cross-reactivity to only full length RBP. Further binding studies suggest this antibody recognizes a novel antigenic site distinct from antibodies described in chapter II, as well as in the literature. This antibody, while poorly neutralizing in vitro, protected hamsters from NiV_B challenge. CryoEM of HENV-270 complexed with HeV-RBP showed this mAb to bind a region distal to the ephrin-B2 binding site. Alanine mutagenesis identified two critical residues in the C-terminus of the RBP stalk domain, L181 and G183, that when substituted for alanine abrogates binding by HENV-270. This region, and these residues specifically, has been implicated in the fusogenicity of henipaviruses, further suggesting HENV-270 functions by blocking RBP triggering of F directly.

Viruses within the flavivirus genus represent a massive global public health burden, with a majority of the world's population living in a region with at least one endemic flavivirus. YFV is a re-emerging flavivirus with a high case fatality ratio that is spread via *Aedes* spp. mosquitoes. While there is an efficacious vaccine for YFV, large populations of unvaccinated people, as well as a lack of a therapeutics to treat YFV disease, make this a pathogen that requires development of novel treatment and vaccine options. To this end, I isolated a panel of monoclonal antibodies targeting the YFV envelope protein from a panel of YFV vaccine subjects. While most mAbs displayed poor neutralization profiles, YFV-136 was highly potent against both vaccine and fully virulent strains. Epitope mapping and escape mutagenesis studies discovered a critical residue, H67, on domain II of YFV-E that is critical for binding. Mechanistic studies suggested YFV-136 functions primarily at a pre-attachment step. Finally, this mAb showed therapeutic efficacy in hamsters and a novel murine model of YFV infection. These studies outlined a mechanism of

neutralization used by a human antibody elicited by YFV vaccination and provided a potential therapeutic candidate to be used in humans suffering from YFV infection.

Caveats

Antibody source

My work spanning both henipaviruses and YFV discuss the isolation of antibodies from subjects with vaccine-elicited immunity. In the case of the anti-henipavirus work, these mAbs were elicited by an unapproved vaccine antigen originally intended for use in equine populations. While the lack of approval is a caveat to the work described in this document, the ability of this vaccine to elicit a robust humoral response in a human subject bodes well for future vaccine studies using RBP as a candidate antigen. YFV, on the other hand, is a well-validated vaccine that has been used in millions of humans. In both cases, it is possible (and absolutely certain in the case of the henipavirus work) that natural infection elicits a humoral response that a) is more potent, b) targets different antigenic sites, and c) targets different viral proteins. Point c) is of specific interest, as anti-F immunity is completely absent in the henipavirus-immune subject panned in this study. With studies showing antibodies targeting HeV-F and NiV-F being highly functional both *in vitro* and *in vivo*, it is imperative that future studies analyze responses in human subjects with natural immunity against both surface glycoproteins.

Screening biases in antibody discovery

All antibody isolation campaigns performed in pursuit of my thesis aims were done so using hybridoma technology. Biases were mitigated in the case of YFV by using numerous screening

techniques on the front end, including binding assays against recombinant protein and infected cells, as well as virus neutralization assays. The small size of this antibody panel was simply a matter of low circulating memory B cell frequencies in this donor. The anti-henipavirus mAbs, however, were isolated using an ELISA screen for binding to recombinantly-produced antigens. It is highly likely that using other techniques would yield diverse antibodies against sites not properly presented on antigen bound to ELISA plates. Using antigen-specific B cell sorting, for instance, may have yielded antibodies that could assemble complex quaternary epitopes on the BCR. Additionally, the source of B cells likely introduced bias into my screening approach. The approach used to isolate mAbs throughout this thesis only allowed for isolation of circulating memory B cells that were permissible to EBV infection. This leaves out two crucial B cell compartments: circulating plasmablasts and long-lived plasma cells (LLPCs). This is especially important considering that the majority of serum antibodies are derived from LLPCs, as memory B cells do not actively secrete large amounts of antibody. Recent work from Adimab has highlighted the concept that LLPCs, on average, display higher levels of somatic hypermutation, suggesting antibodies derived from this compartment may display superior antiviral potency (Shehata, Maurer et al. 2019). This cellular compartment may represent a rich source of therapeutic monoclonal antibodies. While extraction of bone marrow is invasive and will likely be more difficult to obtain than PBMC samples, it behooves investigators studying henipavirus and flavivirus humoral responses to tap into this largely untouched resource.

Model systems: pseudotyped and chimeric viruses

Front end screening approaches for neutralization potency of antibodies in this thesis used *bona fide* virus, whether it be HeV, NiV, or YFV. That being said, for chapters II and III, all synergy

studies were done using either pseudotyped VSV or chimeric CedV. While the CedV chimeras likely represent a biologically similar system to pathogenic henipaviruses, the system has not been fully validated for its ability to recapitulate packaging of HeV or NiV RBP and F into virions in a similar fashion. Concurrently, the morphology of CedV virions is largely unknown. These are important considerations when thinking about stoichiometry of antibody binding and occupancy needed to achieve virus neutralization (Pierson, Xu et al. 2007). In the case of the pseudotyped NiV_B-VSV studies, this system is only able to undergo one round of replication and requires the combination of two viral genomes with each bearing a distinct glycoprotein of NiV_B. No data on synergistic neutralization of *bona fide* henipaviruses was shown here, a caveat that must be addressed in future studies in order to claim synergistic neutralization of HeV and NiV.

Hamster models of NiV_B and YFV

Numerous animal models for evaluating small molecule and biologic therapeutics exist for HeV, NiV, and YFV. The studies detailed in this document all utilized the hamster model of infection. The hamster model of NiV_B does not fully recapitulate the human condition. While humans can experience both respiratory and neurological disease manifestations simultaneously, Syrian golden hamsters display disparate disease courses depending on the dose and route of inoculation. The massive inoculum used for these studies led to rapid respiratory disease, with surviving animals experiencing neurological disease in a separate, later phase of disease. The implications of this distinct disease course on antibody therapy are unknown. Therefore, future work must address these concerns by using animal models that better recapitulate henipavirus disease, such as ferrets and/or AGMs. A different set of concerns plague the Syrian golden hamster model of YFV. Unlike henipaviruses, YFV induces a disease state in hamsters that

largely mirrors the human condition, including viscerotropic disease with liver damage. This is a far more tractable model than the murine model, which requires a complete ablation of interferon signaling, either by genetic knockout or antibody blockade.

Future Directions

Part I: Future directions for chapters II - IV

Human antibodies elicited by natural infection

As highlighted in the "caveats" section, these studies describe antibodies isolated from a human with exposure to a HeV equine vaccine. One open question relates to the human humoral response to the henipavirus F protein. It is likely that natural infection (or vaccination for that matter, though no F-based vaccines have entered trials for henipaviruses) would elicit highly functional antibodies against F, as well as antibodies against RBP that bind to novel sites only presented when RBP is particle-bound. Throughout my graduate studies, we made attempts to acquire human PBMCs from a survivor of Hendra virus infection in Australia, but numerous complications, coupled to the COVID-19 pandemic, prevented us from getting these precious samples. We have also made strides in finding few survivors of NiV but have not been able to finalize details.

Allosteric alterations of RBP that allow for synergy

Studies herein and by others have shown with high confidence that binding by ephrin-B2 induced conformational rearrangements to RBP that are required for the fusogenic activity of F. Despite these findings, there is almost no high-resolution structural information that informs the precise structural rearrangements by RBP following receptor binding. While these studies were not meant to unravel basic mechanisms of paramyxovirus fusion, these antibodies may provide a useful tool in probing this question. One tool that could be employed to better address these questions is cryo-electron tomography using the chimeric CedV constructs described in my synergy studies. This would have the potential to address numerous gaps in knowledge. First, it would allow us to show that the viral morphology and glycoprotein packaging of these chimerae mirrors that of HeV and NiV, further validating these viruses as a model to be used in future studies. Second, it would allow for elucidation of basic mechanisms of henipavirus fusion by capturing the native glycoproteins in a membrane-bound state within a viral membrane. I would hypothesize we would see RBP in close proximity to both pre- and post-fusion F, and that those in close contact with post-fusion F would be in a "heads-up" conformation with the C-terminus of the stalk domain exposed. In the presence of HENV-270, this region would be sterically hindered from interacting with F, leaving the F proteins in close proximity in the pre-fusion conformation.

Contribution of Fc effector functions to *in vivo* efficacy

Because antibodies are bifunctional molecules, Fc effector functions may play a crucial role in antibody-mediated protection from henipaviruses. Because henipaviruses bud from the host cell plasma membrane, it is possible that opsonization of infected cells by these antibodies is one

mechanism by which they can mediate protection. Conversely, antibody-dependent enhancement, a phenomenon observed in the clinic for DENV infection, may play a role in the pathogenesis of henipaviruses. Both possibilities must be explored in order to progress these molecules into the clinic. In our bispecific antibody studies *in vivo*, we did evaluate whether enhanced Fc effector function, by way of removal of the fucose moiety on the Fc glycans (afucosylation), augmented or diminished therapeutic efficacy. In both instances, no change in protection was observed. While this suggests that Fc effector functions play a minimal role, it is still possible that complete loss of these effector functions may impact the therapeutic efficacy, especially in the case of the monoclonal antibodies. Multiple antibody platforms with amino acid substitutions in the Fc domain have been developed to abrogate binding of antibodies to Fc gamma receptors. In order to best assess the contribution of Fc effector functions to in vivo protection, HENV-103, HENV-117, and HENV-270 should be chimerized into an Fc backbone bearing the LALA-PG amino acid substitutions (Lo, Kim et al. 2017). We would then need to test WT and LALA-PG antibodies in a side-by-side study in hamsters, or better yet, a larger animal model of infection. These studies would inform how our mAbs could be formulated for use in humans.

Antibody cocktails directed against RBP and F

Human subject limitations, described above, forced these studies to narrow in on therapeutic antibodies targeting RBP. These antibodies, while potent and protective, target only one out of two potential targets of antibody therapeutics for henipaviruses. Recent studies by multiple groups have described potent, cross-reactive mAbs with therapeutic potential against HeV and NiV F. With this in mind, it is appropriate to assess the efficacy of RBP + F antibody cocktails

both *in vitro* and *in vivo*. These antibodies would use vastly differing mechanisms to achieve neutralization, making them likely to display synergistic potency *in vitro*. As with HENV-103 and HENV-117, future studies could use chimeric CedV, VSV, or WT virus to assess synergy of one of these two mAbs with an anti-F mAb in a matrix approach, followed by validation in the hamster model of NiV_B. Excitingly, this approach does not have to be limited to a two-antibody cocktail. In fact, in the case of Ebolavirus infection, cocktails containing three or more antibodies show excellent activity in symptomatic humans. This opens up the potential to test a three-antibody cocktail containing HENV-103, HENV-117, and a potent, cross-reactive F mAb. This approach would vastly decrease the likelihood that escape mutants would be generated with the added benefit of synergistic potency.

Cross-reactivity to other emerging henipaviruses

Antibodies in these studies, specifically those with therapeutic potential, were assessed for their ability to bind and neutralize multiple distinct henipavirus species. Because these viruses share roughly 83% amino acid identity in RBP, the presence of cross-reactive mAbs is far from surprising. While it is important for mAbs to be efficacious against both HeV and NiV isolates, future studies need to take this a step further. Over the last decade, novel paramyxoviruses that share the receptor tropism of HeV and NiV have been isolated from animal reservoirs, namely bat populations. Concurrently, serological studies in Sub-Saharan Africa have found humans with NiV seropositivity, though this has largely come in the absence of clinical disease (Pernet, Schneider et al. 2014). These studies have eerie similarity to CoV studies in the 2010's, which found bats harboring novel CoVs with the ability to target human ACE2 and replicate in human airway epithelial cells. As we know, this was followed by a pandemic of a similar virus, SARS-

CoV-2, resulting in millions of deaths worldwide. Moving forward, it behooves us to identify pan-henipavirus antibodies that are functional against not only HeV and NiV, but also these emergent henipaviruses that have not yet been confirmed to cause disease in humans. In our previous studies describing HENV-26 and HENV-32, I showed that these antibodies, which bind to conserved regions of RBP, do not cross-react with CedV or Ghana virus (GhV), two bat-borne henipaviruses which have confirmed tropism for ephrin-B2. Despite this, we have a few options for pursuing broadly reactive, pan-henipavirus mAbs.

Non-human primate studies to benchmark the HENV-103 and HENV-117 cocktail against standard of care options

Our small animal model studies suggest that HENV-103 and HENV-117, when given as a cocktail, may represent the most potent therapeutic option for prophylaxis or treatment of henipavirus diseases. Unfortunately, the studies highlighted here did not properly compare this cocktail with the antibody currently farthest along in the development pipeline, m102.4. Not only has m102.4 been shown to be protective in numerous animal models including non-human primates but it has been established as tolerable in a phase I clinical trial. Because of this, the development of the HENV-103 and HENV-117 cocktail rests on the ability to show that its efficacy and potency exceeds that of m102.4. While we are convinced the potency of this cocktail *in vitro* far exceeds that of m102.4, it is imperative that directly compare both treatment options side-by-side. To do this, we can use the African Green monkey model of NiV_B disease. As discussed previously, m102.4 treatment failed to rescue animals when given at days 5 and 7 post inoculation. Using this exact model, we can administer m102.4, HENV-103 and HENV-117 cocktail, or an isotype control to animals 5 and 7 days after inoculation with NiV_B (via

intratracheal route). We would expect all animals treated with m102.4 or an isotype control to succumb to infection. If HENV-103 and HENV-117 can rescue animals this late in disease, we will be able to confidently say that our antibody cocktail represents the next generation of biologics against these viruses and is worthy of further clinical development. Even if the efficacy of our cocktail is the same as m102.4, the benefit of a cocktail in preventing escape mutations makes it an attractive therapeutic candidate.

Part II: Future directions for chapter V

Antibody-dependent enhancement (ADE) potential of YFV-136

The absolute conservation of the fusion loop epitope of the flavivirus E protein has driven concerns for antibody dependent enhancement (ADE). In this scenario, infection by one flavivirus leads to the generation of antibodies against FLE, a site that has proven to be immunodominant in prior studies. In a subsequent infection, a recall response is dominated by FLE antibodies, which generally bind with high affinity, but are poorly neutralizing (Rogers, Goodwin et al. 2017). This allows for uptake of these immune complexes into FcgR-bearing cells, and ultimately allowing for replication and propagation of virus in these cell types. This concept has been well-described in the case of DENV infection, where infection by one serotype correlates with severe disease after infection with a different serotype (Dejnirattisai, Jumnainsong et al. 2010). This has led to the essential failure of the Sanofi vaccine, in which immune-naïve children showed clear clinical worsening of disease after being infected after vaccination (Wilder-Smith, Flasche et al. 2019). Concerns for ADE were exacerbated after the 2016 Zika epidemic, where multiple *in vitro* studies have shown that sera raised against DENV

can enhance ZIKV infection (Dejnirattisai, Supasa et al. 2016, Bardina, Bunduc et al. 2017, Brown, Singh et al. 2019). While this has not yet been borne out in the clinic, concerns remain that ADE could potentially be a problem across the viral family.

To flesh out whether YFV antibodies can enhance other flaviviruses, or vice versa, large scale epidemiological studies are likely to be needed. Looking at the propensity for severe disease in persons with a confirmed previous infection with an orthologous flavivirus might suggest whether severe disease correlates with previous sero-status. An obvious, easily achievable future study could assess the ability of FLE mAbs isolated in this study to mediate DENV ADE *in vitro*. To do so, immune complexes could be incubated with K562 or U937 (monocyte lines bearing Fcg receptors) cells and assessed by flow cytometry. These cells are otherwise refractory to infection by DENV, but antibodies able to mediate ADE will allow for infection. To date, few studies have assessed ADE in the context of YFV infection (Barrett and Gould 1986, Gould and Buckley 1989). If FLE mAbs in this study can be shown to mediate ADE in vitro, in vivo studies should be performed to confirm this phenotype in a murine model of infection. If confirmed, this may inform further clinical studies that will assess whether YFV vaccination is recommended for those living in areas where other flaviviruses are endemic.

Genetic analysis of survivors vs. vaccinees to assess YFV-136-like antibody repertoire frequency

My work regarding YFV-136 confirmed previous studies that suggested antibodies with the VH4-4/VL1-51 heavy and light chain pairings are enriched in the context of YFV-17D vaccination, and that these antibodies target a similar antigenic site on DII. One possible

explanation for the widespread success of this vaccine is the ability for it to elicit a public clonotype that contributes to the majority of the function seen in serum antibody responses to YFV. This possibility leads to two distinct but connected questions. First, what percentage of the serum neutralizing antibody response is made up by antibodies that target this antigenic site? To address this, serum depletion studies should be done to selectively deplete antibodies that target the YFV-136 antigenic site. This approach has been previously used by our collaborators to probe the antibody response to sequential infections by Dengue virus (Patel, Longo et al. 2017). If we observe a massive loss of neutralization activity after depletion of these antibodies, this would indicate that this site is absolutely critical for the efficacy of the YFV-17D vaccine. Follow-up studies should also do this in the context of convalescent survivors of YFV infection to assess the contribution of this antigenic site during natural infection.

A second component of studying the contribution of YFV-136-like antibodies would be a large-scale genetic analysis of YFV-17D vaccinees. Recent studies by our lab and others have taken massive sequencing datasets to dissect differences and similarities of human antibody responses across a population (Briney, Inderbitzin et al. 2019, Soto, Bombardi et al. 2019). These tools have been deployed to assess responses to specific pathogens, and to determine if certain antibodies are elicited across a population (Setliff, McDonnell et al. 2018). In the context of this project, a cohort of YFV-17D vaccinees could be sampled for memory B cells, which would then be subjected to next generation single cell sequencing. This would allow us to see whether this VH4-4/VL1-51 is enriched after vaccination. Concurrently, we would also be able to perform lineage analysis to find antibody sequences that have undergone further somatic hypermutation, potentially making them even more potent than YFV-136. In a reciprocal approach, we could

express the germline revertant of YFV-136, where we remove any amino acid substitutions introduced by somatic hypermutation. If this antibody, termed an unmutated common ancestor (Edupuganti, Mgodi et al.), displays potent activity against YFV *in vitro*, this would further suggest that eliciting germline encoded antibodies against the YFV-136 antigenic site that are highly functional could explain the successes of YFV-17D.

Part III: Future directions for antiviral antibody discovery

New high-throughput approaches for rapidly identifying optimal antibody cocktails

In the past decade, high-throughput antibody discovery platforms have been built to allow for rapid identification of lead candidates against both self and non-self targets. Companies and academic institutions alike have mobilized these platforms during the SARS-CoV-2 pandemic with marked success. In my project, and many others seeking to discover antiviral antibodies, a cocktail approach has been taken for reasons described throughout this dissertation. The process of discovering antibody cocktails with desirable properties (synergistic activity, refractory to escape, etc.) can be laborious and time consuming, requiring numerous virological and biochemical assays that must be performed after discovery has already been completed. While this approach has yielded tremendously powerful cocktail therapeutic candidates, front-end approaches for identifying antibody pairs on the front end of the discovery process could move provide a massive boon to the field of antiviral antibody discovery.

Achieving this platform development is likely to be convoluted, requiring the multiplexing of numerous, diverse technologies coupled to computational tools that may or may not be available.

One approach could be to incorporate a display technology, such as the once described by the Bloom laboratory, to build in a mutational screening step. In this scenario, antibodies would be discovered against a target antigen using antigen specific B cell sorting followed by single cell RNA sequencing. All sequences corresponding to a binding antibody could be expressed in microscale, with each mAb incubated with the display library bearing a full mutagenesis library of the target of interest. In this scenario, each antibody would have an escape mutation profile. One could imagine this dataset could be computationally analyzed for antibody pairs with orthogonal escape profiles. This rich dataset could be coupled to functional data, such as neutralization or ability to block antigen-ligand interactions and it could be used to properly choose the most promising pairs on the front end. While we might be years away from any sort of implementation of such technological streamlining, it is exciting to imagine the potential of such a discovery effort.

Leveraging principles of antibody-mediated virus neutralization to design better vaccines

While antibodies certainly have the potential to serve an important role in mitigating disease caused by viral infections, vaccines are ultimately needed to completely stop a pathogenic virus from spreading through a population. Historically, vaccine discovery has been done almost completely empirically without an understanding of principles that guide vaccine efficacy. Yellow fever is a perfect example, where to this day, we lack an understanding of why the vaccine strain is attenuated or why it is so efficacious. Only recently have we begun to tap into our knowledge of how the humoral arm of the immune system combats viral infections to rationally develop vaccines. For example, respiratory syncytial virus (RSV) and SARS-CoV-2, have type I fusion glycoproteins that contain almost all protective antigenic sites in the pre-

fusion conformation (McLellan, Chen et al. 2013, McLellan, Chen et al. 2013, Hsieh, Goldsmith et al. 2020). Numerous groups have now used stabilizing amino acid substitutions, such as disulfide bridges, cavity filling substitutions, and flexible region stabilizing substitutions to preferentially lock these proteins into the pre-fusion conformation (Crank, Ruckwardt et al. 2019). While these represent critical leaps in terms of developing vaccinees, we are beginning to develop capabilities to take this a step further.

An approach that could be universally applied to almost any viral target would be scaffolding the minimal portions of a viral glycoprotein that are responsible for eliciting potent and protective antibodies. This concept weds principles of antibody-based neutralization, antigen design, and computational methods and has been applied to vaccine development for numerous pathogens with varying degrees of success (Correia, Ban et al. 2010, Ofek, Guenaga et al. 2010, Correia, Bates et al. 2014). For both flaviviruses and henipaviruses, where we have discovered sites of vulnerability (specifically a site on YFV that appears to elicit a public antibody response), we could use these methods to scaffold the epitopes of our most potently neutralizing antibodies. In one scenario, we could even take the epitopes of HENV-103 and HENV-117 and scaffold these onto a single immunogen. This has the potential to elicit only potently neutralizing antibodies that we have validated functionally, while also a) safeguarding against mutational escape and b) providing the added bonus of synergy. Taking it one step further, we may be able to generate pan-henipavirus immunogens to safeguard against emergent viruses within this family. Incorporation of technology such as COBRA, which uses computational methods to generate influenza vaccine candidates that a elicit broadly protective humoral response, is one possibility (Crevar, Carter et al. 2015). My hope is that the data outlined in this dissertation, specifically the

knowledge about the sites of vulnerability I have highlighted, form a foundation for these future studies.

Rethinking how we construct antiviral antibody cocktails

Traditionally, and with sound reasoning, antiviral cocktails have been constructed using antibodies that target distinct, non-overlapping antigenic sites. This has been done to ensure simultaneous engagement by each member of the cocktail. The rationale can be described as two-fold: prevention of mutational escape, and potential for synergistic potency. While it is likely that this approach is viable in most situations, recent work in SARS-CoV-2 has shown that we can, perhaps, be more thoughtful in our approach. Jesse Bloom's group, using a yeast display system, showed that highly potent antibodies against overlapping antigenic sites may compete for binding, but have completely orthogonal escape profiles (Starr, Greaney et al. 2021). Excitingly, when antibodies such as these are combined *in vitro*, escape from neutralization is completely abrogated. In a follow up study, this technology was applied to antibodies from Regeneron and Eli Lilly that are currently in the clinic. The results for Regeneron's product, a cocktail of two mAbs against different sites on the receptor binding domain of spike, highlighted that even this approach may result in mutational escape. In this case, an amino acid substitution at a site distal from either antibody binding site resulted in escape.

Moving forward, technology that comprehensively maps all possible amino acid substitutions should be applied to all antiviral antibodies moving into the clinic. Secondarily, the idea of synergy, while tempting, should take a back seat to concerns of mutational escape. Our studies, while compelling in correlating *in vitro* and *in vivo* synergy, represent a small portion of studies

that have been able to show this phenotype. Instead, a focus on prevention of mutational escape should be prioritized. The Bloom group's high throughput mapping technology, as mentioned above, may represent a platform for assessing escape profiles very early in the discovery process for numerous viral (and potentially bacterial) targets. This will assure that all lead candidates are validated for their ability to prevent escape, likely preventing massive clinical failures.

Is antibody therapy a viable option for viral diseases dominated by immune-mediated pathologies in poorly-accessible tissue compartments?

The SARS-CoV-2 pandemic has been a significant opportunity to showcase how monoclonal antibodies can be used as a frontline treatment for people experiencing symptoms induced by a pandemic virus. Some of the largest pharmaceutical companies mobilized their platforms to develop antibodies targeting the spike protein of SARS-CoV-2, which were quickly moved into the clinic for trials in subjects experiencing severe COVID-19. While it is difficult to draw conclusions on the usefulness of antibody treatments for henipavirus disease from SARS-CoV-2, there might be some lessons to be learned. First, in the case of immune-mediated pathology (such as acute respiratory distress syndrome, a pathological process sometimes shared between COVID-19 and disease caused by Nipah virus), antibody treatment late in infection appeared to be ineffective. Eli Lilly, a company with one of the leading mAb treatment candidates for COVID-19, halted their phase 3 trial that focused on severe, hospitalized patients due to its clear ineffectiveness. Small molecule antivirals have also suffered a similar fate in late stage trials. More hopeful were the trials looking at ambulatory patients with mild COVID-19 symptoms. In these patients, rates of hospitalization were decreased when antibody therapy was administered early in infection.

A second obstacle that antibody therapy must overcome is the blood-brain barrier (BBB). Because the majority of subjects with Hendra or Nipah virus infection present with neurological symptoms, it is likely an antibody therapy will need to directly access this immune-privileged site. To date, a few strategies to achieve this CNS bioavailability have been tried with varying results. The most direct method used in the clinic is direct administration into CNS compartments such as the cerebrospinal fluid, or directly into CNS tumors in the case of cancer. Perhaps one of the most intriguing avenues for CNS delivery is the "trojan horse" approach. Here, antibodies are coupled to a protein or molecule that can hijack host transport systems at the BBB to allow for active transport. Potential receptors that could be used include transferrin receptor (Tfr), human insulin receptor (HIR), and other mono- and bi-directional transporters (Skarlatos, Yoshikawa et al. 1995). A receptor-specific antibody could also be used, which negates the need for use of a substrate specific for these receptors (for example, a bispecific antibody with both pathogen and receptor binding capabilities). The "trojan horse" approach has previously been used to deliver antiviral antibodies to the appropriate site, but the BBB is still a matter requiring further work (Wec, Nyakatura et al. 2016). Finally, alternatives to full length antibodies have been explored. One example is single chain antibody technology. Sometimes referred to as "nanobodies," these small proteins have the ability to cross the BBB, and numerous studies have highlighted their efficacy in treatment of infectious and non-infectious indications (Muruganandam, Tanha et al. 2002, Rossey, Gilman et al. 2017, Huo, Le Bas et al. 2020).

Antibody delivery platforms – cutting costs, decreasing dose, extending half-life

Let's assume antibodies can be used to treat Hendra and Nipah virus disease long after the onset of symptoms. This would mean antibody therapy would likely be the preferred standard of care for patients experiencing severe disease. As it currently stands, a single infusion of antibody is likely to cost thousands of dollars. For example, use of Synagis in premature infants to prevent RSV can result in an out-of-pocket cost from thousands to tens of thousands of dollars depending on insurance coverage. At this price point, treatment would likely be prohibitively expensive for widespread use of antibody against Hendra or Nipah virus. A number of technologies have been developed that may be able to reduce the costs associated with production of antibody therapeutics on a massive scale.

First, and perhaps most obvious now that we have experienced the COVID pandemic, is nucleic acid technology. Companies have begun using RNA and DNA platforms for delivery of not only vaccine antigens, but also antibody therapeutics. For example, Moderna has mobilized their RNA technology for delivery of a monoclonal antibody targeting Chikungunya virus (CHIKV) (Kose, Fox et al. 2019). This molecule, termed mRNA-1944, has been shown to be safe and tolerated in a Phase 1 clinical trial, and has shown promising potency in pre-clinical studies. DNA delivery has also been explored for antibody delivery. AstraZeneca and the Wistar Institute have collaborated to move MEDI3902, and anti-bacterial bispecific antibody, into a DNA delivery vector, and have shown this to be a successful approach in animal models of infection (Patel, DiGiandomenico et al. 2017). Viral vectors, such as Ad5 or adeno-associated virus (AAV), have also been used to deliver a nucleic acid payload encoding antibody heavy and light

chain genes. RSV and HIV, for example, have been targeted in pre-clinical studies using this approach with promising efficacy (Skaricic, Traube et al. 2008, Balazs, Chen et al. 2011).

These platforms offer a promising alternative to recombinant antibody therapy for both pre- and post-exposure administration of HENV-103/HENV-117 cocktails. The complication with using an antibody cocktail in the context of these platforms is the potential for heavy and light chain mispairing. That being said, this can be circumvented in a few ways. For one, each antibody can be delivered to distal sites, making it less likely that pairings will be mismatched. A second approach would be to genetically fuse heavy and light chains such that the entire antibody is expressed as a single polypeptide. This can be achieved by removing the CH1 and CL domains and directly fusing the VH and VL to the Fc domain. This is known as scFv-Fc (Bujak, Matasci et al. 2014). This platform offers some advantages in expressibility profiles, and has already been considered for therapeutic use (Sokolowska-Wedzina, Chodaczek et al. 2017). Finally, a re-exploration of bispecific modalities may be needed to assure that the potency of HENV-103 and HENV-117 would be maintained within a single molecule. While our studies have not shown a superior profile to the antibody cocktail, other bispecific arrangements may offer the opportunity to achieve the potency of the mAb combo (Thanabalasuriar, Scott et al. 2019).

To decrease the need for multiple doses of antibody, increasing potency and half-life will work to achieve both goals. The lead candidates described herein, while already exceptionally potent against their respective viruses, could be further engineered using in vitro affinity maturation approaches to boost potency. This would allow for a lower dose to achieve the same potency, inherently cutting costs. While in vitro affinity maturation has the potential to introduce non-

native amino acid sequences that are potentially immunogenic, engineered mAbs targeting SARS-CoV-2 have shown to avoid these pitfalls while displaying superior breadth and potency (Rappazzo, Tse et al. 2021). Concomitantly, increasing half-life will negate the need for a multi-dose regimen, again helping to massively decrease the cost of treatment. As with abrogation of Fc effector functions, multiple groups have introduced amino acid substitutions into Fc that increase FcRn affinity, thus increasing *in vivo* half-life. The most well-established platform, YTE, is already being considered for the next generation of RSV immunoprophylaxis by AstraZeneca (Zhu, McLellan et al. 2017). Recently, the Georgiou group has published has developed the DHS-IgG backbone, which is shown to be optimized for half-life extension without compromising other Fc effector mechanisms (Lee, Kang et al. 2019). Taken together, the technologies highlighted here have the potential to make these antibodies widely available for use in the event of a YFV or henipavirus epidemic or pandemic, affording us a valuable resource to treat and protect people in rapid fashion.

BIBLIOGRAPHY

(2010). "Yellow fever fact sheet." Wkly Epidemiol Rec **85**(5): 33-36.

Abdiche, Y. N., A. Miles, J. Eckman, D. Foletti, T. J. Van Blarcom, Y. A. Yeung, J. Pons and A. Rajpal (2014). "High-throughput epitope binning assays on label-free array-based biosensors can yield exquisite epitope discrimination that facilitates the selection of monoclonal antibodies with functional activity." PLoS One **9**(3): e92451.

Adams, P. D., P. V. Afonine, G. Bunkoczi, V. B. Chen, I. W. Davis, N. Echols, J. J. Headd, L. W. Hung, G. J. Kapral, R. W. Grosse-Kunstleve, A. J. McCoy, N. W. Moriarty, R. Oeffner, R. J. Read, D. C. Richardson, J. S. Richardson, T. C. Terwilliger and P. H. Zwart (2010). "PHENIX: a comprehensive Python-based system for macromolecular structure solution." Acta Crystallogr D Biol Crystallogr **66**(Pt 2): 213-221.

Aguilar, H. C., Z. A. Ataman, V. Aspericueta, A. Q. Fang, M. Stroud, O. A. Negrete, R. A. Kammerer and B. Lee (2009). "A novel receptor-induced activation site in the Nipah virus attachment glycoprotein (G) involved in triggering the fusion glycoprotein (F)." J Biol Chem **284**(3): 1628-1635.

Aguilar, H. C. and R. M. Iorio (2012). "Henipavirus membrane fusion and viral entry." Curr Top Microbiol Immunol **359**: 79-94.

Akey, D. L., W. C. Brown, S. Dutta, J. Konwerski, J. Jose, T. J. Jurkiw, J. DelProposto, C. M. Ogata, G. Skiniotis, R. J. Kuhn and J. L. Smith (2014). "Flavivirus NS1 structures reveal surfaces for associations with membranes and the immune system." Science **343**(6173): 881-885.

Allison, S. L., J. Schalich, K. Stiasny, C. W. Mandl and F. X. Heinz (2001). "Mutational evidence for an internal fusion peptide in flavivirus envelope protein E." J Virol **75**(9): 4268-4275.

Amaya, M. and C. C. Broder (2020). "Vaccines to emerging viruses: Nipah and Hendra." Annu Rev Virol **7**(1): 447-473.

Andino, R. and E. Domingo (2015). "Viral quasispecies." Virology **479-480**: 46-51.

Arunkumar, G., R. Chandni, D. T. Mourya, S. K. Singh, R. Sadanandan, P. Sudan, B. Bhargava, P. Nipah Investigators and G. Health Study (2019). "Outbreak Investigation of Nipah Virus Disease in Kerala, India, 2018." J Infect Dis **219**(12): 1867-1878.

Arunkumar, G., S. Devadiga, A. K. McElroy, S. Prabhu, S. Sheik, J. Abdulmajeed, S. Robin, A. Sushama, A. Jayaram, S. Nittur, M. Shakir, K. G. S. Kumar, C. Radhakrishnan, K. Sakeena, J. Vasudevan, K. J. Reena, R. L. Sarita, J. D. Klena, C. F. Spiropoulou, K. F. Laserson and S. T. Nichol (2019). "Adaptive Immune Responses in Humans During Nipah Virus Acute and Convalescent Phases of Infection." Clin Infect Dis **69**(10): 1752-1756.

Avanzato, V. A., K. Y. Oguntuyo, M. Escalera-Zamudio, B. Gutierrez, M. Golden, S. L. Kosakovsky Pond, R. Pryce, T. S. Walter, J. Seow, K. J. Doores, O. G. Pybus, V. J. Munster, B. Lee and T. A. Bowden (2019). "A structural basis for antibody-mediated neutralization of Nipah virus reveals a site of vulnerability at the fusion glycoprotein apex." Proc Natl Acad Sci U S A **116**(50): 25057-25067.

Bajic, G., M. J. Maron, Y. Adachi, T. Onodera, K. R. McCarthy, C. E. McGee, G. D. Sempowski, Y. Takahashi, G. Kelsoe, M. Kuraoka and A. G. Schmidt (2019). "Influenza Antigen Engineering Focuses Immune Responses to a Subdominant but Broadly Protective Viral Epitope." Cell Host Microbe **25**(6): 827-835 e826.

Baker, K. S., S. Todd, G. Marsh, A. Fernandez-Loras, R. Suu-Ire, J. L. N. Wood, L. F. Wang, P. R. Murcia and A. A. Cunningham (2012). "Co-circulation of diverse paramyxoviruses in an urban African fruit bat population." J Gen Virol **93**(Pt 4): 850-856.

Balazs, A. B., J. Chen, C. M. Hong, D. S. Rao, L. Yang and D. Baltimore (2011). "Antibody-based protection against HIV infection by vectored immunoprophylaxis." Nature **481**(7379): 81-84.

Bangaru, S., S. Lang, M. Schotsaert, H. A. Vanderven, X. Zhu, N. Kose, R. Bombardi, J. A. Finn, S. J. Kent, P. Gilchuk, I. Gilchuk, H. L. Turner, A. Garcia-Sastre, S. Li, A. B. Ward, I. A. Wilson and J. E. Crowe, Jr. (2019). "A Site of Vulnerability on the Influenza Virus Hemagglutinin Head Domain Trimer Interface." Cell **177**(5): 1136-1152 e1118.

Bardina, S. V., P. Bunduc, S. Tripathi, J. Duehr, J. J. Frere, J. A. Brown, R. Nachbagauer, G. A. Foster, D. Krysztof, D. Tortorella, S. L. Stramer, A. Garcia-Sastre, F. Krammer and J. K. Lim (2017). "Enhancement of Zika virus pathogenesis by preexisting antiflavivirus immunity." Science **356**(6334): 175-180.

Barr, J., C. Smith, I. Smith, C. de Jong, S. Todd, D. Melville, A. Broos, S. Crameri, J. Haining, G. Marsh, G. Crameri, H. Field and L. F. Wang (2015). "Isolation of multiple novel paramyxoviruses from pteropid bat urine." J Gen Virol **96**(Pt 1): 24-29.

Barrett, A. D. and E. A. Gould (1986). "Antibody-mediated early death in vivo after infection with yellow fever virus." J Gen Virol **67 (Pt 11)**: 2539-2542.

Bauer, J. H. and N. P. Hudson (1928). "The Incubation Period of Yellow Fever in the Mosquito." J Exp Med **48**(1): 147-153.

Bennett, M. R., R. G. Bombardi, N. Kose, E. H. Parrish, M. B. Nagel, R. A. Petit, T. D. Read, K. L. Schey, I. P. Thomsen, E. P. Skaar and J. E. Crowe (2019). "Human mAbs to Staphylococcus aureus IsdA Provide Protection Through Both Heme-Blocking and Fc-Mediated Mechanisms." J Infect Dis **219**(8): 1264-1273.

Benson, M. D., M. I. Romero, M. E. Lush, Q. R. Lu, M. Henkemeyer and L. F. Parada (2005). "Ephrin-B3 is a myelin-based inhibitor of neurite outgrowth." Proc Natl Acad Sci U S A **102**(30): 10694-10699.

Boder, E. T. and K. D. Wittrup (1997). "Yeast surface display for screening combinatorial polypeptide libraries." Nat Biotechnol **15**(6): 553-557.

Bonaparte, M. I., A. S. Dimitrov, K. N. Bossart, G. Crameri, B. A. Mungall, K. A. Bishop, V. Choudhry, D. S. Dimitrov, L. F. Wang, B. T. Eaton and C. C. Broder (2005). "Ephrin-B2 ligand is a functional receptor for Hendra virus and Nipah virus." Proc Natl Acad Sci U S A **102**(30): 10652-10657.

Borisevich, V., B. Lee, A. Hickey, B. DeBuysscher, C. C. Broder, H. Feldmann and B. Rockx (2016). "Escape From Monoclonal Antibody Neutralization Affects Henipavirus Fitness In Vitro and In Vivo." J Infect Dis **213**(3): 448-455.

Bose, S., T. S. Jardetzky and R. A. Lamb (2015). "Timing is everything: Fine-tuned molecular machines orchestrate paramyxovirus entry." Virology **479-480**: 518-531.

Bose, S., B. D. Welch, C. A. Kors, P. Yuan, T. S. Jardetzky and R. A. Lamb (2011). "Structure and mutagenesis of the parainfluenza virus 5 hemagglutinin-neuraminidase stalk domain reveals a four-helix bundle and the role of the stalk in fusion promotion." J Virol **85**(24): 12855-12866.

Bossart, K. N., G. Crameri, A. S. Dimitrov, B. A. Mungall, Y. R. Feng, J. R. Patch, A. Choudhary, L. F. Wang, B. T. Eaton and C. C. Broder (2005). "Receptor binding, fusion inhibition, and induction of cross-reactive neutralizing antibodies by a soluble G glycoprotein of Hendra virus." J Virol **79**(11): 6690-6702.

Bossart, K. N., D. L. Fusco and C. C. Broder (2013). "Paramyxovirus entry." Adv Exp Med Biol **790**: 95-127.

Bossart, K. N., T. W. Geisbert, H. Feldmann, Z. Zhu, F. Feldmann, J. B. Geisbert, L. Yan, Y. R. Feng, D. Brining, D. Scott, Y. Wang, A. S. Dimitrov, J. Callison, Y. P. Chan, A. C. Hickey, D. S. Dimitrov, C. C. Broder and B. Rockx (2011). "A neutralizing human monoclonal antibody protects african green monkeys from hendra virus challenge." Sci Transl Med **3**(105): 105ra103.

Bossart, K. N., Z. Zhu, D. Middleton, J. Klippel, G. Crameri, J. Bingham, J. A. McEachern, D. Green, T. J. Hancock, Y. P. Chan, A. C. Hickey, D. S. Dimitrov, L. F. Wang and C. C. Broder (2009). "A neutralizing human monoclonal antibody protects against lethal disease in a new ferret model of acute nipah virus infection." PLoS Pathog **5**(10): e1000642.

Bottom-Tanzer, S. F., K. Rybkina, J. N. Bell, C. A. Alabi, C. Mathieu, M. Lu, S. Biswas, M. Vasquez, M. Porotto, J. A. Melero, V. Mas and A. Moscona (2019). "Inhibiting Human Parainfluenza Virus Infection by Preactivating the Cell Entry Mechanism." mBio **10**(1).

Bowden, T. A., A. R. Aricescu, R. J. Gilbert, J. M. Grimes, E. Y. Jones and D. I. Stuart (2008). "Structural basis of Nipah and Hendra virus attachment to their cell-surface receptor ephrin-B2." Nat Struct Mol Biol **15**(6): 567-572.

Bowden, T. A., M. Crispin, D. J. Harvey, E. Y. Jones and D. I. Stuart (2010). "Dimeric architecture of the Hendra virus attachment glycoprotein: evidence for a conserved mode of assembly." J Virol **84**(12): 6208-6217.

Bowers, P. M., R. A. Horlick, T. Y. Neben, R. M. Toobian, G. L. Tomlinson, J. L. Dalton, H. A. Jones, A. Chen, L. Altobell, 3rd, X. Zhang, J. L. Macomber, I. P. Krapf, B. F. Wu, A. McConnell, B. Chau, T. Holland, A. D. Berkebile, S. S. Neben, W. J. Boyle and D. J. King (2011). "Coupling mammalian cell surface display with somatic hypermutation for the discovery and maturation of human antibodies." Proc Natl Acad Sci U S A **108**(51): 20455-20460.

Boyaka, P. N. (2017). "Inducing Mucosal IgA: A Challenge for Vaccine Adjuvants and Delivery Systems." J Immunol **199**(1): 9-16.

Brack, C., M. Hirama, R. Lenhard-Schuller and S. Tonegawa (1978). "A complete immunoglobulin gene is created by somatic recombination." Cell **15**(1): 1-14.

Bradel-Tretheway, B. G., J. L. R. Zamora, J. A. Stone, Q. Liu, J. Li and H. C. Aguilar (2019). "Nipah and Hendra Virus Glycoproteins Induce Comparable Homologous but Distinct Heterologous Fusion Phenotypes." J Virol **93**(13).

Breit, T. M., I. L. Wolvers-Tettero, A. Beishuizen, M. A. Verhoeven, E. R. van Wering and J. J. van Dongen (1993). "Southern blot patterns, frequencies, and junctional diversity of T-cell receptor-delta gene rearrangements in acute lymphoblastic leukemia." Blood **82**(10): 3063-3074.

Briney, B., A. Inderbitzin, C. Joyce and D. R. Burton (2019). "Commonality despite exceptional diversity in the baseline human antibody repertoire." Nature **566**(7744): 393-397.

Brochet, X., M. P. Lefranc and V. Giudicelli (2008). "IMGT/V-QUEST: the highly customized and integrated system for IG and TR standardized V-J and V-D-J sequence analysis." Nucleic Acids Res. **36**(Web Server issue): W503-508.

Broder, C. C., K. Xu, D. B. Nikolov, Z. Zhu, D. S. Dimitrov, D. Middleton, J. Pallister, T. W. Geisbert, K. N. Bossart and L. F. Wang (2013). "A treatment for and vaccine against the deadly Hendra and Nipah viruses." Antiviral Res **100**(1): 8-13.

Brown, J. A., G. Singh, J. A. Acklin, S. Lee, J. E. Duehr, A. N. Chokola, J. J. Frere, K. W. Hoffman, G. A. Foster, D. Krysztof, R. Cadagan, A. R. Jacobs, S. L. Stramer, F. Krammer, A. Garcia-Sastre and J. K. Lim (2019). "Dengue Virus Immunity Increases Zika Virus-Induced Damage during Pregnancy." Immunity **50**(3): 751-762 e755.

Bujak, E., M. Matasci, D. Neri and S. Wulhfard (2014). "Reformatting of scFv antibodies into the scFv-Fc format and their downstream purification." Methods Mol Biol **1131**: 315-334.

Bukreyev, A., L. Yang, J. Fricke, L. Cheng, J. M. Ward, B. R. Murphy and P. L. Collins (2008). "The secreted form of respiratory syncytial virus G glycoprotein helps the virus evade antibody-mediated restriction of replication by acting as an antigen decoy and through effects on Fc receptor-bearing leukocytes." J Virol **82**(24): 12191-12204.

Calvert, A. E., K. L. Dixon, J. Piper, S. L. Bennett, B. A. Thibodeaux, A. D. Barrett, J. T. Roehrig and C. D. Blair (2016). "A humanized monoclonal antibody neutralizes yellow fever virus strain 17D-204 in vitro but does not protect a mouse model from disease." Antiviral Res **131**: 92-99.

Casadevall, A., E. Dadachova and L. A. Pirofski (2004). "Passive antibody therapy for infectious diseases." Nat Rev Microbiol **2**(9): 695-703.

Casadevall, A. and M. D. Scharff (1994). "Serum therapy revisited: animal models of infection and development of passive antibody therapy." Antimicrob Agents Chemother **38**(8): 1695-1702.

Chadha, M. S., J. A. Comer, L. Lowe, P. A. Rota, P. E. Rollin, W. J. Bellini, T. G. Ksiazek and A. Mishra (2006). "Nipah virus-associated encephalitis outbreak, Siliguri, India." Emerg Infect Dis **12**(2): 235-240.

Chambers, T. J., C. S. Hahn, R. Galler and C. M. Rice (1990). "Flavivirus genome organization, expression, and replication." Annu Rev Microbiol **44**: 649-688.

Chan, Y. P., M. Lu, S. Dutta, L. Yan, J. Barr, M. Flora, Y. R. Feng, K. Xu, D. B. Nikolov, L. F. Wang, G. Skiniotis and C. C. Broder (2012). "Biochemical, conformational, and immunogenic analysis of soluble trimeric forms of henipavirus fusion glycoproteins." J Virol **86**(21): 11457-11471.

Chao, L. H., D. E. Klein, A. G. Schmidt, J. M. Pena and S. C. Harrison (2014). "Sequential conformational rearrangements in flavivirus membrane fusion." Elife **3**: e04389.

Chen, P., A. Nirula, B. Heller, R. L. Gottlieb, J. Boscia, J. Morris, G. Huhn, J. Cardona, B. Mocherla, V. Stosor, I. Shawa, A. C. Adams, J. Van Naarden, K. L. Custer, L. Shen, M. Durante, G. Oakley, A. E. Schade, J. Sabo, D. R. Patel, P. Klekotka, D. M. Skovronsky and B.-. Investigators (2021). "SARS-CoV-2 Neutralizing Antibody LY-CoV555 in Outpatients with Covid-19." N Engl J Med **384**(3): 229-237.

Chen, Y., T. Maguire, R. E. Hileman, J. R. Fromm, J. D. Esko, R. J. Linhardt and R. M. Marks (1997). "Dengue virus infectivity depends on envelope protein binding to target cell heparan sulfate." Nat Med **3**(8): 866-871.

Chippaux, J. P. and A. Chippaux (2018). "Yellow fever in Africa and the Americas: a historical and epidemiological perspective." J Venom Anim Toxins Incl Trop Dis **24**: 20.

Chua, K. B., K. J. Goh, K. T. Wong, A. Kamarulzaman, P. S. Tan, T. G. Ksiazek, S. R. Zaki, G. Paul, S. K. Lam and C. T. Tan (1999). "Fatal encephalitis due to Nipah virus among pig-farmers in Malaysia." Lancet **354**(9186): 1257-1259.

Chua, K. B., C. L. Koh, P. S. Hooi, K. F. Wee, J. H. Khong, B. H. Chua, Y. P. Chan, M. E. Lim and S. K. Lam (2002). "Isolation of Nipah virus from Malaysian Island flying-foxes." Microbes Infect **4**(2): 145-151.

Chua, K. B., E. M. Wong, B. C. Cropp and A. D. Hyatt (2007). "Role of electron microscopy in Nipah virus outbreak investigation and control." Med J Malaysia **62**(2): 139-142.

Chung, K. M., G. E. Nybakken, B. S. Thompson, M. J. Engle, A. Marri, D. H. Fremont and M. S. Diamond (2006). "Antibodies against West Nile Virus nonstructural protein NS1 prevent

lethal infection through Fc gamma receptor-dependent and -independent mechanisms." J Virol **80**(3): 1340-1351.

Clayton, B. A., D. Middleton, J. Bergfeld, J. Haining, R. Arkinstall, L. Wang and G. A. Marsh (2012). "Transmission routes for nipah virus from Malaysia and Bangladesh." Emerg Infect Dis **18**(12): 1983-1993.

Colling, A., R. Lunt, J. Bergfeld, L. McNabb, K. Halpin, S. Juzva, K. Newberry, C. Morrissy, C. Loomes, S. Warner, I. Diallo, P. Kirkland, C. C. Broder, G. Carlile, M. H. Loh, C. Waugh, L. Wright, J. Watson, D. Eagles, K. Zuelke, S. McCullough and P. Daniels (2018). "A network approach for provisional assay recognition of a Hendra virus antibody ELISA: test validation with low sample numbers from infected horses." J Vet Diagn Invest **30**(3): 362-369.

Correia, B. E., Y. E. Ban, M. A. Holmes, H. Xu, K. Ellingson, Z. Kraft, C. Carrico, E. Boni, D. N. Sather, C. Zenobia, K. Y. Burke, T. Bradley-Hewitt, J. F. Bruhn-Johannsen, O. Kalyuzhniy, D. Baker, R. K. Strong, L. Stamatatos and W. R. Schief (2010). "Computational design of epitope-scaffolds allows induction of antibodies specific for a poorly immunogenic HIV vaccine epitope." Structure **18**(9): 1116-1126.

Correia, B. E., J. T. Bates, R. J. Loomis, G. Baneyx, C. Carrico, J. G. Jardine, P. Rupert, C. Correnti, O. Kalyuzhniy, V. Vittal, M. J. Connell, E. Stevens, A. Schroeter, M. Chen, S. Macpherson, A. M. Serra, Y. Adachi, M. A. Holmes, Y. Li, R. E. Klevit, B. S. Graham, R. T. Wyatt, D. Baker, R. K. Strong, J. E. Crowe, Jr., P. R. Johnson and W. R. Schief (2014). "Proof of principle for epitope-focused vaccine design." Nature **507**(7491): 201-206.

Crank, M. C., T. J. Ruckwardt, M. Chen, K. M. Morabito, E. Phung, P. J. Costner, L. A. Holman, S. P. Hickman, N. M. Berkowitz, I. J. Gordon, G. V. Yamshchikov, M. R. Gaudinski, A. Kumar, L. A. Chang, S. M. Moin, J. P. Hill, A. T. DiPiazza, R. M. Schwartz, L. Kueltzo, J. W. Cooper, P. Chen, J. A. Stein, K. Carlton, J. G. Gall, M. C. Nason, P. D. Kwong, G. L. Chen, J. R. Mascola, J. S. McLellan, J. E. Ledgerwood, B. S. Graham and V. R. C. S. Team (2019). "A proof of concept for structure-based vaccine design targeting RSV in humans." Science **365**(6452): 505-509.

Crennell, S., T. Takimoto, A. Portner and G. Taylor (2000). "Crystal structure of the multifunctional paramyxovirus hemagglutinin-neuraminidase." Nat Struct Biol **7**(11): 1068-1074.

Crevar, C. J., D. M. Carter, K. Y. Lee and T. M. Ross (2015). "Cocktail of H5N1 COBRA HA vaccines elicit protective antibodies against H5N1 viruses from multiple clades." Hum Vaccin Immunother **11**(3): 572-583.

Crill, W. D. and J. T. Roehrig (2001). "Monoclonal antibodies that bind to domain III of dengue virus E glycoprotein are the most efficient blockers of virus adsorption to Vero cells." J Virol **75**(16): 7769-7773.

Crowe, J. E., Jr. (2017). "Principles of Broad and Potent Antiviral Human Antibodies: Insights for Vaccine Design." Cell Host Microbe **22**(2): 193-206.

Cunha, M. S., R. M. Tubaki, R. M. T. de Menezes, M. Pereira, G. S. Caleiro, E. Coelho, L. D. C. Saad, N. Fernandes, J. M. Guerra, J. S. Nogueira, J. L. Summa, A. A. C. Coimbra, T. Zwarg, S. S. Witkin, L. F. Mucci, M. Timenetsky, E. C. Sabino and J. T. de Deus (2020). "Possible non-sylvatic transmission of yellow fever between non-human primates in Sao Paulo city, Brazil, 2017-2018." Sci Rep **10**(1): 15751.

Currie, W. (1803). "Observations on the Treatment of the Malignant Yellow Fever, Which Prevailed Partially in the City and Liberties of Philadelphia, in the Summer and Autumn of 1802." Med Phys J **9**(48): 97-103.

Daffis, S., R. E. Kontermann, J. Korimbocus, H. Zeller, H. D. Klenk and J. Ter Meulen (2005). "Antibody responses against wild-type yellow fever virus and the 17D vaccine strain: characterization with human monoclonal antibody fragments and neutralization escape variants." Virology **337**(2): 262-272.

Dang, H. V., Y. P. Chan, Y. J. Park, J. Snijder, S. C. Da Silva, B. Vu, L. Yan, Y. R. Feng, B. Rockx, T. W. Geisbert, C. E. Mire, C. C. Broder and D. Veesler (2019). "An antibody against the F glycoprotein inhibits Nipah and Hendra virus infections." Nat Struct Mol Biol **26**(10): 980-987.

Davis, E. H., A. S. Beck, A. E. Strother, J. K. Thompson, S. G. Widen, S. Higgs, T. G. Wood and A. D. T. Barrett (2019). "Attenuation of Live-Attenuated Yellow Fever 17D Vaccine Virus Is Localized to a High-Fidelity Replication Complex." mBio **10**(5).

de La Vega, M. A., G. Wong, G. P. Kobinger and X. Qiu (2015). "The multiple roles of sGP in Ebola pathogenesis." Viral Immunol **28**(1): 3-9.

de Sousa-Pereira, P. and J. M. Woof (2019). "IgA: Structure, Function, and Developability." Antibodies (Basel) **8**(4).

Dejnirattisai, W., A. Jumnainsong, N. Onsirisakul, P. Fitton, S. Vasanawathana, W. Limpitikul, C. Puttikhunt, C. Edwards, T. Duangchinda, S. Supasa, K. Chawansuntati, P. Malasit, J. Mongkolsapaya and G. Screaton (2010). "Cross-reacting antibodies enhance dengue virus infection in humans." Science **328**(5979): 745-748.

Dejnirattisai, W., P. Supasa, W. Wongwiwat, A. Rouvinski, G. Barba-Spaeth, T. Duangchinda, A. Sakuntabhai, V. M. Cao-Lormeau, P. Malasit, F. A. Rey, J. Mongkolsapaya and G. R. Screaton (2016). "Dengue virus sero-cross-reactivity drives antibody-dependent enhancement of infection with zika virus." Nat Immunol **17**(9): 1102-1108.

Deng, Y. Q., J. X. Dai, G. H. Ji, T. Jiang, H. J. Wang, H. O. Yang, W. L. Tan, R. Liu, M. Yu, B. X. Ge, Q. Y. Zhu, E. D. Qin, Y. J. Guo and C. F. Qin (2011). "A broadly flavivirus cross-neutralizing monoclonal antibody that recognizes a novel epitope within the fusion loop of E protein." PLoS One **6**(1): e16059.

Dimasi, N., R. Fleming, H. Wu and C. Gao (2019). "Molecular engineering strategies and methods for the expression and purification of IgG1-based bispecific bivalent antibodies." Methods **154**: 77-86.

Dong, J., R. W. Cross, M. P. Doyle, N. Kose, J. J. Mousa, E. J. Annand, V. Borisevich, K. N. Agans, R. Sutton, R. Nargi, M. Majedi, K. A. Fenton, W. Reichard, R. G. Bombardi, T. W. Geisbert and J. E. Crowe, Jr. (2020). "Potent Henipavirus Neutralization by Antibodies Recognizing Diverse Sites on Hendra and Nipah Virus Receptor Binding Protein." Cell **183**(6): 1536-1550 e1517.

Douam, F. and A. Ploss (2018). "Yellow Fever Virus: Knowledge Gaps Impeding the Fight Against an Old Foe." Trends Microbiol **26**(11): 913-928.

Drexler, J. F., V. M. Corman, M. A. Muller, G. D. Maganga, P. Vallo, T. Binger, F. Gloza-Rausch, V. M. Cottontail, A. Rasche, S. Yordanov, A. Seebens, M. Knornschild, S. Oppong, Y. Adu Sarkodie, C. Pongombo, A. N. Lukashev, J. Schmidt-Chanasit, A. Stocker, A. J. Carneiro, S. Erbar, A. Maisner, F. Fronhoffs, R. Buettner, E. K. Kalko, T. Kruppa, C. R. Franke, R. Kallies, E. R. Yandoko, G. Herrler, C. Reusken, A. Hassanin, D. H. Kruger, S. Matthee, R. G. Ulrich, E. M. Leroy and C. Drosten (2012). "Bats host major mammalian paramyxoviruses." Nat Commun **3**: 796.

Dunbar, J., K. Krawczyk, J. Leem, C. Marks, J. Nowak, C. Regep, G. Georges, S. Kelm, B. Popovic and C. M. Deane (2016). "SAbPred: a structure-based antibody prediction server." Nucleic Acids Res **44**(W1): W474-478.

Dups, J., D. Middleton, M. Yamada, P. Monaghan, F. Long, R. Robinson, G. A. Marsh and L. F. Wang (2012). "A new model for Hendra virus encephalitis in the mouse." PLoS One **7**(7): e40308.

Edeling, M. A., M. S. Diamond and D. H. Fremont (2014). "Structural basis of Flavivirus NS1 assembly and antibody recognition." Proc Natl Acad Sci U S A **111**(11): 4285-4290.

Edupuganti, S., N. Mgodi, S. T. Karuna, P. Andrew, E. Rudnicki, N. Kochar, A. deCamp, R. De La Grecca, M. Anderson, C. Karg, I. Tindale, E. Greene, G. B. Broder, J. Lucas, J. Hural, J. A. Gallardo-Cartagena, P. Gonzales, I. Frank, M. Sobieszczyk, M. M. Gomez Lorenzo, D. Burns, P. L. Anderson, M. D. Miner, J. Ledgerwood, J. R. Mascola, P. B. Gilbert, M. S. Cohen, L. Corey and H. H. s. group (2021). "Feasibility and Successful Enrollment in a Proof-of-Concept HIV Prevention Trial of VRC01, a Broadly Neutralizing HIV-1 Monoclonal Antibody." J Acquir Immune Defic Syndr **87**(1): 671-679.

Egelman, E. H., S. S. Wu, M. Amrein, A. Portner and G. Murti (1989). "The Sendai virus nucleocapsid exists in at least four different helical states." J Virol **63**(5): 2233-2243.

Elshuber, S., S. L. Allison, F. X. Heinz and C. W. Mandl (2003). "Cleavage of protein prM is necessary for infection of BHK-21 cells by tick-borne encephalitis virus." J Gen Virol **84**(Pt 1): 183-191.

Emsley, P. and K. Cowtan (2004). "Coot: model-building tools for molecular graphics." Acta Crystallogr D Biol Crystallogr **60**(Pt 12 Pt 1): 2126-2132.

Epstein, J. H., S. J. Anthony, A. Islam, A. M. Kilpatrick, S. Ali Khan, M. D. Balkey, N. Ross, I. Smith, C. Zambrana-Torrelio, Y. Tao, A. Islam, P. L. Quan, K. J. Olival, M. S. U. Khan, E. S.

Gurley, M. J. Hossein, H. E. Field, M. D. Fielder, T. Briese, M. Rahman, C. C. Broder, G. Crameri, L. F. Wang, S. P. Luby, W. I. Lipkin and P. Daszak (2020). "Nipah virus dynamics in bats and implications for spillover to humans." Proc Natl Acad Sci U S A **117**(46): 29190-29201.

Escaffre, O., V. Borisevich, J. R. Carmical, D. Prusak, J. Prescott, H. Feldmann and B. Rockx (2013). "Henipavirus pathogenesis in human respiratory epithelial cells." J Virol **87**(6): 3284-3294.

Fenouillet, E., J. C. Gluckman and I. M. Jones (1994). "Functions of HIV envelope glycans." Trends Biochem Sci **19**(2): 65-70.

Ferrara, F. and N. Temperton (2018). "Pseudotype neutralization assays: From laboratory bench to data analysis." Methods Protoc **1**(1).

Fibriansah, G., K. D. Ibarra, T. S. Ng, S. A. Smith, J. L. Tan, X. N. Lim, J. S. Ooi, V. A. Kostyuchenko, J. Wang, A. M. de Silva, E. Harris, J. E. Crowe, Jr. and S. M. Lok (2015). "DENGUE VIRUS. Cryo-EM structure of an antibody that neutralizes dengue virus type 2 by locking E protein dimers." Science **349**(6243): 88-91.

Field, H. E. (2016). "Hendra virus ecology and transmission." Curr Opin Virol **16**: 120-125.

Flajnik, M. F. and M. Kasahara (2010). "Origin and evolution of the adaptive immune system: genetic events and selective pressures." Nat Rev Genet **11**(1): 47-59.

Flyak, Andrew I., Philipp A. Ilinykh, Charles D. Murin, T. Garron, X. Shen, Marnie L. Fusco, T. Hashiguchi, Zachary A. Bornholdt, James C. Slaughter, G. Sapparapu, C. Klages, Thomas G. Ksiazek, Andrew B. Ward, Erica O. Saphire, A. Bukreyev and James E. Crowe (2015). "Mechanism of Human Antibody-Mediated Neutralization of Marburg Virus." Cell **160**(5): 893-903.

Foss, S., M. Bottermann, A. Jonsson, I. Sandlie, L. C. James and J. T. Andersen (2019). "TRIM21-From Intracellular Immunity to Therapy." Front Immunol **10**: 2049.

Gaythorpe, K. A., A. Hamlet, K. Jean, D. Garkauskas Ramos, L. Cibrelus, T. Garske and N. Ferguson (2021). "The global burden of yellow fever." Elife **10**.

Geisbert, T. W., K. Bobb, V. Borisevich, J. B. Geisbert, K. N. Agans, R. W. Cross, A. N. Prasad, K. A. Fenton, H. Yu, T. R. Fouts, C. C. Broder and A. S. Dimitrov (2021). "A single dose investigational subunit vaccine for human use against Nipah virus and Hendra virus." NPJ Vaccines **6**(1): 23.

Geisbert, T. W., K. M. Daddario-DiCaprio, A. C. Hickey, M. A. Smith, Y. P. Chan, L. F. Wang, J. J. Mattapallil, J. B. Geisbert, K. N. Bossart and C. C. Broder (2010). "Development of an acute and highly pathogenic nonhuman primate model of Nipah virus infection." PLoS One **5**(5): e10690.

Geisbert, T. W., C. E. Mire, J. B. Geisbert, Y. P. Chan, K. N. Agans, F. Feldmann, K. A. Fenton, Z. Zhu, D. S. Dimitrov, D. P. Scott, K. N. Bossart, H. Feldmann and C. C. Broder (2014).

"Therapeutic treatment of Nipah virus infection in nonhuman primates with a neutralizing human monoclonal antibody." Sci Transl Med **6**(242): 242ra282.

Gershman, M. D., K. M. Angelo, J. Ritchey, D. P. Greenberg, R. D. Muhammad, G. Brunette, M. S. Cetron and M. J. Sotir (2017). "Addressing a Yellow Fever Vaccine Shortage - United States, 2016-2017." MMWR Morb Mortal Wkly Rep **66**(17): 457-459.

Gilchuk, I. M., S. Bangaru, P. Gilchuk, R. P. Irving, N. Kose, R. G. Bombardi, N. J. Thornburg, C. B. Creech, K. M. Edwards, S. Li, H. L. Turner, W. Yu, X. Zhu, I. A. Wilson, A. B. Ward and J. E. Crowe, Jr. (2019). "Influenza H7N9 Virus Neuraminidase-Specific Human Monoclonal Antibodies Inhibit Viral Egress and Protect from Lethal Influenza Infection in Mice." Cell Host Microbe **26**(6): 715-728 e718.

Gilchuk, P., R. G. Bombardi, J. H. Erasmus, Q. Tan, R. Nargi, C. Soto, P. Abbink, T. J. Suscovich, L. A. Durnell, A. Khandhar, J. Archer, J. Liang, M. E. Fouch, E. Davidson, B. J. Doranz, T. Jones, E. Larson, S. Ertel, B. Granger, J. Fuerte-Stone, V. Roy, T. Broge, T. C. Linnekin, C. H. Linde, M. J. Gorman, J. Nkolola, G. Alter, S. G. Reed, D. H. Barouch, M. S. Diamond, J. E. Crowe, Jr., N. Van Hoeven, L. B. Thackray and R. H. Carnahan (2020). "Integrated pipeline for the accelerated discovery of antiviral antibody therapeutics." Nat Biomed Eng **4**(11): 1030-1043.

Gilchuk, P., N. Kuzmina, P. A. Ilinykh, K. Huang, B. M. Gunn, A. Bryan, E. Davidson, B. J. Doranz, H. L. Turner, M. L. Fusco, M. S. Bramble, N. A. Hoff, E. Binshtein, N. Kose, A. I. Flyak, R. Flinko, C. Orlandi, R. Carnahan, E. H. Parrish, A. M. Sevy, R. G. Bombardi, P. K. Singh, P. Mukadi, J. J. Muyembe-Tamfum, M. D. Ohi, E. O. Saphire, G. K. Lewis, G. Alter, A. B. Ward, A. W. Rimoin, A. Bukreyev and J. E. Crowe, Jr. (2018). "Multifunctional Pan-ebolavirus Antibody Recognizes a Site of Broad Vulnerability on the Ebolavirus Glycoprotein." Immunity **49**(2): 363-374 e310.

Gilchuk, P., C. D. Murin, J. C. Milligan, R. W. Cross, C. E. Mire, P. A. Ilinykh, K. Huang, N. Kuzmina, P. X. Altman, S. Hui, B. M. Gunn, A. L. Bryan, E. Davidson, B. J. Doranz, H. L. Turner, T. Alkutkar, R. Flinko, C. Orlandi, R. Carnahan, R. Nargi, R. G. Bombardi, M. E. Vodzak, S. Li, A. Okoli, M. Ibeawuchi, B. Ohiaeri, G. K. Lewis, G. Alter, A. Bukreyev, E. O. Saphire, T. W. Geisbert, A. B. Ward and J. E. Crowe, Jr. (2020). "Analysis of a Therapeutic Antibody Cocktail Reveals Determinants for Cooperative and Broad Ebolavirus Neutralization." Immunity **52**(2): 388-403 e312.

Giudicelli, V. and M. P. Lefranc (2011). "IMGT/junctionanalysis: IMGT standardized analysis of the V-J and V-D-J junctions of the rearranged immunoglobulins (IG) and T cell receptors (TR)." Cold Spring Harb. Protoc. **2011**(6): 716-725.

Goh, K. J., C. T. Tan, N. K. Chew, P. S. Tan, A. Kamarulzaman, S. A. Sarji, K. T. Wong, B. J. Abdullah, K. B. Chua and S. K. Lam (2000). "Clinical features of Nipah virus encephalitis among pig farmers in Malaysia." N Engl J Med **342**(17): 1229-1235.

Goldstein, M., J. Fergie and L. R. Krilov (2021). "Impact of the 2014 American Academy of Pediatrics Policy on RSV Hospitalization in Preterm Infants in the United States." Infect Dis Ther.

Gomez Roman, R., L. F. Wang, B. Lee, K. Halpin, E. de Wit, C. C. Broder, M. Rahman, P. Kristiansen and M. Saville (2020). "Nipah@20: Lessons learned from another virus with pandemic potential." mSphere **5**(4).

Gould, E. A. and A. Buckley (1989). "Antibody-dependent enhancement of yellow fever and Japanese encephalitis virus neurovirulence." J Gen Virol **70 (Pt 6)**: 1605-1608.

Greaney, A. J., T. N. Starr, P. Gilchuk, S. J. Zost, E. Binshtein, A. N. Loes, S. K. Hilton, J. Huddleston, R. Eguia, K. H. D. Crawford, A. S. Dingens, R. S. Nargi, R. E. Sutton, N. Suryadevara, P. W. Rothlauf, Z. Liu, S. P. J. Whelan, R. H. Carnahan, J. E. Crowe and J. D. Bloom (2020). "Complete mapping of mutations to the SARS-CoV-2 spike receptor-binding domain that escape antibody recognition." bioRxiv.

Greaney, A. J., T. N. Starr, P. Gilchuk, S. J. Zost, E. Binshtein, A. N. Loes, S. K. Hilton, J. Huddleston, R. Eguia, K. H. D. Crawford, A. S. Dingens, R. S. Nargi, R. E. Sutton, N. Suryadevara, P. W. Rothlauf, Z. Liu, S. P. J. Whelan, R. H. Carnahan, J. E. Crowe, Jr. and J. D. Bloom (2021). "Complete Mapping of Mutations to the SARS-CoV-2 Spike Receptor-Binding Domain that Escape Antibody Recognition." Cell Host Microbe **29**(1): 44-57 e49.

Guillaume, V., H. Contamin, P. Loth, M. C. Georges-Courbot, A. Lefeuvre, P. Marianneau, K. B. Chua, S. K. Lam, R. Buckland, V. Deubel and T. F. Wild (2004). "Nipah virus: vaccination and passive protection studies in a hamster model." J Virol **78**(2): 834-840.

Guillaume, V., H. Contamin, P. Loth, I. Grosjean, M. C. Courbot, V. Deubel, R. Buckland and T. F. Wild (2006). "Antibody prophylaxis and therapy against Nipah virus infection in hamsters." J Virol **80**(4): 1972-1978.

Guirakhoo, F., K. Pugachev, J. Arroyo, C. Miller, Z. X. Zhang, R. Weltzin, K. Georgakopoulos, J. Catalan, S. Ocran, K. Draper and T. P. Monath (2002). "Viremia and immunogenicity in nonhuman primates of a tetravalent yellow fever-dengue chimeric vaccine: genetic reconstructions, dose adjustment, and antibody responses against wild-type dengue virus isolates." Virology **298**(1): 146-159.

Gurley, E. S., J. M. Montgomery, M. J. Hossain, M. Bell, A. K. Azad, M. R. Islam, M. A. Molla, D. S. Carroll, T. G. Ksiazek, P. A. Rota, L. Lowe, J. A. Comer, P. Rollin, M. Czub, A. Grolla, H. Feldmann, S. P. Luby, J. L. Woodward and R. F. Breiman (2007). "Person-to-person transmission of Nipah virus in a Bangladeshi community." Emerg Infect Dis **13**(7): 1031-1037.

Hackett, B. A. and S. Cherry (2018). "Flavivirus internalization is regulated by a size-dependent endocytic pathway." Proc Natl Acad Sci U S A **115**(16): 4246-4251.

Halpin, K., A. D. Hyatt, R. Fogarty, D. Middleton, J. Bingham, J. H. Epstein, S. A. Rahman, T. Hughes, C. Smith, H. E. Field, P. Daszak and G. Henipavirus Ecology Research (2011). "Pteropid bats are confirmed as the reservoir hosts of henipaviruses: a comprehensive experimental study of virus transmission." Am J Trop Med Hyg **85**(5): 946-951.

Halpin, K., P. L. Young, H. E. Field and J. S. Mackenzie (2000). "Isolation of Hendra virus from pteropid bats: a natural reservoir of Hendra virus." J Gen Virol **81**(Pt 8): 1927-1932.

Hammarlund, E., A. Thomas, I. J. Amanna, L. A. Holden, O. D. Slayden, B. Park, L. Gao and M. K. Slifka (2017). "Plasma cell survival in the absence of B cell memory." Nat Commun **8**(1): 1781.

Hansen, J., A. Baum, K. E. Pascal, V. Russo, S. Giordano, E. Wloga, B. O. Fulton, Y. Yan, K. Koon, K. Patel, K. M. Chung, A. Hermann, E. Ullman, J. Cruz, A. Rafique, T. Huang, J. Fairhurst, C. Libertiny, M. Malbec, W. Y. Lee, R. Welsh, G. Farr, S. Pennington, D. Deshpande, J. Cheng, A. Watty, P. Bouffard, R. Babb, N. Levenkova, C. Chen, B. Zhang, A. Romero Hernandez, K. Saotome, Y. Zhou, M. Franklin, S. Sivapalasingam, D. C. Lye, S. Weston, J. Logue, R. Haupt, M. Frieman, G. Chen, W. Olson, A. J. Murphy, N. Stahl, G. D. Yancopoulos and C. A. Kyratsous (2020). "Studies in humanized mice and convalescent humans yield a SARS-CoV-2 antibody cocktail." Science **369**(6506): 1010-1014.

Hardy, R. R. and K. Hayakawa (2015). "Perspectives on fetal derived CD5+ B1 B cells." Eur J Immunol **45**(11): 2978-2984.

Hellert, J., J. Buchrieser, F. Larrous, A. Minola, G. D. de Melo, L. Soriaga, P. England, A. Haouz, A. Telenti, O. Schwartz, D. Corti, H. Bourhy and F. A. Rey (2020). "Structure of the prefusion-locking broadly neutralizing antibody RVC20 bound to the rabies virus glycoprotein." Nat Commun **11**(1): 596.

Hernaez, B. and A. Alcami (2018). "New insights into the immunomodulatory properties of poxvirus cytokine decoy receptors at the cell surface." F1000Res **7**.

Homaira, N., M. Rahman, M. J. Hossain, J. H. Epstein, R. Sultana, M. S. Khan, G. Podder, K. Nahar, B. Ahmed, E. S. Gurley, P. Daszak, W. I. Lipkin, P. E. Rollin, J. A. Comer, T. G. Ksiazek and S. P. Luby (2010). "Nipah virus outbreak with person-to-person transmission in a district of Bangladesh, 2007." Epidemiol Infect **138**(11): 1630-1636.

Hossain, M. J., E. S. Gurley, J. M. Montgomery, M. Bell, D. S. Carroll, V. P. Hsu, P. Formenty, A. Croisier, E. Bertherat, M. A. Faiz, A. K. Azad, R. Islam, M. A. Molla, T. G. Ksiazek, P. A. Rota, J. A. Comer, P. E. Rollin, S. P. Luby and R. F. Breiman (2008). "Clinical presentation of nipah virus infection in Bangladesh." Clin Infect Dis **46**(7): 977-984.

Howell, K. A., J. M. Brannan, C. Bryan, A. McNeal, E. Davidson, H. L. Turner, H. Vu, S. Shulenin, S. He, A. Kuehne, A. S. Herbert, X. Qiu, B. J. Doranz, F. W. Holtsberg, A. B. Ward, J. M. Dye and M. J. Aman (2017). "Cooperativity Enables Non-neutralizing Antibodies to Neutralize Ebolavirus." Cell Rep **19**(2): 413-424.

Hsieh, C. L., J. A. Goldsmith, J. M. Schaub, A. M. DiVenere, H. C. Kuo, K. Javanmardi, K. C. Le, D. Wrapp, A. G. Lee, Y. Liu, C. W. Chou, P. O. Byrne, C. K. Hjorth, N. V. Johnson, J. Ludes-Meyers, A. W. Nguyen, J. Park, N. Wang, D. Amengor, J. J. Lavinder, G. C. Ippolito, J. A. Maynard, I. J. Finkelstein and J. S. McLellan (2020). "Structure-based design of prefusion-stabilized SARS-CoV-2 spikes." Science **369**(6510): 1501-1505.

Huo, J., A. Le Bas, R. R. Ruza, H. M. E. Duyvesteyn, H. Mikolajek, T. Malinauskas, T. K. Tan, P. Rijal, M. Dumoux, P. N. Ward, J. Ren, D. Zhou, P. J. Harrison, M. Weckener, D. K. Clare, V. K. Vogirala, J. Radecke, L. Moynie, Y. Zhao, J. Gilbert-Jaramillo, M. L. Knight, J. A. Tree, K.

R. Buttigieg, N. Coombes, M. J. Elmore, M. W. Carroll, L. Carrique, P. N. M. Shah, W. James, A. R. Townsend, D. I. Stuart, R. J. Owens and J. H. Naismith (2020). "Neutralizing nanobodies bind SARS-CoV-2 spike RBD and block interaction with ACE2." Nat Struct Mol Biol **27**(9): 846-854.

Ianevski, A., L. He, T. Aittokallio and J. Tang (2020). "SynergyFinder: a web application for analyzing drug combination dose-response matrix data." Bioinformatics.

Janeway, C. A., Jr. and R. Medzhitov (2002). "Innate immune recognition." Annu Rev Immunol **20**: 197-216.

Jardetzky, T. S. and R. A. Lamb (2014). "Activation of paramyxovirus membrane fusion and virus entry." Curr Opin Virol **5**: 24-33.

Jennings, R. G. (1878). "The Quarantine at Little Rock, Arkansas, during August, September, and October, 1878, against the Yellow Fever Epidemic in Memphis and the Mississippi Valley." Public Health Pap Rep **4**: 223-227.

Jeske, D. J., J. Jarvis, C. Milstein and J. D. Capra (1984). "Junctional diversity is essential to antibody activity." J Immunol **133**(3): 1090-1092.

Jin, J., J. G. Galaz-Montoya, M. B. Sherman, S. Y. Sun, C. S. Goldsmith, E. T. O'Toole, L. Ackerman, L. A. Carlson, S. C. Weaver, W. Chiu and G. Simmons (2018). "Neutralizing Antibodies Inhibit Chikungunya Virus Budding at the Plasma Membrane." Cell Host Microbe **24**(3): 417-428 e415.

Johnson, S., C. Oliver, G. A. Prince, V. G. Hemming, D. S. Pfarr, S. C. Wang, M. Dormitzer, J. O'Grady, S. Koenig, J. K. Tamura, R. Woods, G. Bansal, D. Couchenour, E. Tsao, W. C. Hall and J. F. Young (1997). "Development of a humanized monoclonal antibody (MEDI-493) with potent in vitro and in vivo activity against respiratory syncytial virus." J Infect Dis **176**(5): 1215-1224.

Johnston, S. C., T. Briese, T. M. Bell, W. D. Pratt, J. D. Shamblin, H. L. Esham, G. C. Donnelly, J. C. Johnson, L. E. Hensley, W. I. Lipkin and A. N. Honko (2015). "Detailed analysis of the African green monkey model of Nipah virus disease." PLoS One **10**(2): e0117817.

Juan-Giner, A., D. Kimathi, K. H. Grantz, M. Hamaluba, P. Kazooba, P. Njuguna, G. Fall, M. Dia, N. S. Bob, T. P. Monath, A. D. Barrett, J. Hombach, E. M. Mulogo, I. Ampeire, H. K. Karanja, D. Nyehangane, J. Mwanga-Amumpaire, D. A. T. Cummings, P. Bejon, G. M. Warimwe and R. F. Grais (2021). "Immunogenicity and safety of fractional doses of yellow fever vaccines: a randomised, double-blind, non-inferiority trial." Lancet **397**(10269): 119-127.

Julander, J. G., B. A. Thibodeaux, J. D. Morrey, J. T. Roehrig and C. D. Blair (2014). "Humanized monoclonal antibody 2C9-cIgG has enhanced efficacy for yellow fever prophylaxis and therapy in an immunocompetent animal model." Antiviral Res **103**: 32-38.

Junjhon, J., T. J. Edwards, U. Utaipat, V. D. Bowman, H. A. Holdaway, W. Zhang, P. Keelapang, C. Puttikhunt, R. Perera, P. R. Chipman, W. Kasinrerk, P. Malasit, R. J. Kuhn and N.

Sittisombut (2010). "Influence of pr-M cleavage on the heterogeneity of extracellular dengue virus particles." J Virol **84**(16): 8353-8358.

Junjhon, J., M. Lausumpao, S. Supasa, S. Noisakran, A. Songjaeng, P. Saraithong, K. Chaichoun, U. Utaipat, P. Keelapang, A. Kanjanahaluethai, C. Puttikhunt, W. Kasinrerk, P. Malasit and N. Sittisombut (2008). "Differential modulation of prM cleavage, extracellular particle distribution, and virus infectivity by conserved residues at nonfurin consensus positions of the dengue virus pr-M junction." J Virol **82**(21): 10776-10791.

Junt, T., E. A. Moseman, M. Iannacone, S. Massberg, P. A. Lang, M. Boes, K. Fink, S. E. Henrickson, D. M. Shayakhmetov, N. C. Di Paolo, N. van Rooijen, T. R. Mempel, S. P. Whelan and U. H. von Andrian (2007). "Subcapsular sinus macrophages in lymph nodes clear lymph-borne viruses and present them to antiviral B cells." Nature **450**(7166): 110-114.

Kabsch, W. (2010). "Xds." Acta Crystallogr D Biol Crystallogr **66**(Pt 2): 125-132.

Kajihara, M., A. Marzi, E. Nakayama, T. Noda, M. Kuroda, R. Manzoor, K. Matsuno, H. Feldmann, R. Yoshida, Y. Kawaoka and A. Takada (2012). "Inhibition of Marburg virus budding by nonneutralizing antibodies to the envelope glycoprotein." J Virol **86**(24): 13467-13474.

Kaufmann, B., M. R. Vogt, J. Goudsmit, H. A. Holdaway, A. A. Aksyuk, P. R. Chipman, R. J. Kuhn, M. S. Diamond and M. G. Rossmann (2010). "Neutralization of West Nile virus by cross-linking of its surface proteins with Fab fragments of the human monoclonal antibody CR4354." Proc Natl Acad Sci U S A **107**(44): 18950-18955.

Kessler, M. K., D. J. Becker, A. J. Peel, N. V. Justice, T. Lunn, D. E. Crowley, D. N. Jones, P. Eby, C. A. Sanchez and R. K. Plowright (2018). "Changing resource landscapes and spillover of henipaviruses." Ann N Y Acad Sci **1429**(1): 78-99.

Kohler, G. and C. Milstein (1975). "Continuous cultures of fused cells secreting antibody of predefined specificity." Nature **256**(5517): 495-497.

Kose, N., J. M. Fox, G. Sapparapu, R. Bombardi, R. N. Tennekoon, A. D. de Silva, S. M. Elbashir, M. A. Theisen, E. Humphris-Narayanan, G. Ciaramella, S. Himansu, M. S. Diamond and J. E. Crowe, Jr. (2019). "A lipid-encapsulated mRNA encoding a potently neutralizing human monoclonal antibody protects against chikungunya infection." Sci Immunol **4**(35).

Kraemer, M. U. G., N. R. Faria, R. C. Reiner, Jr., N. Golding, B. Nikolay, S. Stasse, M. A. Johansson, H. Salje, O. Faye, G. R. W. Wint, M. Niedrig, F. M. Shearer, S. C. Hill, R. N. Thompson, D. Bisanzio, N. Taveira, H. H. Nax, B. S. R. Pradelski, E. O. Nsoesie, N. R. Murphy, Bogoch, II, K. Khan, J. S. Brownstein, A. J. Tatem, T. de Oliveira, D. L. Smith, A. A. Sall, O. G. Pybus, S. I. Hay and S. Cauchemez (2017). "Spread of yellow fever virus outbreak in Angola and the Democratic Republic of the Congo 2015-16: a modelling study." Lancet Infect Dis **17**(3): 330-338.

Kuhn, R. J., W. Zhang, M. G. Rossmann, S. V. Pletnev, J. Corver, E. Lenches, C. T. Jones, S. Mukhopadhyay, P. R. Chipman, E. G. Strauss, T. S. Baker and J. H. Strauss (2002). "Structure of

dengue virus: implications for flavivirus organization, maturation, and fusion." Cell **108**(5): 717-725.

Laing, E. D., C. K. Navaratnarajah, S. Cheliout Da Silva, S. R. Petzing, Y. Xu, S. L. Sterling, G. A. Marsh, L. F. Wang, M. Amaya, D. B. Nikolov, R. Cattaneo, C. C. Broder and K. Xu (2019). "Structural and functional analyses reveal promiscuous and species specific use of ephrin receptors by Cedar virus." Proc Natl Acad Sci U S A **116**(41): 20707-20715.

Lawrence, M. C., N. A. Borg, V. A. Streltsov, P. A. Pilling, V. C. Epa, J. N. Varghese, J. L. McKimm-Breschkin and P. M. Colman (2004). "Structure of the haemagglutinin-neuraminidase from human parainfluenza virus type III." J Mol Biol **335**(5): 1343-1357.

Lazar, G. A., W. Dang, S. Karki, O. Vafa, J. S. Peng, L. Hyun, C. Chan, H. S. Chung, A. Eivazi, S. C. Yoder, J. Vielmetter, D. F. Carmichael, R. J. Hayes and B. I. Dahiyat (2006). "Engineered antibody Fc variants with enhanced effector function." Proc Natl Acad Sci U S A **103**(11): 4005-4010.

Lee, B. and Z. A. Ataman (2011). "Modes of paramyxovirus fusion: a Henipavirus perspective." Trends Microbiol **19**(8): 389-399.

Lee, C. H., T. H. Kang, O. Godon, M. Watanabe, G. Delidakis, C. M. Gillis, D. Sterlin, D. Hardy, M. Cogne, L. E. Macdonald, A. J. Murphy, N. Tu, J. Lee, J. R. McDaniel, E. Makowski, P. M. Tessier, A. S. Meyer, P. Bruhns and G. Georgiou (2019). "An engineered human Fc domain that behaves like a pH-toggle switch for ultra-long circulation persistence." Nat Commun **10**(1): 5031.

Lee, J., D. R. Boutz, V. Chromikova, M. G. Joyce, C. Vollmers, K. Leung, A. P. Horton, B. J. DeKosky, C. H. Lee, J. J. Lavinder, E. M. Murrin, C. Chrysostomou, K. H. Hoi, Y. Tsybovsky, P. V. Thomas, A. Druz, B. Zhang, Y. Zhang, L. Wang, W. P. Kong, D. Park, L. I. Popova, C. L. Dekker, M. M. Davis, C. E. Carter, T. M. Ross, A. D. Ellington, P. C. Wilson, E. M. Marcotte, J. R. Mascola, G. C. Ippolito, F. Krammer, S. R. Quake, P. D. Kwong and G. Georgiou (2016). "Molecular-level analysis of the serum antibody repertoire in young adults before and after seasonal influenza vaccination." Nat Med **22**(12): 1456-1464.

Leung, K., A. Klaus, B. K. Lin, E. Laks, J. Biele, D. Lai, A. Bashashati, Y. F. Huang, R. Aniba, M. Moksa, A. Steif, A. M. Mes-Masson, M. Hirst, S. P. Shah, S. Aparicio and C. L. Hansen (2016). "Robust high-performance nanoliter-volume single-cell multiple displacement amplification on planar substrates." Proc Natl Acad Sci U S A **113**(30): 8484-8489.

Li, Y., R. Li, M. Wang, Y. Liu, Y. Yin, X. Zai, X. Song, Y. Chen, J. Xu and W. Chen (2020). "Fc-Based Recombinant Henipavirus Vaccines Elicit Broad Neutralizing Antibody Responses in Mice." Viruses **12**(4).

Liu, J., K. M. Coffin, S. C. Johnston, A. M. Babka, T. M. Bell, S. Y. Long, A. N. Honko, J. H. Kuhn and X. Zeng (2019). "Nipah virus persists in the brains of nonhuman primate survivors." JCI Insight **4**(14).

Liu, Q., J. A. Stone, B. Bradel-Tretheway, J. Dabundo, J. A. Benavides Montano, J. Santos-Montanez, S. B. Biering, A. V. Nicola, R. M. Iorio, X. Lu and H. C. Aguilar (2013). "Unraveling a three-step spatiotemporal mechanism of triggering of receptor-induced Nipah virus fusion and cell entry." PLoS Pathog **9**(11): e1003770.

Lo, M., H. S. Kim, R. K. Tong, T. W. Bainbridge, J. M. Vernes, Y. Zhang, Y. L. Lin, S. Chung, M. S. Dennis, Y. J. Zuchero, R. J. Watts, J. A. Couch, Y. G. Meng, J. K. Atwal, R. J. Brezski, C. Spiess and J. A. Ernst (2017). "Effector-attenuating Substitutions That Maintain Antibody Stability and Reduce Toxicity in Mice." J Biol Chem **292**(9): 3900-3908.

Lo, M. K., F. Feldmann, J. M. Gary, R. Jordan, R. Bannister, J. Cronin, N. R. Patel, J. D. Klena, S. T. Nichol, T. Cihlar, S. R. Zaki, H. Feldmann, C. F. Spiropoulou and E. de Wit (2019). "Remdesivir (GS-5734) protects African green monkeys from Nipah virus challenge." Sci Transl Med **11**(494).

Lo, M. K., L. Lowe, K. B. Hummel, H. M. Sazzad, E. S. Gurley, M. J. Hossain, S. P. Luby, D. M. Miller, J. A. Comer, P. E. Rollin, W. J. Bellini and P. A. Rota (2012). "Characterization of Nipah virus from outbreaks in Bangladesh, 2008-2010." Emerg Infect Dis **18**(2): 248-255.

Loomis, R. J., G. B. E. Stewart-Jones, Y. Tsybovsky, R. T. Caringal, K. M. Morabito, J. S. McLellan, A. L. Chamberlain, S. T. Nugent, G. B. Hutchinson, L. A. Kueltzo, J. R. Mascola and B. S. Graham (2020). "Structure-Based Design of Nipah Virus Vaccines: A Generalizable Approach to Paramyxovirus Immunogen Development." Front Immunol **11**: 842.

Lu, X., H. Xiao, S. Li, X. Pang, J. Song, S. Liu, H. Cheng, Y. Li, X. Wang, C. Huang, T. Guo, J. Ter Meulen, S. Daffis, J. Yan, L. Dai, Z. Rao, H. D. Klenk, J. Qi, Y. Shi and G. F. Gao (2019). "Double Lock of a Human Neutralizing and Protective Monoclonal Antibody Targeting the Yellow Fever Virus Envelope." Cell Rep **26**(2): 438-446 e435.

Luby, S. P. (2013). "The pandemic potential of Nipah virus." Antiviral Res **100**(1): 38-43.

Luby, S. P., M. Rahman, M. J. Hossain, L. S. Blum, M. M. Husain, E. Gurley, R. Khan, B. N. Ahmed, S. Rahman, N. Nahar, E. Kenah, J. A. Comer and T. G. Ksiazek (2006). "Foodborne transmission of Nipah virus, Bangladesh." Emerg Infect Dis **12**(12): 1888-1894.

Luis, A. D., T. J. O'Shea, D. T. S. Hayman, J. L. N. Wood, A. A. Cunningham, A. T. Gilbert, J. N. Mills and C. T. Webb (2015). "Network analysis of host-virus communities in bats and rodents reveals determinants of cross-species transmission." Ecol Lett **18**(11): 1153-1162.

Lynch, R. M., L. Tran, M. K. Louder, S. D. Schmidt, M. Cohen, C. C. T. Members, R. Dersimonian, Z. Euler, E. S. Gray, S. Abdool Karim, J. Kirchherr, D. C. Montefiori, S. Sibeko, K. Soderberg, G. Tomaras, Z. Y. Yang, G. J. Nabel, H. Schuitemaker, L. Morris, B. F. Haynes and J. R. Mascola (2012). "The development of CD4 binding site antibodies during HIV-1 infection." J Virol **86**(14): 7588-7595.

Maar, D., B. Harmon, D. Chu, B. Schulz, H. C. Aguilar, B. Lee and O. A. Negrete (2012). "Cysteines in the stalk of the nipah virus G glycoprotein are located in a distinct subdomain critical for fusion activation." J Virol **86**(12): 6632-6642.

Marsh, G. A., C. de Jong, J. A. Barr, M. Tachedjian, C. Smith, D. Middleton, M. Yu, S. Todd, A. J. Foord, V. Haring, J. Payne, R. Robinson, I. Broz, G. Crameri, H. E. Field and L. F. Wang (2012). "Cedar virus: a novel Henipavirus isolated from Australian bats." PLoS Pathog **8**(8): e1002836.

Martin, G., C. Yanez-Arenas, C. Chen, R. K. Plowright, R. J. Webb and L. F. Skerratt (2018). "Climate change could increase the geographic extent of Hendra virus spillover risk." Ecohealth **15**(3): 509-525.

Matsuda, F., K. Ishii, P. Bourvagnet, K. Kuma, H. Hayashida, T. Miyata and T. Honjo (1998). "The complete nucleotide sequence of the human immunoglobulin heavy chain variable region locus." J Exp Med **188**(11): 2151-2162.

McCafferty, J., A. D. Griffiths, G. Winter and D. J. Chiswell (1990). "Phage antibodies: filamentous phage displaying antibody variable domains." Nature **348**(6301): 552-554.

McCoy, A. J., R. W. Grosse-Kunstleve, P. D. Adams, M. D. Winn, L. C. Storoni and R. J. Read (2007). "Phaser crystallographic software." J Appl Crystallogr **40**(Pt 4): 658-674.

McLellan, J. S., M. Chen, M. G. Joyce, M. Sastry, G. B. Stewart-Jones, Y. Yang, B. Zhang, L. Chen, S. Srivatsan, A. Zheng, T. Zhou, K. W. Graepel, A. Kumar, S. Moin, J. C. Boyington, G. Y. Chuang, C. Soto, U. Baxa, A. Q. Bakker, H. Spits, T. Beaumont, Z. Zheng, N. Xia, S. Y. Ko, J. P. Todd, S. Rao, B. S. Graham and P. D. Kwong (2013). "Structure-based design of a fusion glycoprotein vaccine for respiratory syncytial virus." Science **342**(6158): 592-598.

McLellan, J. S., M. Chen, S. Leung, K. W. Graepel, X. Du, Y. Yang, T. Zhou, U. Baxa, E. Yasuda, T. Beaumont, A. Kumar, K. Modjarrad, Z. Zheng, M. Zhao, N. Xia, P. D. Kwong and B. S. Graham (2013). "Structure of RSV fusion glycoprotein trimer bound to a prefusion-specific neutralizing antibody." Science **340**(6136): 1113-1117.

Mei, H. E., I. Wirries, D. Frolich, M. Brisslert, C. Giesecke, J. R. Grun, T. Alexander, S. Schmidt, K. Luda, A. A. Kuhl, R. Engelmann, M. Durr, T. Scheel, M. Bokarewa, C. Perka, A. Radbruch and T. Dorner (2015). "A unique population of IgG-expressing plasma cells lacking CD19 is enriched in human bone marrow." Blood **125**(11): 1739-1748.

Meissner, H. C., R. C. Welliver, S. A. Chartrand, B. J. Law, L. E. Weisman, H. L. Dorkin and W. J. Rodriguez (1999). "Immunoprophylaxis with palivizumab, a humanized respiratory syncytial virus monoclonal antibody, for prevention of respiratory syncytial virus infection in high risk infants: a consensus opinion." Pediatr Infect Dis J **18**(3): 223-231.

Merz, D. C., A. Scheid and P. W. Choppin (1980). "Importance of antibodies to the fusion glycoprotein of paramyxoviruses in the prevention of spread of infection." J Exp Med **151**(2): 275-288.

Middleton, D. (2014). "Hendra virus." Vet Clin North Am Equine Pract **30**(3): 579-589.

Middleton, D., J. Pallister, R. Klein, Y. R. Feng, J. Haining, R. Arkinstall, L. Frazer, J. A. Huang, N. Edwards, M. Wareing, M. Elhay, Z. Hashmi, J. Bingham, M. Yamada, D. Johnson, J.

White, A. Foord, H. G. Heine, G. A. Marsh, C. C. Broder and L. F. Wang (2014). "Hendra virus vaccine, a one health approach to protecting horse, human, and environmental health." Emerg Infect Dis **20**(3): 372-379.

Miglietta, R., C. Pastori, A. Venuti, C. Ochsenbauer and L. Lopalco (2014). "Synergy in monoclonal antibody neutralization of HIV-1 pseudoviruses and infectious molecular clones." J Transl Med **12**: 346.

Mire, C. E., Y. P. Chan, V. Borisevich, R. W. Cross, L. Yan, K. N. Agans, H. V. Dang, D. Veesler, K. A. Fenton, T. W. Geisbert and C. C. Broder (2019). "A Cross-Reactive Humanized Monoclonal Antibody Targeting Fusion Glycoprotein Function Protects Ferrets Against Lethal Nipah Virus and Hendra Virus Infection." J Infect Dis.

Mire, C. E., Y. P. Chan, V. Borisevich, R. W. Cross, L. Yan, K. N. Agans, H. V. Dang, D. Veesler, K. A. Fenton, T. W. Geisbert and C. C. Broder (2020). "A cross-reactive humanized monoclonal antibody targeting fusion glycoprotein function protects ferrets against lethal Nipah virus and Hendra virus infection." J Infect Dis **221**(Supplement_4): S471-S479.

Mire, C. E., J. B. Geisbert, K. N. Agans, K. M. Versteeg, D. J. Deer, B. A. Satterfield, K. A. Fenton and T. W. Geisbert (2019). "Use of single-injection recombinant Vesicular Stomatitis Virus vaccine to protect nonhuman primates against lethal Nipah virus disease." Emerg Infect Dis **25**(6): 1144-1152.

Mire, C. E., B. A. Satterfield, J. B. Geisbert, K. N. Agans, V. Borisevich, L. Yan, Y. P. Chan, R. W. Cross, K. A. Fenton, C. C. Broder and T. W. Geisbert (2016). "Pathogenic Differences between Nipah Virus Bangladesh and Malaysia Strains in Primates: Implications for Antibody Therapy." Sci Rep **6**: 30916.

Mire, C. E., K. M. Versteeg, R. W. Cross, K. N. Agans, K. A. Fenton, M. A. Whitt and T. W. Geisbert (2013). "Single injection recombinant vesicular stomatitis virus vaccines protect ferrets against lethal Nipah virus disease." Virol J **10**: 353.

Modhiran, N., H. Song, L. Liu, C. Bletchly, L. Brillault, A. A. Amarilla, X. Xu, J. Qi, Y. Chai, S. T. M. Cheung, R. Traves, Y. X. Setoh, S. Bibby, C. A. P. Scott, M. E. Freney, N. D. Newton, A. A. Khromykh, K. J. Chappell, D. A. Muller, K. J. Stacey, M. J. Landsberg, Y. Shi, G. F. Gao, P. R. Young and D. Watterson (2021). "A broadly protective antibody that targets the flavivirus NS1 protein." Science **371**(6525): 190-194.

Monath, T. P. and P. F. Vasconcelos (2015). "Yellow fever." J Clin Virol **64**: 160-173.

Morens, D. M. and A. S. Fauci (2020). "Emerging pandemic diseases: How we got to COVID-19." Cell **182**(5): 1077-1092.

Mulangu, S., L. E. Dodd, R. T. Davey, Jr., O. Tshiani Mbaya, M. Proschan, D. Mukadi, M. Lusakibanza Manzo, D. Nzolo, A. Tshomba Oloma, A. Ibanda, R. Ali, S. Coulibaly, A. C. Levine, R. Grais, J. Diaz, H. C. Lane, J. J. Muyembe-Tamfum, P. W. Group, B. Sivahera, M. Camara, R. Kojan, R. Walker, B. Dighero-Kemp, H. Cao, P. Mukumbayi, P. Mbala-Kingebeni, S. Ahuka, S. Albert, T. Bonnett, I. Crozier, M. Duvenhage, C. Proffitt, M. Teitelbaum, T.

Moench, J. Aboulhab, K. Barrett, K. Cahill, K. Cone, R. Eckes, L. Hensley, B. Herpin, E. Higgs, J. Ledgerwood, J. Pierson, M. Smolskis, Y. Sow, J. Tierney, S. Sivapalasingam, W. Holman, N. Gettinger, D. Vallee, J. Nordwall and P. C. S. Team (2019). "A Randomized, Controlled Trial of Ebola Virus Disease Therapeutics." N Engl J Med **381**(24): 2293-2303.

Muller, D. A. and P. R. Young (2013). "The flavivirus NS1 protein: molecular and structural biology, immunology, role in pathogenesis and application as a diagnostic biomarker." Antiviral Res **98**(2): 192-208.

Murray, K., R. Rogers, L. Selvey, P. Selleck, A. Hyatt, A. Gould, L. Gleeson, P. Hooper and H. Westbury (1995). "A novel morbillivirus pneumonia of horses and its transmission to humans." Emerg Infect Dis **1**(1): 31-33.

Murray, K., P. Selleck, P. Hooper, A. Hyatt, A. Gould, L. Gleeson, H. Westbury, L. Hiley, L. Selvey, B. Rodwell and et al. (1995). "A morbillivirus that caused fatal disease in horses and humans." Science **268**(5207): 94-97.

Murray, P. K. (1996). "The evolving story of the equine morbillivirus." Aust Vet J **74**(3): 214.

Muruganandam, A., J. Tanha, S. Narang and D. Stanimirovic (2002). "Selection of phage-displayed llama single-domain antibodies that transmigrate across human blood-brain barrier endothelium." FASEB J **16**(2): 240-242.

Navaratnarajah, C. K., A. R. Generous, I. Yousaf and R. Cattaneo (2020). "Receptor-mediated cell entry of paramyxoviruses: Mechanisms, and consequences for tropism and pathogenesis." J Biol Chem **295**(9): 2771-2786.

Negrete, O. A., D. Chu, H. C. Aguilar and B. Lee (2007). "Single amino acid changes in the Nipah and Hendra virus attachment glycoproteins distinguish ephrinB2 from ephrinB3 usage." J Virol **81**(19): 10804-10814.

Negrete, O. A., E. L. Levroney, H. C. Aguilar, A. Bertolotti-Ciarlet, R. Nazarian, S. Tajyar and B. Lee (2005). "EphrinB2 is the entry receptor for Nipah virus, an emergent deadly paramyxovirus." Nature **436**(7049): 401-405.

Negrete, O. A., M. C. Wolf, H. C. Aguilar, S. Enterlein, W. Wang, E. Muhlberger, S. V. Su, A. Bertolotti-Ciarlet, R. Flick and B. Lee (2006). "Two key residues in ephrinB3 are critical for its use as an alternative receptor for Nipah virus." PLoS Pathog **2**(2): e7.

Norrby, E. (2007). "Yellow fever and Max Theiler: the only Nobel Prize for a virus vaccine." J Exp Med **204**(12): 2779-2784.

O'Sullivan, J. D., A. M. Allworth, D. L. Paterson, T. M. Snow, R. Boots, L. J. Gleeson, A. R. Gould, A. D. Hyatt and J. Bradfield (1997). "Fatal encephalitis due to novel paramyxovirus transmitted from horses." Lancet **349**(9045): 93-95.

Ofek, G., F. J. Guenaga, W. R. Schief, J. Skinner, D. Baker, R. Wyatt and P. D. Kwong (2010). "Elicitation of structure-specific antibodies by epitope scaffolds." Proc Natl Acad Sci U S A **107**(42): 17880-17887.

Ohi, M., Y. Li, Y. Cheng and T. Walz (2004). "Negative staining and image classification - powerful tools in modern electron microscopy." Biol Proced Online **6**: 23-34.

Pager, C. T., W. W. Craft, Jr., J. Patch and R. E. Dutch (2006). "A mature and fusogenic form of the Nipah virus fusion protein requires proteolytic processing by cathepsin L." Virology **346**(2): 251-257.

Pager, C. T. and R. E. Dutch (2005). "Cathepsin L is involved in proteolytic processing of the Hendra virus fusion protein." J Virol **79**(20): 12714-12720.

Pascal, K. E., D. Dudgeon, J. C. Trefry, M. Anantpadma, Y. Sakurai, C. D. Murin, H. L. Turner, J. Fairhurst, M. Torres, A. Rafique, Y. Yan, A. Badithe, K. Yu, T. Potocky, S. L. Bixler, T. B. Chance, W. D. Pratt, F. D. Rossi, J. D. Shamblin, S. E. Wollen, J. M. Zelko, R. Carrion, Jr., G. Worwa, H. M. Staples, D. Burakov, R. Babb, G. Chen, J. Martin, T. T. Huang, K. Erlandson, M. S. Willis, K. Armstrong, T. M. Dreier, A. B. Ward, R. A. Davey, M. L. M. Pitt, L. Lipsich, P. Mason, W. Olson, N. Stahl and C. A. Kyratsous (2018). "Development of Clinical-Stage Human Monoclonal Antibodies That Treat Advanced Ebola Virus Disease in Nonhuman Primates." J Infect Dis **218**(suppl_5): S612-S626.

Patel, A., A. DiGiandomenico, A. E. Keller, T. R. F. Smith, D. H. Park, S. Ramos, K. Schultheis, S. T. C. Elliott, J. Mendoza, K. E. Broderick, M. C. Wise, J. Yan, J. Jiang, S. Flingai, A. S. Khan, K. Muthumani, L. Humeau, L. I. Cheng, L. Wachter-Rosati, C. K. Stover, N. Y. Sardesai and D. B. Weiner (2017). "An engineered bispecific DNA-encoded IgG antibody protects against Pseudomonas aeruginosa in a pneumonia challenge model." Nat Commun **8**(1): 637.

Patel, B., P. Longo, M. J. Miley, M. Montoya, E. Harris and A. M. de Silva (2017). "Dissecting the human serum antibody response to secondary dengue virus infections." PLoS Negl Trop Dis **11**(5): e0005554.

Paton, N. I., Y. S. Leo, S. R. Zaki, A. P. Auchus, K. E. Lee, A. E. Ling, S. K. Chew, B. Ang, P. E. Rollin, T. Umapathi, I. Sng, C. C. Lee, E. Lim and T. G. Ksiazek (1999). "Outbreak of Nipah-virus infection among abattoir workers in Singapore." Lancet **354**(9186): 1253-1256.

Peel, A. J., K. Wells, J. Giles, V. Boyd, A. Burroughs, D. Edson, G. Crameri, M. L. Baker, H. Field, L. F. Wang, H. McCallum, R. K. Plowright and N. Clark (2019). "Synchronous shedding of multiple bat paramyxoviruses coincides with peak periods of Hendra virus spillover." Emerg Microbes Infect **8**(1): 1314-1323.

Pernet, O., B. S. Schneider, S. M. Beaty, M. LeBreton, T. E. Yun, A. Park, T. T. Zachariah, T. A. Bowden, P. Hitchens, C. M. Ramirez, P. Daszak, J. Mazet, A. N. Freiberg, N. D. Wolfe and B. Lee (2014). "Evidence for henipavirus spillover into human populations in Africa." Nat Commun **5**: 5342.

Pettersen, E. F., T. D. Goddard, C. C. Huang, G. S. Couch, D. M. Greenblatt, E. C. Meng and T. E. Ferrin (2004). "UCSF Chimera--a visualization system for exploratory research and analysis." J Comput Chem **25**(13): 1605-1612.

Pierson, T. C. and M. S. Diamond (2020). "The continued threat of emerging flaviviruses." Nat Microbiol **5**(6): 796-812.

Pierson, T. C., Q. Xu, S. Nelson, T. Oliphant, G. E. Nybakken, D. H. Fremont and M. S. Diamond (2007). "The stoichiometry of antibody-mediated neutralization and enhancement of West Nile virus infection." Cell Host Microbe **1**(2): 135-145.

Playford, E. G., T. Munro, S. M. Mahler, S. Elliott, M. Gerometta, K. L. Hoger, M. L. Jones, P. Griffin, K. D. Lynch, H. Carroll, D. El Saadi, M. E. Gilmour, B. Hughes, K. Hughes, E. Huang, C. de Bakker, R. Klein, M. G. Scher, I. L. Smith, L. F. Wang, S. B. Lambert, D. S. Dimitrov, P. P. Gray and C. C. Broder (2020). "Safety, tolerability, pharmacokinetics, and immunogenicity of a human monoclonal antibody targeting the G glycoprotein of henipaviruses in healthy adults: a first-in-human, randomised, controlled, phase 1 study." Lancet Infect Dis **20**(4): 445-454.

Plemper, R. K., A. L. Hammond, D. Gerlier, A. K. Fielding and R. Cattaneo (2002). "Strength of envelope protein interaction modulates cytopathicity of measles virus." J Virol **76**(10): 5051-5061.

Plowright, R. K., P. Eby, P. J. Hudson, I. L. Smith, D. Westcott, W. L. Bryden, D. Middleton, P. A. Reid, R. A. McFarlane, G. Martin, G. M. Tabor, L. F. Skerratt, D. L. Anderson, G. Crameri, D. Quammen, D. Jordan, P. Freeman, L. F. Wang, J. H. Epstein, G. A. Marsh, N. Y. Kung and H. McCallum (2015). "Ecological dynamics of emerging bat virus spillover." Proc Biol Sci **282**(1798): 20142124.

Pontejo, S. M., A. Alejo and A. Alcami (2015). "Poxvirus-encoded TNF decoy receptors inhibit the biological activity of transmembrane TNF." J Gen Virol **96**(10): 3118-3123.

Prasad, V. M., A. S. Miller, T. Klose, D. Sirohi, G. Buda, W. Jiang, R. J. Kuhn and M. G. Rossmann (2017). "Structure of the immature Zika virus at 9 A resolution." Nat Struct Mol Biol **24**(2): 184-186.

Puerta-Guardo, H., D. R. Glasner, D. A. Espinosa, S. B. Biering, M. Patana, K. Ratnasiri, C. Wang, P. R. Beatty and E. Harris (2019). "Flavivirus NS1 Triggers Tissue-Specific Vascular Endothelial Dysfunction Reflecting Disease Tropism." Cell Rep **26**(6): 1598-1613 e1598.

Qiu, X., Y. Lei, P. Yang, Q. Gao, N. Wang, L. Cao, S. Yuan, X. Huang, Y. Deng, W. Ma, T. Ding, F. Zhang, X. Wu, J. Hu, S. L. Liu, C. Qin, X. Wang, Z. Xu and Z. Rao (2018). "Structural basis for neutralization of Japanese encephalitis virus by two potent therapeutic antibodies." Nat Microbiol **3**(3): 287-294.

Queensland Government, B. Q. (2020, 28 Jul 2020). "A summary of incidents of Hendra virus (HeV) in horses for Queensland and New South Wales since 1994." Retrieved 14 Feb 2021, 2021, from https://www.business.qld.gov.au/industries/service-industries-professionals/service-industries/veterinary-surgeons/guidelines-hendra/incident-summary.

Rappazzo, C. G., L. V. Tse, C. I. Kaku, D. Wrapp, M. Sakharkar, D. Huang, L. M. Deveau, T. J. Yockachonis, A. S. Herbert, M. B. Battles, C. M. O'Brien, M. E. Brown, J. C. Geoghegan, J. Belk, L. Peng, L. Yang, Y. Hou, T. D. Scobey, D. R. Burton, D. Nemazee, J. M. Dye, J. E. Voss, B. M. Gunn, J. S. McLellan, R. S. Baric, L. E. Gralinski and L. M. Walker (2021). "Broad and potent activity against SARS-like viruses by an engineered human monoclonal antibody." Science **371**(6531): 823-829.

Reed, W., J. Carroll, A. Agramonte and J. W. Lazear (1900). "The Etiology of Yellow Fever-A Preliminary Note." Public Health Pap Rep **26**: 37-53.

Rey, F. A., F. X. Heinz, C. Mandl, C. Kunz and S. C. Harrison (1995). "The envelope glycoprotein from tick-borne encephalitis virus at 2 A resolution." Nature **375**(6529): 291-298.

Rey, F. A., K. Stiasny and F. X. Heinz (2017). "Flavivirus structural heterogeneity: implications for cell entry." Curr Opin Virol **24**: 132-139.

Reyes-Sandoval, A. and J. E. Ludert (2019). "The Dual Role of the Antibody Response Against the Flavivirus Non-structural Protein 1 (NS1) in Protection and Immuno-Pathogenesis." Front Immunol **10**: 1651.

Rima, B., A. Balkema-Buschmann, W. G. Dundon, P. Duprex, A. Easton, R. Fouchier, G. Kurath, R. Lamb, B. Lee, P. Rota, L. Wang and C. Ictv Report (2019). "ICTV Virus Taxonomy Profile: Paramyxoviridae." J Gen Virol **100**(12): 1593-1594.

Rissanen, I., A. A. Ahmed, K. Azarm, S. Beaty, P. Hong, S. Nambulli, W. P. Duprex, B. Lee and T. A. Bowden (2017). "Idiosyncratic Mojiang virus attachment glycoprotein directs a host-cell entry pathway distinct from genetically related henipaviruses." Nat Commun **8**: 16060.

Rockx, B., K. N. Bossart, F. Feldmann, J. B. Geisbert, A. C. Hickey, D. Brining, J. Callison, D. Safronetz, A. Marzi, L. Kercher, D. Long, C. C. Broder, H. Feldmann and T. W. Geisbert (2010). "A novel model of lethal Hendra virus infection in African green monkeys and the effectiveness of ribavirin treatment." J Virol **84**(19): 9831-9839.

Rockx, B., D. Brining, J. Kramer, J. Callison, H. Ebihara, K. Mansfield and H. Feldmann (2011). "Clinical outcome of henipavirus infection in hamsters is determined by the route and dose of infection." J Virol **85**(15): 7658-7671.

Rodriguez, J. J., L. F. Wang and C. M. Horvath (2003). "Hendra virus V protein inhibits interferon signaling by preventing STAT1 and STAT2 nuclear accumulation." J Virol **77**(21): 11842-11845.

Rogers, T. F., E. C. Goodwin, B. Briney, D. Sok, N. Beutler, A. Strubel, R. Nedellec, K. Le, M. E. Brown, D. R. Burton and L. M. Walker (2017). "Zika virus activates de novo and cross-reactive memory B cell responses in dengue-experienced donors." Sci Immunol **2**(14).

Rossey, I., M. S. Gilman, S. C. Kabeche, K. Sedeyn, D. Wrapp, M. Kanekiyo, M. Chen, V. Mas, J. Spitaels, J. A. Melero, B. S. Graham, B. Schepens, J. S. McLellan and X. Saelens (2017).

"Potent single-domain antibodies that arrest respiratory syncytial virus fusion protein in its prefusion state." Nat Commun **8**: 14158.

Santiago, C., M. L. Celma, T. Stehle and J. M. Casasnovas (2010). "Structure of the measles virus hemagglutinin bound to the CD46 receptor." Nat Struct Mol Biol **17**(1): 124-129.

Sasaki, M., A. Setiyono, E. Handharyani, I. Rahmadani, S. Taha, S. Adiani, M. Subangkit, H. Sawa, I. Nakamura and T. Kimura (2012). "Molecular detection of a novel paramyxovirus in fruit bats from Indonesia." Virol J **9**: 240.

Satterfield, B. A., R. W. Cross, K. A. Fenton, K. N. Agans, C. F. Basler, T. W. Geisbert and C. E. Mire (2015). "The immunomodulating V and W proteins of Nipah virus determine disease course." Nat Commun **6**: 7483.

Schatz, D. G., M. A. Oettinger and D. Baltimore (1989). "The V(D)J recombination activating gene, RAG-1." Cell **59**(6): 1035-1048.

Schramm, C. A. and D. C. Douek (2018). "Beyond Hot Spots: Biases in Antibody Somatic Hypermutation and Implications for Vaccine Design." Front Immunol **9**: 1876.

Schrodinger, LLC (2015). The PyMOL Molecular Graphics System, Version 1.8.

Schroeder, H. W., Jr. and L. Cavacini (2010). "Structure and function of immunoglobulins." J Allergy Clin Immunol **125**(2 Suppl 2): S41-52.

Schulz, J. E., S. N. Seifert, J. T. Thompson, V. Avanzato, S. L. Sterling, L. Yan, M. C. Letko, M. J. Matson, R. J. Fischer, A. Tremeau-Bravard, J. F. R. Seetahal, V. Ramkissoon, J. Foster, T. Goldstein, S. J. Anthony, J. H. Epstein, E. D. Laing, C. C. Broder, C. V. F. Carrington, T. Schountz and V. J. Munster (2020). "Serological Evidence for Henipa-like and Filo-like Viruses in Trinidad Bats." J Infect Dis **221**(Suppl 4): S375-S382.

Selvey, L. A., R. M. Wells, J. G. McCormack, A. J. Ansford, K. Murray, R. J. Rogers, P. S. Lavercombe, P. Selleck and J. W. Sheridan (1995). "Infection of humans and horses by a newly described morbillivirus." Med J Aust **162**(12): 642-645.

Setliff, I., W. J. McDonnell, N. Raju, R. G. Bombardi, A. A. Murji, C. Scheepers, R. Ziki, C. Mynhardt, B. E. Shepherd, A. A. Mamchak, N. Garrett, S. A. Karim, S. A. Mallal, J. E. Crowe, Jr., L. Morris and I. S. Georgiev (2018). "Multi-Donor Longitudinal Antibody Repertoire Sequencing Reveals the Existence of Public Antibody Clonotypes in HIV-1 Infection." Cell Host Microbe **23**(6): 845-854 e846.

Shehata, L., D. P. Maurer, A. Z. Wec, A. Lilov, E. Champney, T. Sun, K. Archambault, I. Burnina, H. Lynaugh, X. Zhi, Y. Xu and L. M. Walker (2019). "Affinity Maturation Enhances Antibody Specificity but Compromises Conformational Stability." Cell Rep **28**(13): 3300-3308 e3304.

Simmonds, P., P. Becher, J. Bukh, E. A. Gould, G. Meyers, T. Monath, S. Muerhoff, A. Pletnev, R. Rico-Hesse, D. B. Smith, J. T. Stapleton and C. Ictv Report (2017). "ICTV Virus Taxonomy Profile: Flaviviridae." J Gen Virol **98**(1): 2-3.

Skaricic, D., C. Traube, B. De, J. Joh, J. Boyer, R. G. Crystal and S. Worgall (2008). "Genetic delivery of an anti-RSV antibody to protect against pulmonary infection with RSV." Virology **378**(1): 79-85.

Skarlatos, S., T. Yoshikawa and W. M. Pardridge (1995). "Transport of [125I]transferrin through the rat blood-brain barrier." Brain Res **683**(2): 164-171.

Slon Campos, J. L., J. Mongkolsapaya and G. R. Screaton (2018). "The immune response against flaviviruses." Nat Immunol **19**(11): 1189-1198.

Smit, J. M., B. Moesker, I. Rodenhuis-Zybert and J. Wilschut (2011). "Flavivirus cell entry and membrane fusion." Viruses **3**(2): 160-171.

Smith, E. C. (2017). "The not-so-infinite malleability of RNA viruses: Viral and cellular determinants of RNA virus mutation rates." PLoS Pathog **13**(4): e1006254.

Smith, I. and L. F. Wang (2013). "Bats and their virome: an important source of emerging viruses capable of infecting humans." Curr Opin Virol **3**(1): 84-91.

Smith, S. A., U. K. Nivarthi, R. de Alwis, N. Kose, G. Sapparapu, R. Bombardi, K. M. Kahle, J. M. Pfaff, S. Lieberman, B. J. Doranz, A. M. de Silva and J. E. Crowe, Jr. (2016). "Dengue Virus prM-Specific Human Monoclonal Antibodies with Virus Replication-Enhancing Properties Recognize a Single Immunodominant Antigenic Site." J Virol **90**(2): 780-789.

Smith, S. A., Y. Zhou, N. P. Olivarez, A. H. Broadwater, A. M. de Silva and J. E. Crowe, Jr. (2012). "Persistence of circulating memory B cell clones with potential for dengue virus disease enhancement for decades following infection." J. Virol. **86**(5): 2665-2675.

Sokolowska-Wedzina, A., G. Chodaczek, J. Chudzian, A. Borek, M. Zakrzewska and J. Otlewski (2017). "High-Affinity Internalizing Human scFv-Fc Antibody for Targeting FGFR1-Overexpressing Lung Cancer." Mol Cancer Res **15**(8): 1040-1050.

Soman Pillai, V., G. Krishna and M. Valiya Veettil (2020). "Nipah virus: Past outbreaks and future containment." Viruses **12**(4).

Soto, C., R. G. Bombardi, A. Branchizio, N. Kose, P. Matta, A. M. Sevy, R. S. Sinkovits, P. Gilchuk, J. A. Finn and J. E. Crowe, Jr. (2019). "High frequency of shared clonotypes in human B cell receptor repertoires." Nature **566**(7744): 398-402.

Spiropoulou, C. F. (2019). "Nipah Virus Outbreaks: Still Small but Extremely Lethal." J Infect Dis **219**(12): 1855-1857.

Stadlbauer, D., X. Zhu, M. McMahon, J. S. Turner, T. J. Wohlbold, A. J. Schmitz, S. Strohmeier, W. Yu, R. Nachbagauer, P. A. Mudd, I. A. Wilson, A. H. Ellebedy and F. Krammer (2019).

"Broadly protective human antibodies that target the active site of influenza virus neuraminidase." Science **366**(6464): 499-504.

Stark, H. (2010). "GraFix: stabilization of fragile macromolecular complexes for single particle cryo-EM." Methods Enzymol **481**: 109-126.

Starr, T. N., A. J. Greaney, A. Addetia, W. W. Hannon, M. C. Choudhary, A. S. Dingens, J. Z. Li and J. D. Bloom (2021). "Prospective mapping of viral mutations that escape antibodies used to treat COVID-19." Science **371**(6531): 850-854.

Stavnezer, J., J. E. Guikema and C. E. Schrader (2008). "Mechanism and regulation of class switch recombination." Annu Rev Immunol **26**: 261-292.

Steffen, D. L., K. Xu, D. B. Nikolov and C. C. Broder (2012). "Henipavirus mediated membrane fusion, virus entry and targeted therapeutics." Viruses **4**(2): 280-308.

Sweileh, W. M. (2017). "Global research trends of World Health Organization's top eight emerging pathogens." Global Health **13**(1): 9.

Tan, C. T., K. J. Goh, K. T. Wong, S. A. Sarji, K. B. Chua, N. K. Chew, P. Murugasu, Y. L. Loh, H. T. Chong, K. S. Tan, T. Thayaparan, S. Kumar and M. R. Jusoh (2002). "Relapsed and late-onset Nipah encephalitis." Ann Neurol **51**(6): 703-708.

Tassaneetrithep, B., T. H. Burgess, A. Granelli-Piperno, C. Trumpfheller, J. Finke, W. Sun, M. A. Eller, K. Pattanapanyasat, S. Sarasombath, D. L. Birx, R. M. Steinman, S. Schlesinger and M. A. Marovich (2003). "DC-SIGN (CD209) mediates dengue virus infection of human dendritic cells." J Exp Med **197**(7): 823-829.

Thanabalasuriar, A., B. N. V. Scott, M. Peiseler, M. E. Willson, Z. Zeng, P. Warrener, A. E. Keller, B. G. J. Surewaard, E. A. Dozier, J. T. Korhonen, L. I. Cheng, M. Gadjeva, C. K. Stover, A. DiGiandomenico and P. Kubes (2019). "Neutrophil Extracellular Traps Confine Pseudomonas aeruginosa Ocular Biofilms and Restrict Brain Invasion." Cell Host Microbe **25**(4): 526-536 e524.

Thanabalasuriar, A., B. G. Surewaard, M. E. Willson, A. S. Neupane, C. K. Stover, P. Warrener, G. Wilson, A. E. Keller, B. R. Sellman, A. DiGiandomenico and P. Kubes (2017). "Bispecific antibody targets multiple Pseudomonas aeruginosa evasion mechanisms in the lung vasculature." J Clin Invest **127**(6): 2249-2261.

Theiler, M. and H. H. Smith (1937). "The Effect of Prolonged Cultivation in Vitro Upon the Pathogenicity of Yellow Fever Virus." J Exp Med **65**(6): 767-786.

Theiler, M. and H. H. Smith (1937). "The Use of Yellow Fever Virus Modified by in Vitro Cultivation for Human Immunization." J Exp Med **65**(6): 787-800.

Thibodeaux, B. A., N. C. Garbino, N. M. Liss, J. Piper, J. J. Schlesinger, C. D. Blair and J. T. Roehrig (2012). "A humanized IgG but not IgM antibody is effective in prophylaxis and therapy

of yellow fever infection in an AG129/17D-204 peripheral challenge mouse model." Antiviral Res **94**(1): 1-8.

Tsimbalyuk, S., E. M. Cross, M. Hoad, C. M. Donnelly, J. A. Roby and J. K. Forwood (2020). "The Intrinsically Disordered W Protein Is Multifunctional during Henipavirus Infection, Disrupting Host Signalling Pathways and Nuclear Import." Cells **9**(8).

Uchida, S., R. Horie, H. Sato, C. Kai and M. Yoneda (2018). "Possible role of the Nipah virus V protein in the regulation of the interferon beta induction by interacting with UBX domain-containing protein1." Sci Rep **8**(1): 7682.

Velayutham, T. S., S. Kumar, X. Zhang, N. Kose, D. H. Walker, G. Winslow, J. E. Crowe, Jr. and J. W. McBride (2019). "Ehrlichia chaffeensis Outer Membrane Protein 1-Specific Human Antibody-Mediated Immunity Is Defined by Intracellular TRIM21-Dependent Innate Immune Activation and Extracellular Neutralization." Infect Immun **87**(12).

Vidgen, M. E., C. de Jong, K. Rose, J. Hall, H. E. Field and C. S. Smith (2015). "Novel paramyxoviruses in Australian flying-fox populations support host-virus co-evolution." J Gen Virol **96**(Pt 7): 1619-1625.

Vogt, M. R., K. A. Dowd, M. Engle, R. B. Tesh, S. Johnson, T. C. Pierson and M. S. Diamond (2011). "Poorly neutralizing cross-reactive antibodies against the fusion loop of West Nile virus envelope protein protect in vivo via Fcgamma receptor and complement-dependent effector mechanisms." J Virol **85**(22): 11567-11580.

Voigt, K., M. Hoffmann, J. F. Drexler, M. A. Muller, C. Drosten, G. Herrler and N. Kruger (2019). "Fusogenicity of the Ghana Virus (Henipavirus: Ghanaian bat henipavirus) Fusion Protein is Controlled by the Cytoplasmic Domain of the Attachment Glycoprotein." Viruses **11**(9).

Walls, A. C., X. Xiong, Y. J. Park, M. A. Tortorici, J. Snijder, J. Quispe, E. Cameroni, R. Gopal, M. Dai, A. Lanzavecchia, M. Zambon, F. A. Rey, D. Corti and D. Veesler (2020). "Unexpected Receptor Functional Mimicry Elucidates Activation of Coronavirus Fusion." Cell **183**(6): 1732.

Walsh, M. G., A. Wiethoelter and M. A. Haseeb (2017). "The impact of human population pressure on flying fox niches and the potential consequences for Hendra virus spillover." Sci Rep **7**(1): 8226.

Wang, L. F., M. Yu, E. Hansson, L. I. Pritchard, B. Shiell, W. P. Michalski and B. T. Eaton (2000). "The exceptionally large genome of Hendra virus: support for creation of a new genus within the family Paramyxoviridae." J Virol **74**(21): 9972-9979.

Weatherman, S., H. Feldmann and E. de Wit (2018). "Transmission of henipaviruses." Curr Opin Virol **28**: 7-11.

Wec, A. Z., D. Haslwanter, Y. N. Abdiche, L. Shehata, N. Pedreno-Lopez, C. L. Moyer, Z. A. Bornholdt, A. Lilov, J. H. Nett, R. K. Jangra, M. Brown, D. I. Watkins, C. Ahlm, M. N. Forsell, F. A. Rey, G. Barba-Spaeth, K. Chandran and L. M. Walker (2020). "Longitudinal dynamics of

the human B cell response to the yellow fever 17D vaccine." Proc Natl Acad Sci U S A **117**(12): 6675-6685.

Wec, A. Z., E. K. Nyakatura, A. S. Herbert, K. A. Howell, F. W. Holtsberg, R. R. Bakken, E. Mittler, J. R. Christin, S. Shulenin, R. K. Jangra, S. Bharrhan, A. I. Kuehne, Z. A. Bornholdt, A. I. Flyak, E. O. Saphire, J. E. Crowe, Jr., M. J. Aman, J. M. Dye, J. R. Lai and K. Chandran (2016). "A "Trojan horse" bispecific-antibody strategy for broad protection against ebolaviruses." Science **354**(6310): 350-354.

Wec, A. Z., D. Wrapp, A. S. Herbert, D. P. Maurer, D. Haslwanter, M. Sakharkar, R. K. Jangra, M. E. Dieterle, A. Lilov, D. Huang, L. V. Tse, N. V. Johnson, C. L. Hsieh, N. Wang, J. H. Nett, E. Champney, I. Burnina, M. Brown, S. Lin, M. Sinclair, C. Johnson, S. Pudi, R. Bortz, 3rd, A. S. Wirchnianski, E. Laudermilch, C. Florez, J. M. Fels, C. M. O'Brien, B. S. Graham, D. Nemazee, D. R. Burton, R. S. Baric, J. E. Voss, K. Chandran, J. M. Dye, J. S. McLellan and L. M. Walker (2020). "Broad neutralization of SARS-related viruses by human monoclonal antibodies." Science **369**(6504): 731-736.

Welch, B. D., P. Yuan, S. Bose, C. A. Kors, R. A. Lamb and T. S. Jardetzky (2013). "Structure of the parainfluenza virus 5 (PIV5) hemagglutinin-neuraminidase (HN) ectodomain." PLoS Pathog **9**(8): e1003534.

Welch, S. R., N. L. Tilston, M. K. Lo, S. L. M. Whitmer, J. R. Harmon, F. E. M. Scholte, J. R. Spengler, W. P. Duprex, S. T. Nichol and C. F. Spiropoulou (2020). "Inhibition of Nipah virus by defective interfering particles." J Infect Dis **221**(Supplement_4): S460-S470.

Wessel, A. W., N. Kose, R. G. Bombardi, V. Roy, W. Chantima, J. Mongkolsapaya, M. A. Edeling, C. A. Nelson, I. Bosch, G. Alter, G. R. Screaton, D. H. Fremont, J. E. Crowe, Jr. and M. S. Diamond (2020). "Antibodies targeting epitopes on the cell-surface form of NS1 protect against Zika virus infection during pregnancy." Nat Commun **11**(1): 5278.

Wilder-Smith, A., S. Flasche and P. G. Smith (2019). "Vaccine-attributable severe dengue in the Philippines." Lancet **394**(10215): 2151-2152.

Williamson, L. E., T. Gilliland, Jr., P. K. Yadav, E. Binshtein, R. Bombardi, N. Kose, R. S. Nargi, R. E. Sutton, C. L. Durie, E. Armstrong, R. H. Carnahan, L. M. Walker, A. S. Kim, J. M. Fox, M. S. Diamond, M. D. Ohi, W. B. Klimstra and J. E. Crowe, Jr. (2020). "Human Antibodies Protect against Aerosolized Eastern Equine Encephalitis Virus Infection." Cell **183**(7): 1884-1900 e1823.

Winn, M. D., C. C. Ballard, K. D. Cowtan, E. J. Dodson, P. Emsley, P. R. Evans, R. M. Keegan, E. B. Krissinel, A. G. Leslie, A. McCoy, S. J. McNicholas, G. N. Murshudov, N. S. Pannu, E. A. Potterton, H. R. Powell, R. J. Read, A. Vagin and K. S. Wilson (2011). "Overview of the CCP4 suite and current developments." Acta Crystallogr D Biol Crystallogr **67**(Pt 4): 235-242.

Wong, J. J. W., T. A. Young, J. Zhang, S. Liu, G. P. Leser, E. A. Komives, R. A. Lamb, Z. H. Zhou, J. Salafsky and T. S. Jardetzky (2017). "Monomeric ephrinB2 binding induces allosteric changes in Nipah virus G that precede its full activation." Nat Commun **8**(1): 781.

Wong, K. T., I. Grosjean, C. Brisson, B. Blanquier, M. Fevre-Montange, A. Bernard, P. Loth, M. C. Georges-Courbot, M. Chevallier, H. Akaoka, P. Marianneau, S. K. Lam, T. F. Wild and V. Deubel (2003). "A golden hamster model for human acute Nipah virus infection." Am J Pathol **163**(5): 2127-2137.

Wu, C., H. Ying, C. Grinnell, S. Bryant, R. Miller, A. Clabbers, S. Bose, D. McCarthy, R. R. Zhu, L. Santora, R. Davis-Taber, Y. Kunes, E. Fung, A. Schwartz, P. Sakorafas, J. Gu, E. Tarcsa, A. Murtaza and T. Ghayur (2007). "Simultaneous targeting of multiple disease mediators by a dual-variable-domain immunoglobulin." Nat Biotechnol **25**(11): 1290-1297.

Wu, H., D. S. Pfarr, S. Johnson, Y. A. Brewah, R. M. Woods, N. K. Patel, W. I. White, J. F. Young and P. A. Kiener (2007). "Development of motavizumab, an ultra-potent antibody for the prevention of respiratory syncytial virus infection in the upper and lower respiratory tract." J Mol Biol **368**(3): 652-665.

Wu, H., D. S. Pfarr, G. A. Losonsky and P. A. Kiener (2008). "Immunoprophylaxis of RSV infection: advancing from RSV-IGIV to palivizumab and motavizumab." Curr Top Microbiol Immunol **317**: 103-123.

Wu, J. T., C. M. Peak, G. M. Leung and M. Lipsitch (2016). "Fractional dosing of yellow fever vaccine to extend supply: a modelling study." Lancet **388**(10062): 2904-2911.

Wu, Z., L. Yang, F. Yang, X. Ren, J. Jiang, J. Dong, L. Sun, Y. Zhu, H. Zhou and Q. Jin (2014). "Novel Henipa-like virus, Mojiang Paramyxovirus, in rats, China, 2012." Emerg Infect Dis **20**(6): 1064-1066.

Xu, K., C. C. Broder and D. B. Nikolov (2012). "Ephrin-B2 and ephrin-B3 as functional henipavirus receptors." Semin Cell Dev Biol **23**(1): 116-123.

Xu, K., Y. P. Chan, B. Bradel-Tretheway, Z. Akyol-Ataman, Y. Zhu, S. Dutta, L. Yan, Y. Feng, L. F. Wang, G. Skiniotis, B. Lee, Z. H. Zhou, C. C. Broder, H. C. Aguilar and D. B. Nikolov (2015). "Crystal Structure of the Pre-fusion Nipah Virus Fusion Glycoprotein Reveals a Novel Hexamer-of-Trimers Assembly." PLoS Pathog **11**(12): e1005322.

Xu, K., B. Rockx, Y. Xie, B. L. DeBuysscher, D. L. Fusco, Z. Zhu, Y. P. Chan, Y. Xu, T. Luu, R. Z. Cer, H. Feldmann, V. Mokashi, D. S. Dimitrov, K. A. Bishop-Lilly, C. C. Broder and D. B. Nikolov (2013). "Crystal structure of the Hendra virus attachment G glycoprotein bound to a potent cross-reactive neutralizing human monoclonal antibody." PLoS Pathog **9**(10): e1003684.

Yoneda, M., V. Guillaume, H. Sato, K. Fujita, M. C. Georges-Courbot, F. Ikeda, M. Omi, Y. Muto-Terao, T. F. Wild and C. Kai (2010). "The nonstructural proteins of Nipah virus play a key role in pathogenicity in experimentally infected animals." PLoS One **5**(9): e12709.

Young, P. L., K. Halpin, P. W. Selleck, H. Field, J. L. Gravel, M. A. Kelly and J. S. Mackenzie (1996). "Serologic evidence for the presence in Pteropus bats of a paramyxovirus related to equine morbillivirus." Emerg Infect Dis **2**(3): 239-240.

Yu, L., X. Liu, X. Ye, W. Su, X. Zhang, W. Deng, J. Luo, M. Xiang, W. Guo, S. Zhang, W. Xu, Q. Yan, Q. Wang, Y. Cui, C. Wu, W. Guo, X. Niu, F. Zhang, C. Lei, L. Qu, L. Chen and L. Feng (2021). "Monoclonal Antibodies against Zika Virus NS1 Protein Confer Protection via Fcgamma Receptor-Dependent and -Independent Pathways." mBio **12**(1).

Yu, X., P. A. McGraw, F. S. House and J. E. Crowe, Jr. (2008). "An optimized electrofusion-based protocol for generating virus-specific human monoclonal antibodies." J Immunol Methods **336**(2): 142-151.

Yu, X., S. Zhang, L. Jiang, Y. Cui, D. Li, D. Wang, N. Wang, L. Fu, X. Shi, Z. Li, L. Zhang and X. Wang (2015). "Structural basis for the neutralization of MERS-CoV by a human monoclonal antibody MERS-27." Sci Rep **5**: 13133.

Yuan, P., G. P. Leser, B. Demeler, R. A. Lamb and T. S. Jardetzky (2008). "Domain architecture and oligomerization properties of the paramyxovirus PIV 5 hemagglutinin-neuraminidase (HN) protein." Virology **378**(2): 282-291.

Yuan, P., K. A. Swanson, G. P. Leser, R. G. Paterson, R. A. Lamb and T. S. Jardetzky (2011). "Structure of the Newcastle disease virus hemagglutinin-neuraminidase (HN) ectodomain reveals a four-helix bundle stalk." Proc Natl Acad Sci U S A **108**(36): 14920-14925.

Yuan, P., T. B. Thompson, B. A. Wurzburg, R. G. Paterson, R. A. Lamb and T. S. Jardetzky (2005). "Structural studies of the parainfluenza virus 5 hemagglutinin-neuraminidase tetramer in complex with its receptor, sialyllactose." Structure **13**(5): 803-815.

Zhang, S., V. A. Kostyuchenko, T. S. Ng, X. N. Lim, J. S. G. Ooi, S. Lambert, T. Y. Tan, D. G. Widman, J. Shi, R. S. Baric and S. M. Lok (2016). "Neutralization mechanism of a highly potent antibody against Zika virus." Nat Commun **7**: 13679.

Zhong, L., L. Haynes, E. B. Struble, A. Tamin, M. L. Virata-Theimer and P. Zhang (2009). "Antibody-mediated synergy and interference in the neutralization of SARS-CoV at an epitope cluster on the spike protein." Biochem Biophys Res Commun **390**(3): 1056-1060.

Zhu, Q., J. S. McLellan, N. L. Kallewaard, N. D. Ulbrandt, S. Palaszynski, J. Zhang, B. Moldt, A. Khan, C. Svabek, J. M. McAuliffe, D. Wrapp, N. K. Patel, K. E. Cook, B. W. M. Richter, P. C. Ryan, A. Q. Yuan and J. A. Suzich (2017). "A highly potent extended half-life antibody as a potential RSV vaccine surrogate for all infants." Sci Transl Med **9**(388).

Zhu, Z., K. N. Bossart, K. A. Bishop, G. Crameri, A. S. Dimitrov, J. A. McEachern, Y. Feng, D. Middleton, L. F. Wang, C. C. Broder and D. S. Dimitrov (2008). "Exceptionally potent cross-reactive neutralization of Nipah and Hendra viruses by a human monoclonal antibody." J Infect Dis **197**(6): 846-853.

Zhu, Z., A. S. Dimitrov, K. N. Bossart, G. Crameri, K. A. Bishop, V. Choudhry, B. A. Mungall, Y. R. Feng, A. Choudhary, M. Y. Zhang, Y. Feng, L. F. Wang, X. Xiao, B. T. Eaton, C. C. Broder and D. S. Dimitrov (2006). "Potent neutralization of Hendra and Nipah viruses by human monoclonal antibodies." J Virol **80**(2): 891-899.

Zost, S. J., P. Gilchuk, J. B. Case, E. Binshtein, R. E. Chen, J. P. Nkolola, A. Schafer, J. X. Reidy, A. Trivette, R. S. Nargi, R. E. Sutton, N. Suryadevara, D. R. Martinez, L. E. Williamson, E. C. Chen, T. Jones, S. Day, L. Myers, A. O. Hassan, N. M. Kafai, E. S. Winkler, J. M. Fox, S. Shrihari, B. K. Mueller, J. Meiler, A. Chandrashekar, N. B. Mercado, J. J. Steinhardt, K. Ren, Y. M. Loo, N. L. Kallewaard, B. T. McCune, S. P. Keeler, M. J. Holtzman, D. H. Barouch, L. E. Gralinski, R. S. Baric, L. B. Thackray, M. S. Diamond, R. H. Carnahan and J. E. Crowe, Jr. (2020). "Potently neutralizing and protective human antibodies against SARS-CoV-2." Nature **584**(7821): 443-449.

Zost, S. J., P. Gilchuk, R. E. Chen, J. B. Case, J. X. Reidy, A. Trivette, R. S. Nargi, R. E. Sutton, N. Suryadevara, E. C. Chen, E. Binshtein, S. Shrihari, M. Ostrowski, H. Y. Chu, J. E. Didier, K. W. MacRenaris, T. Jones, S. Day, L. Myers, F. Eun-Hyung Lee, D. C. Nguyen, I. Sanz, D. R. Martinez, P. W. Rothlauf, L. M. Bloyet, S. P. J. Whelan, R. S. Baric, L. B. Thackray, M. S. Diamond, R. H. Carnahan and J. E. Crowe, Jr. (2020). "Rapid isolation and profiling of a diverse panel of human monoclonal antibodies targeting the SARS-CoV-2 spike protein." Nat Med **26**(9): 1422-1427.